

# **NANOSIZED ZINC BORATE PRODUCTION**

**A Thesis Submitted to  
the Graduate School of Engineering and Sciences of  
İzmir Institute of Technology  
in Partial Fulfillment of the Requirements for the Degree of**

**DOCTOR OF PHILOSOPHY**

**in Chemical Engineering**

**by  
Mehmet GÖNEN**

**July 2009  
İZMİR**

We approve the thesis of **Mehmet GÖNEN**

---

**Prof. Dr. Devrim BALKÖSE**  
Supervisor

---

**Prof. Dr. Muhsin ÇİFTÇİOĞLU**  
Committee Member

---

**Prof. Dr. Mustafa DEMİRCİOĞLU**  
Committee Member

---

**Prof. Dr. Serdar ÖZÇELİK**  
Committee Member

---

**Assoc. Prof. Dr. Oğuz BAYRAKTAR**  
Committee Member

**14 July 2009**

---

**Prof. Dr. Devrim BALKÖSE**  
Head of the Chemical Engineering  
Department

---

**Prof. Dr. Hasan BÖKE**  
Dean of the Graduate School of  
Engineering and Sciences

## ACKNOWLEDGEMENTS

I wish to begin by expressing my deepest appreciation to Prof. Dr. Devrim Balköse for directing my research in İzmir Institute of Technology. Throughout my graduate career, Prof. Dr. Balköse has been both a terrific advisor and an excellent mentor, especially her experience in Chemistry made a significant contribution to the study. I am very proud and privileged to be her not the first but a remarkable Ph.D. candidate in İzmir Institute of Technology.

I want to thank my co-advisor, Prof. Dr. Semra Ülkü, for her contributions to the study. I am also grateful to Prof. Dr. Serdar Özçelik and Assoc. Prof. Dr. Oğuz Bayraktar for their valuable suggestions during the progression of this study. I would like to express my thanks to Prof. Dr. Muhsin Çiftçioğlu and Prof. Dr. Hürriyet Polat for particle size analyses of samples. Prof. Dr. Servet Turan from Material Science and Engineering Department of Anadolu University is greatly acknowledged for TEM analysis.

Eti Maden Holding is greatly appreciated as they provided raw materials, boric acid and borax decahydrate that were utilized in zinc borate synthesis. I would like to express my indebtedness to The Scientific and Technological Research Council of Turkey (TÜBİTAK), which supported the project of “Nano Sized Zinc Borate Production and its Industrial Applications” with a project number;105M358 and provided a scholarship (6 months) for study in United States.

I also thank to Prof. Dr. Ram B. Gupta for giving me a chance to work in his supercritical fluid laboratory and his invaluable suggestions during the study in Auburn, USA. I want to express my appreciation to friends in Dr Gupta’s research group, Adam Byrd, Sandeep Kumar and Ganesh Sanganwar in Auburn University.

In particular, I would like to thank my friends who helped during my research at İzmir Institute of Technology. A special thank you goes to Mrs. Burcu Alp for her help in constructing experimental setup and performing experiments. I want to thank to Mrs. Sevdije Atakul for her discussion and proof reading of my writing. I would like to thank staffs in Material Research Center of İzmir Institute of Technology who performed the characterization of the samples. I want to thank my best friend, Mr. Deniz Şimşek, for his discussion and suggestions, especially at the lunch break and on

the way of cafeteria. I also express the name of my other best friend, Mr. Mehmet Şişman, for his discussion in economics and politics of globalizing world to determine our actions to preserve our existence under these conditions.

Finally, I would like to thank my wife, Nilüfer, my mother, Güllizar, my father Nuri, and my brothers, İsmail and Özgür, for their never ending supports and encouragement. I wish to express my appreciation to my wife's family for their support, as well. I should express my endless love to my son, Efe, as he sensed my hardworking during the writing of thesis and did not make so much trouble, especially in the nights. I will never forget the sacrifices my parents have made during my education, and I am truly thankful for their emphasis on and love for education.

# ABSTRACT

## NANOSIZED ZINC BORATE PRODUCTION

The present study covers both zinc borate synthesis from boric acid-zinc oxide and borax decahydrate-zinc nitrate hexahydrate pairs; treatment of those samples by supercritical carbon dioxide drying, supercritical ethanol drying, and freeze drying techniques to obtain nanosized products. Zinc borate samples before and after supercritical drying were characterized by analytical titration, SEM, XRD, TGA, DSC, FTIR, and N<sub>2</sub> adsorption at 77 K.

The use of oleic acid as a modifying agent, ultrasonic treatment and nanosized zinc oxide in the reaction of zinc oxide and boric acid did not make significant effect in controlling the particle size. However, particle size of zinc borate produced from borax and zinc nitrate has increased with reaction time. Interaction of zinc borates with CO<sub>2</sub> or ethanol at supercritical conditions or compression of crystals by high pressure created by the expansion of water during freezing are possible side effects of the nanoparticle producing processes. Zinc borate (2ZnO·3B<sub>2</sub>O<sub>3</sub>·7H<sub>2</sub>O) having water of crystallization in its structure reacted partially with CO<sub>2</sub> to produce zinc carbonate, however zinc borate (2ZnO·3B<sub>2</sub>O<sub>3</sub>·3H<sub>2</sub>O) containing only hydroxyl groups did not react with CO<sub>2</sub> in supercritical CO<sub>2</sub> drying. While zinc borate (2ZnO·3B<sub>2</sub>O<sub>3</sub>·3H<sub>2</sub>O) decomposed partially and formed anhydrous zinc borate and zinc oxide, zinc borate (ZnO·B<sub>2</sub>O<sub>3</sub>·2H<sub>2</sub>O) decomposed completely and formed only zinc oxide in the supercritical ethanol drying that was carried out at 6.5 MPa and 250 °C. Boric acid formed from the decomposition of both zinc borates was separated by ethanol extraction. If the initial particle size of zinc borate sample was at nano level, it would be possible to obtain nano particles by freeze drying.

# ÖZET

## NANO BOYUTLU ÇİNKO BORAT ÜRETİMİ

Bu çalışma, borik asit-çinko oksit ve boraks-çinko nitrat çiftlerinden çinko borat eldesini; nano boyutlu ürünler elde etmek için ürünlerin süperkritik karbondioksit kurutma, süperkritik etanol kurutma ve dondurarak kurutma teknikleri ile kurutulmasını kapsamaktadır. Çinko borat örnekleri süperkritik kurutma öncesinde ve sonrasında analitik titrasyon, SEM, XRD, TGA, DSC, FTIR analizleri ve 77 K'de azot adsorpsiyonu ile karakterize edilmiştir.

Çinko oksit ve borik asit reaksiyonunda, modifiye ajanı olarak oleik asit kullanımı, ultrasonik dalga, ve nano boyutlu çinko oksit kullanımları son ürünün parçacık boyutunu kontrol etmede etkili olmamıştır. Bununla birlikte, boraks ile çinko nitrattan üretilen çinko boratın parçacık boyutu reaksiyon süresi ile artmıştır. Süperkritik koşullarda çinko boratların CO<sub>2</sub> veya etanol ile etkileşimi, suyun dondurulmasında genişmeden oluşan yüksek basınç sonucu kristallerin sıkıştırılması nano parçacık üretim proseslerindeki olası yan etkilerdir. Yapısında kristal suyu içeren çinko borat (2ZnO·3B<sub>2</sub>O<sub>3</sub>·7H<sub>2</sub>O) süperkritik karbondioksit kurutmada CO<sub>2</sub> ile reaksiyona girmiş ve çinko karbonatı oluşturmuştur. Fakat, yapısında sadece hidroksil grupları içeren çinko borat (2ZnO·3B<sub>2</sub>O<sub>3</sub>·3H<sub>2</sub>O) ise karbondioksit ile bir etkileşim göstermemiştir. 6.5 MPa ve 250 °C'de gerçekleştirilen süperkritik etanol kurutma işleminde 2ZnO·3B<sub>2</sub>O<sub>3</sub>·3H<sub>2</sub>O yapısındaki çinko borat kısmen bozunarak susuz çinko borate ve çinko oksiti oluştururken, ZnO·B<sub>2</sub>O<sub>3</sub>·2H<sub>2</sub>O yapısındaki çinko borat ise tamamen bozunarak sadece çinko oksiti oluşturmuştur. Her iki çinko boratın bozunmasından oluşan borik asit ise etanol ekstraksiyonu ile ayrılmıştır. Çinko boratın başlangıçtaki parçacık boyutu nano boyutta olduğunda, dondurarak kurutma işlemi ile nano parçacık üretimi mümkündür.

# TABLE OF CONTENTS

LIST OF FIGURES .....	xi
LIST OF TABLES .....	xxii
CHAPTER 1. INTRODUCTION .....	1
CHAPTER 2. BORON, BORATE COMPOUNDS AND ZINC BORATE .....	4
2.1. Boric Acid and Borax Decahydrate .....	7
2.2. Metal Borates .....	11
2.3. Zinc Borates .....	13
2.3.1. Applications of Zinc Borates .....	14
2.4. Production Techniques of Metal Borates .....	16
2.4.1. Production of Zinc Borate from Borax and Zinc Salts .....	18
2.4.2. Production of Zinc Borate from Boric Acid and Zinc Oxide ..	23
2.4.3. Nucleation, Growth and Organization in Borate Crystallization .....	30
CHAPTER 3. SUPERCRITICAL FLUIDS .....	36
3.1. Supercritical Fluid (SCF) Properties .....	37
3.1.1. Viscosity .....	41
3.1.2. Diffusion Coefficient .....	43
3.1.3. Thermal Conductivity .....	44
3.1.4. Dielectric Properties .....	44
3.2. Supercritical Fluid Processes .....	44
3.3. Supercritical Fluid Drying .....	45
3.3.1. Supercritical Ethanol Drying .....	47

3.3.2. Supercritical Carbon Dioxide Drying .....	49
CHAPTER 4. MATERIALS AND METHODS .....	53
4.1. Materials .....	53
4.1.1. Boric Acid .....	54
4.1.2. Zinc Oxide .....	54
4.1.3. Disodium Tetraborate Decahydrate (Borax Decahydrate) .....	55
4.1.4. Zinc Nitrate Hexahydrate .....	55
4.2. Methods .....	55
4.2.1. Production of Zinc Borate from Boric Acid and Zinc Oxide ..	56
4.2.2. Production of Zinc Borate from Borax Decahydrate and Zinc Nitrate Hexahydrate .....	60
4.2.3. Supercritical CO <sub>2</sub> Drying of Zinc Borate Species .....	61
4.2.4. Subcritical and Supercritical Ethanol Drying of Zinc Borate Species .....	62
4.2.5. Freeze Drying of Zinc Borate Species .....	64
4.2.6. Analytical Characterization Chemicals and Techniques .....	64
4.2.7. Characterization of Zinc Borate Samples .....	65
CHAPTER 5. RESULTS AND DISCUSSION .....	68
5.1. Characterization of Raw Materials .....	68
5.2. Zinc Borate Production From Boric Acid and Zinc Oxide .....	72
5.2.1. Reaction Mechanism .....	72
5.3. Zinc Borate Production in Magnetically-Stirred Glass Reactor ...	74
5.3.1. Effect of Reaction Temperature .....	74
5.3.2. Effect of Boric Acid Concentration .....	79
5.3.3. Effect of Sonication .....	87
5.3.4. Effect of Zinc Oxide Particle Size .....	91
5.3.5. Effect of Oleic Acid as a Modifying Agent .....	95
5.3.6. Analytical Characterization .....	98
5.4. Zinc Borate Production in Mechanical-Stirred Stainless Steel Reactor .....	102
5.4.1. Effect of Reaction Time .....	102



5.4.2. Analytical Characterization .....	112
5.5. Zinc Borate Production from Borax Decahydrate and Zinc Nitrate Hexahydrate .....	113
5.5.1. Reaction Mechanism .....	113
5.6. Zinc Borate Production in a Magnetically-Stirred Glass Reactor .	114
5.6.1. Effect of Reaction Time .....	114
5.6.2. Analytical Characterization .....	125
5.7. Zinc Borate Production in a Mechanical-Stirred Stainless Steel Reactor .....	127
5.8. Supercritical Carbon Dioxide (CO <sub>2</sub> ) Drying of Zinc Borate Species .....	133
5.8.1. Characterization of Supercritical CO <sub>2</sub> Dried Zinc Borate Produced from Boric Acid and Zinc Oxide .....	134
5.8.2. Supercritical CO <sub>2</sub> Drying of Zinc Borate Produced from Borax Decahydrate and Zinc Nitrate Hexahydrate .....	138
5.8.3. Interaction Between Carbon Dioxide and Zinc Borates .....	145
5.9. Subcritical and Supercritical Ethanol Drying of Zinc Borate Species .....	145
5.9.1. Supercritical Ethanol Drying of Zinc Borate Produced from Boric Acid and Zinc Oxide .....	148
5.9.2. Effect of Temperature in Ethanol Drying .....	154
5.9.3. Supercritical Ethanol Drying of Zinc Borate Produced from Borax Decahydrate and Zinc Nitrate Hexahydrate .....	158
5.9.4. Material Balance Around Supercritical Ethanol Drying Process .....	164
5.10. Freeze Drying of Zinc Borate Species .....	171
5.10.1. Freeze Drying of Zinc Borate Produced in Glass Reactor ...	171
5.10.2. Freeze Drying of Zinc Borate Produced in Stainless Steel Reactor.....	175
5.11. Nucleation, Growth and Phase Transformation in Zinc Borate Crystallization .....	177
 CHAPTER 6. CONCLUSIONS .....	 180



## LIST OF FIGURES

<u>Figure</u>	<u>Page</u>
Figure 2.1. Estimated total borate use by major industrial applications in B <sub>2</sub> O <sub>3</sub> equivalents for the year 2001 .....	5
Figure 2.2. Schematic representation of borate oxoanions a) [B(OH) <sub>4</sub> ] <sup>-</sup> b) [B <sub>3</sub> O <sub>3</sub> (OH) <sub>4</sub> ] <sup>-</sup> c) [B <sub>5</sub> O <sub>6</sub> (OH) <sub>4</sub> ] <sup>-</sup> d) [B <sub>3</sub> O <sub>3</sub> (OH) <sub>5</sub> ] <sup>2-</sup> e) [B <sub>6</sub> O <sub>7</sub> (OH) <sub>6</sub> ] <sup>2-</sup> .	7
Figure 2.3. Solubility-temperature curves for boric acid, borax, sodium pentaborate, and sodium metaborate .....	9
Figure 2.4. Schematic drawings of mannitol and negatively charged borate mannitol complexes .....	11
Figure 2.5. SEM images of a) pure zinc borate particles and modified zinc borate particles (1.00 wt% of oleic acid added) with different zinc sulfate/sodium borate mole ratios: b) 1:1, c) 1:1.5, and d) 1:2.....	20
Figure 2.6. SEM images of samples obtained with different quantities of PEG 300: a) (0 mL), b) (0-1 mL), and c) (10-20 mL) .....	22
Figure 2.7. TG-DTA curves of 4ZnO·B <sub>2</sub> O <sub>3</sub> ·H <sub>2</sub> O nanorods .....	23
Figure 2.8. SEM images of zinc borate particles in the presence of different amounts of water a) 3 mL b) 0.04 mL .....	29
Figure 2.9. Schematic representation of nucleation and growth, phase transformation, and formation of single crystals steps .....	33
Figure 2.10. Schematic illustration of the possible growth mechanisms of 4ZnO·B <sub>2</sub> O <sub>3</sub> ·H <sub>2</sub> O under different initial conditions .....	34
Figure 3.1. Schematic <i>P-T</i> plane phase diagram of a pure substance.....	38
Figure 3.2. Schematic <i>P-V</i> plane phase diagram for a pure substance .....	38
Figure 3.3. Transport properties .....	40
Figure 3.4. Viscosity of carbon dioxide as function of pressure at different temperatures .....	43
Figure 3.5. Schematic diagram of solid-liquid-vapor boundary .....	47

<u>Figure</u>	<u>Page</u>
Figure 4.1. Schematic representation of reactor system: 1) High pressure reactor and surrounding heating block, 2) Split-Ring closure, 3) Thermocouple connection, 4) Pressure gage, 5) Stirrer motor and magnetic drive unit 6) Needle valve and reactor outlet connection 7) Rupture disc 8) Back pressure regulator, 9) Pressure gage, 10) Exit pipe, 11) Needle valve and vessel inlet, 12) Split-Ring closure, 13) Low pressure vessel .....	57
Figure 4.2. Photograph of reactor system .....	58
Figure 4.3. Photograph of impeller used in the stainless steel reactor .....	58
Figure 4.4. Schematic representation of supercritical CO <sub>2</sub> drying system .....	61
Figure 4.5. Schematic representation of supercritical Ethanol drying system ...	63
Figure 5.1. FTIR spectra of a) boric acid and b) zinc oxide .....	69
Figure 5.2. XRD patterns of a) boric acid, b) borax decahydrate and c) zinc oxide .....	70
Figure 5.3. SEM microphotographs of a) boric acid and b) zinc oxide .....	70
Figure 5.4. FTIR spectra of a) borax decahydrate and b) zinc nitrate hexahydrate .....	71
Figure 5.5. FTIR spectra of zinc borate produced at 70 °C (S-1) and 90 °C (S-3) using 3.0 mol.dm <sup>-3</sup> boric acid with B <sub>2</sub> O <sub>3</sub> /ZnO molar ratio of 2.0 for 5.0 h .....	75
Figure 5.6. XRD patterns of zinc borate produced at 70 °C (S-1) and 90 °C (S-3) using 3.0 mol.dm <sup>-3</sup> boric acid with B <sub>2</sub> O <sub>3</sub> /ZnO molar ratio of 2.0 for 5.0 h .....	76
Figure 5.7. Thermograms of zinc borates produced at 70 °C (S-1) and 90 °C (S-3) using 3.0 mol.dm <sup>-3</sup> boric acid with B <sub>2</sub> O <sub>3</sub> /ZnO molar ratio of 2.0 for 5.0 h .....	77
Figure 5.8. SEM microphotographs of zinc borates produced at a) 70 °C (S-1) and b) 90 °C (S-3) using 3.0 mol.dm <sup>-3</sup> boric acid with B <sub>2</sub> O <sub>3</sub> /ZnO molar ratio of 2.0 for 5.0 h .....	78
Figure 5.9. Particle size distribution of zinc borate produced at 70 °C (S-1) using 3.0 mol.dm <sup>-3</sup> boric acid with B <sub>2</sub> O <sub>3</sub> /ZnO molar ratio of 2.0 for 5.0 h, (Malvern Mastersizer 2000) .....	78

<b><u>Figure</u></b>	<b><u>Page</u></b>
Figure 5.10. Particle size distribution of zinc borate produced at 90 °C (S-3) using 3.0 mol.dm <sup>-3</sup> boric acid with B <sub>2</sub> O <sub>3</sub> /ZnO molar ratio of 2.0 for 5.0 h, (Malvern Mastersizer 2000) .....	79
Figure 5.11. FTIR spectra of zinc borates produced using 3.0 mol.dm <sup>-3</sup> (S-3) and 4.0 mol.dm <sup>-3</sup> (S-2) boric acid and zinc oxide according to the B <sub>2</sub> O <sub>3</sub> /ZnO molar ratio of 2.0 at 90 °C for 5 h .....	80
Figure 5.12. XRD patterns of zinc borates produced using 3.0 mol.dm <sup>-3</sup> (S-3) and 4.0 mol.dm <sup>-3</sup> (S-2) boric acid and zinc oxide according to the B <sub>2</sub> O <sub>3</sub> /ZnO molar ratio of 2.0 at 90 °C for 5 h .....	81
Figure 5.13. Thermograms of zinc borates produced using 3.0 mol.dm <sup>-3</sup> (S-3) and 4.0 mol.dm <sup>-3</sup> (S-2) boric acid and zinc oxide according to the B <sub>2</sub> O <sub>3</sub> /ZnO molar ratio of 2.0 at 90 °C for 5 h .....	82
Figure 5.14. SEM microphotograph of zinc borate produced at 90 °C for 5 h, B <sub>2</sub> O <sub>3</sub> /ZnO molar ratio of 2.0, a) 3.0 mol.dm <sup>-3</sup> boric acid (S-3); b) 4.0 mol.dm <sup>-3</sup> boric acid (S-2) .....	83
Figure 5.15. Particle size distribution of zinc borate produced at 90 °C (S-2) using 4.0 mol.dm <sup>-3</sup> boric acid with B <sub>2</sub> O <sub>3</sub> /ZnO molar ratio of 2.0 for 5.0 h, (Malvern Mastersizer 2000) .....	83
Figure 5.16. FTIR spectrum of zinc borate produced at 90 °C for 5 h, at B <sub>2</sub> O <sub>3</sub> /ZnO molar ratio of 2.0 and 4.7 mol.dm <sup>-3</sup> boric acid (S-4) .....	84
Figure 5.17. XRD pattern of zinc borate produced at 90 °C for 5 h, at B <sub>2</sub> O <sub>3</sub> /ZnO molar ratio of 2.0, 4.7 mol.dm <sup>-3</sup> boric acid (S-4) .....	85
Figure 5.18. Thermogram of zinc borate produced at 90 °C for 5h, at B <sub>2</sub> O <sub>3</sub> /ZnO molar ratio of 2.0 and 4.7 mol.dm <sup>-3</sup> boric acid (S-4) .....	86
Figure 5.19. SEM microphotograph of zinc borate produced at 90 °C for 5 h, at B <sub>2</sub> O <sub>3</sub> /ZnO molar ratio of 2.0 and 4.7 mol.dm <sup>-3</sup> boric acid (S-4) .....	86
Figure 5.20. Particle size distribution of zinc borate produced at 90 °C for 5 h, at B <sub>2</sub> O <sub>3</sub> /ZnO molar ratio of 2.0 and 4.7 mol.dm <sup>-3</sup> boric acid (S-4), (Malvern Mastersizer 2000) .....	87
Figure 5.21. FTIR spectrum of zinc borate produced at 90 °C for 5h, at B <sub>2</sub> O <sub>3</sub> /ZnO molar ratio of 2.0, 4.7 mol.dm <sup>-3</sup> boric acid and under sonication (S-5) .....	89

<b><u>Figure</u></b>	<b><u>Page</u></b>
Figure 5.22. XRD pattern of zinc borate produced at 90 °C for 5 h, B <sub>2</sub> O <sub>3</sub> /ZnO molar ratio of 2.0, 4.7 mol.dm <sup>-3</sup> boric acid and under sonication (S-5) .....	89
Figure 5.23. Thermogram of zinc borate produced at 90 °C for 5 h, at B <sub>2</sub> O <sub>3</sub> /ZnO molar ratio of 2.0, 4.7 mol.dm <sup>-3</sup> boric acid and under sonication (S-5) .....	90
Figure 5.24. SEM microphotographs of zinc borate produced at 90 °C for 5 h, at B <sub>2</sub> O <sub>3</sub> /ZnO molar ratio of 2.0, 4.7 mol.dm <sup>-3</sup> boric acid and under sonication (S-5) .....	91
Figure 5.25. Particle size distribution of zinc borate produced at 90 °C for 5 h, at B <sub>2</sub> O <sub>3</sub> /ZnO molar ratio of 2.0, 4.7 mol.dm <sup>-3</sup> boric acid and under sonication (S-5), (Malvern Mastersizer 2000) .....	91
Figure 5.26. FTIR spectrum of zinc borate produced at 90 °C for 5h, at B <sub>2</sub> O <sub>3</sub> /ZnO molar ratio of 2.0, 4.7 mol.dm <sup>-3</sup> boric acid, and using nano zinc oxide (S-6) .....	92
Figure 5.27. XRD pattern of zinc borate produced at 90 °C for 5 h, at B <sub>2</sub> O <sub>3</sub> /ZnO molar ratio of 2.0, 4.7 mol.dm <sup>-3</sup> boric acid and using nano zinc oxide (S-6) .....	93
Figure 5.28. Thermogram of zinc borate produced at 90 °C for 5 h, at B <sub>2</sub> O <sub>3</sub> /ZnO molar ratio of 2.0, 4.7 mol.dm <sup>-3</sup> boric acid and using nano zinc oxide (S-6) .....	93
Figure 5.29. SEM microphotographs of zinc borate produced at 90 °C for 5 h, at B <sub>2</sub> O <sub>3</sub> /ZnO molar ratio of 2.0, 4.7 mol.dm <sup>-3</sup> boric acid and using nano zinc oxide (S-6) .....	94
Figure 5.30. Particle size distribution of zinc borate produced at 90 °C for 5 h, at B <sub>2</sub> O <sub>3</sub> /ZnO molar ratio of 2.0, 4.7 mol.dm <sup>-3</sup> boric acid and using nano zinc oxide (S-6), (Malvern Mastersizer 2000) .....	94
Figure 5.31. FTIR spectrum of zinc borate produced at 90 °C for 5 h, at B <sub>2</sub> O <sub>3</sub> /ZnO molar ratio of 2.0, 4.7 mol.dm <sup>-3</sup> boric acid and using oleic acid as modifying agent and ethanol (S-7) .....	95

<b><u>Figure</u></b>	<b><u>Page</u></b>
Figure 5.32. XRD pattern of zinc borate produced at 90 °C for 5 h, at B <sub>2</sub> O <sub>3</sub> /ZnO molar ratio of 2.0, 4.7 mol.dm <sup>-3</sup> boric acid and using oleic acid as modifying agent and ethanol (S-7) .....	96
Figure 5.33. Thermogram of zinc borate produced at 90 °C for 5 h, B <sub>2</sub> O <sub>3</sub> /ZnO molar ratio of 2.0, 4.7 mol.dm <sup>-3</sup> boric acid and using oleic acid as modifying agent and ethanol (S-7) .....	96
Figure 5.34. SEM microphotographs of zinc borate produced at 90 °C for 5 h, B <sub>2</sub> O <sub>3</sub> /ZnO molar ratio of 2.0, 4.7 mol.dm <sup>-3</sup> boric acid and using oleic acid as modifying agent and ethanol (S-7) .....	97
Figure 5.35. Particle size distribution of zinc borate produced at 90 °C for 5 h, B <sub>2</sub> O <sub>3</sub> /ZnO molar ratio of 2.0, 4.7 mol.dm <sup>-3</sup> boric acid and using oleic acid as modifying agent and ethanol (S-7), (Malvern Mastersizer 2000) .....	98
Figure 5.36. Schematic structures of some borate minerals, a) frovolite, b) pinnoite and c) vimsite .....	99
Figure 5.37. IR spectra of zinc borate samples produced at 90 °C for a) 2 h (S-8), b) 3 h (S-9), c) 4h (S-10) (initially all samples were heated at 60 °C for 1.5 h) .....	104
Figure 5.38. IR spectra of zinc borate samples produced a) at 90 °C for 4 h (S-10), (initially at 60 °C for 1.5 h), b) at 90 °C for 4 h (S-11) .....	105
Figure 5.39. XRD patterns of zinc borate samples produced at 90 °C for a) 2 h (S-8), b) 3 h (S-9), c) 4 h (S-10) (initially all samples were heated at 60 °C for 1.5 h) .....	106
Figure 5.40. XRD patterns of zinc borate samples produced a) at 90 °C for 4 h (S-10), (initially at 60 °C for 1.5 h) b) at 90 °C for 4 h (S-11).....	106
Figure 5.41. Thermograms of zinc borate samples produced at 90 °C for a) 2 h (S-8), b) 3 h (S-9), c) 4 h (S-10) (initially all samples were heated at 60 °C for 1.5 h) .....	108
Figure 5.42. DSC curves of zinc borate samples produced at 90 °C for a) 2 h (S-8), b) 3 h (S-9), c) 4 h (S-10) (initially all samples were heated at 60 °C for 1.5 h) .....	108

<b><u>Figure</u></b>	<b><u>Page</u></b>
Figure 5.43. Thermograms of zinc borate samples produced a) at 90 °C for 4 h (S-10), (initially at 60 °C for 1.5 h), b) at 90 °C for 4 h (S-11).....	109
Figure 5.44. DSC curves of zinc borate samples produced a) at 90 °C for 4 h (S-10), (initially at 60 °C for 1.5 h), b) at 90 °C for 4 h (S-11) .....	109
Figure 5.45. The particle size of distributions zinc borates produced at 90 °C for a) 2 h (S-8), b) 3 h (S-9), c) 4 h (S-10) (initially all samples were heated at 60 °C for 1.5 h) and produced at only 90 °C for d) 4 h, (Sedigraph) .....	110
Figure 5.46. SEM microphotographs of zinc borates produced at 90 °C for a) 2 h (S-8), b) 3 h (S-9), c) 4 h (S-10) (initially all samples were heated at 60 °C for 1.5 h) and produced at only 90 °C for d) 4 h ....	111
Figure 5.47. SEM microphotograph of zinc borate (S-11) produced at 90 °C for 4 h .....	111
Figure 5.48. FTIR spectra of zinc borates produced from 1 mol.dm <sup>-3</sup> zinc nitrate and 1 mol.dm <sup>-3</sup> borax at 70 °C, mole ratio of borax/zinc nitrate =1.0 for reaction times a) 1 h (S-12), b) 2h (S-13), c) 3 h (S-14) ....	115
Figure 5.49. FTIR spectra of zinc borates produced from 1 mol.dm <sup>-3</sup> zinc nitrate and 1 mol.dm <sup>-3</sup> borax at 70 °C, mole ratio of borax/zinc nitrate =1.0 for reaction times a) 4 h (S-15), b) 5 h (S-16), c) 6 h (S-17), d) 16 h (S-18) .....	117
Figure 5.50. XRD patterns of zinc borates produced from 1 mol.dm <sup>-3</sup> zinc nitrate and 1 mol.dm <sup>-3</sup> borax at 70 °C, mole ratio of borax/zinc nitrate =1.0, for reaction times a) 1 h (S-12), b) 2 h (S-13) .....	118
Figure 5.51. XRD patterns of zinc borates produced from 1 mol.dm <sup>-3</sup> zinc nitrate and 1 mol.dm <sup>-3</sup> borax at 70 °C, mole ratio of borax/zinc nitrate =1.0, for reaction times a) 3 h (S-14), b) 4 h (S-15), c) 5 h (S-16) .....	118
Figure 5.52. XRD patterns of zinc borates produced from 1 mol.dm <sup>-3</sup> zinc nitrate and 1 mol.dm <sup>-3</sup> borax at 70 °C, mole ratio of borax/zinc nitrate =1.0, for reaction times a) 16 h (S-18), b) 6 h (S-17) .....	119



<b><u>Figure</u></b>	<b><u>Page</u></b>
Figure 5.53. Thermograms of zinc borates produced from 1 mol.dm <sup>-3</sup> zinc nitrate and 1 mol.dm <sup>-3</sup> borax at 70 °C, mole ratio of borax/zinc nitrate =1.0, for reaction times a) 1 h (S-12), b) 3 h (S-14) .....	120
Figure 5.54. Thermograms of zinc borates produced from 1 mol.dm <sup>-3</sup> zinc nitrate and 1 mol.dm <sup>-3</sup> borax at 70 °C, mole ratio of borax/zinc nitrate =1.0, for reaction times a) 5 h (S-16), b) 16 h (S-18) .....	121
Figure 5.55. SEM microphotographs of Zinc Borates produced from 1 mol.dm <sup>-3</sup> zinc nitrate and 1 mol.dm <sup>-3</sup> borax at 70 °C, mole ratio of borax/zinc nitrate =1.0, for reaction times a) 1h (S-12), b) 2h (S-13), c) 3h (S-14), d) 4h (S-15), (e) 5h (S-16), f) 6h (S-17) .....	122
Figure 5.56. SEM microphotograph of zinc borate produced from 1 mol.dm <sup>-3</sup> zinc nitrate and 1 mol.dm <sup>-3</sup> borax at 70 °C, mole ratio of borax/zinc nitrate =1.0, for reaction time of 16 h (S-18) .....	123
Figure 5.57. Particle size distribution of zinc borate produced from 1 mol.dm <sup>-3</sup> zinc nitrate and 1 mol.dm <sup>-3</sup> borax at 70 °C, mole ratio of borax/zinc nitrate =1.0, for reaction time of 1 h (S-12), (Malvern Mastersizer 2000) .....	124
Figure 5.58. Particle size distribution of zinc borate produced from 1 mol.dm <sup>-3</sup> zinc nitrate and 1 mol.dm <sup>-3</sup> borax at 70 °C, mole ratio of borax/zinc nitrate =1.0, for reaction time of 3 h (S-14), (Malvern Mastersizer 2000) .....	124
Figure 5.59. Particle size distribution of zinc borate produced from 1 mol.dm <sup>-3</sup> zinc nitrate and 1 mol.dm <sup>-3</sup> borax at 70 °C, mole ratio of borax/zinc nitrate =1.0, for reaction time of 5 h (S-16), (Malvern Mastersizer 2000) .....	125
Figure 5.60. FTIR spectra of zinc borates produced in a reactor for a) 4 h (S-19), b) 5 h (S-20), reaction time at 70 °C .....	127
Figure 5.61. XRD patterns of zinc borates produced in a reactor at 70 °C for a) 4 h and b) 5 h reaction time .....	129
Figure 5.62. TGA thermograms of zinc borate products obtained at the end of a) 4 h and b) 5 h reaction time at 70 °C .....	130

<b><u>Figure</u></b>	<b><u>Page</u></b>
Figure 5.63. DSC curves of zinc borate products obtained at the end of a) 4 h and b) 5h reaction time at 70 °C .....	131
Figure 5.64. SEM microphotographs of zinc borate particles produced in a reactor for reaction time of a) 4 h, b) 5 h at 70 °C .....	131
Figure 5.65. Particle size distribution of zinc borate particles produced in a reactor for reaction time of a) 4 h, b) 5 h at 70 °C, (Sedigraph) .....	132
Figure 5.66. Particle size distribution of zinc borates produced in a reactor for reaction time of a) 4 h, b) 5 h at 70 °C, (Malvern Zetasizer 3000 HSA) .....	133
Figure 5.67. FTIR spectra of zinc borate (S-4) dried a) by SC CO <sub>2</sub> for 2h and b) by conventionally at 110 °C .....	136
Figure 5.68. XRD patterns of zinc borate (S-4) dried a) by SC CO <sub>2</sub> for 2 h and b) by conventionally at 110 °C .....	136
Figure 5.69. SEM microphotographs of zinc borate (S-4) dried a) by conventionally at 110 °C, b) by SC CO <sub>2</sub> .....	137
Figure 5.70. TGA curves of zinc borate (S-4) dried a) by conventionally at 110 °C, b) dried by SC CO <sub>2</sub> for 2 h .....	138
Figure 5.71. FTIR spectra of zinc borate (S-16) dried a) by conventionally at 110°C, by SC CO <sub>2</sub> at different drying time b) 2 h, c) 3 h, d) 4 h) ...	139
Figure 5.72. XRD patterns of zinc borate (S-16) dried a) by conventionally at 110 °C, b) by supercritical CO <sub>2</sub> for 4h .....	140
Figure 5.73. SEM microphotographs of zinc borate (S-16) dried a) by conventionally at 110 °C, by SC CO <sub>2</sub> at different drying time b) 2h, c) 3h, d) 4h .....	141
Figure 5.74. TGA thermograms of zinc borate (S-16) dried a) by conventionally at 110 °C, b) dried by SC CO <sub>2</sub> for 4 h .....	142
Figure 5.75. TGA thermograms of zinc borate (S-16) dried by Supercritical CO <sub>2</sub> for c) 2h, and d) 3h .....	143
Figure 5.76. DSC curves of zinc borate (S-16) dried a) by conventionally at 110 °C, b) dried by SC CO <sub>2</sub> for 4 h .....	143
Figure 5.77. Pressure-temperature relation of ethanol in closed reactor .....	147

<u>Figure</u>	<u>Page</u>
Figure 5.78. The change of temperature and pressure with time in closed reactor	147
Figure 5.79. SEM microphotographs of zinc borate sample (S-4) that were produced from boric acid and zinc oxide at 90 °C and with B <sub>2</sub> O <sub>3</sub> /ZnO molar ratio of 2.0 a) and b) before supercritical drying c) and d) after supercritical drying (ZnB1-SCE) .....	149
Figure 5.80. TEM microphotographs of zinc borate sample (ZnB1-SCE) that were produced from boric acid and zinc oxide at 90 °C and with B <sub>2</sub> O <sub>3</sub> /ZnO molar ratio of 2.0, and dried by supercritical ethanol drying a) 50 nm b)100 nm .....	150
Figure 5.81. FTIR Spectrum of Zinc Borate after Supercritical Drying (ZnB1-SCE) .....	151
Figure 5.82. FTIR spectrum of white powder obtained from ethanol phase .....	152
Figure 5.83. XRD pattern of supercritical ethanol dried zinc borate (ZnB1-SCE) .....	153
Figure 5.84. TGA thermogram of supercritical ethanol dried zinc borate (ZnB1-SCE) .....	154
Figure 5.85. SEM microphotographs of a) commercial product, zinc borates dried by removing ethanol at b) 150 °C (ZnB4-SCE), c) 200 °C (ZnB5-SCE) .....	155
Figure 5.86. Particle size distribution of zinc borate dried by removing ethanol at 200 °C (ZnB5-SCE), (Malvern Zetasizer 3000 HSA) .....	156
Figure 5.87. FTIR spectra of zinc borates dried by removing ethanol at a) 150 °C (ZnB4-SCE), b)200 °C (ZnB5-SCE) .....	157
Figure 5.88. XRD patterns of zinc borates dried by removing ethanol at a) 150 °C (ZnB4-SCE) b) 200 °C (ZnB5-SCE) .....	157
Figure 5.89. SEM microphotographs of supercritical ethanol dried zinc borate (ZnB6-SCE) that were produced from 1.0 mol.dm <sup>-3</sup> borax decahydrate and 1 mol.dm <sup>-3</sup> zinc nitrate hexahydrate at 70 °C for 5 h a) 20.000x, b) 50.000x .....	158

<b><u>Figure</u></b>	<b><u>Page</u></b>
Figure 5.90. TEM microphotographs of supercritical ethanol dried zinc borate (ZnB6-SCE) that were produced from 1.0 mol.dm <sup>-3</sup> Borax decahydrate and 1.0 mol.dm <sup>-3</sup> zinc nitrate hexahydrate at 70 °C for 5 h a) 50 nm, b)100 nm .....	159
Figure 5.91. Particle size distribution of zinc borate that was produced from 1.0 mol.dm <sup>-3</sup> borax decahydrate and 1.0 mol.dm <sup>-3</sup> zinc nitrate hexahydrate at 70 °C for 5 h and conventional dried, (Malvern Mastersizer 2000) .....	159
Figure 5.92. Particle size distribution of zinc borate (ZnB6-SCE) that was produced from 1.0 mol.dm <sup>-3</sup> borax decahydrate and 1.0 mol.dm <sup>-3</sup> zinc nitrate hexahydrate at 70 °C for 5 h, and supercritical ethanol dried, (Malvern Mastersizer 2000) .....	160
Figure 5.93. FTIR spectrum of supercritical ethanol dried zinc borate (ZnB6-SCE) .....	161
Figure 5.94. FTIR spectrum of white powder obtained from ethanol phase .....	162
Figure 5.95. XRD pattern of supercritical ethanol dried zinc borate (ZnB6-SCE) .....	163
Figure 5.96. TGA thermogram of supercritical ethanol dried zinc borate (ZnB6-SCE) .....	164
Figure 5.97. Streams in supercritical ethanol drying system .....	166
Figure 5.98. Nitrogen adsorption isotherms of zinc borate after supercritical ethanol drying (ZnB3-SCE) .....	170
Figure 5.99. Nitrogen adsorption isotherms of zinc borate after supercritical ethanol drying (ZnB7-SCE) .....	170
Figure 5.100. FTIR spectrum of freeze dried zinc borate produced from borax and zinc nitrate (S-21) .....	172
Figure 5.101. XRD pattern of freeze dried zinc borate produced from borax and zinc nitrate (S-21) .....	173
Figure 5.102. TG thermogram of freeze dried zinc borate produced from borax and zinc nitrate (S-21) .....	173
Figure 5.103. SEM microphotographs of freeze dried zinc borate produced from borax and zinc nitrate (S-21) a) 50000x, and b) 35000x .....	174

<b><u>Figure</u></b>	<b><u>Page</u></b>
Figure 5.104. Number-weighted nicomp distribution of freeze dried zinc borate particles (S-21) .....	175
Figure 5.105. FTIR spectrum of freeze dried zinc borate produced from borax and zinc nitrate (S-22) .....	176
Figure 5.106. TGA thermogram of freeze dried zinc borate produced from borax and zinc nitrate (S-22) .....	176
Figure 5.107. SEM microphotographs of freeze dried zinc borate produced from borax and zinc nitrate (S-22) a) 12000x, and b) 50000x .....	177

## LIST OF TABLES

<b><u>Table</u></b>	<b><u>Page</u></b>
Table 2.1. Boron minerals .....	5
Table 2.2. Reserves and resources of boron minerals, 2005 (1000t gross weight) .....	6
Table 2.3. Borate anions and their structures .....	6
Table 2.4. Vibrational bands of hydrated polyborate anions .....	12
Table 2.5. Thermal behaviors of zinc borates .....	14
Table 2.6. Zinc borate functions and applications in polymers .....	15
Table 2.7. XRD data of zinc borate species .....	28
Table 2.8. Studies related with zinc borate production .....	31
Table 3.1. Properties of some supercritical fluids .....	40
Table 3.2. Specific surface area (SSA), porosity and bulk density of Pd-supported alumina aerogels after firing at 1200 °C for 5 h .....	50
Table 3.3. Supercritical fluid drying studies .....	52
Table 4.1. Technical grade, granular, low sulphate boric acid, H <sub>3</sub> BO <sub>3</sub> , chemical analysis .....	54
Table 4.2. Technical grade granular borax decahydrate, Na <sub>2</sub> B <sub>4</sub> O <sub>7</sub> ·10H <sub>2</sub> O, chemical analysis .....	55
Table 4.3. Experimental conditions of reaction between zinc oxide and boric acid in a magnetically stirred glass reactor .....	59
Table 4.4. Experimental conditions of reaction between zinc oxide and boric acid in a mechanically stirred stainless steel reactor .....	59
Table 4.5. Experimental conditions of reaction between borax decahydrate and zinc nitrate hexahydrate .....	60
Table 4.6. Supercritical carbon dioxide drying conditions .....	62
Table 4.7. Supercritical and subcritical ethanol drying conditions .....	63

<b><u>Table</u></b>	<b><u>Page</u></b>
Table 5.1. Major peaks in FTIR spectrum of boric acid .....	69
Table 5.2. XRD data of zinc borate, $ZnO \cdot B_2O_3 \cdot 2H_2O$ .....	76
Table 5.3. ZnO, $B_2O_3$ , $H_2O$ contents, dehydration onset temperature and particle morphology of zinc borate samples .....	101
Table 5.4. Observed frequencies of IR spectra of $2ZnO \cdot 3B_2O_3 \cdot 3H_2O$ and $2ZnO \cdot 3B_2O_3 \cdot 7H_2O$ .....	104
Table 5.5. Dehydration behavior of zinc borates produced at 90 °C for 2 h, 3 h, 4 h (initially samples were heated at 60 °C for 1.5 h) and produced at only 90 °C for 4 h .....	110
Table 5.6. $B(OH)_3$ content, and $B_2O_3/ZnO$ molar ratio and density of solid phase of zinc borates produced at 90 °C for 2 h, 3 h, 4 h (initially samples were heated at 60 °C for 1.5 h) and produced at only 90 °C for 4 h .....	112
Table 5.7. ZnO, $B_2O_3$ , $H_2O$ contents, dehydration onset temperature and particle morphology of samples .....	128
Table 5.8. Composition of the samples .....	135
Table 5.9. Thermal behavior of zinc borate samples .....	144
Table 5.10. Observed peaks in IR spectrum of white powder obtained from ethanol .....	152
Table 5.11. Mass and density of samples obtained from supercritical and subcritical ethanol drying of zinc borates .....	167
Table 5.12. Composition of products: powder remained in reactor and product dissolved ethanol .....	168
Table 5.13. ZnO, $B_2O_3$ , and $H_2O$ contents, dehydration onset temperature and particle morphology of freeze dried zinc borates .....	174
Table 5.14. Analyses of mother liquids in zinc borate production from borax-zinc nitrate and boric acid-zinc oxide pairs .....	178

# CHAPTER 1

## INTRODUCTION

Boron compounds have been increasingly used in a wide range of industries including glass, ceramic, paper, detergent, plastic, textile, metal, pesticide, and nuclear for various purposes. Generally, the number of boron compounds that utilized in industry is in the form of boron oxygen compounds, such as alkaline, alkaline-earth and transition metal hydrated borates. Although some of these compounds occur naturally on the earth's crust, most of them are produced synthetically using chemicals that are obtained from mineral deposits of tincal, ulexite, kernite, colemanite with a suitable metal source. On this point, Turkey has substantial mineral reserve of boron and holding approximately a 72 % share of the total boron deposits in the world (Kar et al., 2006). Eti Maden, state-owned company and unique producer, possesses 31 % of total world production on  $B_2O_3$  basis. The most important boron minerals that Turkey owns are tincal, colemanite, and ulexite. While a small amount of its boron compounds is used domestically, a great amount is exported. Turkey's total income from boron export was pointed as 295 million US\$ for the year 2005 (Kar et al., 2006). In order to increase the income from boron products, Turkey should find the ways of converting raw materials of boron into high value boron products by finding novel application areas and searching a market for those new products.

Boron atom coordinates with oxygen atom in various ways, such as trigonal planar ( $BO_3$ ) and tetrahedral ( $BO_4$ ) structural units thus, there is considerable number of boron compounds containing also B-OH groups (hydroxyl hydrated borates) and they may also contain interstitial water (Schubert et al., 2003). Metal borates, which occur either naturally or produced synthetically, can be classified into two main groups, hydrated and anhydrous borates. Hydrated borates, which comprise the majority of known boron containing minerals and synthetic borates are formed by the reaction of metal cation and borate anion. There are more than one hundred borate minerals and many synthetic borates cited in literature today (Schubert, 2003). One of the industrially



important borate compounds, zinc borate, is an important member of synthetic hydrated metal borates. The industrial importance of the zinc borates has increased substantially in recent years as new zinc borate species were synthesized and utilized by industry. There have been at least seven unique crystalline forms of hydrated zinc borate that have been known since they found an industrial use. Each of which can be prepared selectively using either borax and soluble zinc salt or boric acid and zinc oxide. They are used traditionally in ceramic industry for increasing green body strength, decreasing firing time, temperature and pyroplastic deformation. They are also used in paint industry to act as a corrosion inhibitor, fire retardant, preservative and tannin-stain blocker (Nies and Hulbert, 1970; Schubert et al., 2003). Recently, the use of zinc borates in a few industry branches for instance, plastic and lubricant, has grown considerably with parallel to the synthesis of novel zinc borate kinds and nanosized products.

One of the novel application areas of boron compounds is lubricating oil additives (Erdemir, 2000). Lubricating oil additives generally include organic or organometallic compounds bearing polar groups. Zinc borate is proposed as a candidate additive for lubricant as it contains both zinc and boron atoms in its structure. The preparation of zinc borate with a particle size of 20–50 nm was studied using ethanol supercritical fluid drying technique (Dong and Hu, 1998). In most of its applications, particle size of additive plays a crucial role to reveal its own performance. In the synthesis of zinc borates with different morphologies and chemical compositions, novel methods were proposed and used (Shi et al., 2008 and Tian et al., 2008).

Supercritical fluid processing is an alternative technique for the formation of nanomaterials. This novel material processing technique is used in areas ranging from materials drying, natural products extraction, chemical reactions, sample preparation, particle design, and environmental remediation. The mostly used fluids are carbon dioxide, ethanol, methanol and iso-propanol. There are several studies regarding to the formation of metal borate in nanosize. Supercritical fluid drying technique was used in the formation of nanosized zinc, copper, magnesium borates (Dong and Hu, 1998; Hu et al., 1999 and Hu et al., 1998). In those studies, the detailed characterization of the products before and after supercritical drying was not performed and possible interactions between supercritical solvent and metal borates were not considered. Metal borate species might have undergone a chemical change due to either high pressure or high temperature or both during supercritical fluid drying.

This study has two principal goals. The former one is to determine the parameters for the production of nanosized zinc borate using different boron sources, such as boric acid and borax decahydrate with zinc oxide and soluble zinc salt, respectively. The effects of using nano zinc oxide, sonication and oleic acid as a modifying agent in the reaction of boric acid and zinc oxide were also examined. The latter one is to examine the effects of supercritical fluid drying and freeze drying on the morphological and chemical changes of zinc borate species. Thus, zinc borate samples prepared from different raw materials were dried using supercritical carbon dioxide drying and supercritical ethanol drying and freeze drying to obtain nanosized zinc borates.

In Chapter 2, boron minerals and important producers in the world were introduced. Hydrated metal borates and recent studies related to zinc borate production and their applications in the literature were reviewed. Chapter 3 summarizes supercritical fluid phenomenon, supercritical fluids' unique properties based on their industrial applications and especially, supercritical fluid drying process was discussed. Chapter 4 describes the materials used in the production of zinc borate samples, experimental procedure of synthesis and supercritical fluid drying and freeze drying processes, and characterization methods to analyse the zinc borate species. Chapter 5 includes results of zinc borate production from “boric acid-zinc oxide” and “borax decahydrate-zinc nitrate hexahydrate” pairs and supercritical fluid drying and freeze drying results of those products regarding to the literature data.

## CHAPTER 2

### BORON, BORATE COMPOUNDS AND ZINC BORATE

Boron is an important metalloid whose atomic mass and number are 10.81 and 5, respectively. There are two stable boron isotopes,  $^{10}\text{B}$  and  $^{11}\text{B}$ , which are naturally present at 19.10-20.31 % and 79.69-80.90 %, respectively. Boron has electronic structure  $1s^2 2s^2 2p^1$  and an expected valence of three. Because of the high ionization energies, there is no formation of univalent compounds as for the other Group IIIA elements. Boron forms planar tricovalent compounds,  $\text{BX}_3$ , X=halides, alkyls, etc., having the expected  $120^\circ$  bonding angles. The empty p orbital makes these compounds electron-pair acceptors or *Lewis acid*. Alkyls and halides of aluminum dimerize to make up for the deficiency of electrons, but the boron atom is too small to coordinate strongly. Boron also has a high affinity for oxygen-forming borates, polyborates, borosilicates, peroxoborates, etc.

In nature, boron is an abundant mineral with combination of oxygen and various alkaline and alkaline earth metals e.g., Na, Ca and Mg. The mostly encountered borate minerals are listed in Table 2.1. In those minerals, the primary structural units are trigonal planar ( $\text{BO}_3$ ) and tetrahedral ( $\text{BO}_4$ ) and they may exist as isolated anions, connect each other by sharing oxygen to form rings and cages, or form finite clusters, infinite chains, sheets, and frameworks.

Boric acid (sassolite), borax (tincal), kernite, colemanite, ulexite, probertite, hydroboracite, datolite, and szaibelyite (ascharite) are the boron minerals which have commercial importance. Borax and colemanite are the most important compounds among them. Borate production comes mostly from seven countries: the United States, Turkey, Russia, Iran, Argentina, China, and Peru. Boron reserves of these countries are disclosed in Table 2.2.

The amount of  $\text{B}_2\text{O}_3$  that was consumed in the form of various borate products was estimated as  $1.25 \times 10^6$  metric tons. Figure 2.1 shows the approximate proportions of

boron consumed by different large industries. In these areas, boron compounds are used in the manufacture of various types of vitreous materials, particularly fiberglass, ceramic glazes, and specialty borosilicate glasses that consumed the more than half of the all boron consumption by industry. The other uses of borates in laundry detergents, fertilizers, timber protection, fire retardant in polymers, cleaning products are also important.

Table 2.1. Boron minerals  
(Source: Roskill, 2006)

<b>Type</b>	<b>Mineral</b>	<b>Composition</b>	<b>B<sub>2</sub>O<sub>3</sub> weight percentage</b>
Hydrogen borates	Sassolite (natural boric acid)	H <sub>3</sub> BO <sub>3</sub>	56.3
Sodium borates	Tincal	Na <sub>2</sub> B <sub>4</sub> O <sub>7</sub> ·10H <sub>2</sub> O	36.5
	Tincalconite (mohavite)	Na <sub>2</sub> B <sub>4</sub> O <sub>7</sub> ·5H <sub>2</sub> O	47.8
	Kernite (rasorite)	Na <sub>2</sub> B <sub>4</sub> O <sub>7</sub> ·4H <sub>2</sub> O	51.0
Sodium-calcium borates	Ulexite (boronatrocaltite)	NaCaB <sub>5</sub> O <sub>9</sub> ·8H <sub>2</sub> O	43.0
	Probertite (kramerite)	NaCaB <sub>3</sub> O <sub>9</sub> ·5H <sub>2</sub> O	49.6
Calcium borates	Colemanite	Ca <sub>2</sub> B <sub>6</sub> O <sub>11</sub> ·5H <sub>2</sub> O	50.8
	Priceite (pandermite)	CaB <sub>10</sub> O <sub>19</sub> ·7H <sub>2</sub> O	49.8
Calcium borosilicates	Datolite	CaBSiO <sub>4</sub> OH	24.9
Magnesium borates	Hydroboracite	CaMgB <sub>6</sub> O <sub>11</sub> ·6H <sub>2</sub> O	50.5
	Szaibelyite (ascharite)	MgBO <sub>2</sub> OH	41.4
	Boracite (stassfurite)	Mg <sub>3</sub> B <sub>7</sub> O <sub>13</sub> Cl	62.2

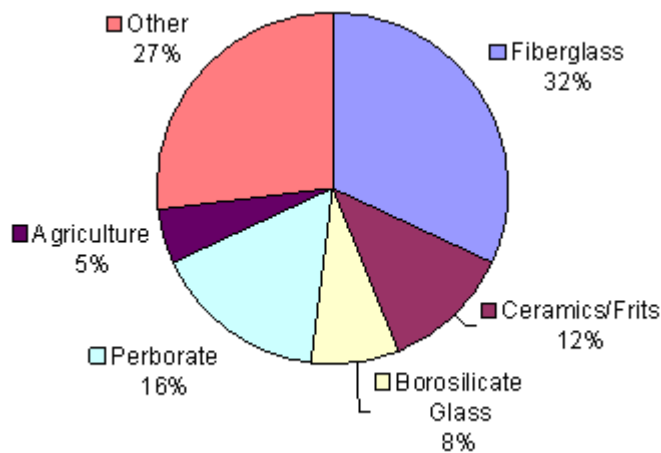


Figure 2.1. Estimated total borate use by major industrial applications in B<sub>2</sub>O<sub>3</sub> equivalents for the year 2001 (Source: Schubert, 2003).

Borate compounds show an ionic character as they contain a boron oxoanion, such as the metaborate anion [B(OH)<sub>4</sub>]<sup>-</sup> in combination with cationic species, such as

Na<sup>+</sup>. For instance, sodium metaborate is Na<sup>+</sup>[B(OH)<sub>4</sub>]<sup>-</sup>, also represented as Na<sub>2</sub>B<sub>2</sub>O<sub>4</sub>·4H<sub>2</sub>O or resolved oxide, NaO·B<sub>2</sub>O<sub>3</sub>·4H<sub>2</sub>O (Schubert, 2005). Table 2.3 lists a number of well known borate anions, including the structural formula and resolved oxide formula for the corresponding compounds formed in combination with monovalent cations (represented by M<sup>+</sup>).

Table 2.2. Reserves and resources of boron minerals, 2005 (1000 t gross weight)  
(Source: Roskill, 2006)

<u>Country</u>	<u>Reserves</u>	<u>Reserve base</u>
Argentina	2,000	9,000
China	25,000	47,000
Iran	1,000	1,000
Peru	4,000	22,000
Russia	40,000	100,000
Turkey	60,000	150,000
USA	40,000	80,000
<b>Total</b>	<b>170,000</b>	<b>410,000</b>

Table 2.3. Borate anions and their structures  
(Source: Schubert, 2005)

<b>Boron Oxoanion</b>	<b>Common Name</b>	<b>Structural Formula Bearing Metal Cation, M<sup>+</sup></b>	<b>Resolved Oxide Formula</b>
[B(OH) <sub>4</sub> ] <sup>-</sup>	metaborate	M[B(OH) <sub>4</sub> ]	M <sub>2</sub> O·B <sub>2</sub> O <sub>3</sub> ·4H <sub>2</sub> O
[B <sub>4</sub> O <sub>5</sub> (OH) <sub>4</sub> ] <sup>2-</sup>	tetraborate	M <sub>2</sub> [B <sub>4</sub> O <sub>5</sub> (OH) <sub>4</sub> ]	M <sub>2</sub> O·2B <sub>2</sub> O <sub>3</sub> ·4H <sub>2</sub> O
[B <sub>5</sub> O <sub>6</sub> (OH) <sub>4</sub> ] <sup>-</sup>	pentaborate	M[B <sub>5</sub> O <sub>6</sub> (OH) <sub>4</sub> ]	M <sub>2</sub> O·5B <sub>2</sub> O <sub>3</sub> ·4H <sub>2</sub> O
[B <sub>3</sub> O <sub>3</sub> (OH) <sub>4</sub> ] <sup>-</sup>	triborate	M[B <sub>3</sub> O <sub>3</sub> (OH) <sub>4</sub> ]	M <sub>2</sub> O·3B <sub>2</sub> O <sub>3</sub> ·4H <sub>2</sub> O
[B <sub>3</sub> O <sub>3</sub> (OH) <sub>5</sub> ] <sup>2-</sup>	triborate	M <sub>2</sub> [B <sub>3</sub> O <sub>3</sub> (OH) <sub>5</sub> ]	2M <sub>2</sub> O·3B <sub>2</sub> O <sub>3</sub> ·5H <sub>2</sub> O
[B <sub>6</sub> O <sub>7</sub> (OH) <sub>6</sub> ] <sup>2-</sup>	hexaborate	M <sub>2</sub> [B <sub>6</sub> O <sub>7</sub> (OH) <sub>6</sub> ]	M <sub>2</sub> O·3B <sub>2</sub> O <sub>3</sub> ·3H <sub>2</sub> O

Chemical structures of these oxoanions are different from each other. For example, the metaborate anion has a tetrahedral form, while the tetraborate anion is a bridged eight member B-O ring, the triborate anion is a six member B-O ring (referred as a boroxyl ring), the pentaborate anion consists of two six-member B-O ring sharing a common boron atom and the hexaborate anion consists of three B-O rings that share three boron atoms and one oxygen atom. Schematic representations of these structures are given in Figure 2.2.

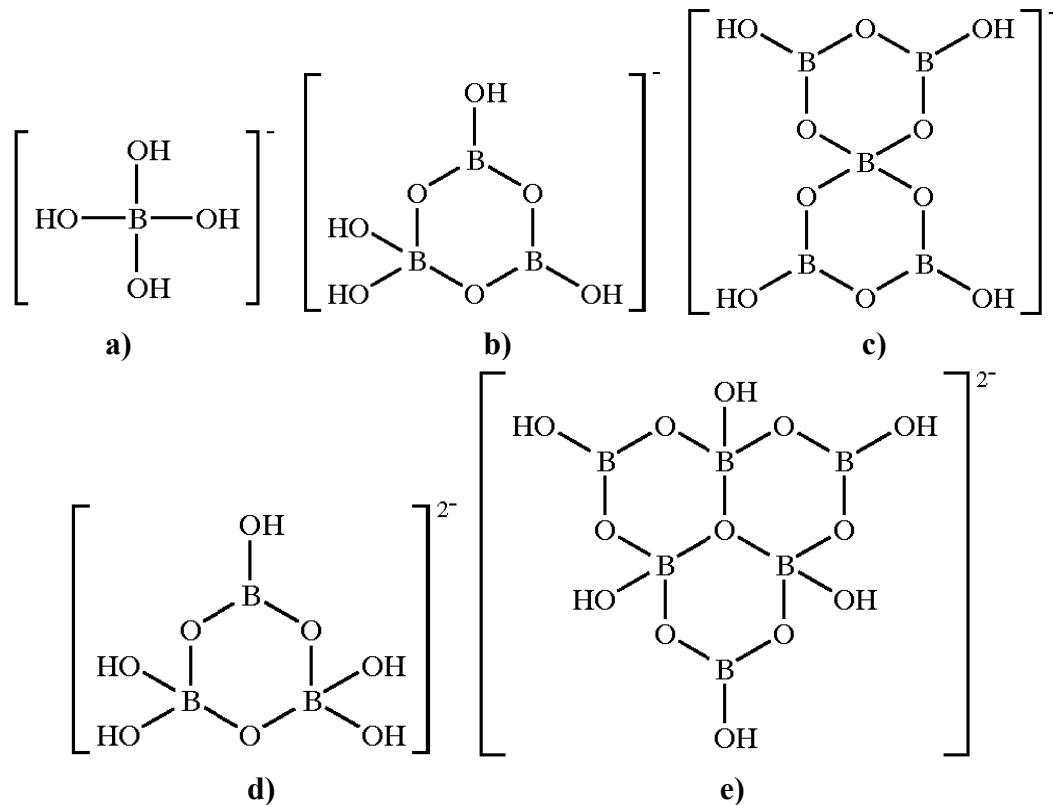


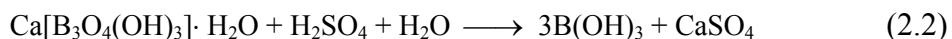
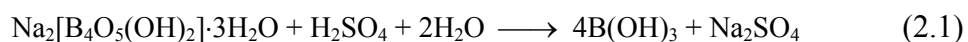
Figure 2.2. Schematic representation of borate oxoanions a)  $[B(OH)_4]^-$ , b)  $[B_3O_3(OH)_4]^-$ , c)  $[B_5O_6(OH)_4]^-$ , d)  $[B_3O_3(OH)_5]^{2-}$ , e)  $[B_6O_7(OH)_6]^{2-}$  ( Source: Schubert, 2005).

In the formation of natural minerals and synthetic borate compounds, these boron oxoanions are either isolated (finite), e.g. connected to adjacent boron oxoanions only by hydrogen bonds and not by oxygen bridges, or alternatively they are directly interconnected through boron-oxygen bonding into infinite chains, sheets or three dimensional frame work structures. Borate minerals and synthetic compounds made up of isolated boron oxoanions containing from one to six boron atoms are quite common (Schubert, 2005).

## 2.1. Boric Acid and Borax Decahydrate

Boric acid, which is commercially an important synthetic reagent, is also known as a orthoboric acid,  $B(OH)_3$ , in literature and it is found naturally as the mineral “Sassolite”. It can be prepared from the reaction of natural borate minerals, such as

kernite or colemanite with mineral acids as indicated in Equations 2.1 and 2.2 (Schubert, 2003).



Orthoboric acid crystallizes from aqueous solution as white, waxy plate that is triclinic. Although boric acid has a melting point (m.p.) of 170.9 °C, when heated slowly it begins to lose some water and forms metaboric acid, HBO<sub>2</sub>, which may exist in one of the three different crystal modifications. Orthorhombic HBO<sub>2</sub>-III or α-form (d= 1.784 g/mL, m.p.= 176 °C) forms first around 130 °C and gradually changes to monoclinic HBO<sub>2</sub>-II or β-form (d= 2.045 g/mL, m.p.= 200.9 °C). At temperatures above 150 °C, dehydration continues to yield viscous liquid phases beyond the metaboric acid composition. The most stable form of metaboric acid, cubic HBO<sub>2</sub>-I or γ-form (d= 2.49 g/mL, mp= 236 °C) crystallizes slowly when mixtures of boric acid and HBO<sub>2</sub>-III are melted in an evacuated, sealed glass bulb and held at 180 °C for several weeks (Briggs, 2001).

The heat of hydration of vitreous boric oxide to crystalline orthoboric acid is -9130 ±39 cal./mole of boric acid and the heat of solution of boric acid to form a 0.05 M solution is -5166 ±39 cal./mole (Adams, 1964). The solubility of boric acid and borax decahydrate in water are shown in Figure 2.3 and solubility of both compounds increase with temperature gradually. The solubility curve of borax decahydrate intersects with the solubility curves of penta-hydrate and tetra-hydrate at 60 °C and 58 °C, respectively. When borax decahydrate is added into saturated solution at above those temperatures, it dissolves with crystallization of penta-hydrate or tetra-hydrate.

The presence of inorganic salts may enhance or depress the aqueous solubility of boric acid: it is increased by potassium chloride as well as by potassium or sodium sulfate but decreased by lithium and sodium chlorides (Briggs, 2001). This is an interesting phenomenon which is used in the preparation of disodium octaborate using a certain amounts of borax and boric acid. Disodium octaborate, which is widely used synthetic product with high boron content, is also known as “Polybor” in the industry.

The highly concentrated aqueous solution of sodium borate was prepared at 20 °C by adjusting the Na/B ratio at 0.22 (pH 6.9) using boric acid (Tsuyumoto et al., 2007).

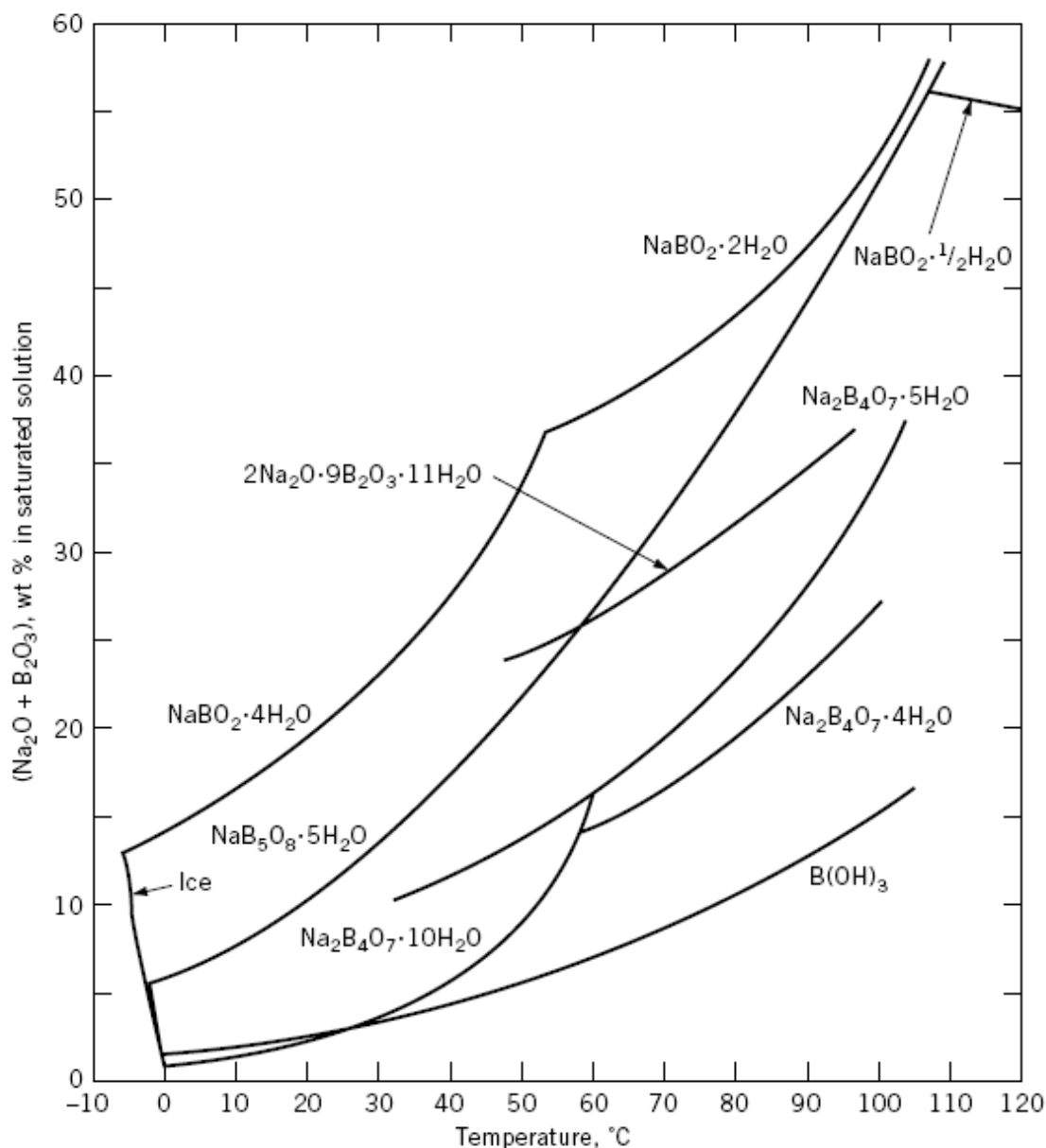


Figure 2.3. Solubility-temperature curves for boric acid, borax, sodium pentaborate, and sodium metaborate (Source: Briggs, 2001).

From the analyses results of Raman Spectroscopy and APCI/MS (atmospheric pressure chemical ionization/mass spectrometry) the presence of polyborate ions of B<sub>9</sub>O<sub>10</sub>(OH)<sub>9</sub><sup>2-</sup>, B<sub>10</sub>O<sub>12</sub>(OH)<sub>8</sub><sup>2-</sup>, B<sub>11</sub>O<sub>14</sub>(OH)<sub>7</sub><sup>2-</sup>, and B<sub>12</sub>O<sub>16</sub>(OH)<sub>6</sub><sup>2-</sup> was determined. The optimum Na/B ratio for the most concentrated sodium borate solution was determined between 0.22 and 0.27, at pH values between 6.9 and 6.5.



Another important issue regarding to the properties of boric acid is that appreciable losses of boric acid occur when aqueous solutions are concentrated by evaporation. Vapor pressure and standard enthalpy of sublimation for solid boric acid was measured using horizontal thermal analysis equipment to which transpiration apparatus adapted in the temperature range of 326-363 K (Pankajavalli et al., 2007). The temperature dependence of the measured values of vapor pressures is expressed as following:

$$\log(P/\text{Pa}) = 26.83(\pm 0.09) - 9094(\pm 246)/T \text{ (K)} \quad (2.3)$$

The standard enthalpy of sublimation,  $\Delta H_{\text{sub}}^{\circ}$ , of  $\text{H}_3\text{BO}_3$  was estimated to be  $174.1 \pm 4.7 \text{ kJ mol}^{-1}$  at the mean temperature of the present measurements, 345 K (Pankajavalli et al., 2007).

The existence of several important polyborate anions, whose salts have been in the structure of many natural and synthetic solid borates and in solution, was determined and explored by Attina and co-workers (1992). Generally, in the determination of boric acid vapor concentration by mass spectroscopy, low temperature sublimation techniques were used. Instead of using sublimation technique, researcher formed polyborate anions in the gas phase by the stepwise addition of  $\text{H}_3\text{BO}_3$  to the  $\text{H}_2\text{BO}_2^-$  anion that was obtained in turn via dissociative electron attachment or by a suitable ion-molecule reaction from gaseous boric acid. Borate anions were detected using Ion cyclotron resonance (ICR) Mass spectrometer and chemical ionization (CI) mass spectrometer. They also found that the character of the  $\text{H}_3\text{BO}_3$  changes in passing from solution to gas phase.

In most of the cases, excessively used boron compounds remain in the aqueous phase and it must be determined quantitatively for checking the experimental accuracy. Boric acid/borate reacts with chemical compounds containing multiple hydroxyl groups (polyols), such as mannitol (Figure 2.4), forming anionic complexes at the neutral pH of water (Geffen et al., 2006).

The borate esters are formed and dissociated spontaneously in a variety of pH dependent equilibrium. Since the acidic protons are released during the complexation, there is simultaneous decrease of pH that leads to reverse the reaction. Thus, in order to maintain stable complexes, decrease in pH should be prevented. The amount of acidification produced upon the addition of polyol is proportional to the extent of borate

esters. Boric acid produces complex with mannitol according to the following equation (Equation 2.4).

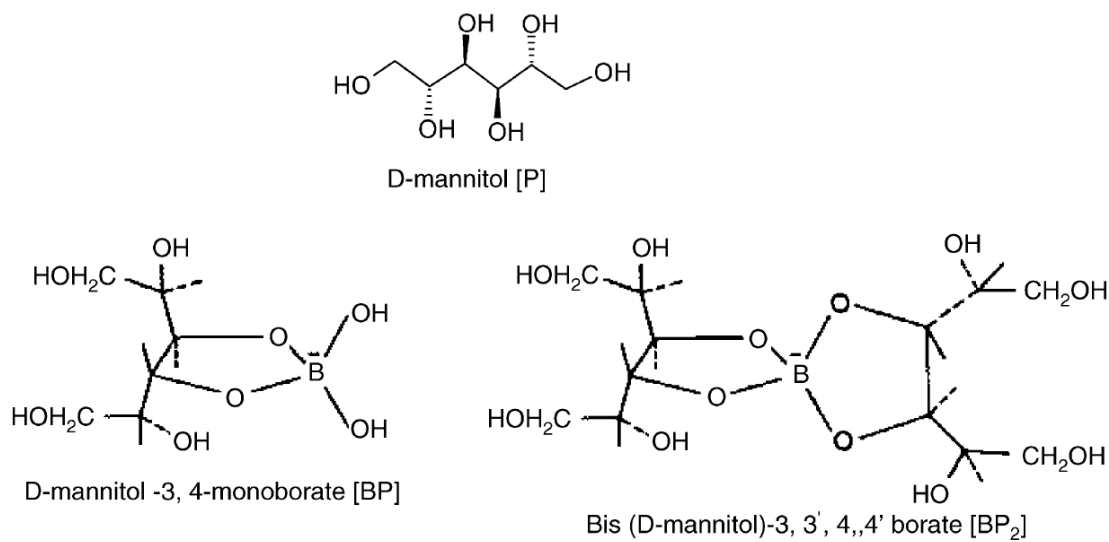
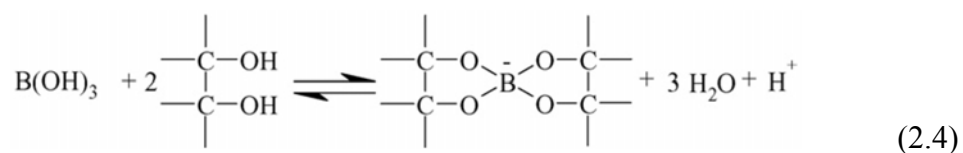


Figure 2.4. Schematic drawings of mannitol and negatively charged borate mannitol complexes (Source: Geffen et al., 2006).

## 2.2. Metal Borates

Crystalline metal borates are made of boron, oxygen, metal and hydrogen atoms. They may contain water molecules as a crystal form and/or hydroxyl groups and in some cases non-borate anions, such as  $\text{Cl}^-$ ,  $(\text{SO}_4)^{2-}$  depending on the metal salt used in the reaction (Waclawska, 1998). They can be found in nature abundantly or they are manufactured synthetically. Borax (sodium borate decahydrate) and colemanite (calcium borate pentahydrate) are two important natural minerals that are utilized in the synthesis of other metal borates, such as zinc, magnesium, copper. The synthetic metal borates and crystalline minerals exhibit considerable structural variety and complexity. Trihedral and tetrahedral boron oxygen structures form fundamental building blocks in crystalline metal borates. Despite the apparent simplicity of these fundamental blocks,

borate structures are usually quite complex. These units may exist as isolated anions as shown in Figure 2.2. Polymerization of these borate anions by elimination of water result in chain formation, furthermore, it gives sheets or three dimensional networks. In addition, borate anions interact with metal cations in complex ways and often display extensive hydrogen bonding integrating their structures (Schubert, 2003).

Jun and co-workers studied and recorded FT-IR and Raman spectra of 27 hydrated borates (Jun et al., 1995). FT-IR and Raman response of chemical structures of these 27 hydrated borates can be grouped according to the configuration of units in the main structure. Table 2.4 shows these distinguished structures in the hydrated borates. The bands of symmetric pulse vibration of the corresponding polyborate anions were also indicated.

Table 2.4. Vibrational bands of hydrated polyborate anions  
(Source: Jun et al., 1995)

<b>Bands (cm<sup>-1</sup>)</b>	<b>Assignment</b>
3600-3300 (IR, Raman)	O-H stretching
2900-2200 (IR)	O-H stretching because of hydrogen bond
1700-1600 (IR)	H-O-H bending (lattice, interstitial water)
1450-1300 (IR)	Asymmetric stretching of B <sub>3</sub> -O
1300-1150 (IR)	In plane bending of B-O-H
1150-1000 (IR, Raman)	Asymmetric stretching of B <sub>4</sub> -O
960-890 (IR, Raman)	Symmetric stretching of B <sub>3</sub> -O
890-740 (IR, Raman)	Symmetric stretching of B <sub>4</sub> -O
750-620 (IR)	Out of plane bending of B <sub>3</sub> -O
650-610 (IR, Raman)	Symmetric pulse vibration of triborate anion and hexaborate anion
590-540 (IR, Raman)	Symmetric pulse vibration of tetraborate anion
560-530 (IR, Raman)	Symmetric pulse vibration of pentaborate anion
590-510 (IR)	Bending of B <sub>3</sub> -O and B <sub>4</sub> -O
500-380 (IR, Raman)	Bending of B <sub>4</sub> -O

IR and Raman represent IR active and Raman active, respectively.

The difficulties in obtaining the vibrational spectroscopy of hydrated borates can be summarized as following:

- The ability of boron atom to coordinate to three and four oxygen atoms enables a wide range of theoretical structural entities to be formulated. Polymerization

by elimination of a water molecule between two hydrated units results in chain formation furthermore; it gives sheets, or networks.

- The bands of O-H deformation modes in hydrated polyborate anions always overlap with the bands of stretching and bending modes of B-O. It is difficult to distinguish these vibration modes.
- Normal coordinate analysis of the spectra of hydrated borates is often impossible as no information is available about the point group of isolated molecule, the site group of hydrated borates, as well as the vibrational units being large molecules with low symmetry (Jun et al., 1995).

### 2.3. Zinc Borates

Zinc borate is a synthetic hydrated metal borate. There are various kinds of crystalline hydrated zinc borates. These have compositions  $\text{ZnO}\cdot\text{B}_2\text{O}_3\cdot 1.12\text{H}_2\text{O}$ ,  $\text{ZnO}\cdot\text{B}_2\text{O}_3\cdot 2\text{H}_2\text{O}$ ,  $6\text{ZnO}\cdot 5\text{B}_2\text{O}_3\cdot 3\text{H}_2\text{O}$ ,  $2\text{ZnO}\cdot 3\text{B}_2\text{O}_3\cdot 7\text{H}_2\text{O}$ ,  $2\text{ZnO}\cdot 3\text{B}_2\text{O}_3\cdot 3\text{H}_2\text{O}$ ,  $4\text{ZnO}\cdot\text{B}_2\text{O}_3\cdot\text{H}_2\text{O}$ ,  $3\text{ZnO}\cdot 5\text{B}_2\text{O}_3\cdot 14\text{H}_2\text{O}$ , and  $\text{ZnO}\cdot 5\text{B}_2\text{O}_3\cdot 4.5\text{H}_2\text{O}$ . In these products,  $\text{B}_2\text{O}_3/\text{ZnO}$  molar ratio changes from 0.25 to 5 and it determines the characteristics of the product (Schubert, 1995).

Zinc borates have been used in industry since the 1940s,  $2\text{ZnO}\cdot 3\text{B}_2\text{O}_3\cdot 7\text{H}_2\text{O}$  and  $3\text{ZnO}\cdot 5\text{B}_2\text{O}_3\cdot 14\text{H}_2\text{O}$  had been primarily utilized in the earlier period. However, these compounds had a limited range of applications due to their low dehydration temperatures. Today, the most important commercial zinc borate has a chemical composition of  $\text{Zn}[\text{B}_3\text{O}_4(\text{OH})_3]$  and it has a relatively high dehydration onset temperature ( $>290^\circ\text{C}$ ). When this product was synthesized initially, its composition was assigned as  $\text{ZnO}\cdot 3\text{B}_2\text{O}_3\cdot 3.5\text{H}_2\text{O}$  which is inconsistent with more recent physical data (Schubert et al., 2003). The water content and dehydration temperatures of various zinc borates are summarized in Table 2.5.

In the comparison of these zinc borate species, it can be deduced that  $2\text{ZnO}\cdot 3\text{B}_2\text{O}_3\cdot 7\text{H}_2\text{O}$ ,  $\text{ZnO}\cdot\text{B}_2\text{O}_3\cdot 2\text{H}_2\text{O}$  and  $3\text{ZnO}\cdot 5\text{B}_2\text{O}_3\cdot 14\text{H}_2\text{O}$  have considerably low dehydration temperatures with respect to the dehydration temperatures of  $4\text{ZnO}\cdot\text{B}_2\text{O}_3\cdot\text{H}_2\text{O}$  and  $\text{ZnO}\cdot 3\text{B}_2\text{O}_3\cdot 3\text{H}_2\text{O}$ . Especially, the zinc borate type of  $4\text{ZnO}\cdot\text{B}_2\text{O}_3\cdot\text{H}_2\text{O}$  was developed for the polymer systems that require high processing

temperature at which polymer additive must be stable and do not interact with the other chemicals.

Table 2.5. Thermal behaviors of zinc borates

Zinc Borate Type	H <sub>2</sub> O (%) <sup>*</sup>	Dehydration Temperature (°C)	Reference
3ZnO·5B <sub>2</sub> O <sub>3</sub> ·14H <sub>2</sub> O	29.85	100-200	(Schubert et al., 2003)
2ZnO·3B <sub>2</sub> O <sub>3</sub> ·7H <sub>2</sub> O	25.32	100-250	(Briggs, 2001)
2ZnO·3B <sub>2</sub> O <sub>3</sub> ·3H <sub>2</sub> O	12.69	290	(Schubert et al., 2003)
ZnO·B <sub>2</sub> O <sub>3</sub> ·2H <sub>2</sub> O	19.25	100-250	(Briggs, 2001)
4ZnO·B <sub>2</sub> O <sub>3</sub> ·H <sub>2</sub> O	4.35	415	(Schubert, 1995)

\*: H<sub>2</sub>O content (wt. %) was determined from chemical formula of the product.

### 2.3.1. Applications of Zinc Borates

A series of hydrated zinc borates have been developed for use as fire-retardant additives in coatings and polymers. As a polymer additive, it serves as a fire retardant synergist, char promoter, anti-drip agent, smoke and afterglow suppressant, and modifier of electrical and optical properties. Worldwide consumption of these zinc salts is several thousand metric tons per year. A substantial portion of this total is used in vinyl plastics where zinc borates are added alone or in combination with other fire retardants such as antimony oxide or alumina trihydrate.

Zinc Borate can be used as a fire retardant in PVC, Polyolefins, Elastomers, Polyamides, and Epoxy resins as given in Table 2.6. The recent developments in this area were reviewed by Shen and co-workers (2008). In halogen-containing systems, zinc borate is used in conjunction with antimony oxide, while in halogen-free systems; it is normally used in conjunction with alumina trihydrate, magnesium hydroxide, or red phosphorus. In some particular applications, zinc borate can be used alone.

Zinc borates act through:

- zinc halide or zinc oxyhalide that accelerate the decomposition of halogen sources and promote char formation.

- by the B<sub>2</sub>O<sub>3</sub> moiety released, a low melting glass, that can stabilize the char. B<sub>2</sub>O<sub>3</sub> released can also promote the formation of ceramic formation in systems containing ATH or magnesium hydroxide.
- the endothermic, stepwise release of water that can promote the formation of foamy char.

Table 2.6. Zinc borate functions and applications in polymers  
(Source: Luzenac, 2009)

Polymer Type	Functions	Applications
Flexible PVC, Rigid PVC	<ul style="list-style-type: none"> <li>• Smoke suppressant</li> <li>• Flame retardant</li> <li>• Synergist of antimony trioxide</li> <li>• Char promoter</li> </ul>	Conveyor belting, car interior trim, roofing membrane, flooring, wires & cables, wall coverings
Polyolefins, EVA	<ul style="list-style-type: none"> <li>• Smoke suppressant / Char promoter</li> <li>• Afterglow suppressant</li> <li>• Improves elongation properties</li> <li>• Anti-arcing agent</li> </ul>	Wire & cable, foam insulation, electrical parts
Polyamides	<ul style="list-style-type: none"> <li>• Anti-arcing and anti-tracking agent</li> <li>• Synergist of halogen sources</li> <li>• Afterglow suppressant</li> <li>• Used in both halogen containing and halogen free nylons</li> </ul>	Electrical components, adhesives
Elastomers, SBR, Silicone, EPDM, Neoprene	<ul style="list-style-type: none"> <li>• Smoke suppressant</li> <li>• Afterglow suppressant</li> <li>• Char promoter</li> <li>• Anti-arcing and anti-tracking agent</li> </ul>	Wire & cable, conveyor belting, roofing membrane, foam insulation, flooring insulator, coatings, sealants
Thermoset resins (Epoxy, Unsaturated Polyester, Urethane, Phenolics.)	<ul style="list-style-type: none"> <li>• Smoke suppressant</li> <li>• Char promoter</li> <li>• Partial or complete replacement of antimony trioxide</li> </ul>	Intumescent coatings, encapsulant, panelling, containers, foam, adhesives, electrical parts

The influence of zinc borates ( $3\text{ZnO}\cdot 5\text{B}_2\text{O}_3\cdot 3.5\text{H}_2\text{O}$  and  $3\text{ZnO}\cdot 5\text{B}_2\text{O}_3\cdot 7.5\text{H}_2\text{O}$ ) on chlorine containing coatings was studied by Giudice and Benitez (2001). The chlorinated alkyd resin was used as film forming material (24.9 % by weight of chlorine on solids) in paint formulations. When this compound is exposed to high temperature, it decomposes by releasing free radicals which combine with air oxygen by complex reactions. Antimony trioxide, titanium dioxide and talc are commonly used pigments in paints. As antimony trioxide is not suitable with halogenated organics, zinc borates were proposed as fire retardant material to replace antimony trioxide in this study.

When antimony trioxide and chlorinated alkyd resin are exposed to heat they form antimony trichloride and/or antimony oxychloride.

Giudice and Benitez reported that after burning, paints including zinc borates in their composition as fire retardant pigment generated an anhydrous compound which forms a glassy layer that prevents the further oxidation of the char. Both types of zinc borate have shown an excellent performance over the antimony trioxide due to their endothermic behaviors. Zinc borate type of  $(3\text{ZnO}\cdot 5\text{B}_2\text{O}_3\cdot 7.5\text{H}_2\text{O})$  gave better performance than the one  $(3\text{ZnO}\cdot 5\text{B}_2\text{O}_3\cdot 3.5\text{H}_2\text{O})$  in fire tests. The higher number of hydrated water molecules that was released at higher temperatures diffused and absorbed a greater amount of heat which increases flame retardancy and heat build up.

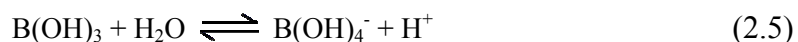
Another study regarding the use of zinc borate species  $(3\text{ZnO}\cdot 5\text{B}_2\text{O}_3\cdot 3\text{H}_2\text{O}$  and  $4\text{ZnO}\cdot \text{B}_2\text{O}_3\cdot \text{H}_2\text{O})$  in the presence of other fire retardants, such as magnesium hydroxide was performed by Genovese and Shanks (2007). The structural and thermal alterations of these commercial fire retardants were examined considering the specific chemical reaction and phase changes. Generally, metal hydroxides reduce significantly the heat release rate through absorption of heat during conversion of its metal oxide. Formation of water, followed by vaporization, decreases the heat and dilutes the volatiles from polymer degradation. Zinc borate species exhibit also dehydration with increasing temperature by the condensation of hydroxyl groups in the structure. Various structural changes of zinc borate  $(3\text{ZnO}\cdot 5\text{B}_2\text{O}_3\cdot 3\text{H}_2\text{O})$  during the heating were determined using differential thermal analysis and wide-angle X-ray spectroscopy. Magnesium orthoborate  $(3\text{MgO}\cdot \text{B}_2\text{O}_3)$  and ZnO was formed as a new crystalline phase at the temperatures greater than 500 °C. However, from zinc borate  $(4\text{ZnO}\cdot \text{B}_2\text{O}_3\cdot \text{H}_2\text{O})$ , ZnO was primary product of heating and no solid state reaction took place between zinc borate and MgO.

## **2.4. Production Techniques of Metal Borates**

Borate salts or complexes of every metal can be prepared according to the data on the literature (Briggs, 2001). For most metals, a series of hydrated and anhydrous compounds can be prepared by varying the raw materials, their ratio, and/or reaction

conditions. Some of them have gained a commercial importance in a few industry branches namely, ceramic, polymer, paint and wood.

The least hydrolyzed form of boron in aqueous solution is boric acid,  $B(OH)_3$ . The basic hydrolysis reaction involving boric acid is the rapid and reversible formation of the borate ion in which boron exhibits tetrahedral coordination with  $sp^3$  hybridization:



Reaction 2.5 becomes significant above pH 7, and  $B(OH)_4^-$  anion is the predominant solution species above pH 11. An equilibrium constant for reaction (Equation 2.5) was reported as  $5.80 \times 10^{-10}$  at 25 °C (Briggs, 2001). At intermediate pH and boric acid concentration greater than about 0.05 M, polyborate anions are formed rapidly and reversibly according to the reaction between boric acid and borate ion given in Equation 2.6.



Polymerization is not observed above pH 11 since borate anions repel each other and since tetrahedrally coordinated boron without any available d orbitals is coordinatively saturated and unable to participate in the  $sp^3 d$  intermediate required for condensation via  $S_N$  mechanism (Brinker and Scherer, 1990). Below pH 4, polymerization is inhibited because the OH ligands on boric acid are not sufficiently strong nucleophiles to have an affinity for other boric acid molecules.

The hydrated metal borates are usually prepared by mixing aqueous solutions or suspensions of the metal oxides, sulfates and boric acid or alkali metal borates, such as borax. The products formed from basic solutions are often sparingly-soluble amorphous solids having variable compositions. The products having crystalline structure are generally obtained from slightly acidic solutions.

Depending on the pH, cation present, and the temperature, a variety of hydrated polyborates can appear as saturating solid phases. There are some rules for the structures of polyborate anions in solution:



- Boron atoms occur in trigonal planar  $\text{BO}_3$  and tetrahedral  $\text{BO}_4$  groups that have a formal charge of 0 and -1, respectively.
- The basic structure of the polyborates is a six membered ring of alternating boron and oxygen atoms.
- To be stable, a ring must contain one or two tetrahedral boron atoms.
- Rings may be refused as tetrahedral boron atoms.
- Long chain polyanions may be formed from the rings by repeated dehydration (Brinker and Scherer, 1990).

Anhydrous metal borates may be prepared by heating the hydrated salts to 300-500 °C or by direct fusion of the metal oxide with boric acid or  $\text{B}_2\text{O}_3$ . Many of anhydrous products having  $\text{B}_2\text{O}_3$  form vitreous phases over certain ranges of composition.

#### **2.4.1. Production of Zinc Borate from Borax and Zinc Salts**

Zinc borate,  $2\text{ZnO}\cdot 3\text{B}_2\text{O}_3\cdot 7\text{H}_2\text{O}$ , can be produced from borax, sodium borate decahydrate, ( $\text{Na}_2\text{O}\cdot 2\text{B}_2\text{O}_3\cdot 10\text{H}_2\text{O}$ ) and various salts of zinc such as, sulfate, chloride, carbonate, nitrate and etc. Borax solution is initially prepared by considering the solubility of the borax at the temperature of 70 °C according to Figure 2.3. Borax starts to lose its hydration water at around 60 °C and it forms tetra and or penta hydrated sodium borates. Then aqueous solution of zinc salt at the same temperature is added into borax solution under vigorous mixing. It was found from X-ray analysis that the product formed was orthorhombic (Briggs, 2001). Zinc borates with composition of  $2\text{ZnO}\cdot 3\text{B}_2\text{O}_3\cdot 7\text{H}_2\text{O}$  and  $\text{ZnO}\cdot \text{B}_2\text{O}_3\cdot 2\text{H}_2\text{O}$  starts to lose water when heated from 130 to 250 °C.

When zinc borate is produced from soluble sodium borate decahydrate and soluble zinc salt, final product contains sodium salt as impurities depending on the type of zinc salt used in the reaction e.g.,  $(\text{SO}_4)^{2-}$ ,  $(\text{NO}_3)^-$ ,  $\text{Cl}^-$  and etc. in large quantities. The use of zinc borates containing such impurities in plastic materials to provide flame retarding property, it is possible that electric properties of plastic equipment deteriorated

since there are impurities in the additive causing poor insulation and dielectric breakdown after the use of extended periods (Sawada et al., 2004). In order to remove those impurities from the final product, washing and filtration unit operations become substantially important.

Crystalline and hydrophobic zinc borate ( $\text{Zn}_2\text{B}_6\text{O}_{11}\cdot 3\text{H}_2\text{O}$ ) nanodiscs were successfully prepared by a wet method using  $\text{Na}_2\text{B}_4\text{O}_7\cdot 10\text{H}_2\text{O}$  and  $\text{ZnSO}_4\cdot 7\text{H}_2\text{O}$  in the presence oleic acid as the modifying agent in aqueous solution (Tian et al., 2006). In the production procedure, 100 mL of 0.1 M borax solution was firstly mixed with 30 mL of absolute ethanol containing certain amount of oleic acid at 70 °C and 20 mL of 1 M zinc sulfate solution was added drop wise to previous solution while being stirred for a period of 0.5 h. After addition of zinc sulfate was completed the whole mixture was stirred at 70 °C for 6.5 h. Finally, reaction mixture was filtered and washed successively by water and ethanol to remove unreacted components, oleic acid and by-products and dried at 80 °C in oven. The microstructures and morphology of the as-obtained samples were studied by X-ray diffraction (XRD), infrared spectra (IR), scanning electron microscopy (SEM) equipped with an energy dispersive X-ray spectrophotometer (EDS) and thermogravimetric analysis (TGA). They found from the measurement of the active ratio that  $\text{Zn}_2\text{B}_6\text{O}_{11}\cdot 3\text{H}_2\text{O}$  samples were hydrophobic. It was indicated that the as-prepared materials displayed nanodisc morphology with average diameters from 100 to 500 nm and the thicknesses were about 30 nm. Moreover, the friction coefficient of the base oil was decreased by the addition of hydrophobic zinc borate nanodiscs. TGA analysis indicated that the mass loss was 12.79 % from 120 to 440 °C, which corresponded to the loss of three molar equivalents of the crystal water and it can be compared with calculated value of 12.69 % for  $2\text{ZnO}\cdot 3\text{B}_2\text{O}_3\cdot 3\text{H}_2\text{O}$ .

Tian and co-workers (2008) studied the production of hydrophobic zinc borate nanoplates from borax decahydrate and zinc sulfate heptahydrate in the presence of oleic acid as a modifying agent. In the reaction, 100mL of 0.1M aqueous borax solution was mixed with 20 mL ethanol and oleic acid mixture at 70 °C then, 20 mL 2 M zinc sulfate heptahydrate solution was added drop wise to the first solution and the reaction was carried out for 6.5 h at  $\text{pH}<7$ . The ultimate mixture was washed by water and ethanol to remove unreacted raw materials and byproducts and dried at 80 °C in an oven. From the SEM microphotographs, the effect of oleic acid and raw materials molar ratio can be seen in Figure 2.5. In the absence of oleic acid, the zinc borate was in the shape of polyhedral thin flakes (Figure 2.5.a). As the mole number of borax decahydrate

increased from 1 to 2, the shape of formed zinc borate changed significantly as seen in Figure 2.5.b and Figure 2.5.c. The diameters of the plates changed between 100 nm to 500 nm with the thickness of about 30 nm. In the thermal behaviour examination by TGA, mass loss of the zinc borate was determined as 12.79 % which corresponds to the loss of three molar equivalents of water and it is very close to theoretical value of 12.69 %. While zinc borate formed in the absence of oleic acid started to lose mass at 240 °C and the other one which was obtained in the presence of oleic acid began to lose mass at 260 °C. Although the water content of zinc borate is equal to the water content of  $2\text{ZnO}\cdot 3\text{B}_2\text{O}_3\cdot 3\text{H}_2\text{O}$ , thermal stability of the prepared product is different than zinc borate type of  $2\text{ZnO}\cdot 3\text{B}_2\text{O}_3\cdot 3\text{H}_2\text{O}$ .

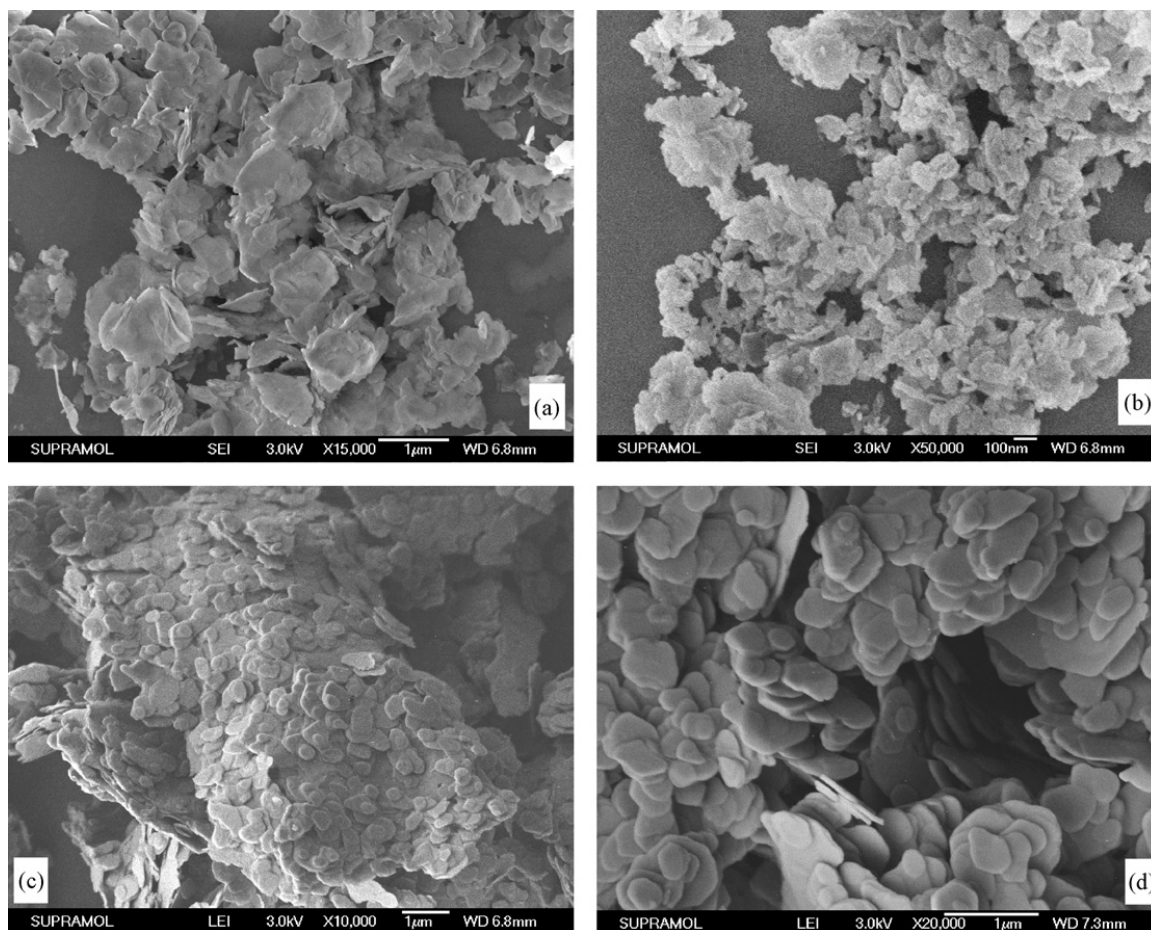


Figure 2.5. SEM images of a) pure zinc borate particles and modified zinc borate particles (1.00 wt % of oleic acid added) with different zinc sulfate/sodium borate mole ratios: b) 1:1, c) 1:1.5, and d) 1:2 (Source: Tian et al., 2008).

Another important examination for the synthesis of zinc borate was the determination of hydrophobic and hydrophilic behaviour of the product and the effect of

oleic acid on this behaviour. As expected, increasing the amount of oleic acid increased the relative contact angle showing that surface of zinc borate became hydrophobic unlike the pure zinc borate surface property. This zinc borate type had potential applications as a lubricating additive since particles were in the shape of nanoplates and hydrophobic. The anticipated problem might be the thermal behaviour of product under heavy loading conditions in lubrication process.

The synthesis of zinc borate type of  $4\text{ZnO}\cdot\text{B}_2\text{O}_3\cdot\text{H}_2\text{O}$  was studied using borax decahydrate and zinc sulfate heptahydrate by Shi and co-workers (2008a). Reactions were carried out in different temperature ranges (80-180 °C), at different pH ranges from 3 to 10, reaction times (9-48 h), raw materials' concentration and in the presence of surfactant PEG 300 of different quantities (0-20 mL). The optimum initial pH range was pointed out as 8-9 and at pH values of 3, 6, and 10 no product formation was reported. In the production of zinc borate from borax and water soluble zinc salt, the initial pH of the mixture has a significant role. The formed product, zinc borate, decomposes in acidic solutions, on the other hand, in basic solutions zinc oxide is produced instead of zinc borate (Shi et al., 2008a). The reaction temperature between 90 and 180 °C was stated as adequate for synthesis of  $4\text{ZnO}\cdot\text{B}_2\text{O}_3\cdot\text{H}_2\text{O}$  crystals. The reaction time was also examined based on the morphological alteration of product and increasing reaction time caused random orientation of nanorods. At low concentrations such as, 0.0125 M, 0.25 M, and 0.50 M zinc borate type of  $4\text{ZnO}\cdot\text{B}_2\text{O}_3\cdot\text{H}_2\text{O}$  was obtained at 100 and 120 °C for 24 h reaction time. While at the reaction temperature of 120 °C for 0.75 M reactant salt concentrations, no product was formed, at 160 °C zinc borate was obtained for same concentration under same reaction time of 24 h.

The effect of surfactant PEG 300 on the formation zinc borate was investigated by adding various amounts of surfactant (0-20 mL) into reaction media with conditions of 0.25 M raw materials' concentration at 100 °C for 24 h reaction time. As it can be seen from Figure 2.6., the PEG 300 significantly affected the morphology of zinc borate. For instance, while irregular particles were formed in the absence of PEG 300, rod-like particles were formed in the presence of 10-20 mL of PEG 300. That formed zinc borate of  $4\text{ZnO}\cdot\text{B}_2\text{O}_3\cdot\text{H}_2\text{O}$  had pure phase and monoclinic crystalline structure was determined by Shi and co-workers based on XRD data.

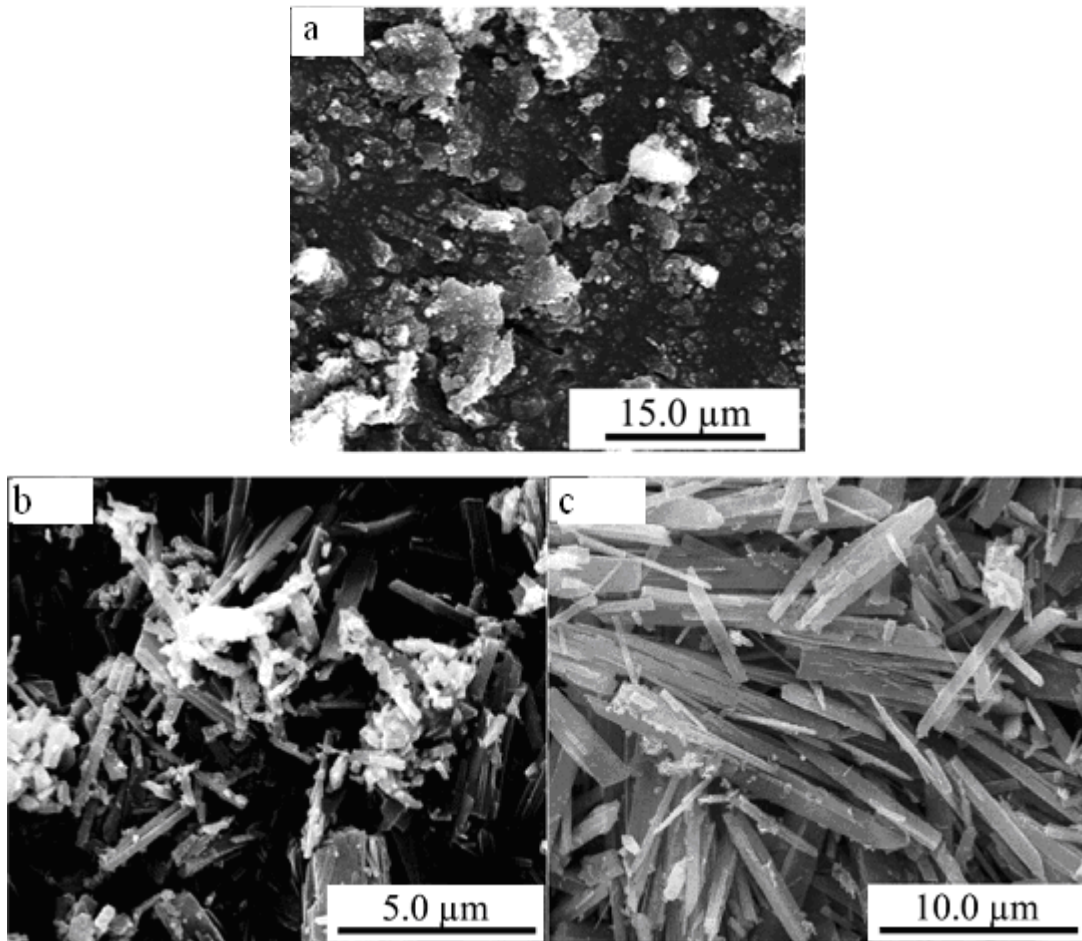


Figure 2.6. SEM images of samples obtained with different quantities of PEG 300: a) (0 mL), b) (0-1 mL), and c) (10-20 mL) (Source: Shi et al., 2008a).

Thermal behaviour of  $4\text{ZnO}\cdot\text{B}_2\text{O}_3\cdot\text{H}_2\text{O}$  was studied by Shi and co-workers (2007). As shown in Figure 2.7., zinc borate began to lose mass at  $100\text{ }^\circ\text{C}$  showing that it contained some unbound water. On the other hand, it lost 4.72 % of its water from  $415\text{ }^\circ\text{C}$  to  $600\text{ }^\circ\text{C}$ , corresponding to theoretical water content of  $4\text{ZnO}\cdot\text{B}_2\text{O}_3\cdot\text{H}_2\text{O}$ .

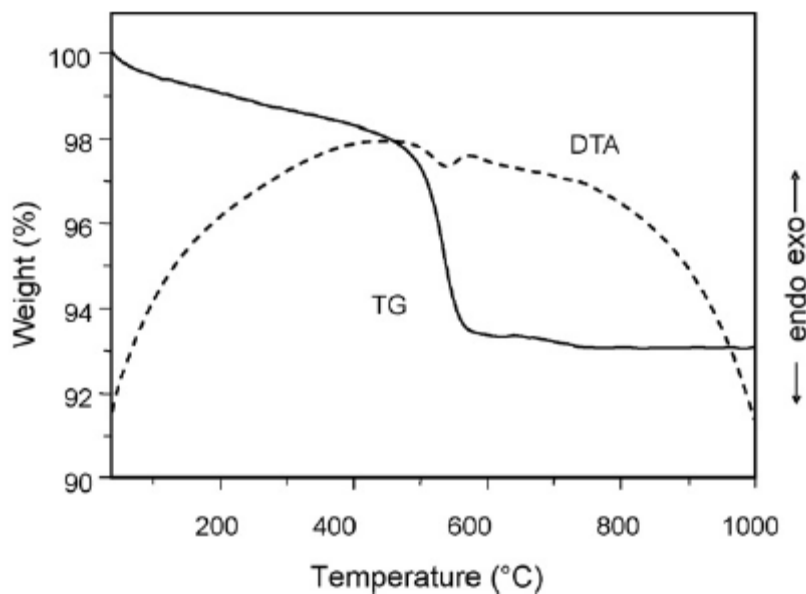


Figure 2.7. TG-DTA curves of  $4\text{ZnO}\cdot\text{B}_2\text{O}_3\cdot\text{H}_2\text{O}$  nanorods (Source: Shi et al., 2007).

In the production of metal borates from borax decahydrate and soluble metal salt, modifying agents such as oleic acid, PEG 300 and other types of surfactants are studied to control morphology and size of particles. When borax decahydrate was dissolved in water it forms borate anion ( $\text{B}_4\text{O}_7^{2-}$ ) and polyborate anions are formed by condensation of aforementioned anions. A highly concentrated aqueous solution of sodium borate with 5.24 mol/kg of boron was prepared at 20 °C by adjusting the Na/B ratio to 0.22 at pH 6.9 (Tsuyumoto et al., 2007). That value was twice more than the solubility of sodium borate 2.49 mol/kg of boron that was prepared at 20 °C. It is anticipated that the formation of polyborates in the reaction media influences the composition and morphology of the ultimate borate product.

#### 2.4.2. Production of Zinc Borate from Boric Acid and Zinc Oxide

Zinc borate,  $2\text{ZnO}\cdot 3\text{B}_2\text{O}_3\cdot 3\text{H}_2\text{O}$ , can also be produced by reaction of zinc oxide and boric acid in hot water at 90-100 °C. The composition  $2\text{ZnO}\cdot 3\text{B}_2\text{O}_3\cdot 3.5\text{H}_2\text{O}$  was assigned to the product by workers who first prepared this compound and recognized its usefulness (Nies and Hulbert, 1970). This composition has been used extensively in technical and trade literature to describe the zinc borate. However, this composition is

incompatible with more recent information of the same product. For instance, both elemental analysis and TGA data indicated that water content was lower than the one ( $3.5 \text{ H}_2\text{O}$ ), which was conventionally accepted. The composition of  $2\text{ZnO}\cdot 3\text{B}_2\text{O}_3\cdot 3\text{H}_2\text{O}$  is accepted as a correct representation for the zinc borate. The composition  $2\text{ZnO}\cdot 3\text{B}_2\text{O}_3\cdot 3.5\text{H}_2\text{O}$  suggests a tetrameric structure, which has been proposed repeatedly in the trade literature, whereas  $2\text{ZnO}\cdot 3\text{B}_2\text{O}_3\cdot 3\text{H}_2\text{O}$  corresponds to a fully polymerized structural unit.

The structure of zinc borate, used in trade and scientific literature as  $2\text{ZnO}\cdot 3\text{B}_2\text{O}_3\cdot 3.5\text{H}_2\text{O}$ , was revised by Schubert and co-workers (2003). They prepared and characterized single crystals of zinc borate. Following method was used for the single crystal synthesis: Firstly, an aqueous zinc chloride solution was prepared by dissolving enough zinc oxide with 6 M HCl to produce a solution having pH 4. Secondly, this solution was added drop wise into concentrated boric acid solution at  $95^\circ\text{C}$  under mixing until a significant pH decrease. Single crystal was formed on the surface of the vessel after maintaining the solution at  $95^\circ\text{C}$  for one day. The obtained single crystal was used in XRD analysis and it represented the bulk of the material. Schubert and co-workers have shown firstly that the exact structure zinc borate is  $2\text{ZnO}\cdot 3\text{B}_2\text{O}_3\cdot 3\text{H}_2\text{O}$  instead of  $2\text{ZnO}\cdot 3\text{B}_2\text{O}_3\cdot 3.5\text{H}_2\text{O}$ . The oxide formula of  $2\text{ZnO}\cdot 3\text{B}_2\text{O}_3\cdot 3\text{H}_2\text{O}$  was pointed as  $\text{Zn}[\text{B}_3\text{O}_4(\text{OH})_3]$  in which polymerized triborate anions form complex with zinc cation and hydrogen bonding between chains.

The parameters, such as, mixing effects (types of propeller, mixing rate, presence of baffle in the reactor), reaction kinetics, temperature, pressure, reactants ratio and concentration, are considerably important for heterogeneous reactions. In the production of zinc borate with composition of  $2\text{ZnO}\cdot 3\text{B}_2\text{O}_3\cdot 3\text{H}_2\text{O}$ , reaction takes place between solid zinc oxide and dissolved boric acid in aqueous media. Particle size of ultimate product is one of the important parameters that determine the application area of the product. Shete and co-workers (2004) studied the effect of hydrodynamic and operating conditions for the formation of zinc borate in a batch stirred reactor. In this reaction, while boric acid was soluble in water, zinc oxide was insoluble. Therefore, authors had following assumptions for the heterogeneous reaction system:

1. Both zinc oxide particles and zinc borate particles were assumed to be spherical.
2. Zinc oxide particles were assumed to be insoluble.

3. Boric acid ions in boric acid solution reacted with zinc oxide particles on the surface of the latter.

Based on these assumptions, fluid-particle system forming an insoluble product has been treated by using an unreacted-core model (Shete et al., 2004). According to this model, the following successive steps that were first proposed by Levenspiel (1972) have been considered for the reaction of zinc oxide and boric acid.

**Step 1:** Borate anions that formed according to the Equation 2.5, diffuse from the bulk of the boric acid solution to the surface of zinc oxide particles (physical).

**Step 2:** Penetration and diffusion of borate ions through the blanket of ash layer covering the unreacted core to the surface of unreacted core of zinc oxide (physical).

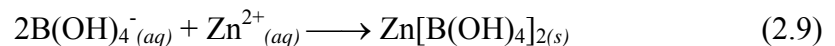
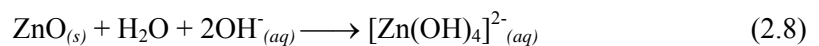
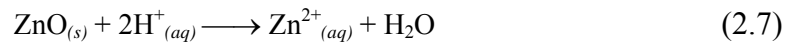
**Step 3:** Reaction of borate ions with zinc oxide particles at the reaction zone (chemical).

**Step 4:** Formation of zinc borate and diffusion of co-product water molecule through the ash layer covering the unreacted core back to the bulk phase (physical).

**Step 5:** It was proposed that peeling of zinc borate layer due to shear/collisions etc.

The point in this model that has not been considered intensively is the behavior of zinc oxide (ZnO). It is an amphoteric compound that means it shows an acidic character in bases and basic behavior in acids (Chang, 1994). ZnO dissolves according to Equations 2.7 or 2.8 in the presence of H<sup>+</sup> cations or OH<sup>-</sup> anions, respectively. Since boric acid solution produces H<sup>+</sup> cations, ZnO must show a basic character and dissolves according to the Equation 2.7.

Formed zinc cations react with borate anions as shown in Equation 2.9. Initial product transforms into different zinc borate species depending on temperature, pH and other parameters.





The reaction between zinc oxide and boric acid usually reaches completion in 3-4 hours and it depends on various other parameters (Shete et al., 2004). They observed that mixing parameters showed an influence on the particle size of the zinc borate. Three different impellers, disc turbine, six-bladed pitched blade turbine, and three-bladed hydrofoil impeller were used in the reactions where each impeller operated at its minimum suspension speed. Three-bladed hydrofoil impeller having higher minimum suspension speed ( $10 \text{ rev}\cdot\text{s}^{-1}$ ) produced zinc borate with lowest mean particle size of 10  $\mu\text{m}$ . The other impeller types gave the higher mean diameter compared with the hydrofoil type. Increasing the stirring rate provided a higher conversion and lower crystal size of the product. Rather than type of the impeller, stirring speed affected the particle size. Another point they examined was the reaction temperature, a complete conversion was achieved after 3.5 h at  $110 \text{ }^\circ\text{C}$  and 4.5 h at  $90 \text{ }^\circ\text{C}$ . On the other hand, at temperatures greater than  $100 \text{ }^\circ\text{C}$ , the system should be over atmospheric pressure, zinc borate has a tendency to hydrolyze to give zinc hydroxide and boric acid under these conditions. Based on this fact, reaction temperature, which is greater than  $100 \text{ }^\circ\text{C}$ , can not be used in this reaction.

Sawada and co-workers (2004) studied the production and application of zinc borate ( $2\text{ZnO}\cdot 3\text{B}_2\text{O}_3\cdot 3\text{H}_2\text{O}$ ) which was mainly used as flame-retarding and smoke suppressing agent (Sawada et al., 2004). The reaction was conducted in two steps. In the former one, zinc oxide and boric acid reacted together at a substantially stoichiometric ratio and a relatively low temperature, such as from  $45$  to  $65 \text{ }^\circ\text{C}$  to form fine crystals of zinc borate. The formation of fine crystalline zinc borate was easily confirmed by an increase in the viscosity of the reaction system. The viscosity of the reaction mixture rises since the solid-liquid ratio of the mixture increases. A substantial amount of water in the mixture is bonded to zinc borate structure in the form of either hydroxyl groups or crystal water. The loss of water from reaction medium increases the viscosity of the mixture. The zinc borate, which is formed at lower reaction temperature, is the zinc borate type of  $2\text{ZnO}\cdot 3\text{B}_2\text{O}_3\cdot 7\text{H}_2\text{O}$  (Eltepe et al., 2007). In the second step, the formed fine crystals were aged by maintaining the reaction system at a relatively high temperature, such as  $70$  to  $110 \text{ }^\circ\text{C}$ . In this part of reaction, the formed zinc borate,  $2\text{ZnO}\cdot 3\text{B}_2\text{O}_3\cdot 7\text{H}_2\text{O}$ , was converted into  $2\text{ZnO}\cdot 3\text{B}_2\text{O}_3\cdot 3\text{H}_2\text{O}$ . In addition, decreasing viscosity indicated the formation of  $2\text{ZnO}\cdot 3\text{B}_2\text{O}_3\cdot 3\text{H}_2\text{O}$ , as the water content has increased in the mixture. They characterized the final products using electron microscope and X-ray diffraction equipment. They found that the individual zinc borate

particles were rhombic hexahedrons, the length of a side of each particle was measured between 0.3-7.0  $\mu\text{m}$ . The volume based median diameter was found between 1.0-6.0  $\mu\text{m}$  as confirmed by the SEM microphotographs (Sawada et al., 2004). The major peaks from XRD pattern were tabulated for zinc borate ( $2\text{ZnO}\cdot 3\text{B}_2\text{O}_3\cdot 3\text{H}_2\text{O}$ ) as given below (Table 2.7). For the zinc borate with a formula of  $2\text{ZnO}\cdot 3\text{B}_2\text{O}_3\cdot 3\text{H}_2\text{O}$ , characteristic XRD peak is located at  $18^\circ$   $2\theta$  value. The major peaks of zinc borate,  $2\text{ZnO}\cdot 3\text{B}_2\text{O}_3\cdot 7\text{H}_2\text{O}$ , are also summarized in Table 2.7. Both of those specific peaks in patterns are going to clarify the type of product synthesized in the reaction.

In order to increase the reaction rate in the first step, authors added seed crystal of zinc borate in an amount from 0.5 to 10 parts by weight per 100 parts by weight of the  $\text{B}_2\text{O}_3$  component of boric acid. The molar ratio of  $\text{B}_2\text{O}_3/\text{ZnO}$  was 2.0 and it was same for all the runs.

Gürhan and co-workers (2009) studied the production of zinc borate having the molecular formula of  $2\text{ZnO}\cdot 3\text{B}_2\text{O}_3\cdot 3.5\text{H}_2\text{O}$  considering the effects of reaction parameters on the properties of product as well as the reaction kinetics. Production of zinc borate from the reaction of boric acid and zinc oxide in the presence of seed crystals was performed in a continuously stirred, temperature-controlled 1.5 L batch reactor. Samples taken in regular time intervals during the experiments were analyzed quantitatively to determine the concentration of zinc oxide and boron oxide in the solid as well as for the conversion of zinc oxide to zinc borate versus time.

They suggested that the reaction between zinc oxide and boric acid fitted to the logistic model which was mostly used for growth in biological systems. The reaction rate, reaction completion time, composition and particle size distribution of zinc borate samples were examined by varying the following parameters: Different reactants ratio ( $\text{H}_3\text{BO}_3:\text{ZnO}$ , the initial molar ratio of boric acid to zinc oxide) of 3:1, 3.5:1, 5:1 and 7:1, the particle size of zinc oxide (10 and 25  $\mu\text{m}$ ), stirring rate (275, 400, 800 and 1600 rpm), temperature (75, 85 and 95  $^\circ\text{C}$ ) and the size of seed crystals (10 and 2  $\mu\text{m}$ ). Zinc borate samples obtained were analyzed for particle size distribution. They concluded that the reaction rate increased with the increases in  $\text{H}_3\text{BO}_3:\text{ZnO}$  molar ratio, stirring rate and temperature. Thus, the time needed for the completion of reaction decreased. On the other hand, the size of zinc borate seed had no significant effect on reaction rate and completion time. Particle size of zinc borate was affected by stirring rate but after a limit (800 rpm), increasing mixing rate did not induce any significant change in the

particle size of the product. That the particle size of zinc oxide did not have a significant effect on the reaction rate and the final size of zinc borate was reported. The average particle sizes of the zinc borate products were in the range 4.3–16.6  $\mu\text{m}$  (wet dispersion analysis). Optimum experimental conditions for producing fine zinc borate (3-5  $\mu\text{m}$ ) were summarized as follows:  $\text{H}_3\text{BO}_3\text{:ZnO}$  molar ratio of 5:1, zinc oxide particle size of 10-25  $\mu\text{m}$ , stirring rate of 800-1600 rpm reaction temperature of 85-95  $^\circ\text{C}$  and seed particle size of 2-10  $\mu\text{m}$ .

Table 2.7. XRD data of zinc borate species  
(Source: Sawada et al., 2004)

<b>2<math>\theta</math></b>	<b>d Spacing (<math>\text{\AA}</math>)</b>	<b>Relative Intensity (<math>I/I_{100}</math>)x100</b>
<b><math>2\text{ZnO}\cdot 3\text{B}_2\text{O}_3\cdot 3\text{H}_2\text{O}</math></b>		
18.0	4.91	100
20.6	4.31	78
21.7	4.08	75
22.5	3.95	22
23.7	3.75	75
24.1	3.69	40
27.5	3.32	22
28.7	3.11	63
<b><math>2\text{ZnO}\cdot 3\text{B}_2\text{O}_3\cdot 7\text{H}_2\text{O}</math></b>		
12.8	6.92	100
17.2	5.14	15
19.4	4.58	16
25.2	3.53	15
26.1	3.41	48
29.1	3.06	28
35.4	2.54	16
36.5	2.46	17
42.6	2.12	14
50.3	1.81	13

In this study, authors did not take into account the formation of different zinc borate types in the reaction of boric acid and zinc oxide. They assumed that zinc borate of  $2\text{ZnO}\cdot 3\text{B}_2\text{O}_3\cdot 3.5\text{H}_2\text{O}$  was formed as the only product in the reaction. The formation of other zinc borate types with a different chemical structure at initial periods of reaction was reported in the literature (Sawada et al, 2004; Eltepe et al., 2007). This fact should be considered in conversion calculation. Otherwise, this assumption would lead to mistakes in reaction rate and conversion calculations.

An industrially important zinc borate,  $2\text{ZnO}\cdot 3\text{B}_2\text{O}_3\cdot 3\text{H}_2\text{O}$ , was synthesized from boric acid and zinc oxide (Shi et al., 2008b) using a rheological phase reaction method. In this method, the promising idea, the use of a little amount of water in the reaction, was examined. This technique could find use in metal borate production processes when environmental legislations are strictly enforced to minimize the amount of waste streams. In order to complete use of raw materials, stoichiometric amounts of zinc oxide and boric acid were used in the reaction. The reactions were carried out at temperatures between 80-95 °C for different reaction periods and various amounts of water. Although longer reaction times (8-10 h) are required to produce zinc borate in this technique, it can be preferred for large scale production as there is no need for separations of product from unreacted raw materials and by-products, and no waste water.

No impurity phases were detected in XRD analysis of final product when even a drop of water was used in the reaction that indicated all the reactants were converted into product. The particle size of  $2\text{ZnO}\cdot 3\text{B}_2\text{O}_3\cdot 3\text{H}_2\text{O}$ , is of great importance to its industrial applications. The particle size of zinc borate samples that were synthesized in the presence of 3 mL and 0.04 mL of water at 95 °C for 8 h of reaction time was about 19  $\mu\text{m}$  and 96  $\mu\text{m}$ , respectively. The reason of different particle size of zinc borate samples is the amount of water used in the reaction. The product has smaller particle size if more water is added to the reactants' mixture (Figure 2.8). The amount of water in the reactants is also responsible for the reaction time. If less water is used in the reaction, the collision chance of molecules decreases and it induces longer reaction times.

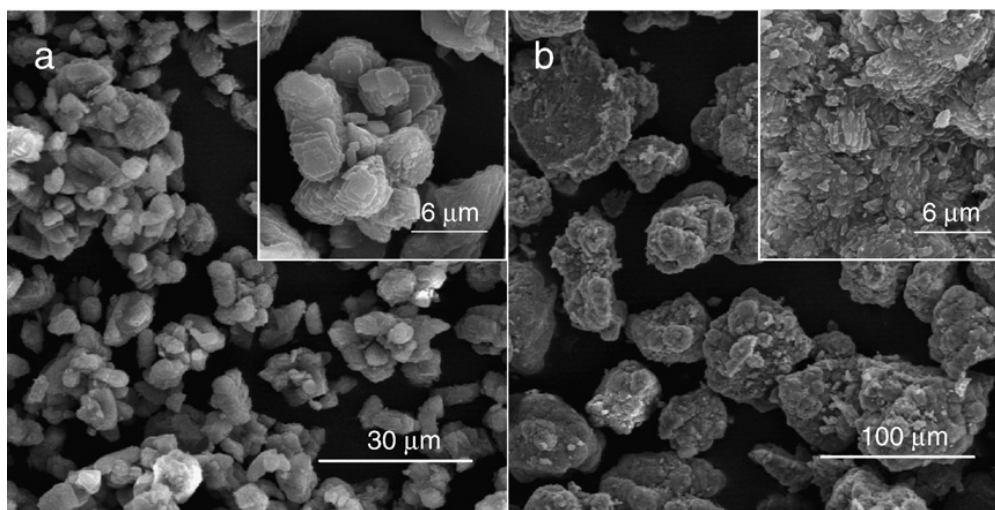


Figure 2.8. SEM images of zinc borate particles in the presence of different amounts of water a) 3 mL b) 0.04 mL (Source: Shi et al., 2008b).

Table 2.8 summarizes the studies of zinc borate synthesis from both boric acid and borax decahydrate. Zinc borate of  $2\text{ZnO}\cdot 3\text{B}_2\text{O}_3\cdot 3\text{H}_2\text{O}$  that was usually produced from boric acid and zinc oxide was determined from this review. On the other hand, the use of borax and soluble zinc salts for the production of zinc borate of  $2\text{ZnO}\cdot 3\text{B}_2\text{O}_3\cdot 3\text{H}_2\text{O}$  was proposed by Tian and co-workers (2006). Hence, both borax decahydrate and boric acid have been decided to be used in the synthesis of nanosized zinc borate.

### **2.4.3. Nucleation, Growth and Organization in Borate Crystallization**

Reactions leading to crystallization of products are of great importance in the production of many industrial chemicals, such as metal borates, metal salts and etc. A sparingly soluble product, zinc borate, precipitates in the reactions of “borax decahydrate-zinc nitrate hexahydrate” and “boric acid-zinc oxide”. In those heterogeneous reactions, while borax decahydrate, boric acid and zinc nitrate hexahydrate are easily soluble in water, solubility of zinc oxide is related to the dissolution of boric acid in which  $\text{H}^+$  proton is released. Nucleation, crystal growth and interaction of those formed particles occur simultaneously and rapidly in precipitation.

There are several important characteristics in precipitation reactions. First, precipitated products are sparingly soluble and need a relatively high supersaturation to form. Second, nucleation dominates the precipitation process due to the high supersaturation. Third, because of high particle concentration and small crystal size, aggregation may occur and it greatly affects the properties of ultimate product. Fourth, supersaturation inducing the precipitation usually results from a chemical reaction. Thus, precipitation is sometimes called as reactive crystallization (Karpinski and Wey, 2002). As nucleation and growth mechanisms are important for controlling the particle size of product, studies related to zinc borate synthesis based on nucleation and crystal growth were reviewed in literature.

Table 2.8. Studies related with zinc borate production

Raw Materials	Purpose	Reaction Conditions	Product Type	Reference
Borax, zinc sulfate, NaOH	Zinc borate synthesis	At room temp. 18-20 h reaction time	$2\text{ZnO} \cdot 3\text{B}_2\text{O}_3 \cdot 7\text{H}_2\text{O}$	(Myhren and Nelson 1946)
Borax, $\text{ZnCl}_2$ , $\text{Zn}(\text{SO})_4$ , NaOH and $\text{H}_2\text{O}$	Production of zinc borate having lower water content	At 95 °C, 24 h reaction time, seed crystal utilized.	$2\text{ZnO} \cdot 3\text{B}_2\text{O}_3 \cdot 3.5\text{H}_2\text{O}$	(Nies and Hulbert, 1970)
$\text{ZnO}$ , $\text{B}(\text{OH})_3$ , and $\text{H}_2\text{O}$	Novel zinc borate synthesis	At 100 °C, 5 h reaction time	$4\text{ZnO} \cdot \text{B}_2\text{O}_3 \cdot \text{H}_2\text{O}$	(Schubert, 1995)
$\text{ZnO}$ , $\text{B}(\text{OH})_3$ , HCl and $\text{H}_2\text{O}$	Clarify zinc borate structure	At 95 °C, 24 h reaction time	$2\text{ZnO} \cdot 3\text{B}_2\text{O}_3 \cdot 3\text{H}_2\text{O}$ or $\text{Zn}[\text{B}_3\text{O}_4(\text{OH})_3]$	(Schubert et al., 2003)
Borax, $\text{Zn}(\text{SO})_4$	Zinc borate production by hydrothermal technique	Between 80-180 °C, 9-48 h reaction time, at pH= 3-10, and surfactant	$4\text{ZnO} \cdot \text{B}_2\text{O}_3 \cdot \text{H}_2\text{O}$	(Shi et al., 2008b)
$\text{ZnO}$ , $\text{B}(\text{OH})_3$ , and $\text{H}_2\text{O}$	Determination of parameters which affect both reaction and product	Propeller type, reaction temp. and period, reactants' ratio, ZnO particle size	$2\text{ZnO} \cdot 3\text{B}_2\text{O}_3 \cdot 3\text{H}_2\text{O}$	(Shete et al., 2004; (Gürhan et al., 2009)
$\text{ZnO}$ , $\text{B}(\text{OH})_3$ , and $\text{H}_2\text{O}$	Zinc borate synthesis using two-step technique	Step 1: at 60 °C for 90 min and Step 2: at 90 °C for 4 h Seed crystal utilized.	$2\text{ZnO} \cdot 3\text{B}_2\text{O}_3 \cdot 3\text{H}_2\text{O}$	(Sawada et al., 2004), (Eltepe et al., 2007).
Borax and zinc sulfate	Hydrophobic zinc borate nanodiscs	At 70 °C, 6.5 h reaction time and oleic acid	$\text{Zn}_2\text{B}_6\text{O}_{11} \cdot 3\text{H}_2\text{O}$	(Tian et al, 2006, 2008)
$\text{ZnO}$ , $\text{B}(\text{OH})_3$ , and $\text{H}_2\text{O}$	Zinc borate production by rheological phase technique	Reaction temperature: 95 °C, Reaction period: 8 h, $\text{H}_2\text{O}$ amount used in the reaction: 0-18.7 cm <sup>3</sup> .	$2\text{ZnO} \cdot 3\text{B}_2\text{O}_3 \cdot 3\text{H}_2\text{O}$	(Shi et al., 2008a).

Crystal growth of zinc borate from reaction of boric acid and zinc oxide was studied by Gürhan and co-workers (2009) using *logistic model*, in which rate law was given by Equation 2.10.

$$X = \frac{X^*}{1 + \left( \frac{X^*}{X_o} - 1 \right) e^{-kt}} \quad (2.10)$$

where  $X_o$  is the critical initial concentration of zinc borate,  $X$  is the zinc borate concentration (M) in the slurry reactor,  $X^*$  is the maximum zinc borate concentration (M), and  $k$  is the specific growth rate (1/h). When  $X$  is equal to  $X^*$ , the crystal growth rate is zero. They reported  $k$  values in the range of 0.039 and 0.165 for different reaction conditions. Production of zinc borate crystals was explained by following mechanism: Nucleation of zinc borate crystals on the surface of zinc oxide occurred first, and followed by growth around nuclei, and then the rupture of zinc borate crystals from the crust formed on zinc oxide surface. They reported that the growth mechanism of zinc borate crystals could be explained by a logistic model rather than by shrinking core model that was suggested by Shete and co-workers (2004).

A monodisperse micro/nano single crystals of  $2\text{ZnO} \cdot 3\text{B}_2\text{O}_3 \cdot 3\text{H}_2\text{O}$  was synthesized by Liu and co-workers (2009). In the synthesis, they prepared precursor by mixing boric acid dissolved in ammonia solution with zinc sulphate solution at 40 °C for 3 h. Then, product was obtained by heating the precursor in an oven at 150 °C for 3 h. An amorphous precursor was converted into crystalline product in the second heating step. They pointed out that there were three main steps as illustrated in Figure 2.9. These are nucleation and growth, phase transformation, and formation of single crystals. They reported that particle size of single crystals could be controlled by varying treatment temperature of precursor. Actually, the release of borate anions from ammonium-borate complex was controlled by changing the treatment temperature.

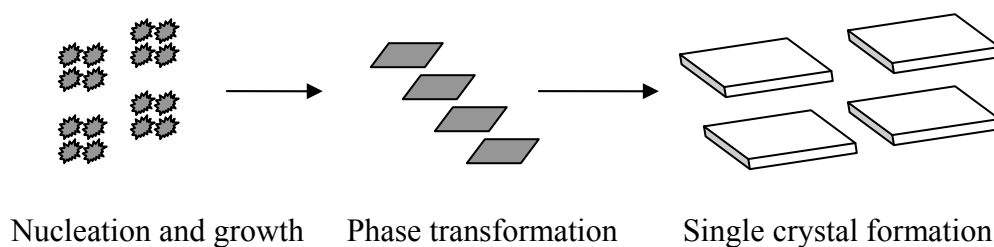


Figure 2.9. Schematic representation of nucleation and growth, phase transformation, and formation of single crystals steps (Source: Liu et al., 2009).

Nano/micro structures of  $4\text{ZnO}\cdot\text{B}_2\text{O}_3\cdot\text{H}_2\text{O}$  with different morphologies were synthesized by a hydrothermal technique in the presence of surfactant polyethylene glycol-300 (PEG 300) borax decahydrate and zinc sulphate heptahydrate (Shi et al., 2008a; Shi et al., 2009). Since PEG has both hydrophilic  $-\text{O}-$  and hydrophobic  $-\text{CH}_2-\text{CH}_2-$  groups in its structure, it dissolves in water with extension of its chains. Active oxygen sites on PEG chains interact with metal ions ( $\text{Zn}^{2+}$ ) and the nucleation and crystal growth of  $4\text{ZnO}\cdot\text{B}_2\text{O}_3\cdot\text{H}_2\text{O}$  are confined within chains. Crystal formation process for zinc borate was summarized as follows: interaction between zinc species and PEG chains, formation of nuclei, and growth of nuclei with the template direction reagent. They reported that the both temperature and PEG 300 played a critical role in controlling the particle size and morphology of zinc borate of  $4\text{ZnO}\cdot\text{B}_2\text{O}_3\cdot\text{H}_2\text{O}$ . It was also pointed that the amount of surfactant had a great effect on the morphology of the resulting product as shown in Figure 2.10. While nanowire morphology was obtained at 1 mL PEG use, nanorods were formed at 3 mL PEG use. Zinc borate with nano lamellar structure was synthesized at  $90\text{ }^\circ\text{C}$  reaction temperature as PEG molecules lost their linear structures as depicted in Figure 2.10. Rotating molecules around C–O bond induced conformations in PEG chains.

A nano-flake-like zinc borate  $2\text{ZnO}\cdot 2.2\text{B}_2\text{O}_3\cdot 3\text{H}_2\text{O}$  was prepared via coordination homogeneous precipitation method using ammonia, zinc nitrate and borax as raw materials (Ting et al., 2009). First, zinc cations reacted with ammonia to form a complex in the presence of borax in aqueous phase. Second, complex solution was diluted and reaction was carried out at  $45\text{ }^\circ\text{C}$ . In order to control particle size of zinc borate, release of zinc cations were controlled by decomposing the complex formed from zinc cations and ammonium depending on reaction temperature. When the zinc cations reach a certain amount, the zinc borate precipitates in the solution. They reported that crystalline zinc borates can only be obtained for reaction times of 12 h and



15 h. At the initial periods of reaction, nucleation of zinc borate occurs and then growth process takes place for further reaction times. Since final products were dried in vacuum oven at 70 °C for even 12 h, hydroxyl groups or water of crystallization in the structure of zinc borate could not be removed. If final product was dried at higher temperatures, phase transformation or new structure formation would take place.

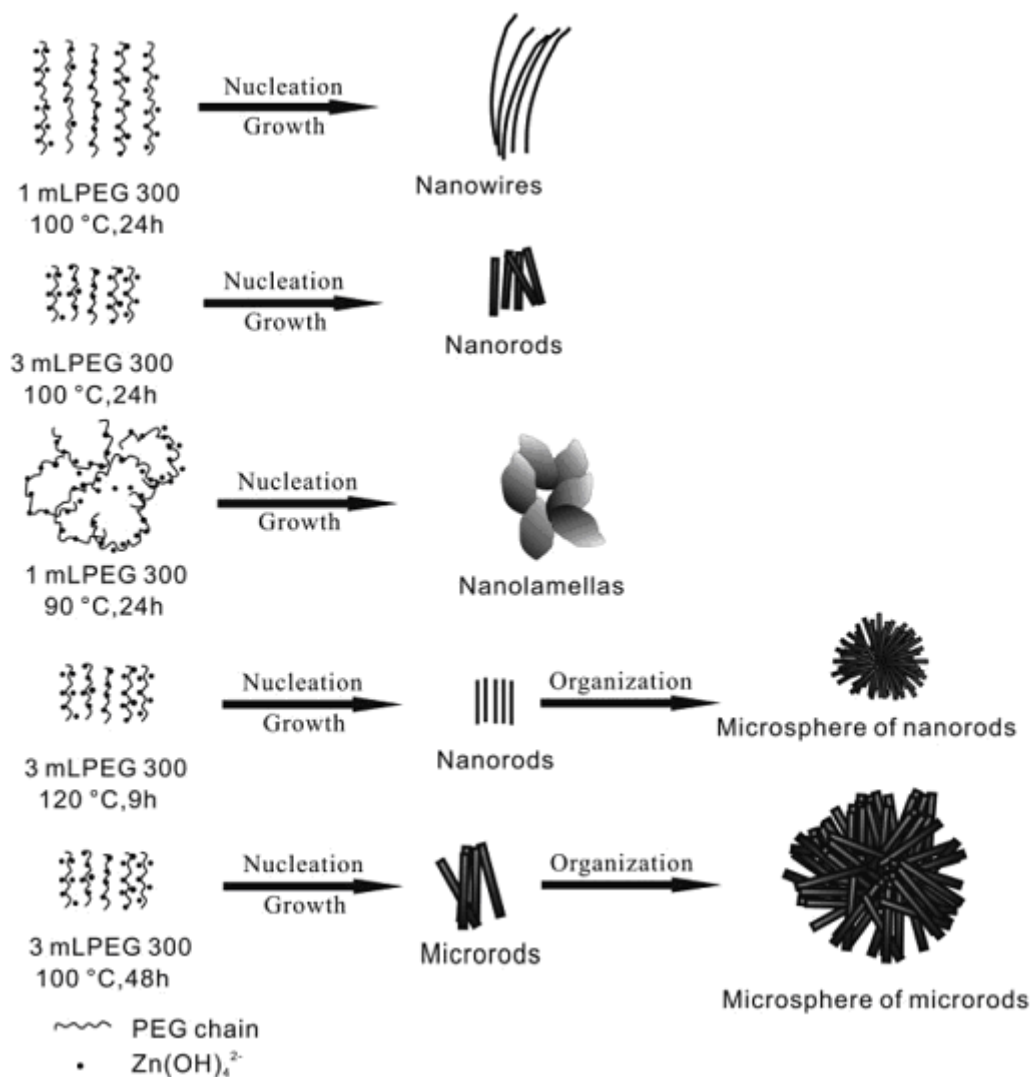


Figure 2.10. Schematic illustration of the possible growth mechanisms of  $4\text{ZnO}\cdot\text{B}_2\text{O}_3\cdot\text{H}_2\text{O}$  under different initial conditions (Source: Shi et al., 2008a).

In zinc borate production either using borax decahydrate or boric acid as a boron source, controlled release of one of reactants or addition of modifying agent were used to control particle size and morphology of the product. Since zinc borates are sparingly soluble in water (Lide, 2004), as soon as two reactant solutions are mixed they precipitate. But, the analysis of this apparently simple operation can be extremely

difficult. On the other hand, both nucleation and growth mechanisms in metal borate precipitation process are not completely understood. In the synthesis of zinc borate from borax decahydrate-zinc nitrate hexahydrate and boric acid-zinc oxide the data given above should be considered.

## CHAPTER 3

### SUPERCRITICAL FLUIDS

The purpose of this chapter is to acquaint the reader with the unusual properties of supercritical fluids and their applications in various industries. The most important properties, such as physico-chemical and fundamental transport properties are explained based on the mostly used supercritical fluids e.g., ethanol, carbon dioxide and water. Additionally, the application areas of supercritical fluids are exploited and especially, the supercritical fluid drying process is reviewed. In this novel area, there are so many steps that are going to be taken as the awareness of green technologies has been realized. Particularly, the application of supercritical fluid drying in the production of diverse compounds from catalyst to aerogels was introduced.

Since the discovery of supercritical fluid phenomenon by *Cagniard de la Tour* in 1822, a lot of progress has been attained in this area. It can be said that supercritical fluids studies made a boom in 1990s and many short courses or summer schools were held to gather the new scientists all around the world into this novel area. The most of developments regarding the supercritical fluids have emerged in the last three decades, in the extraction of chemicals, foods, pharmaceuticals, fragrances, flavors, nutraceuticals, and pesticides; polymerization, biological reactions, and various organic and inorganic chemical reactions; etching of semiconductors; supercritical drying of aerogels; textile dyeing and dry cleaning; manufacturing of micro and nanoparticles. Today most of the studies regarding supercritical fluid processes focused on drug synthesis, drug development, drug delivery, food industry, pharmaceutical and cosmetic industries, textile and polymer industries.

The basic definition of supercritical fluid could be made as following: When a gas is compressed to a sufficiently high pressure, it becomes liquid. If, on the other hand, the gas that is heated above a specific temperature can not be liquefied regardless of the pressure applied. It does not matter how high pressure is exerted on the hot gas. That temperature is called as the critical temperature ( $T_c$ ) and corresponding vapor

pressure is called as critical pressure ( $P_c$ ). The state of substance above these conditions is known as supercritical fluid (SCF). The supercritical fluid has both the gaseous property of being able to penetrate anything, and the liquid property of being able to dissolve materials. Both the capability of some supercritical fluids to replace toxic solvents and tunable solvent properties has led to the current scientific and industrial interest in supercritical fluids.

Currently, particular attention is being paid to the uses of supercritical fluids especially, in fields of reaction, separation, drying and materials processing (nano materials and nano structured materials, thin films, coatings).

### 3.1 Supercritical Fluid (SCF) Properties

Figure 3.1 is the phase diagram of a pure substance in a two coordinate system: P pressure, (P) and temperature, (T). For every substance, there is a value of T and P where liquid phase and gaseous phase have the same density. They are the coordinates of the so called critical point, which ends the liquid-vapor coexistence curve. The area corresponding to temperature and pressure beyond the critical point coordinated is the supercritical region. The fluid in this region is called as a supercritical fluid (SCF).

At the critical point, the density of gas phase becomes equal to that of the liquid phase and the interface between liquid and gas disappears. Thus, supercritical fluid shows unique properties that are different from those of either gases or liquids under standard conditions. The macroscopic behavior of those fluids can be described by mechanical and thermal instabilities. These instabilities result from the singular behavior of some properties, such as isothermal compressibility,  $K_T$ ;

$$K_T = -\frac{1}{V} \left( \frac{\partial V}{\partial P} \right)_T \quad (3.1)$$

where  $V$  is molar volume, which tends to infinity at the critical point (Cansell et al., 2003).

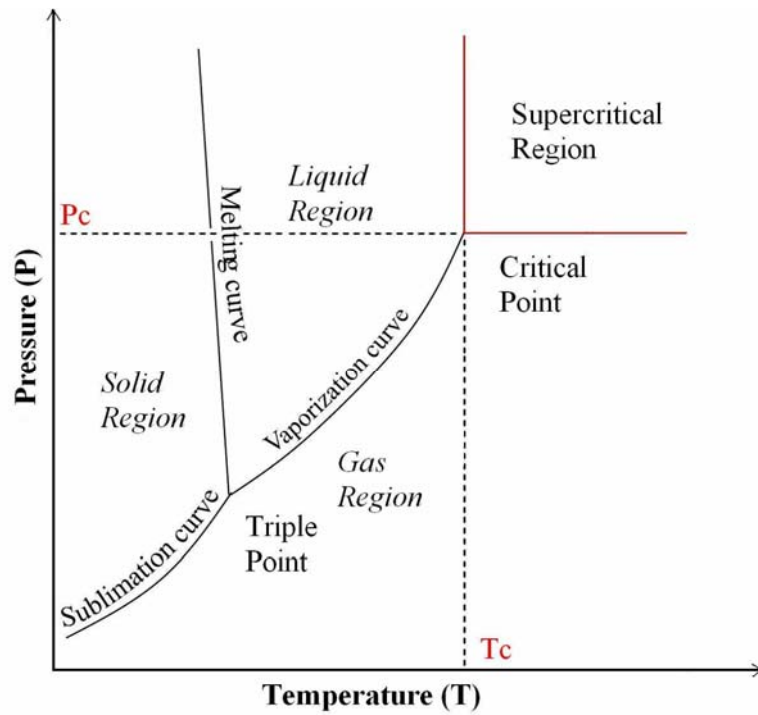


Figure 3.1 Schematic  $P$ - $T$  plane phase diagram of a pure substance.

Figure 3.2 shows the  $P$ - $V$  diagram of a pure substance. Isotherms are obtained using cubic equation of state, which is capable of representing both liquid and vapor behaviors. For the isotherm  $T > T_c$ , at which system is in supercritical region, pressure is

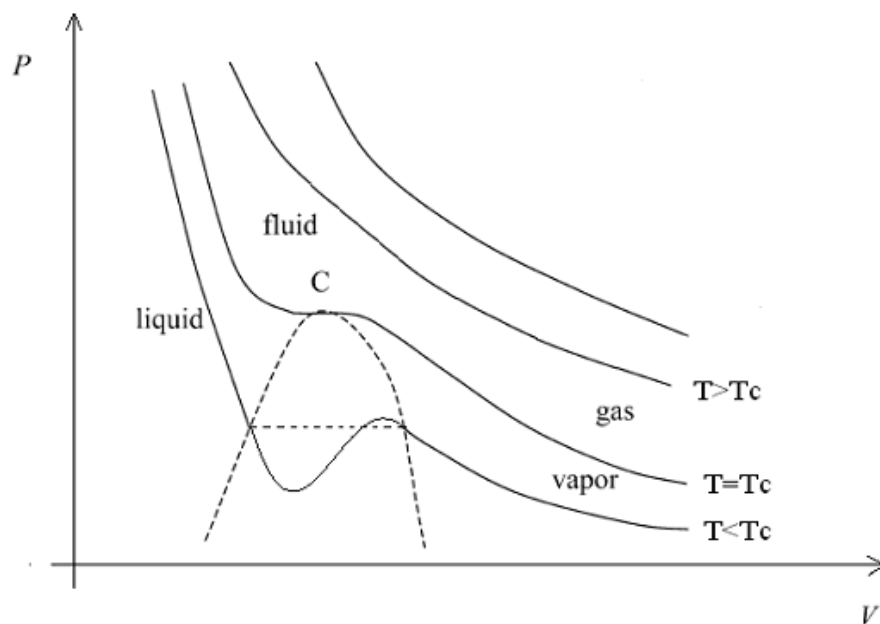


Figure 3.2 Schematic  $P$ - $V$  plane phase diagram for a pure substance.

a monotonically decreasing function with increasing molar volume. All the supercritical isotherms have finite slope everywhere, but the slope may be very small (the compressibility very high) in the vicinity of the critical isochore. When  $T$  is equal to  $T_c$ , the isotherm has a horizontal inflection in which the change of pressure with respect to volume change is zero (slope zero). At this point, isothermal compressibility is infinite and the limit of mechanical stability is reached. From this behavior, it can be inferred that along with isothermal compressibility  $K_T$ , the isobaric heat capacity  $C_P$ , and expansion coefficient  $\alpha_p$ , become infinite at the critical point. These properties are unusually large in the supercritical region (Sengers, 2000). For the isotherm  $T < T_c$ , the pressure decreases rapidly in the liquid region with increasing  $V$ ; after crossing the saturated liquid line it goes through minimum rises to a maximum, and then decreases, crossing the saturated vapor line and continuing into the vapor region. Experimental isotherms do not exhibit that smooth transition from the liquid to vapor region; rather they contain a horizontal segment within two-phase region in which both saturated liquid and vapor coexist. The behaviour, shown by a horizontal dashed line in Figure 3.2 is not analytical, and the fluctuation of the isotherm in two phase region is unrealistic behaviour of equation of state (Smith et al., 1996). Under this condition ( $T < T_c$ ), pressure, temperature and chemical potential, called field variables, are equal in coexisting phases. On the other hand, volume, density, enthalpy, entropy, which are called as density variables, are not equal in two phases (Sengers, 2000).

The mostly used supercritical fluids and their properties are given in Table 3.1. Carbon dioxide is usually preferred supercritical fluid since it is non toxic, non-flammable, and inexpensive and having mild critic temperature ( $T_c = 31.1\text{ }^\circ\text{C}$ ) and other properties could be seen in Table 3.1. The important properties of supercritical fluids will be reviewed based on those well known substances (water, carbon dioxide, and ethanol) so that unusual properties can be comprehended without difficulty. As it is accepted that supercritical fluids have densities that are intermediate between those of liquid and vapors, it may sound logical to assume their properties are also intermediate. This is valid for many properties, but not for all.

In most of the chemical engineering processes, heat and mass transfers involve for conversion of matter. In order to evaluate the transfer processes in various media, non-dimensional numbers, such as Reynolds number (flow effect), Prandlt number (for heat transfer), Schmidt number (for mass transfer) and including all of them Nusselt number are usually used. The comparison of conventional and supercritical fluids was

done by Subra and Jestin (1999) using the non dimensional numbers for heat and mass transfers. Figure 3.3 shows the general behavior of liquids, gases, and supercritical fluids regarding Pr and Sc numbers.

Table 3.1 Properties of some supercritical fluids  
(Source: Smith et al., 1996)

Fluid	Normal Boiling Point (°C)	Critical Constants		
		Pressure (bar)	Temperature (°C)	Density (g.cm <sup>-3</sup> )
Carbon Dioxide	-78.5	73.8	31.1	0.468
Ethane	-88	48.8	32.2	0.203
Ethanol	78.5	61.4	240.8	0.276
Ethylene	-103.7	50.4	9.3	0.200
Propane	-44.5	42.5	96.7	0.220
Propylene	-47.7	46.2	91.9	0.23
Benzene	80.1	48.9	289.0	0.302
Toluene	110.0	41.1	318.6	0.290
Ammonia	-33.4	112.8	132.5	0.240
Water	100.0	220.5	374.2	0.272

Supercritical fluids are much better than gases in transferring both heat and mass as indicated in Figure 3.3. When they are compared to liquids, performances in mass transport are lesser while heat transport efficiencies can attain a comparable level (Subra and Jestin, 1999).

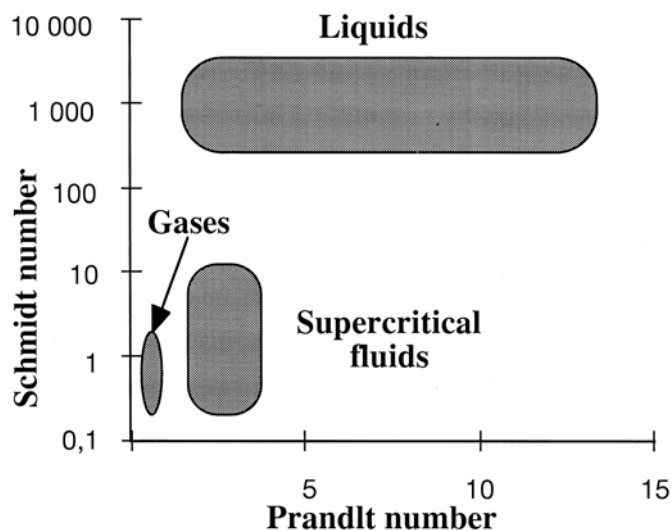


Figure 3.3 Transport properties  
(Source: Subra and Jestin, 1999).

### 3.1.1 Viscosity

The viscosity of a fluid measures its tendency to dissipate energy when disturbed from equilibrium by the imposition of a flow field. The viscosity is defined by the linear, phenomenological relationship known as Newton's law (Arai et al., 2002). When a shear stress is applied to a fluid, motion of the fluid occurs and a velocity gradient is established in the fluid. If the shear stress per unit area at any point is divided by the velocity gradient, the ratio obtained can be defined as the viscosity of the fluid. The coefficient of the shear stress of a flowing fluid or viscosity is defined by the linear relation:

$$\tau = -\eta \left( \frac{d_u}{d_z} \right) \quad (3.2)$$

where  $\tau$  is the shear stress resulting from the applied velocity gradient  $\left( \frac{d_u}{d_z} \right)$ , normal to the direction of the flow. The proportionality constant,  $\eta$ , is simply called viscosity and depends on the thermodynamic state variables, such as its temperature and pressure (or density) (Mukhopadhyay, 2000). In order to grasp the variation of viscosity of a supercritical fluid with respect to other variables e.g., pressure, temperature and density, one should comprehend response in both liquid and gas phases. For this aim, a brief review for viscosity of both liquid and gas phases will be made.

The viscosity of low density gases is independent of pressure (or density) and can be expressed as a function of temperature. In this case, the viscosity is proportional to the square root of the absolute temperature  $T$ , and dilute gases become more viscous at higher temperatures. This behaviour is certified by simple kinetic theory. In this theory, the gaseous viscosity of spherically symmetric monatomic molecules at low pressure is expressed by the following equation:

$$\eta = \left( \frac{\rho v l}{3} \right) \quad (3.3)$$



where  $\rho$  is density of the gas,  $v$  is the average velocity, and  $l$  is the mean free path. As the pressure dependency of the density is offset by that of the mean free path, the viscosity is almost constant over the low-pressure region. Since average velocity is proportional to  $T^{1/2}$ , the viscosity is proportional to  $T^{1/2}$ .

On the other hand, as the pressure increases further, the viscosity also becomes greater. This difference in the pressure dependency of viscosity between a dilute gas and a dense gas is caused by the variations in the mechanisms of momentum transfer. In a dilute gas, it is the molecules that transport the momentum, while in the dense gas transport of momentum occurs over nonzero distance on collision. The molecular interaction plays an important role in momentum transport in dense fluids.

The liquid viscosity decreases exponentially with increasing temperature. This can be explained by the formation of a hole or increase of the free volume. In order to represent this viscosity behavior, many models have been proposed, as a rigorous theoretical treatment is hardly possible for liquid viscosity analysis (Arai et al, 2002).

In general, the isothermal viscosity of a SCF solvent increases with increasing pressure. It decreases with an increase in temperature at a constant pressure up to a minimum as in the case of liquid, then increases with temperature as in the case of a gas at high reduced temperatures. The change of viscosity with respect to temperature and pressure variation was examined for carbon dioxide using the data provided by Zabaloy and co-workers (2005). Figure 3.4 shows the viscosity as a function of pressure at different temperatures e.g., 310, 380 and 900 K. For instance, at 310 K, which is 5 K above  $T_c$ , viscosity ascends abruptly around  $P_c$  then rises gradually with increasing pressure. And at 380 K, viscosity starts to increase smoothly beyond the critical pressure. Finally, at 900 K, viscosity is not affected significantly from the pressure alteration. At constant pressure, which is around critical pressure, viscosity firstly decreases then increases with rising temperature. But, far way from the  $P_c$ , viscosity decreases with increasing temperature.

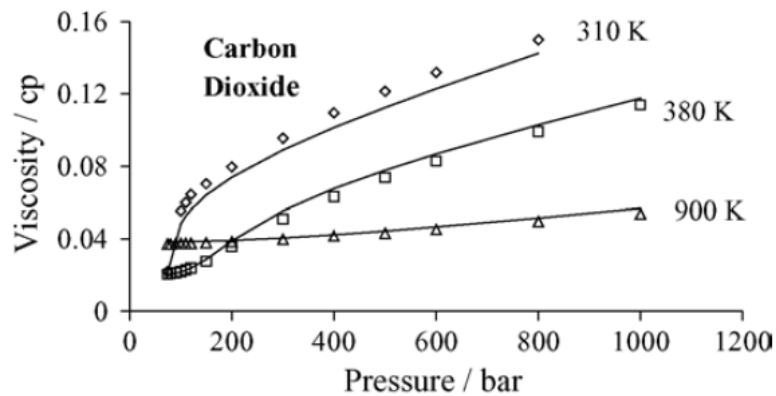


Figure 3.4. Viscosity of carbon dioxide as function of pressure at different temperatures (Source: Zabaloy et al., 2005).

### 3.1.2. Diffusion Coefficient

The phenomena of momentum, heat and mass transfer in fluids are analogous. The transferred quantities are proportional to the gradients of velocity, temperature, and concentration, and phenomenological relationships are referred to as Newton's law, Fourier's law and Fick's law, respectively. Since supercritical fluids are used in most of the unit operations for separation, the value of binary diffusion coefficient rather than self diffusion coefficient is required. But, limited experimental data are available for diffusion in supercritical fluids.

Diffusion coefficients in supercritical fluids are said to be intermediate of those in gases and liquids. Diffusion coefficients in gaseous systems at ambient or low pressures are well represented by the Chapman-Enskog kinetic theory. At higher pressures, the modified theories, or the rough hard sphere theory can give a good representation under limited conditions, so that the expression does not fully cover supercritical fluids, or liquid-like dense fluids. At the mixture critical point, the binary diffusion coefficient approaches zero. The limiting mutual diffusion coefficients at infinite dilution of naphthalene, phenanthrene, and hexachlorobenzene were measured by Akgerman et al. (1996) in the temperature range of 308-328 K and at pressures between 96.4 and 249 bar.

### **3.1.3. Thermal Conductivity**

Thermal conductivity,  $k$ , is a property that gives information about how the material conducts heat. Like viscosity, thermal conductivity increases with density. The thermal conductivities of pure fluids diverge at critical point about half as strongly as the isobaric heat capacity, and therefore the thermal diffusivity,  $k/\rho C_p$ , goes to zero (Sengers, 2000).

### **3.1.4 Dielectric Properties**

The dielectric constant of a solvent is a relative measure of its polarity. For example, water (very polar) has a dielectric constant of 80.10 at 20 °C while n-hexane (very non-polar) has a dielectric constant of 1.89 at 20 °C (Lide, 2004). This information is of great value when designing separation, sample preparation and chromatography techniques in analytical chemistry. Dielectric constant of water usually drops gradually from 80 while the temperature is increased from room temperature toward critical temperature. The critical-point value of the dielectric constant is about 4.0 and undergoes a sharp change at critical point and falls below 2.0 at 25 MPa and 700 K (Sengers, 2000). Under those conditions, water is a low dielectric fluid, and poor solvent for electrolytes and good solvent for organics.

## **3.2 Supercritical Fluid Processes**

Supercritical processes have gained importance since the environmental and health considerations of humanity have developed intensively and capabilities of supercritical fluids have been understood much deeply. Supercritical fluids are widely used in many fields, such as pharmacy, food industry, analytical and preparative separations, organic and inorganic synthesis, waste management, materials processing

(nanomaterials, nanostructured materials, thin films, coating), porous materials, and earth science (Cansell et al., 2003). Applications of supercritical fluids can be summarized as following (Sengers, 2000):

- Supercritical Fluid Extraction (SFE),
- Supercritical Fluid Chromatography (SFC),
- Hydrothermal Processing
- Hydrothermal Destruction of Hazardous Waste
- Polymer Processing.

Since the pharmaceutical and drug materials are sensitive to heat treatment, it is difficult to grind them using conventional size reduction techniques. At this point, the use of supercritical fluids for the fine particle synthesis emerged as an alternative technique. For this purpose, processes that have been developed for the fine particle synthesis are as following: Rapid Expansion of supercritical solutions (RESS) (Matson et al., 1987), supercritical anti-solvent (SAS) (Gallagher et al., 1989), particles from gas saturated solutions (PGSS) (Knez and Weidner, 2003), and supercritical anti-solvent process with enhanced mass transfer (SAS-EM) (Chattopadhyay and Gupta, 2001). They are based on the physical transformation of matter.

When the recent studies have been examined, it is clearly seen that most of the studies have focused on two main areas: The separation of active agents from natural products or from reaction mixture and the production of pharmaceutical materials within the limit of desired particle size. Particle formation using the supercritical fluids (SCF) involves minimal or no use of organic solvents, while the processing conditions are relatively mild. In contrast to the conventional particle formation methods, where a larger particle is originally formed and then converted into the desired size, SCF technology involves the growing of particles in a controlled fashion to attain the desired morphology (Vemavarapu et al., 2005).

### **3.3 Supercritical Fluid Drying**

Supercritical fluid drying technique was firstly proposed by Kistler for the production of aerogel production (Kistler, 1941). Since shrinkage and cracking are

produced by capillary forces during conventional drying, these problems can be avoided by removing the liquid from the pores above the critical temperature ( $T_c$ ) and critical pressure ( $P_c$ ) of the liquid. As indicated in the phase diagram in Figure 3.5, there is no longer any distinction between the liquid and vapor phases: the densities become equal; there is no liquid-vapor interface and no capillary pressure. The capillary pressure ( $P$ ) associated with the liquid and vapor interface within a pore is given by

$$P = \left( \frac{2\sigma \cos(\theta)}{r} \right) \quad (3.4)$$

where  $\sigma$  is surface tension,  $\theta$  is the contact angle between liquid and solid, and  $r$  is the pore radius.

In the process of supercritical drying, a sol or wet gel is placed into an autoclave and heated along a path such as one indicated by arrow in Figure 3.5. The pressure and temperature are increased in such a way that the phase boundary is not crossed, once the critical point is passed, the solvent is vented at a constant temperature which is greater than critical temperature ( $>T_c$ ). Supercritical fluid drying is mostly associated with freeze drying as they both remove the solvent from solid in a different way. Solvents or liquids are first frozen in the solid matrix than they are sublimed from the material. While freeze drying is generally preferred in the drying of biological samples and proteins (Jovanovic et al., 2006), supercritical fluid drying is utilized in the drying of micro electronic devices (Weibel and Ober, 2003 and Wahlbrink et al., 2007). Supercritical carbon dioxide drying has been recently started to be used in temperature sensitive materials drying as carbon dioxide has low critical temperature. Supercritical fluid drying is used not only for inorganic materials but also for organic materials. Lysozyme particle formation using supercritical fluid drying was studied by Bouchard and co-workers (Bouchard et al., 2007). Depending on the process conditions, e.g., ethanol fraction, use of antisolvent, three different particle morphologies were identified: agglomerated nano particles, micro spheres and irregular micro particles.

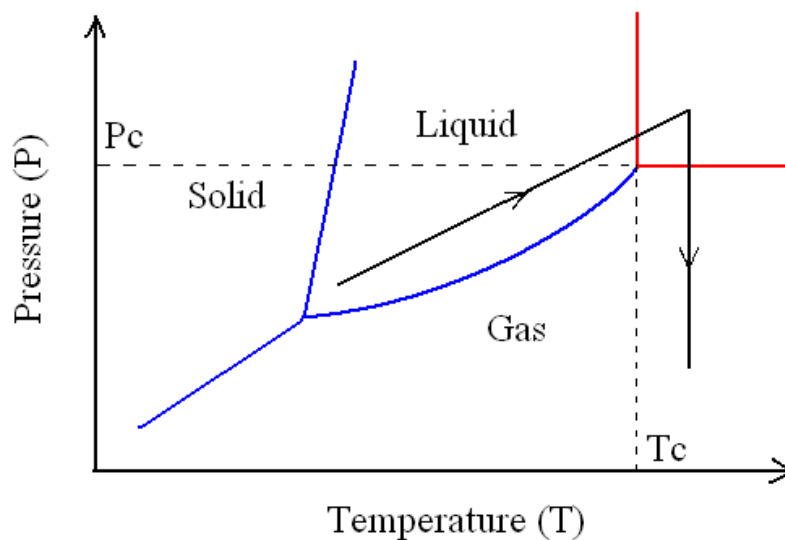


Figure 3.5. Schematic diagram of solid-liquid-vapor boundary.

In aerogel preparation, two step techniques associated with alcohol removing and further dilution and gelation in a non-alcoholic solvent has been used. Acetone, ether and acetonitrile were successfully utilized (Kocon et al., 1998). Strategies that are effective in maintaining the integrity of a gel network during drying are based on minimizing the capillary pressure or eliminating it totally. The minimization of the capillary pressure has been achieved by using solvents that have lower surface tension than that of water ( $72.8 \text{ mN}\cdot\text{m}^{-1}$ ) or that of alcohol ( $22.3 \text{ mN}\cdot\text{m}^{-1}$ ). A complete removal of capillary pressure can be obtained by using supercritical drying in which no phase boundary occurs between liquid and gas phases (Ward and Ko, 1995).

The production of nanosized metal borates was studied using supercritical ethanol drying and supercritical  $\text{CO}_2$  drying (Dong and Hu, 1998; Hu et al., 2002).

### 3.3.1. Supercritical Ethanol Drying

Supercritical ethanol drying (SCED) is generally preferred when the ethanol initially is present as a continuous phase of the system or components of the mixture, especially as it happens in aerogel synthesis. Since the ethanol can be brought into supercritical state just by heating, system pressure is increased first by heating and then keeping the temperature constant above critical temperature, ethanol is released slowly

from the system. In some cases ethanol is extracted by another supercritical solvent without forming any capillary pressure. Both of the above applications are used in research.

The preparation of zirconia aerogel was studied by Cao and co-workers (2002). The preparation consisted of two consecutive steps: alcohothermal synthesis and supercritical fluid drying treatment. In the first step, zirconia alcogel was prepared by using zirconium nitrate and absolute ethanol in autoclave. The mixture was maintained at 383 K for 60 min and then was allowed to cool to room temperature. The obtained alcogel was aged at the room temperature for 60 min. In the second step the resultant alcogel was supercritically dried by 210 mL of ethanol in a 500 mL autoclave. The autoclave was pressurized to 7.0 MPa with high purity nitrogen and was heated to 280 °C with the rate of 2 °C.min<sup>-1</sup> to form supercritical ethanol (553 K, 11.0 MPa). The autoclaved sample was allowed to dry slowly (2 mL ethanol/min) under supercritical condition for 1 h. The larger surface area as well as pore volume and a well developed porosity were obtained for zirconia aerogel in alcohothermal and supercritical drying techniques.

The preparation of silica aerogel from rice hull ash by applying supercritical carbon dioxide drying was studied by Tang and Wang (2005). The rice hull ash having higher silica content was used as a silica source. Silica was extracted by using sodium hydroxide solution and final solution was sodium silicate. Then it was neutralized by sulfuric acid solution to obtain silica gel. After washing by water and solvent exchange with ethanol, the aged gel was dried to produce silica aerogel by supercritical carbon dioxide drying. In the supercritical drying, the prepared silica gel was placed into extraction autoclave whose volume was 50 mL. The system was pressurized by CO<sub>2</sub> to 16 MPa at 25 °C for 24 h. It was assumed that the ethanol in the silica gel was replaced by liquid CO<sub>2</sub> in this period. Then the autoclave was heated to 40 °C with constant pressure of 16 MPa. Dynamic drying was applied with CO<sub>2</sub> flow rate of 1.5 mol.h<sup>-1</sup> for 4 h at 40 °C and 16 MPa. The silica gel obtained had a specific surface area of 597.7 m<sup>2</sup>.g<sup>-1</sup> and bulk density of 38.0 kg.m<sup>-3</sup>. The diameters of the pores inside the aerogel were between 10-60 nm.

The production of nanosized crystalline zinc borate using supercritical ethanol drying technique was prepared by Dong and Hu (1998). The obtained precipitate from the reaction of borax and zinc nitrate was washed by absolute ethanol and filtered. Supercritical ethanol drying was performed by heating sample and liquid ethanol in a

closed vessel up to 536 K and corresponding pressure of 8.3 MPa with heating rate of 5 K.min<sup>-1</sup>. The system was maintained under these conditions for 30 min and then ethanol was released into a pipe containing nitrogen very slowly. They claim that zinc borate with particle size of 20-50 nm was obtained and it improved wear resistance and load carrying capacity of 500 SN base oil by reducing the friction coefficient. In fact, authors did not take into account the interaction of zinc borate obtained from borax with ethanol under supercritical conditions. According to their characterization of the sample after supercritical ethanol drying, XRD pattern of the sample includes ZnO characteristic peaks at 2θ value of 31°, 34°, 36° which meant that zinc borate decomposed partially during supercritical ethanol drying. The other peaks in the XRD pattern showed the presence of anhydrous zinc borate or diborontrioxide.

### **3.3.2. Supercritical Carbon Dioxide Drying**

Since supercritical carbon dioxide has a lower critical temperature (31.1 °C), it is generally preferred in the drying of labile biological samples and other temperature sensitive organic materials. Supercritical CO<sub>2</sub> drying has been utilized in many applications owing to the fact that carbon dioxide is inexpensive, environmentally benign, not flammable, non toxic and can be regenerated easily by a cycle system. The preparation of nanometer sized copper borate with supercritical carbon dioxide drying was studied by Hu and co-workers (Hu et al., 1999). There are some points in the characterization of copper borate need clarification in this study. For instance, thermal behavior of copper borate was not examined; the interaction between copper borate and supercritical CO<sub>2</sub> was not taken into account.

Supercritical drying was also used to form a high surface area and pore volume in catalyst preparation. Alumina aerogel catalysts were prepared by Mizushima and Hori (1995) using two supercritical drying methods (supercritical ethanol drying and ethanol extraction by supercritical carbon dioxide). In the first method, palladium supported alumina aerogel was prepared in autoclave at 270 °C and 26.5 MPa. In the latter, the solvent of the alumina gel was extracted by using supercritical CO<sub>2</sub> at 80°C and 15.7 MPa. The properties of the two catalysts obtained from two different



techniques are given in Table 3.2. Catalyst A prepared by supercritical ethanol drying exhibited a high specific surface area of  $112.8 \text{ m}^2.\text{g}^{-1}$  after firing at  $1200 \text{ }^\circ\text{C}$  for 5 h, while the catalyst B prepared by ethanol extraction using supercritical carbon dioxide, had specific surface area of  $5.2 \text{ m}^2.\text{g}^{-1}$  due to alumina phase transformation.

Table 3.2 Specific surface area (SSA), porosity and bulk density of Pd-supported alumina aerogels after firing at  $1200^\circ\text{C}$  for 5 h (Source: Mizushima and Hori 1995).

Sample	SSA ( $\text{m}^2/\text{g}$ )	Porosity (%)	Bulk Density ( $\text{g}.\text{cm}^{-3}$ )
Aerogel Catalyst A	112.8	90.2	0.23
Aerogel Catalyst B	5.2	38.0	2.5

In the examination of biological samples in transmission electron microscopy (TEM), they need to be dried without destructing their physical structure and decomposing their chemical composition. They are usually dried by using supercritical carbon dioxide since it has low critical temperature which does not decompose biological materials. The supercritical drying of proteins (lysozyme and myoglobin) was studied by Jovanovic and co-workers (2006). In fact they studied the effects of sucrose and trehalose on protein stability during the supercritical drying. As a supercritical fluid, the mixture of carbon dioxide and ethanol was used.

The supercritical fluid aided preparation of aerogels and their characterization were studied by Sunol and co-workers (1995). In their study, inorganic oxide gels ( $\text{NiO}/\text{Al}_2\text{O}_3$ ) were prepared by sol-gel method and then dried using supercritical solvent extraction and supercritical drying to obtain aerogel catalyst as porous powder. Supercritical  $\text{CO}_2$  was used to extract the butanol and methanol that were used in sol-gel step. In the supercritical drying step, butanol and methanol mixture was brought to a supercritical condition and then supercritical fluid was removed slowly from the gel.  $\text{NiO}/\text{Al}_2\text{O}_3$  aerogels in the form of porous powder were produced using supercritical  $\text{CO}_2$  extraction at  $35 \text{ }^\circ\text{C}$  and 100 atm within 40 minutes under  $\text{CO}_2$  flow rate of  $1.4 \text{ l}.\text{min}^{-1}$ . In this study, authors used  $\text{CO}_2$  in the supercritical alcohol drying instead of inert gas.

When ethanol is used as a supercritical solvent for removing water from sample, it is necessary to recover that ethanol for reuse in the system. Since water and ethanol form an azeotropic mixture it is not possible to purify ethanol by conventional

techniques, such as distillation. Instead, vacuum distillation, extraction and distillation, membrane separation are used for obtaining a high purity. All these separation techniques are expensive and they make the supercritical fluid drying process unaffordable. On the other hand, the use of clinoptilolite type natural zeolite for removing the water from aqueous ethanol was proposed by Tihminlioğlu and Ülkü (1996). In this liquid adsorption process, the intraparticle diffusion was pointed out as a main resistance. The utilization of this method for separating ethanol from water with higher purity might make the supercritical ethanol drying method more feasible.

Supercritical fluid drying studies from literature were summarized as given in Table 3.3. Supercritical ethanol drying has been used mostly for aerogel synthesis, in which removal of solvent (ethanol) is critical step. Deformations or collapse of three dimensional network of aerogel structure is prevented by supercritical ethanol drying. However, since ethanol is a flammable solvent, especially in supercritical state, supercritical ethanol drying technique becomes dangerous or it requires some safety precautions. Thus, extraction of ethanol at low temperature by another supercritical fluid, which has lower critical temperature and be less dangerous, e.g., carbon dioxide was proposed and used for aerogel and nanoparticle synthesis.

Supercritical ethanol drying was used for synthesizing nanosized metal (zinc, titanium, and magnesium) borates to prevent particle agglomeration. Thermal stability of metal borates and interactions with solvent during supercritical ethanol drying are important points that were not considered in previous studies (Dong and Hu., 1998; Hu and Dong, 1998; Hu et al., 2002).

Table 3.3. Supercritical fluid drying studies

<b>Dried Matter</b>	<b>Removed Solvent</b>	<b>Supercritical Fluid</b>	<b>Pressure (MPa)</b>	<b>Temperature (°C)</b>	<b>Drying time (h)</b>	<b>Reference</b>
NiO/Al <sub>2</sub> O <sub>3</sub> aerogel	Butanol-methanol	Carbon dioxide	10	35	0.67	(Sunol et al., 1995)
Alumina aerogel	Ethanol	Ethanol	26.5	270	-	(Mizushima and Hori, 1995)
	Ethanol	Carbon dioxide	15.7	80	-	
Copper Borate	n-propanol, benzene	Carbon dioxide	6-6.5	40°	2.5	(Hu et al., 1999)
Zinc Borate	Ethanol	Ethanol	8.3	263	0.5	(Dong and Hu, 1998)
Titanium borate	Ethanol	Ethanol	-	263	0.5	(Hu and Dong, 1998)
Magnesium Borate	Ethanol	Ethanol	8.3	263	0.5	(Hu et al., 2002)
Zirconia aerogel	Ethanol	Ethanol	11	280	1.0	(Cao et al., 2002)
Silica aerogel	Ethanol	Carbon dioxide	16	40	4.0	(Tang and Wang, 2005)
Lysozyme and myoglobin	Ethanol-Carbon dioxide	Carbon dioxide	10	37	0.27	(Jovanovic et al., 2006)

-: No information given.

## CHAPTER 4

### MATERIALS AND METHODS

#### 4.1 Materials

The chemicals used in this study can be divided into two main groups: Raw materials utilized in the production of zinc borate and the materials used in the supercritical fluid drying of zinc borate samples. Zinc borate was produced using both analytical grade and industrial grade boron chemicals. At the beginning of the study, industrial grade boric acid (99.9 %) and borax decahydrate (99.9 %) obtained from Eti Maden were used in the synthesis of zinc borate. In the second part, sodium borate decahydrate (99.5-105.0%) from Sigma-Aldrich, boric acid (99.99 %) from Aldrich, micronized zinc oxide and nanosized zinc oxide, particle size <100 nm (99.9 %) from Sigma-Aldrich, zinc nitrate hexahydrate (99.9 %) from Fluka were used in the production of zinc borate species. Oleic acid obtained from Sigma-Aldrich (99.0 %) was used in reactions as a modifying agent. D-Mannitol used in titration was supplied from Sigma-Aldrich. De-ionized water obtained from purification system, ethanol (99.9 %) and methanol (99.9 %) from Aldrich were used in experiments.

CO<sub>2</sub> (99.9 %) was obtained from Air Gas Company and ethanol (99.8 %) from Riedel were used in supercritical carbon dioxide and ethanol drying, respectively. N<sub>2</sub> supplied by Karbogaz was also used to remove oxygen in supercritical ethanol drying. The zinc borate samples produced in our laboratory and a commercial zinc borate (2ZnO·3B<sub>2</sub>O<sub>3</sub>·3.5H<sub>2</sub>O) that was supplied by US Borax Inc. were used in supercritical ethanol drying.

### 4.1.1. Boric Acid

Boric acid contains the elements boron, oxygen, and hydrogen ( $H_3BO_3$ ). Boric acid is white, odorless, and nearly tasteless. The important property of boric acid is its boron oxide content and is graded according to this value. The  $B_2O_3$  content of the boric acid used in experiments was minimum 56.25 % by weight. One of the important parameters in the use of boric acid is to pay attention to the variation of its solubility as a function of temperature. Figure 2.3. shows the solubility of boric acid in water. The properties of boric acid given by Eti Maden are summarized in Table 4.1.

Table 4.1. Technical grade, granular, low sulphate boric acid,  $H_3BO_3$ , chemical analysis (Source: Eti Maden, 2009)

Component	Unit	Content
$B_2O_3$	%	56.25 min.
Purity	%	99.90 min.
$SO_4$	ppm	130 max.
Cl	ppm	15 max.
Fe	ppm	10 max.

### 4.1.2. Zinc Oxide

Zinc oxide occurs naturally as mineral zincite. It is an amorphous white or yellowish powder, insoluble in water and alcohol but soluble in acid and alkali. Zinc oxide particles may be spherical, acicular or nodular depending on the manufacturing process. The particle shape is important for maximizing physical properties. Zinc oxide is an amphoteric oxide which exhibits both acidic and basic properties depending on the medium where it is present.

### 4.1.3. Disodium Tetraborate Decahydrate (Borax Decahydrate)

Disodium Tetraborate Decahydrate is an important boron mineral which has a chemical formula of  $\text{Na}_2\text{B}_4\text{O}_7 \cdot 10\text{H}_2\text{O}$  or  $\text{Na}_2\text{O} \cdot 2\text{B}_2\text{O}_3 \cdot 10\text{H}_2\text{O}$ . It has monoclinic crystal structure and is widely used in the production of other borate derivatives. The properties of borax decahydrate is given in Table 4.2

Table 4.2 Technical grade granular borax decahydrate,  $\text{Na}_2\text{B}_4\text{O}_7 \cdot 10\text{H}_2\text{O}$ , chemical analysis (Source: Eti Maden, 2009)

Component	Unit	Content
$\text{B}_2\text{O}_3$	%	36.47 min.
Purity	%	99.90 min.
$\text{SO}_4$	ppm	70 max.
Cl	ppm	50 max.
Fe	ppm	10 max.

Borax dissolves easily in water forming borate anion and sodium cation. The solubility plot of borax in water is given in Figure 2.3.

### 4.1.4. Zinc Nitrate Hexahydrate

Zinc nitrate hexahydrate is a white tetragonal crystal; melting point  $36.5\text{ }^\circ\text{C}$ ; losing all water at  $105\text{ }^\circ\text{C}$  to form anhydrous one. It is soluble in alcohol and water.

## 4.2. Methods

Zinc borate species were produced by using two different boron sources. In the first one, zinc borate was produced from reaction of boric acid and zinc oxide. In the latter, zinc borate was prepared by using borax decahydrate and zinc nitrate hexahydrate. The reactions were carried out in  $0.25\text{ dm}^3$  glass bottle on a magnetic stirrer and  $0.30\text{ dm}^3$  (2.5 inches in diameter and 4 inches inside depth) stainless steel

reactor with mechanical stirrer. Temperature of reaction media was maintained using a heating tape on the reaction vessel that was controlled by a temperature controller.

#### 4.2.1. Production of Zinc Borate from Boric Acid and Zinc Oxide

In the production of zinc borate from boric acid and zinc oxide a mechanical-stirred stainless steel reactor or a magnetically-stirred glass reactor was used. The mechanical stirred reactor, which is part of supercritical ethanol drying system, is shown in Figure 4.1. The photograph of this reactor system that was utilized in both zinc borate synthesis and supercritical ethanol drying of zinc borate samples is shown in Figure 4.2. Temperature controller and pressure gauge features are given in Appendix A. Detailed drawing of reactor system (vessels and pipelining) is given in Appendix B.

**Production in a Magnetically Stirred Glass Reactor:** The reaction between boric acid and zinc oxide was carried out at 70 °C and 90 °C for 5 h and by using a B<sub>2</sub>O<sub>3</sub>/ZnO molar ratio of 2.0 (Sawada et al., 2004) and at different concentrations of boric acid with the mixing rate of 155 rpm in glass reactor. The effect of nanosized zinc oxide in the reaction was also examined. In the experiments, ZnO was added into boric acid solution at the reaction temperature of 90 °C. Experimental conditions are given in Table 4.3.

To remove the unreacted boric acid from formed product, the prepared precipitates were washed several times using de-ionized water. Zn, B(OH)<sub>3</sub> contents and pH of the mother liquid and wash water were measured.

The effect of ultrasonic treatment in the reaction between zinc oxide and boric acid was examined. In the generation of ultrasonic waves, 600 W, 20 kHz sonic generators (Ace Glass Inc) and titanium horn (Sonic and Materials Inc) were used. The reaction was carried out in the 30% of maximum amplitude.

**Production in a Mechanically Stirred Stainless Steel Reactor:** The effect of reaction time and comparison of one step process with two step process were examined using the mixing rate of 900 rpm in mechanical stirring reactor. The details of experiments performed in mechanical stirring reactor are given in Table 4.4.

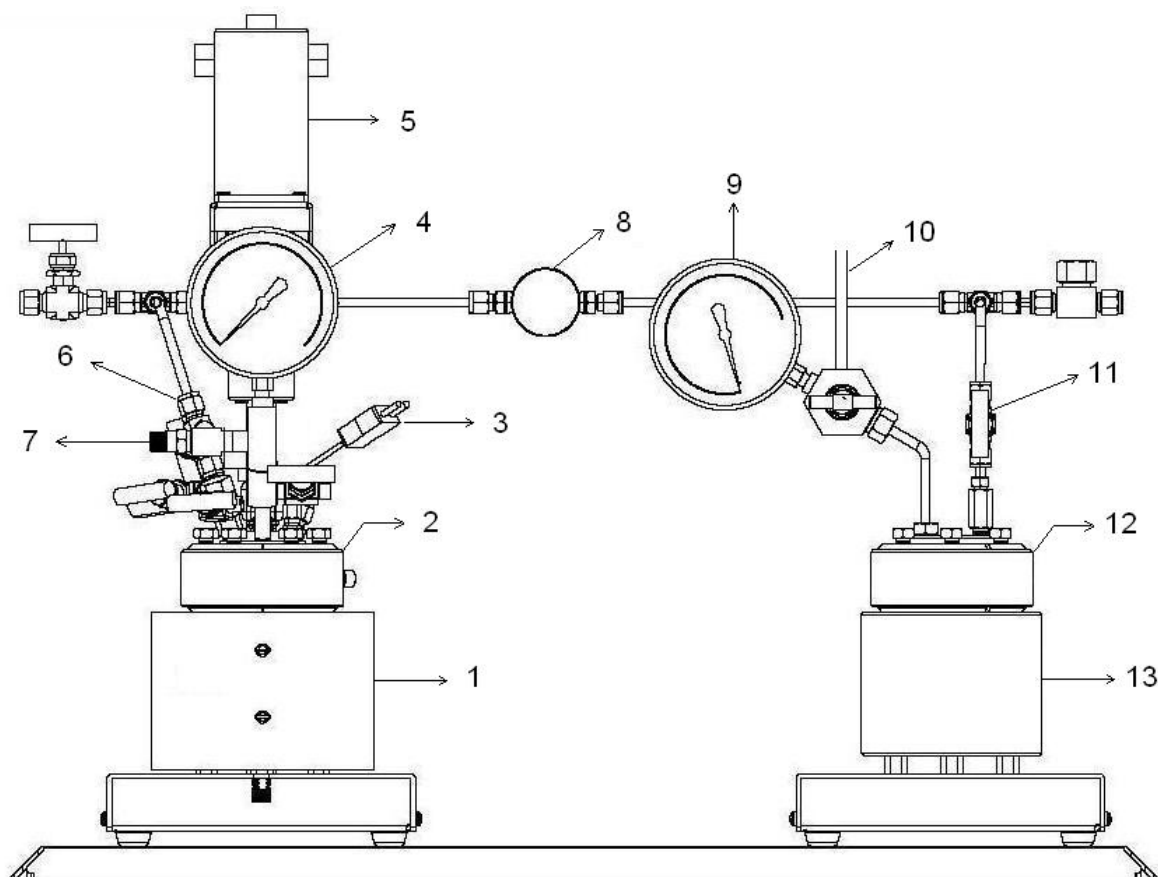


Figure 4.1. Schematic representation of reactor system: 1) High pressure reactor and surrounding heating block, 2) Split-Ring closure, 3) Thermocouple connection, 4) Pressure gage, 5) Stirrer motor and magnetic drive unit 6) Needle valve and reactor outlet connection 7) Rupture disc 8) Back pressure regulator, 9) Pressure gage, 10) Exit pipe, 11) Needle valve and vessel inlet, 12) Split-Ring closure, 13) Low pressure vessel.

The impeller used in the reactor is shown in Figure 4.3. It is a four-bladed, turbine type impeller.





Figure 4.2. Photograph of reactor system.



Figure 4.3. Photograph of impeller used in the stainless steel reactor.

Table 4.3. Experimental conditions of reaction between zinc oxide and boric acid in a magnetically stirred glass reactor

Sample	Reaction		Mixing Rate (rpm)	Explanation
	Temp. (°C)	Time (h)		
S-1	70	5.0	155	B <sub>2</sub> O <sub>3</sub> /ZnO molar ratio of 2.0, stoichiometric amount of ZnO and 3.0 mol.dm <sup>-3</sup> 50 mL boric acid
S-2	90	5.0	155	B <sub>2</sub> O <sub>3</sub> /ZnO molar ratio of 2.0, stoichiometric amount of ZnO and 4.0 mol.dm <sup>-3</sup> 50 mL boric acid
S-3	90	5.0	155	B <sub>2</sub> O <sub>3</sub> /ZnO molar ratio of 2.0, stoichiometric amount of ZnO and 3.0 mol.dm <sup>-3</sup> 50 mL boric acid
S-4	90	5.0	155	B <sub>2</sub> O <sub>3</sub> /ZnO molar ratio of 2.0, stoichiometric amount of ZnO and 4.7 mol.dm <sup>-3</sup> 50 mL boric acid
S-5	90	5.0	155	B <sub>2</sub> O <sub>3</sub> /ZnO molar ratio of 2.0, stoichiometric amount of ZnO and 4.7 mol.dm <sup>-3</sup> 50 mL boric acid, under sonication
S-6	90	5.0	155	B <sub>2</sub> O <sub>3</sub> /ZnO molar ratio of 2.0, stoichiometric amount of ZnO and 4.7 mol.dm <sup>-3</sup> 50 mL boric acid, with nano zinc oxide
S-7	90	6.0	155	B <sub>2</sub> O <sub>3</sub> /ZnO molar ratio of 2.0, stoichiometric amount of ZnO and 4.7 mol.dm <sup>-3</sup> 50 mL boric acid, with oleic acid and ethanol

Table 4.4. Experimental conditions of reaction between zinc oxide and boric acid in a mechanically stirred stainless steel reactor

Sample	Reaction		Mixing Rate (rpm)	Explanation
	Temp. (°C)	Time (h)		
S-8*	90	2.0	900	B <sub>2</sub> O <sub>3</sub> /ZnO molar ratio of 2.0, stoichiometric amount of ZnO and 4.7 mol.dm <sup>-3</sup> 100 mL boric acid
S-9*	90	3.0	900	B <sub>2</sub> O <sub>3</sub> /ZnO molar ratio of 2.0, stoichiometric amount of ZnO and 4.7 mol.dm <sup>-3</sup> 100 mL boric acid
S-10*	90	4.0	900	B <sub>2</sub> O <sub>3</sub> /ZnO molar ratio of 2.0, stoichiometric amount of ZnO and 4.7 mol.dm <sup>-3</sup> 100 mL boric acid
S-11	90	4.0	900	B <sub>2</sub> O <sub>3</sub> /ZnO molar ratio of 2.0, stoichiometric amount of ZnO and 4.7 mol.dm <sup>-3</sup> 100 mL boric acid

\*: Reactants firstly mixed at 60 °C for 1.5 h

In order to obtain the zinc borate in nanosized form, oleic acid was added into reactants as a modifying agent. Oleic acid was dispersed in 15 ml of ethanol considering 1.0 % of total reactants' mass and added into reaction media.

## 4.2.2. Production of Zinc Borate from Borax Decahydrate and Zinc Nitrate Hexahydrate

In this part, zinc borate was produced by using 50 ml, 1.0 mol.dm<sup>-3</sup> borax decahydrate and 50 ml, 1.0 mol.dm<sup>-3</sup> zinc nitrate hexahydrate at 70 °C for different reaction times. The experimental conditions of these reactions are given in Table 4.5. The runs between S-12 and S-18 were carried out in a glass reactor and the runs S-19 and S-20 were carried out in stainless steel reactor having turbine type four-bladed impeller.

Table 4.5. Experimental conditions of reaction between borax decahydrate and zinc nitrate hexahydrate

Sample	Reaction		Mixing Rate (rpm)	Explanation
	Temp. (°C)	Time (h)		
S-12	70	1	1100	1.0 mol.dm <sup>-3</sup> 50 mL borax, 1 mol.dm <sup>-3</sup> 50 mL zinc nitrate, mole ratio of borax/zinc nitrate =1.0
S-13	70	2	1100	1.0 mol.dm <sup>-3</sup> 50 mL borax, 1 mol.dm <sup>-3</sup> 50 mL zinc nitrate, mole ratio of borax/zinc nitrate =1.0
S-14	70	3	1100	1.0 mol.dm <sup>-3</sup> 50 mL borax, 1 mol.dm <sup>-3</sup> 50 mL zinc nitrate, mole ratio of borax/zinc nitrate =1.0
S-15	70	4	1100	1.0 mol.dm <sup>-3</sup> 50 mL borax, 1 mol.dm <sup>-3</sup> 50 mL zinc nitrate, mole ratio of borax/zinc nitrate =1.0
S-16	70	5	1100	1.0 mol.dm <sup>-3</sup> 50 mL borax, 1 mol.dm <sup>-3</sup> 50 mL zinc nitrate, mole ratio of borax/zinc nitrate =1.0
S-17	70	6	1100	1 mol.dm <sup>-3</sup> 50 mL borax, 1 mol.dm <sup>-3</sup> 50 mL zinc nitrate, mole ratio of borax/zinc nitrate =1.0
S-18	70	16	1100	1.0 mol.dm <sup>-3</sup> 50 mL borax, 1 mol.dm <sup>-3</sup> 50 mL zinc nitrate, mole ratio of borax/zinc nitrate =1.0
S-19*	70	4	900	1.0 mol.dm <sup>-3</sup> 50 mL borax, 1 mol.dm <sup>-3</sup> 50 mL zinc nitrate, mole ratio of borax/zinc nitrate =1.0
S-20*	70	5	900	1.0 mol.dm <sup>-3</sup> 50 mL borax, 1 mol.dm <sup>-3</sup> 50 mL zinc nitrate, mole ratio of borax/zinc nitrate =1.0
S-21	70	4	550	1.0 mol.dm <sup>-3</sup> 50 mL borax, 1 mol.dm <sup>-3</sup> 50 mL zinc nitrate, mole ratio of borax/zinc nitrate =1.0
S-22*	70	4	900	1.0 mol.dm <sup>-3</sup> 50 mL borax, 1 mol.dm <sup>-3</sup> 50 mL zinc nitrate, mole ratio of borax/zinc nitrate =1.0

\*: Stainless-steel reactor with turbine type impeller was used for those runs.

To remove the unreacted zinc nitrate and sodium borate decahydrate, the prepared precipitates were washed using de-ionized water. Zn, B(OH)<sub>3</sub> contents and pH

were analysed for mother liquid and wash water. Subsequently, zinc borates were washed three times with methanol or ethanol to replace water according to the drying process.

#### 4.2.3. Supercritical CO<sub>2</sub> Drying of Zinc Borate Species

In supercritical CO<sub>2</sub> drying, the prepared zinc borate sample of 4.0 g (wetted by methanol) was firstly packaged in a filter paper pouch and then put into the 0.10 dm<sup>3</sup> extraction autoclave. The autoclave was pressurized with CO<sub>2</sub> up to 10 MPa at 40 °C using a pump (Thar P-50). The CO<sub>2</sub> flow rate was measured by the pump and that value was used in calculation of actual flow rate with the help of calibration factor of pump at 10 MPa and 40 °C. The pressurized CO<sub>2</sub> was sent to extraction vessel through a coil in heating bath at 40 °C. The temperature of extraction vessel was also maintained at 40 °C by a temperature controller and heating tape. Dynamic drying was performed with a CO<sub>2</sub> flow rate of 2.5-3.0 g.min<sup>-1</sup> for different drying times under 10 MPa and 40 °C. Afterwards, the autoclave was slowly depressurized to atmosphere at 40 °C. Finally, supercritical CO<sub>2</sub> dried zinc borate samples were obtained. The schematic drawing of supercritical CO<sub>2</sub> drying system is shown in Figure 4.4.

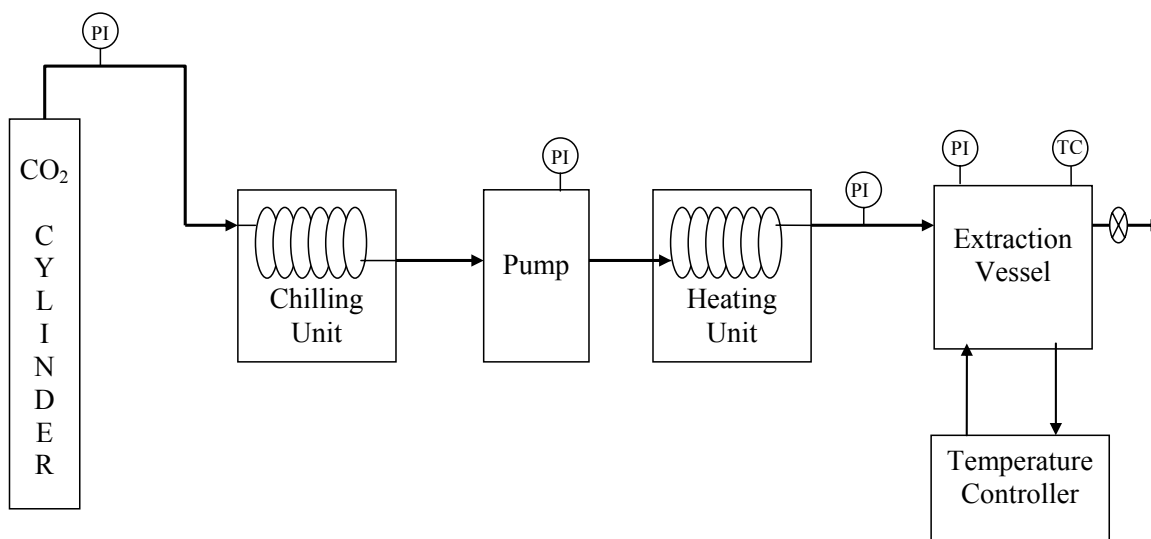


Figure 4.4. Schematic representation of supercritical CO<sub>2</sub> drying system.

The experimental conditions of supercritical CO<sub>2</sub> drying are given in Table 4.6. Drying time between 2-4 h was examined for zinc borate drying.

Table 4.6. Supercritical carbon dioxide drying conditions

<b>Inlet Sample</b>	<b>Outlet Sample</b>	<b>Drying Time (h)</b>	<b>Initial Mass (g)</b>	<b>Final Mass (g)</b>
S-4	S-4-SC	2	2.5	2.4
S-16	S-16-SC1	2	4.0	1.6
S-16	S-16-SC2	3	4.0	1.6
S-16	S-16-SC3	4	3.7	1.5

#### **4.2.4. Subcritical and Supercritical Ethanol Drying of Zinc Borate Species**

The supercritical ethanol drying system that was used in the experiments is shown in Figure 4.5. Zinc borate samples that were produced from borax and boric acid in our laboratory were washed first by ethanol to remove water before supercritical ethanol drying. After washing and drying, approximately 8-10 g of zinc borate sample was placed into 0.30 dm<sup>3</sup> high pressure reactor as shown in Figure 4.1. Commercial zinc borate obtained from US Borax Inc. was directly used in supercritical ethanol drying. The amount of ethanol was calculated as 0.11 dm<sup>3</sup> considering ethanol specific volume at supercritical conditions and reactor volume. Before starting to heat the system, nitrogen gas was passed through the system to remove oxygen in the reactor and pipelines. The supercritical pressure of ethanol (6.5 MPa) was attained by heating the system to 250 °C.

Under these conditions, sample was kept for 30 min and without waiting (0 min) and ethanol was released from system slowly at constant temperature. Finally, nitrogen gas was again used to sweep the remaining ethanol through the system and temperature was brought to the room temperature. Zinc borate samples and supercritical ethanol drying conditions are given in Table 4.7. Both phases obtained at the end of supercritical ethanol drying, (the solid phase remained in the reactor and the liquid phase in the expansion vessel) were characterized.

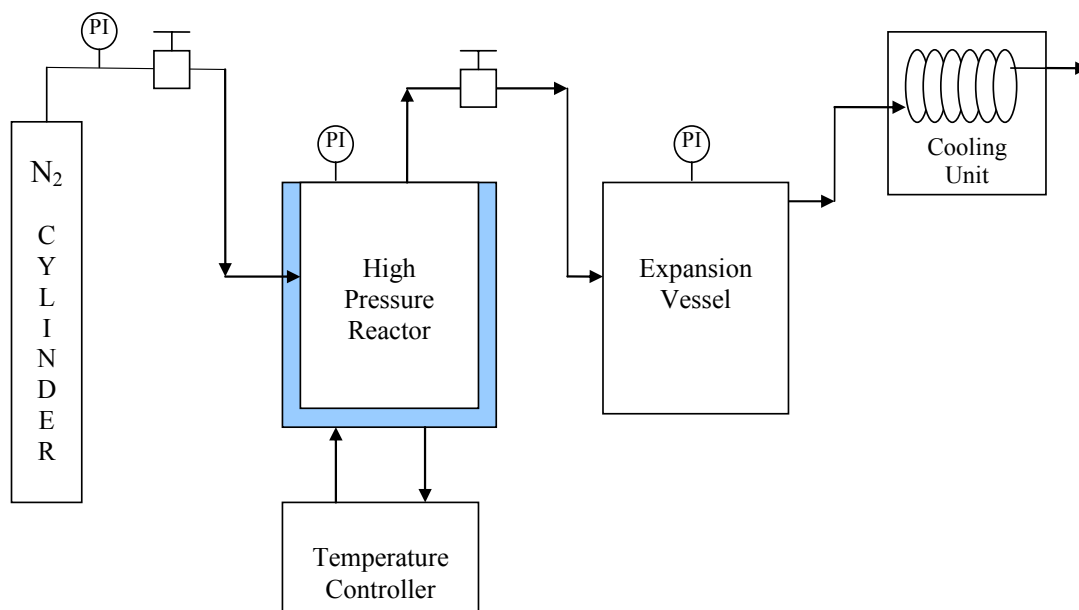


Figure 4.5. Schematic representation of supercritical ethanol drying system.

Table 4.7. Supercritical and subcritical ethanol drying conditions

Inlet Material	Explanation	Conditions	Outlet Product	Period of Drying (min)
S-4	Zinc borate produced from zinc oxide and boric acid	250 °C, 6.5 MPa	ZnB1-SCE	30
ZnB2335	Commercial product (2ZnO·3B <sub>2</sub> O <sub>3</sub> ·3.5H <sub>2</sub> O)	250 °C, 6.5 MPa	ZnB2-SCE	30
ZnB2335	Commercial product (2ZnO·3B <sub>2</sub> O <sub>3</sub> ·3.5H <sub>2</sub> O)	250 °C, 6.5 MPa	ZnB3-SCE	0
ZnB2335	Commercial product (2ZnO·3B <sub>2</sub> O <sub>3</sub> ·3.5H <sub>2</sub> O)	200 °C, 3.0 MPa	ZnB4-SCE*	0
ZnB2335	Commercial product (2ZnO·3B <sub>2</sub> O <sub>3</sub> ·3.5H <sub>2</sub> O)	150 °C, 1.1 MPa	ZnB5-SCE*	0
S-20	Zinc borate produced from borax and zinc nitrate	250 °C, 6.5 MPa	ZnB6-SCE	0
S-20	Zinc borate produced from borax and zinc nitrate	250 °C, 6.5 MPa	ZnB7-SCE	0

\*: Subcritical ethanol drying

In order to determine the interaction of zinc borate with ethanol at subcritical temperature and corresponding pressure, removal of ethanol at 200 °C and 150 °C were

studied. Zinc borate samples and subcritical ethanol drying conditions are given in Table 4.7.

#### 4.2.5. Freeze Drying of Zinc Borate Species

Zinc borates, (S-21 and S-22), whose details introduced in Table 4.5 were dried by freeze drying equipment (Labconco FreeZone-4.5) at temperature of  $-51\text{ }^{\circ}\text{C}$ , and under vacuum of 0.020 mbar until reaching a constant remaining mass.

#### 4.2.6. Analytical Characterization Chemicals and Techniques

Diborontrioxide ( $\text{B}_2\text{O}_3$ ) and zinc oxide ( $\text{ZnO}$ ) contents of zinc borate samples were determined by analytical titration using 0.1 N NaOH and  $0.1\text{ mol}\cdot\text{dm}^{-3}$  EDTA, respectively.

*NaOH Solution*,  $0.1\text{ mol}\cdot\text{dm}^{-3}$ : NaOH solution was used in analytical titration to determine boric acid content of zinc borate after it was dissolved by 6M HCl.

*EDTA Solution*,  $0.01\text{ mol}\cdot\text{dm}^{-3}$ : 3.80 g of disodium dihydrogen ethylenediaminetetraacetate dehydrate was dissolved in 1 L deionized water.

*Buffer Solution*, pH 10: 70 g  $\text{NH}_4\text{Cl}$  was dissolved in 325 mL  $\text{H}_2\text{O}$  and 1135 mL concentric ammonia solution was added and final solution diluted to 2 L by deionized water.

*Indicators*: Erichrome Black T indicator for Zn titration by EDTA, methyl red for HCl titration and phenolphthalein for  $\text{B}(\text{OH})_3$  by NaOH.

In the titration, zinc borate sample was initially dissolved by  $6\text{ mol}\cdot\text{dm}^{-3}$  HCl and completed to 100 mL by deionized  $\text{H}_2\text{O}$  then, 25 mL of that solution was used to determine the Zn content with EDTA titration in the presence of Erichrome Black T indicator and a buffer solution of pH 10. Another 25 mL of that solution, that contains EDTA solution equivalent to zinc ions to prevent the precipitation of Zn with NaOH in the solution, was titrated by 0.1 N NaOH solution in the presence methyl red till color

changes from pale red to yellow. This first titration by NaOH is attributed to the determination of free  $H^+$  ions released by HCl. Mannitol was then added to form a complex with boric acid and releases  $H^+$  proton according to the Equation 2.4 and the resulting solution was titrated with 0.1 N NaOH solution using phenolphthalein as a indicator until color of mixture changes from yellow to deep pink. All the titration experiments were performed twice to obtain more reliable results.

#### **4.2.7. Characterization of Zinc Borate Samples**

The physico-chemical properties of each zinc borate sample were identified by X-Ray diffraction (XRD), Scanning electron microscopy (SEM), Fourier transform infrared spectroscopy (FTIR), and Thermal gravimetric analysis (TGA). Supercritical  $CO_2$  dried zinc borates were characterized by elemental analysis to determine C and H contents. Zinc borate samples produced from boric acid in the stainless-steel reactor was also examined by Differential Scanning Calorimeter (DSC). BET surface area of supercritical ethanol dried zinc borate samples was determined by  $N_2$  adsorption at 77 K. The supercritical ethanol dried zinc borate samples were also examined by transmission electron microscope (TEM). Samples and filtrates were analyzed by analytical titration in order to determine boron and zinc contents.

Densities of zinc borate samples after supercritical ethanol drying were measured using pycnometer (Quantochrome Ultrapycnometer 1000) at 25 °C.

##### **Transmission Electron Microscopy (TEM)**

(TEM), (JEOL JEM 2100F) was used for identification of particle size and morphology of supercritical ethanol dried zinc borate particles. The samples used for TEM characterization were dispersed in absolute ethanol and were sonicated before observation.

##### **Scanning Electron Microscopy (SEM)**

SEM (Philips XL30 SFEG and Zeiss DSM 940) images were used to examine the morphology of the conventional dried and supercritical dried zinc borate particles.



Conductive double sided tape was used to fix the particles to the specimen holder before sputtering them with a thin layer of gold.

### **X-Ray Powder Diffraction (XRD)**

XRD was performed using a X-ray diffractometer (Philips Xpert-Pro). The incident  $\text{CuK}_\alpha$  radiation at 45 kV and 40 mA with 1.54 Å was used in the analysis. The dried sample powders were prepared in a 0.5-mm thick holder. Diffraction patterns were used to determine the type of zinc borate samples. XRD pattern confirms whether the formed zinc borate is amorphous or crystalline.

### **Fourier Transform Infrared Spectroscopy (FTIR)**

Fourier Transform Infrared Spectrometers (Nicolet 360 and Shimadzu 8601) were used to determine chemical structure of the products. Zinc borate-KBr pellets were prepared by mixing 4.0 mg of zinc borate and 196 mg of KBr in an agate mortar and pressing the mixture under 8 tons.

### **Differential Scanning Calorimetry (DSC)**

DSC was performed on a calorimeter (Shimadzu, DSC 50). Dry powder (5-10 mg) was placed in an aluminum pan that was hermetically sealed. For conventional DSC measurements, samples were heated from room temperature to 600 °C at a rate of 10 °C.min<sup>-1</sup>.

### **Thermogravimetric Analysis (TGA)**

Thermal gravimetric analyses (TGA) were carried out by using Shimadzu TGA-51. Zinc borate samples (10-15 mg) were loaded into an alumina pan and heated from room temperature to 600 °C at 10 °C.min<sup>-1</sup> under N<sub>2</sub> flow of 40 mL min<sup>-1</sup>.

### **Conventional Drying of Zinc Borate Samples**

Wet zinc borate samples were dried in an air circulating oven at 110 °C until the constant mass of the sample was attained. The water content of the zinc borate after washing and filtration was measured using moisture analyzer (Sartorius MA 100).

### **Elemental Analysis**

H, C and N content of supercritical carbon dioxide dried zinc borate samples were determined using elemental analyzer (Leco CHNS-932).

### **Particle Size Analysis**

Particle sizes of zinc borate samples were determined using by particle size analyzers (Malvern Mastersizer 2000, Malvern Zetasizer 3000 HSA, and PSS Nicomp 380) and (Sedigraph 5100). While using the zetasizer, samples were dispersed in water by sonication for a while, zinc borate samples were dispersed in water using surfactant for analyzing in Sedigraph.

### **Surface Area Determination**

BET surface area of supercritical ethanol dried samples and freeze dried sample were determined using N<sub>2</sub> adsorption at 77 K in Micromeritics ASAP 2010. Initially samples were degassed at room temperature.

## CHAPTER 5

### RESULTS AND DISCUSSION

Results obtained in this study are going to be introduced in two main sections: The results of zinc borate production from both boric acid and borax decahydrate as a boron source, and the results of supercritical fluid drying and freeze drying of zinc borate species. Supercritical fluid drying results are also subdivided into two groups according to the supercritical fluid used; supercritical carbon dioxide drying and supercritical ethanol drying of the zinc borate species. Before introducing the results, the characterization of reactants are provided and discussed so that any remained reactant in the ultimate product can be easily distinguished.

#### 5.1. Characterization of Raw Materials

The characterization of raw materials is important because of the following reasons; purity of the reactant is vital in the reaction and it determines the quality of the ultimate product and alters its properties. If the purity of raw material is known, it is easily determined that whether there is unreacted raw material in the ultimate product or not. The characterization of boric acid, zinc oxide, borax decahydrate and zinc nitrate hexahydrate was done using FTIR spectroscopy, and X-ray diffraction (XRD).

**Boric Acid and Zinc Oxide:** The FTIR spectra of zinc oxide and boric acid are given in Figure 5.1. The major peaks in Figure 5.1.a and their assigned structure are listed in Table 5.1. The bands at  $1465\text{-}547\text{ cm}^{-1}$  are characteristic peaks of boric acid ( $\text{H}_3\text{BO}_3$ ). The peak at  $400\text{ cm}^{-1}$  wavenumber in Figure 5.1.b belongs to the zinc-oxygen coordination in the IR spectrum. At the same time, the small broad peak at  $3300\text{-}3500\text{ cm}^{-1}$  shows the presence of OH groups or water molecule in the powder product.

XRD patterns of boric acid and zinc oxide utilized in zinc borate production are shown in Figure 5.2. The major peaks in Figure 5.2.a, 14.4°, 27.8°, 30.3°, 31.3°, 40.2°, 41.5°, 42.9°, and 44.3° at 2θ values belong to boric acid which is a layered material with a triclinic crystal structure (Erdemir et al., 1997 and JCPDS 30–0199). All of the peaks at 2θ values of 31.6°, 34.3°, 36.1°, 47.4°, 56.5°, 62.7°, 66.3°, 67.8°, and 69.0° in Figure 5.2.b are well matched with that of bulk ZnO (JCPDS 80–0075) which confirms that the powder used in the production of zinc borate has crystalline structure (Wahab et al., 2007). ZnO having pattern at those 2θ values shows hexagonal structure according to the XRD card data.

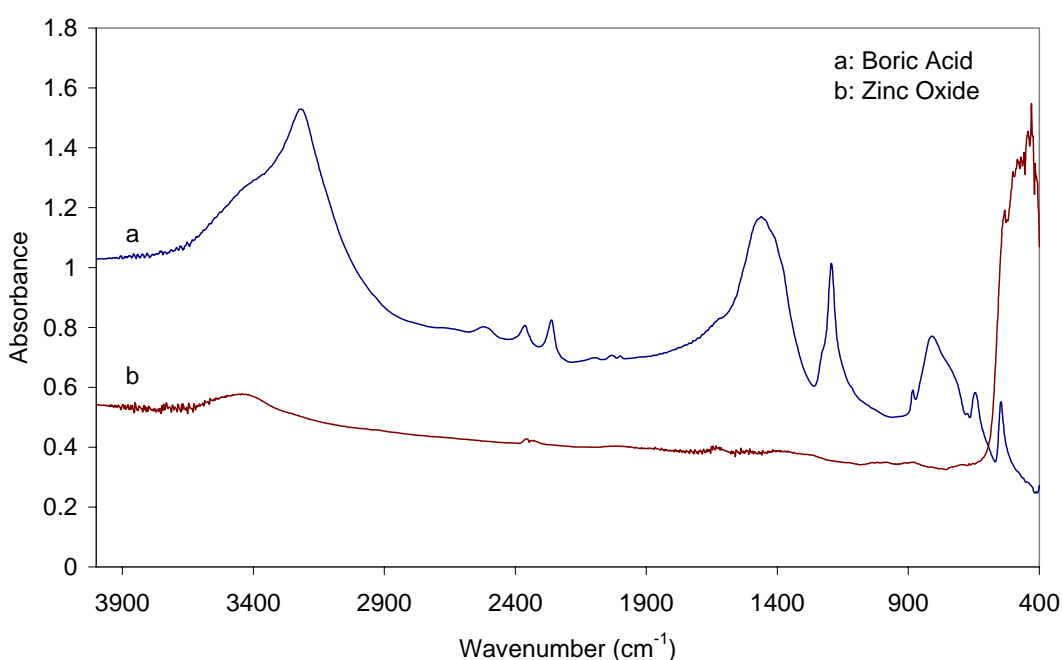


Figure 5.1. FTIR spectra of a) boric acid and b) zinc oxide.

Table 5.1 Major peaks in FTIR spectrum of boric acid  
(Source: Medvedev and Komarevskaya, 2007)

Wavenumber (cm <sup>-1</sup> )	Assigned Structure
3230	O-H stretching
1465	Asymmetric stretching vibrations of B-O in (BO <sub>3</sub> )
1195	B-O-H in plane bending
887	Symmetric stretching vibrations of B-O in (BO <sub>3</sub> )
819	B-O-H out of plane bending
651	Deformation vibration of atoms in B-O
547	B-O-B

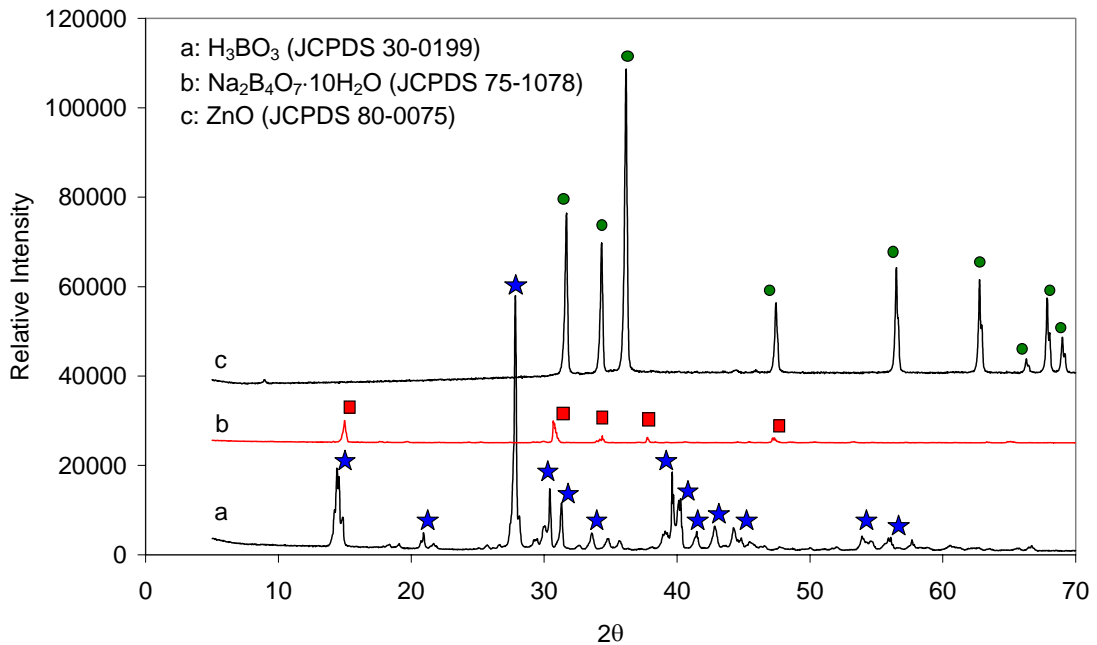


Figure 5.2. XRD patterns of a) boric acid, b) borax decahydrate and c) zinc oxide.

SEM microphotographs of boric acid and zinc oxide are shown in Figure 5.3. It was determined that boric acid particles were between 300-500  $\mu\text{m}$  and zinc oxide particles were smaller than 1.0  $\mu\text{m}$ . Since boric acid is soluble in water, particle size does affect only dissolution rate.

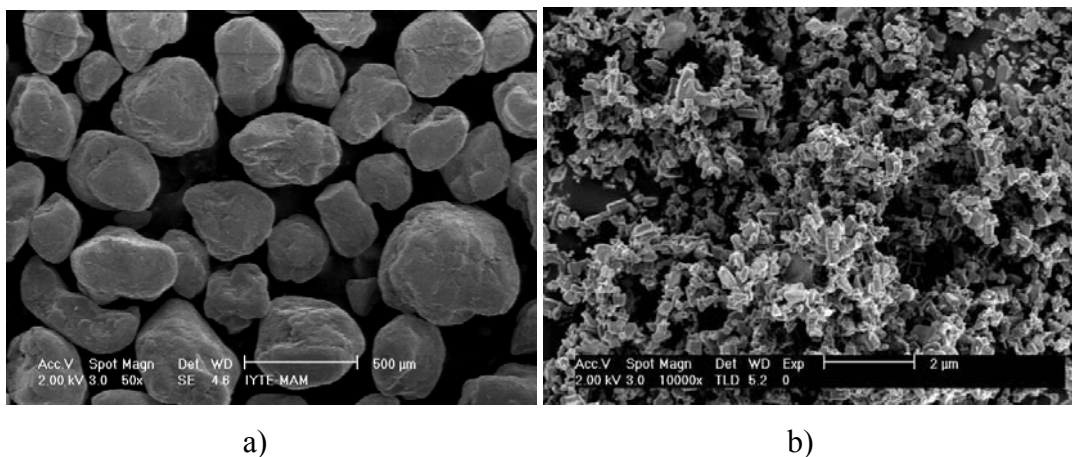


Figure 5.3. SEM microphotographs of a) boric acid and b) zinc oxide

**Borax Decahydrate and Zinc Nitrate Hexahydrate:** Figure 5.4 shows the FTIR spectra of borax decahydrate and zinc nitrate hexahydrate that were used in the zinc borate production. The bands at 1390, 1360 and 1049 $\text{cm}^{-1}$  in Figure 5.4.a are assigned

to the asymmetric stretching ( $\nu_4$ ), symmetric stretching ( $\nu_1$ ) and the N-O stretching ( $\nu_2$ ) (Biswick et al., 2007). The band at  $829\text{ cm}^{-1}$  belongs to asymmetric deformation ( $\nu_2$ ) of nitrate structure. The band at  $1635\text{ cm}^{-1}$  shows that water of crystallization is present in the zinc nitrate structure as it is expected. The broad band at  $3500\text{ cm}^{-1}$  represents the OH groups in water of crystallization. The bands between  $3600\text{--}3200\text{ cm}^{-1}$  in Figure 5.4.b represent the OH groups' coordination in borax structure and hydrogen bonding between OH groups. The bands at  $1695$  and  $1650\text{ cm}^{-1}$  is assigned to the H-O-H bending mode, which shows the compound containing the water of crystallization. The bands at  $1425$ ,  $1360\text{ cm}^{-1}$  and  $1000\text{--}950\text{ cm}^{-1}$  belong to the asymmetric and symmetric stretching vibrations of  $\text{BO}_3$ , respectively. The band at  $1161\text{ cm}^{-1}$  is caused by the vibrations of in-plane bending of B-O-H.

The bands at  $1145\text{--}1045\text{ cm}^{-1}$  and  $837\text{--}829\text{ cm}^{-1}$  are assigned as the asymmetric and symmetric stretching of  $\text{BO}_4$ , respectively. The bands at  $781\text{--}670\text{ cm}^{-1}$  are the out-of-plane bending of B-O-H. The band at  $632\text{ cm}^{-1}$  is assigned to symmetric pulse vibration of triborate anion. The bands at  $545$  and  $460\text{ cm}^{-1}$  are due to the bending of  $\text{BO}_3$  and  $\text{BO}_4$ , respectively (Jun et al., 1995).

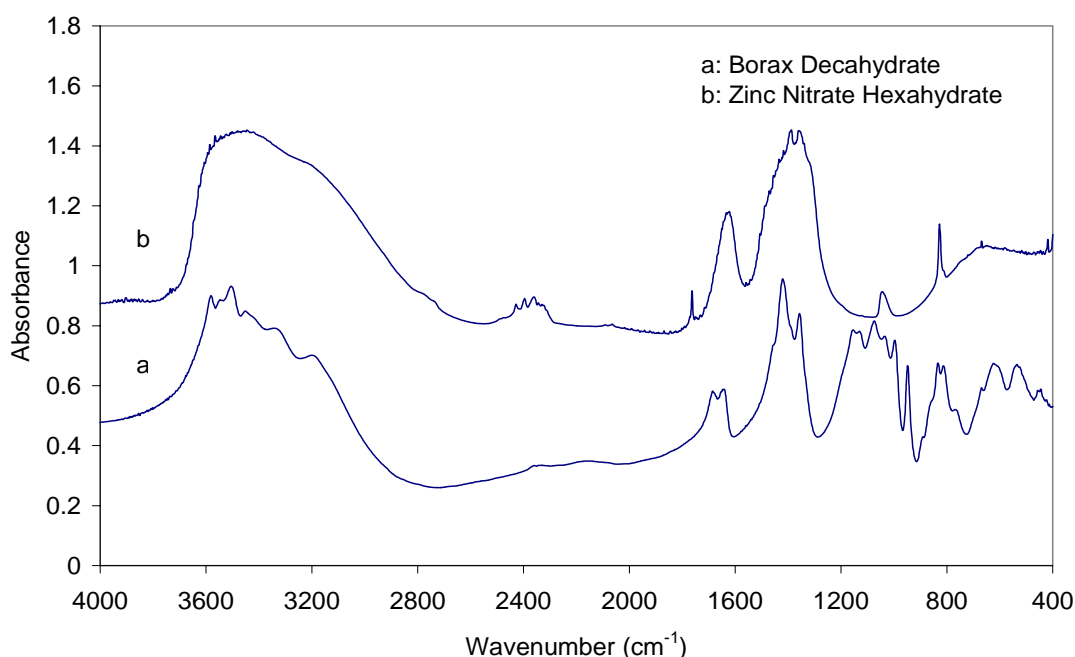


Figure 5.4. FTIR spectra of a) borax decahydrate and b) zinc nitrate hexahydrate.

XRD pattern of borax decahydrate ( $\text{Na}_2\text{B}_4\text{O}_7 \cdot 10\text{H}_2\text{O}$ ) obtained from Eti Maden and used in zinc borate production is shown in Figure 5.2. The major peaks in this pattern are  $14.9^\circ$ ,  $30.6^\circ$ ,  $34.4^\circ$ ,  $37.8^\circ$ ,  $41.5^\circ$ ,  $47.3^\circ$  at  $2\theta$  values belong to borax

decahydrate which has monoclinic structure (JCPDS 75-1078). The observed pattern of borax was also consistent with the pattern given by Waclawska (1995) at  $2\theta$  values between  $10^\circ$ - $50^\circ$ .

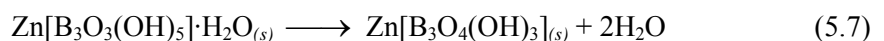
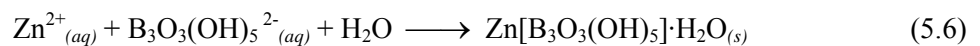
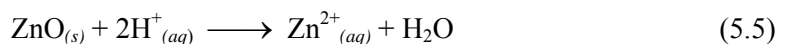
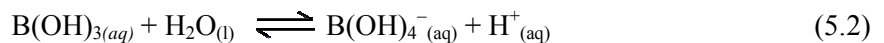
## **5.2. Zinc Borate Production from Boric Acid and Zinc Oxide**

In the production of zinc borate from boric acid and zinc oxide, solubility of boric acid is one of the important parameters which determine reactants' concentration at the reaction temperature. The particle size of zinc oxide is another important parameter since reaction rate is expected to be directly proportional to this property. Although zinc oxide was assumed to be insoluble in the reaction between boric acid and zinc oxide in aqueous phase (Shete et al., 2004), zinc oxide, in fact, dissolves in acidic medium displaying a base property. At this point, particle size of zinc oxide can be the parameter that influences its dissolution rate directly or reaction rate indirectly in the reaction media. In the production of zinc borate from boric acid and zinc oxide, the technique proposed by Sawada and co-workers was used (Sawada et al., 2004). In this technique, two step process including heating periods at  $60^\circ\text{C}$  and  $90^\circ\text{C}$  were applied for 1.5 and 4 h, respectively. In the first step, 1000 mL of  $1.17\text{ mol}\cdot\text{dm}^{-3}$  aqueous solution of boric acid was prepared and to that solution stoichiometric amounts of ZnO was added. Then excess amount of boric acid was added into reaction media keeping the molar ratio of  $\text{B}_2\text{O}_3/\text{ZnO}$  as 2.0. As boric acid is consumed by the reaction, solid boric acid dissolves in aqueous phase depending on solubility at reaction temperature.

### **5.2.1. Reaction Mechanism**

The following reactions occurred in the production of zinc borate from boric acid and zinc oxide (Equations 5.1, 5.2, 5.3, 5.4, 5.5, 5.6 and 5.7). In Equation 5.2, the boric acid reacts with water to form borate anion and a  $\text{H}^+$  proton which provides acidic character. Polyborate anions with the charge of -1 and -2 are formed in Equation 5.3 and

Equation 5.4, respectively. In Equation 5.5, ZnO dissolves in water in the presence of H<sup>+</sup> protons to form Zn<sup>2+</sup> cations in aqueous solution. In Equation 5.6, Zn<sup>2+</sup> cations react with polyborate anion of B<sub>3</sub>O<sub>3</sub>(OH)<sub>5</sub><sup>2-</sup><sub>(aq)</sub> to form insoluble solid Zn[B<sub>3</sub>O<sub>3</sub>(OH)<sub>5</sub>]<sub>(s)</sub>·H<sub>2</sub>O. Zinc borate clusters are initially formed and their concentration increases until a critical supersaturation is reached. As soon as the critical supersaturation value is exceeded, nucleation occurs. Then crystal growth on the formed nuclei takes place via consuming of molecular precursors from the bulk of solution. As zinc borate is sparingly soluble in aqueous phase, it precipitates out as soon as it is formed. All the successive steps happen in zinc borate synthesis from boric acid and zinc oxide. Zinc borate having structural formula of Zn[B<sub>3</sub>O<sub>3</sub>(OH)<sub>5</sub>]<sub>(s)</sub>·H<sub>2</sub>O or oxide formula of 2ZnO·3B<sub>2</sub>O<sub>3</sub>·7H<sub>2</sub>O is the zinc borate type precipitated first (Eltepe et al., 2007). Finally, polymerization of zinc borate (Zn[B<sub>3</sub>O<sub>3</sub>(OH)<sub>5</sub>]<sub>(s)</sub>·H<sub>2</sub>O) by condensation of B-OH and releasing the water of crystallization produces zinc borate (Zn[B<sub>3</sub>O<sub>4</sub>(OH)<sub>3</sub>]<sub>(s)</sub>) that is shown in Equation 5.7. Since boric acid was used in excess amount in the reaction, reaction medium was always acidic and pH was measured as 5.0 in mother liquid at the end of reaction. The presence of ions, such as H<sup>+</sup> protons, borate anions, and Zn<sup>2+</sup> cations is also another point that influences the zinc borate crystallization. Solubility of zinc borates and phase transformations should be considered under those reaction conditions. Boric acid concentration, temperature, use of modifying agent, reaction time are the parameters that influence the type of zinc borate that would be synthesized.





### 5.3. Zinc Borate Production in a Magnetically-Stirred Glass Reactor

#### 5.3.1. Effect of Reaction Temperature

Two step process is generally used in the production of zinc borate from boric acid and zinc oxide (Sawada et al., 2004 and Eltepe et al, 2007). Since the first step is usually carried out at 60 °C in the study of above authors, the effect of a higher reaction temperature was investigated in this part. For this purpose, the reaction between 3.0 mol.dm<sup>-3</sup> 50 mL of boric acid solution and equivalent amount of zinc oxide considering the B<sub>2</sub>O<sub>3</sub>/ZnO molar ratio as 2.0 was studied at 70 °C and 90 °C. The formed products at the end of this step were characterized. FTIR spectrum of zinc borate obtained from boric acid and zinc oxide at 70 °C is shown in Figure 5.5.a. The broad peak being maximum at 3400 cm<sup>-1</sup> wavenumber belongs to hydrogen bonded OH groups in the product. The bending vibration of water peak at 1650 cm<sup>-1</sup> depicts the presence of water of crystallization in the product. The peak at 1360 and 1230 cm<sup>-1</sup> belong to  $\nu_{as}(\text{BO}_3)$  and  $\delta(\text{B-O-H})$ , respectively. The peaks between 1130 and 1000 cm<sup>-1</sup> belong to  $\nu_{as}(\text{BO}_4)$ , and at 839 cm<sup>-1</sup> belongs to  $\nu_s(\text{BO}_4)$ .

In Figure 5.5.b. FTIR spectrum of zinc borate obtained from boric acid and zinc oxide at 90 °C is shown. From this spectrum, it is inferred that it is a completely different type of zinc borate. It does resemble neither 2ZnO·3B<sub>2</sub>O<sub>3</sub>·7H<sub>2</sub>O nor 2ZnO·3B<sub>2</sub>O<sub>3</sub>·3H<sub>2</sub>O. The emerging extra peaks between 2900 and 3400 cm<sup>-1</sup> wavenumber indicate that OH groups bonded to the main borate chain differently. This type of zinc borate also contains a water of crystallization in its structure as it has a peak at 1650 cm<sup>-1</sup> wavenumber. The other characteristic bands involved in boron oxygen coordination were observed between 1400 and 400 cm<sup>-1</sup> wavenumber region. Specifically, peaks at 1430-1317 cm<sup>-1</sup> and at 925 cm<sup>-1</sup> belong to asymmetric and symmetric stretching vibrations of trihedral (BO<sub>3</sub>) boron oxygen coordination, respectively. The peaks at 1182-1020 cm<sup>-1</sup> and 835 cm<sup>-1</sup> are related to asymmetric and symmetric stretching vibrations of tetrahedral (BO<sub>4</sub>) structure.

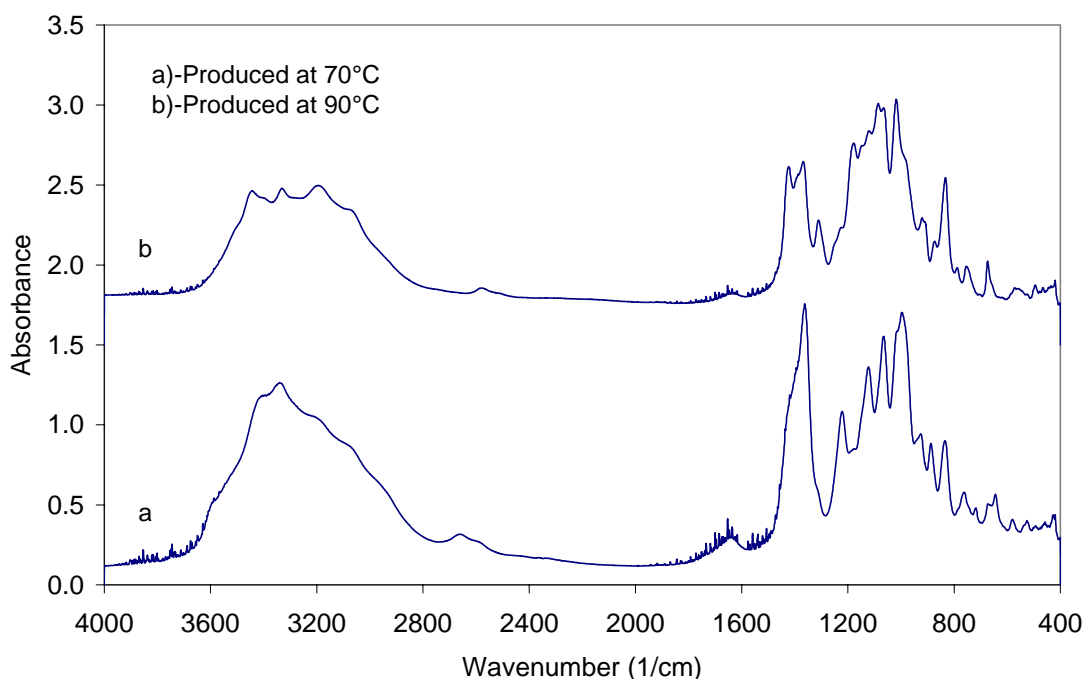


Figure 5.5. FTIR spectra of zinc borate produced at 70 °C (S-1) and 90 °C (S-3) using  $3.0 \text{ mol}\cdot\text{dm}^{-3}$  boric acid with  $\text{B}_2\text{O}_3/\text{ZnO}$  molar ratio of 2.0 for 5.0 h.

XRD pattern of zinc borate produced at 70 °C and for 5 h reaction time is shown in Figure 5.6.a. There are two groups of major peaks at  $2\theta$  values: the first group ( $10.2^\circ$ ,  $20.6^\circ$ ,  $28.1^\circ$ ,  $33.1^\circ$ ,  $36.2^\circ$ ,  $45.9^\circ$  and  $56.7^\circ$ ) represented by star and the second group ( $8.8^\circ$ ,  $12.8^\circ$ ,  $13.0^\circ$ , and  $31.7^\circ$ ) as shown by circle. From these peaks, it was determined that this product is a mixture of  $2\text{ZnO}\cdot 3\text{B}_2\text{O}_3\cdot 7\text{H}_2\text{O}$  (JCPDS 75-0766 and Sawada et al., 2004) and  $\text{ZnO}\cdot\text{B}_2\text{O}_3\cdot 2\text{H}_2\text{O}$ . On the other hand, XRD pattern of zinc borate (Figure 5.6.b.) synthesized at 90 °C revealed that it was pure zinc borate type of  $\text{ZnO}\cdot\text{B}_2\text{O}_3\cdot 2\text{H}_2\text{O}$  as water content value was verified by TGA analysis. The major peaks in Figure 5.6.b. are summarized in Table 5.2. The detailed characterization of zinc borates,  $2\text{ZnO}\cdot 3\text{B}_2\text{O}_3\cdot 7\text{H}_2\text{O}$ ,  $2\text{ZnO}\cdot 3\text{B}_2\text{O}_3\cdot 3\text{H}_2\text{O}$ , and  $4\text{ZnO}\cdot\text{B}_2\text{O}_3\cdot\text{H}_2\text{O}$ , can be found in most of the studies (Sawada et al., 2004, Schubert, 1995). However, definition of XRD pattern of zinc borate,  $\text{ZnO}\cdot\text{B}_2\text{O}_3\cdot 2\text{H}_2\text{O}$ , was made for the first time in this study according to the best of our knowledge.

Table 5.2. XRD data of zinc borate,  $\text{ZnO}\cdot\text{B}_2\text{O}_3\cdot 2\text{H}_2\text{O}$

$2\theta$	d Spacing (Å)	Relative Intensity ( $I/I_{100}$ )x100	Crystallite size (nm)
10.2	8.69	100	37.1
20.6	4.30	16	39.6
27.6	3.23	10	26.0
28.1	3.17	24	31.3
29.6	3.01	12	18.3
30.9	2.89	14	33.5
33.1	2.70	13	41.9
34.1	2.63	20	9.9
36.2	2.48	15	20.8
42.5	2.13	40	4.0
45.9	1.98	43	4.3
56.7	1.62	16	1.6

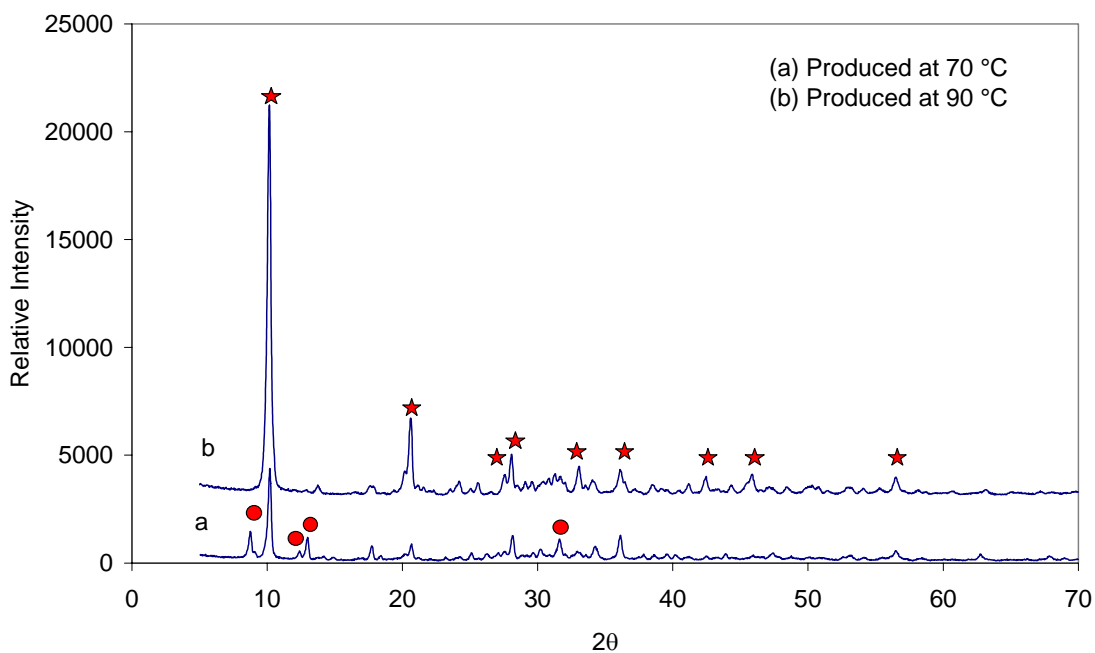


Figure 5.6. XRD patterns of zinc borate produced at 70 °C (S-1) and 90 °C (S-3) using  $3.0 \text{ mol}\cdot\text{dm}^{-3}$  boric acid with  $\text{B}_2\text{O}_3/\text{ZnO}$  molar ratio of 2.0 for 5.0 h.

Thermal behaviour of zinc borate obtained at 70 °C for 5 h reaction time is shown in Figure 5.7.a. In this thermogram, there are two decomposition steps that belong to different zinc borate species. It is depicted that zinc borates  $2\text{ZnO}\cdot 3\text{B}_2\text{O}_3\cdot 7\text{H}_2\text{O}$  and  $\text{ZnO}\cdot\text{B}_2\text{O}_3\cdot 2\text{H}_2\text{O}$  lose their water and hydroxyl groups when heated from 130 to 250 °C (Briggs, 2001). The first step in which mass loss occurs at around 130 °C belong to zinc borate of  $2\text{ZnO}\cdot 3\text{B}_2\text{O}_3\cdot 7\text{H}_2\text{O}$  and the second step where

mass loss starts at around 240 °C pertains to zinc borate species of  $\text{ZnO}\cdot\text{B}_2\text{O}_3\cdot 2\text{H}_2\text{O}$ . The total mass loss was calculated as 22.14 % during the heating of that mixture up to 600 °C. This mass loss is the sum of the mass losses from first and second steps, as 12.71 % and 9.43 %, respectively.

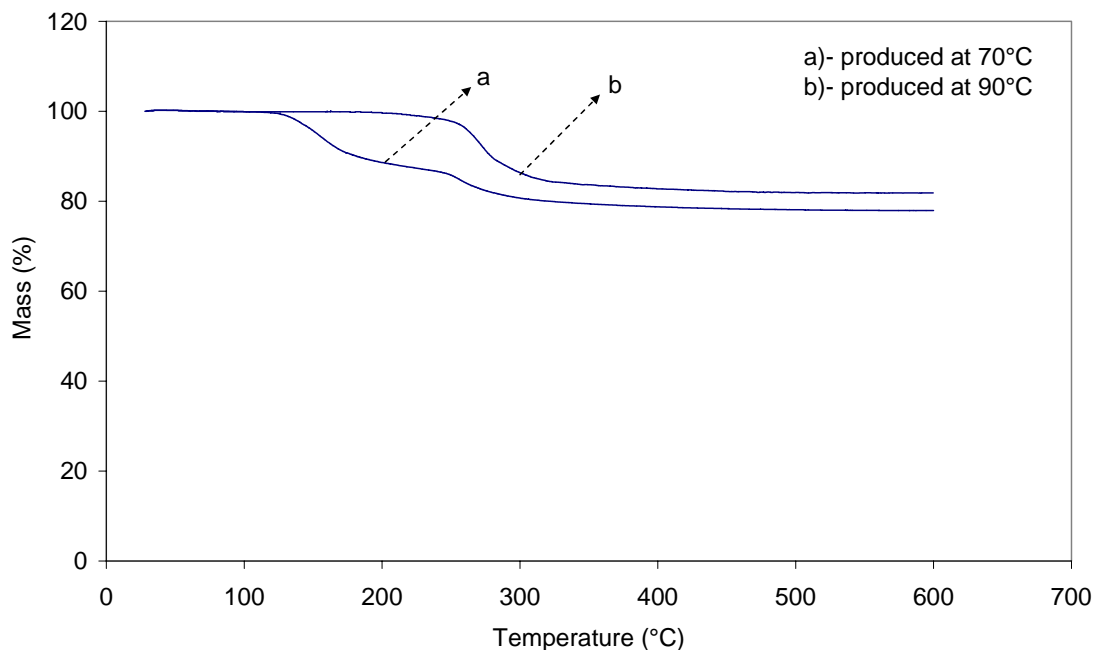


Figure 5.7. Thermograms of zinc borates produced at 70 °C (S-1) and 90 °C (S-3) using  $3.0 \text{ mol}\cdot\text{dm}^{-3}$  boric acid with  $\text{B}_2\text{O}_3/\text{ZnO}$  molar ratio of 2.0 for 5.0 h.

Figure 5.7.b. represents TGA curve of the zinc borate produced at 90 °C for 5 h reaction time. For this type of zinc borate, the total mass loss occurred as 18.16 % when the sample was heated from ambient temperature to 600 °C. Zinc borate sample started to lose mass at around 240 °C and beyond 400 °C no further mass loss was observed till 600 °C. The mass loss of 18.16 % occurred due to the condensation of hydroxyl groups in that temperature range corresponds to water content of  $\text{ZnO}\cdot\text{B}_2\text{O}_3\cdot 2\text{H}_2\text{O}$  and can be compared to the theoretical value of 19.25 %.

SEM microphotographs of zinc borates produced at 70 °C and 90 °C for 5.0 h reaction time are shown in Figure 5.8.a and Figure 5.8.b, respectively. Zinc borate particles obtained at 70 °C are in the form of thin rectangular plates as shown in Figure 5.8.a. While the thickness of these plates is in the range of nanoscale, the length and the width of particles are in the range of 5-10  $\mu\text{m}$  and 1-2  $\mu\text{m}$ , respectively. Figure 5.8.b points out that zinc borate particles produced at 90 °C show a long plate-like

morphology rectangular shape and they are about 50 nm in thickness, 150-200 nm in width and 5-10  $\mu\text{m}$  in length.

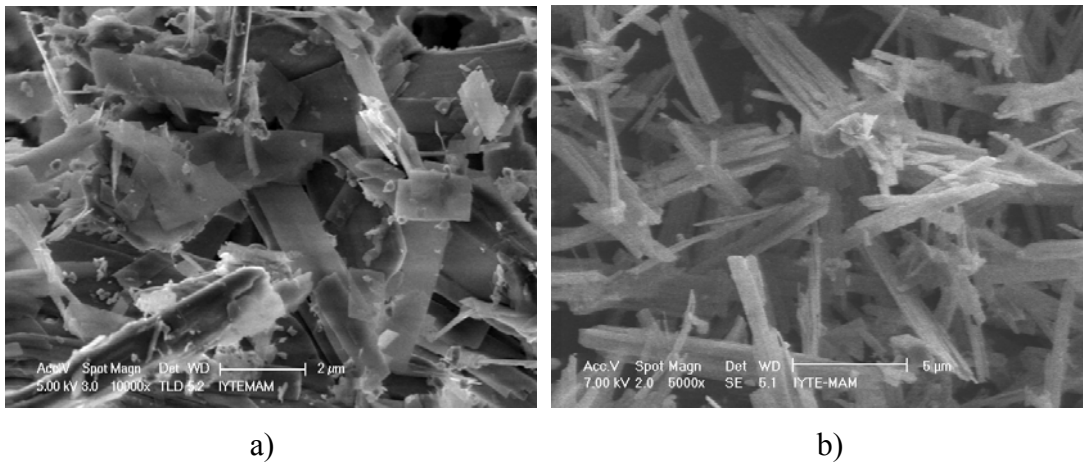


Figure 5.8. SEM microphotographs of zinc borates produced at a) 70 °C (S-1) and b) 90 °C (S-3) using 3.0 mol.dm<sup>-3</sup> boric acid with B<sub>2</sub>O<sub>3</sub>/ZnO molar ratio of 2.0 for 5.0 h.

Particle size distributions of zinc borate samples produced at 70 °C and 90 °C are shown in Figure 5.9 and Figure 5.10, respectively. The volume-weighted mean particle diameter of zinc borates produced at 70 °C and 90 °C was 7.6  $\mu\text{m}$  and 5.9  $\mu\text{m}$ , respectively. Increasing the reaction temperature from 70 °C to 90 °C reduced the mean diameter of the particles. However, agglomeration of particles formed a second small peak just below 100  $\mu\text{m}$  as shown in Figure 5.10.

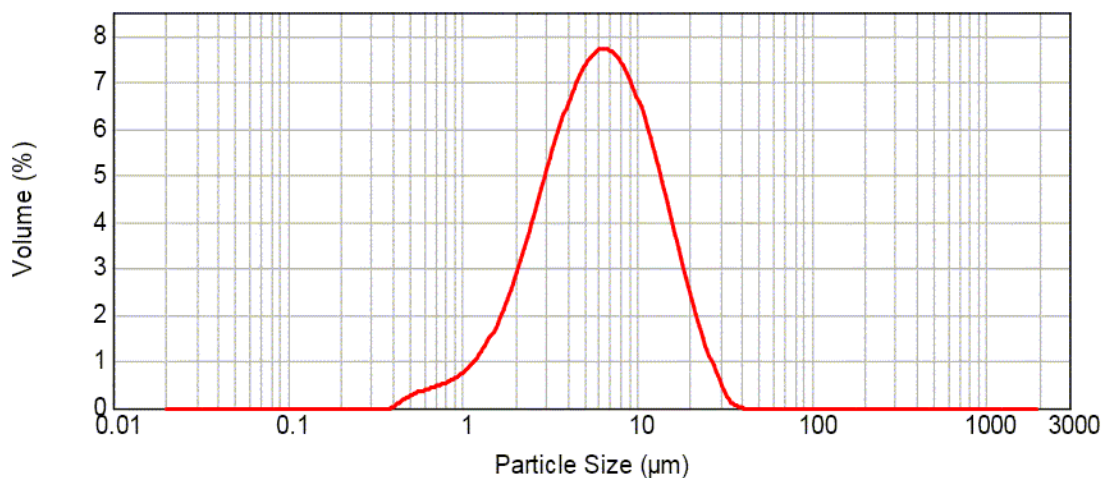


Figure 5.9. Particle size distribution of zinc borate produced at 70 °C (S-1) using 3.0 mol.dm<sup>-3</sup> boric acid with B<sub>2</sub>O<sub>3</sub>/ZnO molar ratio of 2.0 for 5.0 h, (Malvern Mastersizer 2000).

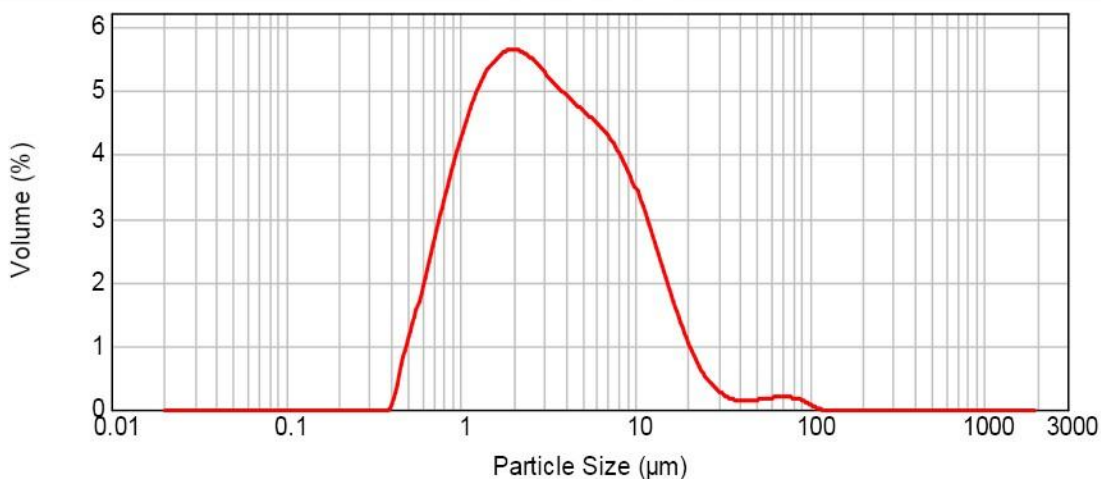


Figure 5.10. Particle size distribution of zinc borate produced at 90 °C (S-3) using 3.0 mol.dm<sup>-3</sup> boric acid with B<sub>2</sub>O<sub>3</sub>/ZnO molar ratio of 2.0 for 5.0 h, (Malvern Mastersizer 2000).

### 5.3.2. Effect of Boric Acid Concentration

The effect of boric acid concentration in the production of zinc borate of 2ZnO·3B<sub>2</sub>O<sub>3</sub>·3H<sub>2</sub>O was examined by Gürhan and co-workers (2009) using seed crystals and Shete and co-workers (2004) without using seed. In both studies, authors focused on the conversion in the reaction with respect to the change in boric acid concentration and zinc oxide consumption. Increasing boric acid concentration in such a reaction usually boosts the reaction rate and diminishes the reaction time. Another advantage in excess boric acid usage is to convert zinc oxide completely in the reaction since it is not possible to separate any unreacted solid zinc oxide from powder product. That phenomenon was observed in both of the studies mentioned above. They assumed that consumption of either boric acid or zinc oxide in the reaction had been used for only the synthesis of zinc borate of 2ZnO·3B<sub>2</sub>O<sub>3</sub>·3H<sub>2</sub>O. On the other hand, Eltepe and co-workers (2007) reported that two different zinc borate species were synthesized in the reaction between boric acid and zinc oxide with elapsing reaction time. Formation of other zinc borate species in the reaction of zinc oxide and boric acid should be considered.

In this part of study, the effect of boric acid concentration (3.0, 4.0, and 4.7 mol.dm<sup>-3</sup>) using equivalent amount of zinc oxide corresponding to the B<sub>2</sub>O<sub>3</sub>/ZnO molar ratio of 2.0 was investigated.

FTIR spectra of zinc borates, which were produced at 3.0 mol.dm<sup>-3</sup> and 4 mol.dm<sup>-3</sup> boric acid concentrations and equivalent amount of zinc oxide using the B<sub>2</sub>O<sub>3</sub>/ZnO molar ratio of 2.0 at 90 °C, are shown in Figure 5.11. From the comparison of those spectra (Figure 5.11.a and b) it is inferred that there is no characteristic difference between them. According to the characterization of spectrum obtained previously (Figure 5.5.b), both spectra have same major peaks and they are zinc borate species of ZnO·B<sub>2</sub>O<sub>3</sub>·2H<sub>2</sub>O. The emerging extra peaks between 2900 and 3400 cm<sup>-1</sup> wavenumber points also that configurations of hydroxyl groups to main borate chain are different than those of other zinc borate species. Thus, the region of spectrum could be used as blueprint for that zinc borate type (ZnO·B<sub>2</sub>O<sub>3</sub>·2H<sub>2</sub>O). This type of zinc borate also contains crystal water in its structure as it has a peak at 1650 cm<sup>-1</sup> wavenumber. The other characteristic bands involved in boron oxygen coordination were observed between 1400 and 400 cm<sup>-1</sup> wavenumber region in its spectrum.

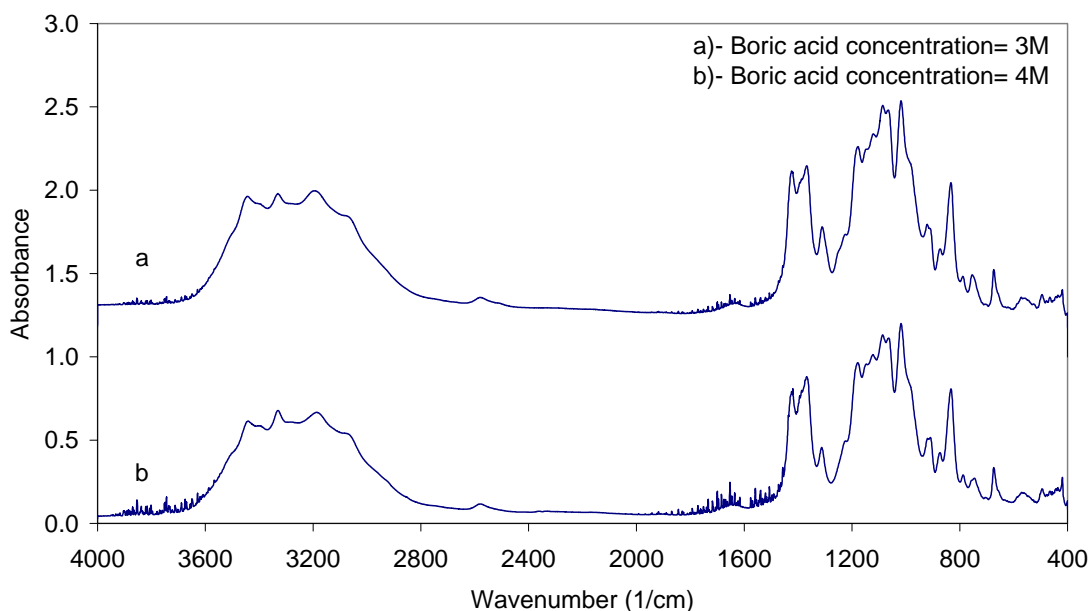


Figure 5.11. FTIR spectra of zinc borates produced using 3.0 mol.dm<sup>-3</sup> (S-3) and 4.0 mol.dm<sup>-3</sup> (S-2) boric acid and zinc oxide according to the B<sub>2</sub>O<sub>3</sub>/ZnO molar ratio of 2.0 at 90 °C for 5 h.

XRD patterns of zinc borates that were synthesized using  $3.0 \text{ mol.dm}^{-3}$  and  $4.0 \text{ mol.dm}^{-3}$  boric acid concentration and equal amount of zinc oxide taking the  $\text{B}_2\text{O}_3/\text{ZnO}$  molar ratio as 2.0 are shown in Figure 5.12. Both patterns exhibit same major peaks as shown in Figure 5.12.a and Figure 5.12.b. The major peaks represented by star in XRD patterns occurred at  $10.2^\circ$ ,  $20.6^\circ$ ,  $28.1^\circ$ ,  $33.1^\circ$ ,  $36.2^\circ$ ,  $45.9^\circ$  and  $56.7^\circ$   $2\theta$  values. Those characteristic peaks belong to the zinc borate of  $\text{ZnO}\cdot\text{B}_2\text{O}_3\cdot 2\text{H}_2\text{O}$ . The type of zinc borate was determined as  $\text{ZnO}\cdot\text{B}_2\text{O}_3\cdot 2\text{H}_2\text{O}$  since it was also supported by both water content and  $\text{B}_2\text{O}_3/\text{ZnO}$  molar ratio. The use of  $3.0 \text{ mol.dm}^{-3}$  and  $4.0 \text{ mol.dm}^{-3}$  boric acid concentration did not have a considerable effect on the type of zinc borate.

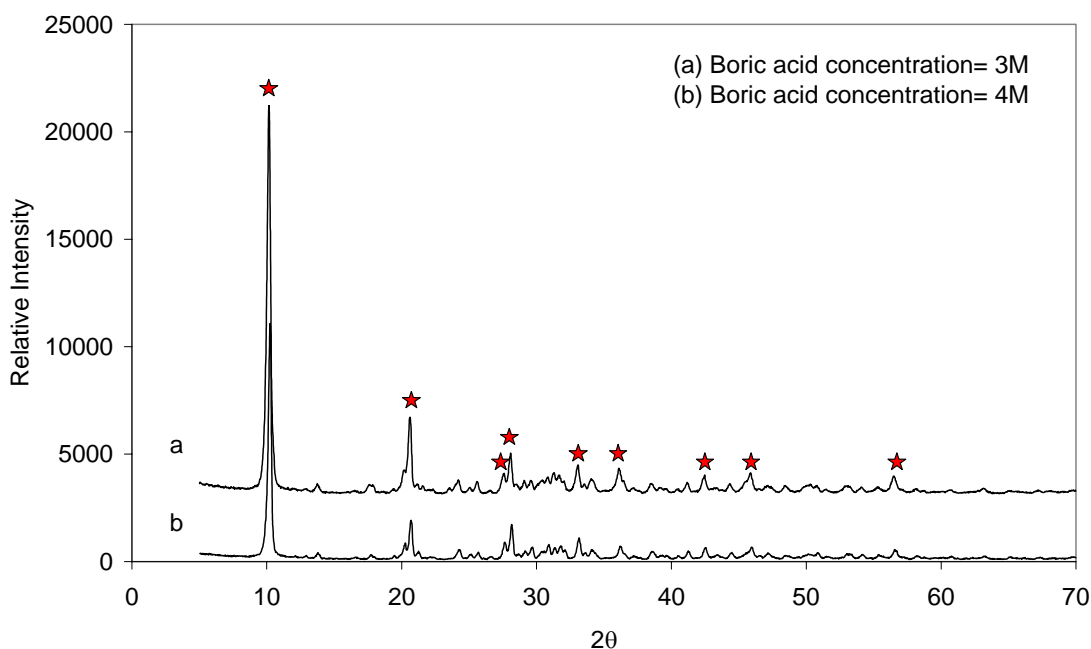


Figure 5.12. XRD patterns of zinc borates produced using a)  $3.0 \text{ mol.dm}^{-3}$  (S-3) and b)  $4.0 \text{ mol.dm}^{-3}$  (S-2) boric acid and zinc oxide according to the  $\text{B}_2\text{O}_3/\text{ZnO}$  molar ratio of 2.0 at  $90^\circ \text{C}$  for 5 h.

Figure 5.13 represents TG plots of the zinc borates produced using different boric acid concentrations, such as  $3.0 \text{ mol.dm}^{-3}$  and  $4.0 \text{ mol.dm}^{-3}$  and equivalent amounts of zinc oxide according to the  $\text{B}_2\text{O}_3/\text{ZnO}$  molar ratio of 2.0 at  $90^\circ \text{C}$  for 5 h reaction time. From the comparison of Figure 5.13.a and Figure 5.13.b there is not a considerable difference between these thermograms. Both thermograms have only one decomposition step between  $200^\circ \text{C}$  and  $400^\circ \text{C}$ . The total mass loss occurred as 18.16% when the samples were heated from ambient temperature to  $600^\circ \text{C}$ . Zinc borate sample started to lose mass at around  $240^\circ \text{C}$  and beyond  $400^\circ \text{C}$  no mass loss was



observed till 600 °C. The mass loss of 18.16 % occurred due to the condensation of hydroxyl groups in that temperature range corresponds to water content of  $\text{ZnO}\cdot\text{B}_2\text{O}_3\cdot 2\text{H}_2\text{O}$  and can be compared to the theoretical water content value of 19.25 %.

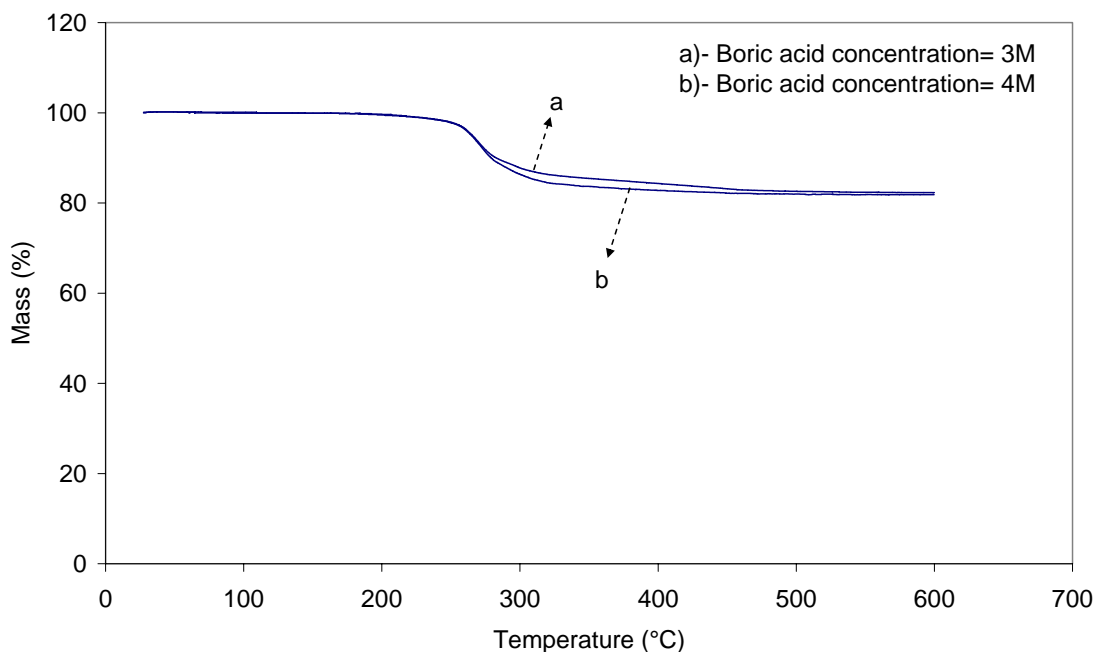


Figure 5.13. Thermograms of zinc borates produced using  $3.0 \text{ mol}\cdot\text{dm}^{-3}$  (S-3) and  $4.0 \text{ mol}\cdot\text{dm}^{-3}$  (S-2) boric acid and zinc oxide according to the  $\text{B}_2\text{O}_3/\text{ZnO}$  molar ratio of 2.0 at  $90 \text{ }^\circ\text{C}$  for 5 h.

SEM photographs of zinc borates produced at  $90 \text{ }^\circ\text{C}$  for 5h with  $\text{B}_2\text{O}_3/\text{ZnO}$  molar ratio of 2.0 and different boric acid concentrations of  $3.0 \text{ mol}\cdot\text{dm}^{-3}$  and  $4.0 \text{ mol}\cdot\text{dm}^{-3}$  are shown in Figure 5.14.a and Figure 5.14.b, respectively. Zinc borate particles are in the form of long lamellar plates for both boric acid concentrations. As it is represented in Figure 5.14.a, the thickness of these plates is in the range of nanoscale, the length and width of them are in the range of  $2\text{-}4 \text{ }\mu\text{m}$  and  $0.5\text{-}1 \text{ }\mu\text{m}$ , respectively. Zinc borate particles show again a plate like morphology about  $50 \text{ nm}$  in thickness,  $150\text{-}200 \text{ nm}$  in width and  $5\text{-}10 \text{ }\mu\text{m}$  in length as given in Figure 5.14.b.

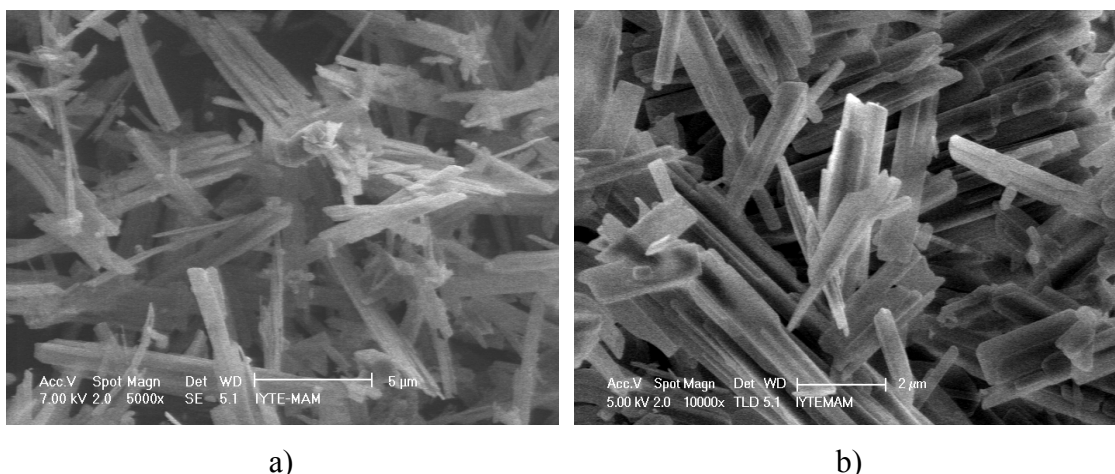


Figure 5.14. SEM microphotograph of zinc borate produced at 90 °C for 5 h,  $B_2O_3/ZnO$  molar ratio of 2.0, a) 3.0 mol.dm<sup>-3</sup> boric acid (S-3); b) 4.0 mol.dm<sup>-3</sup> boric acid (S-2).

Figure 5.15 represents the particle size distribution of zinc borate produced using 4.0 mol.dm<sup>-3</sup> boric acid concentration at 90 °C. From the comparison of Figure 5.10 and Figure 5.15, increasing the boric acid concentration from 3.0 to 4.0 mol.dm<sup>-3</sup> did not bring any significant change in particle size. The volume-weighted mean diameter of the particles was about 4.5 μm. Since these particles agglomerated, mean diameter became larger.

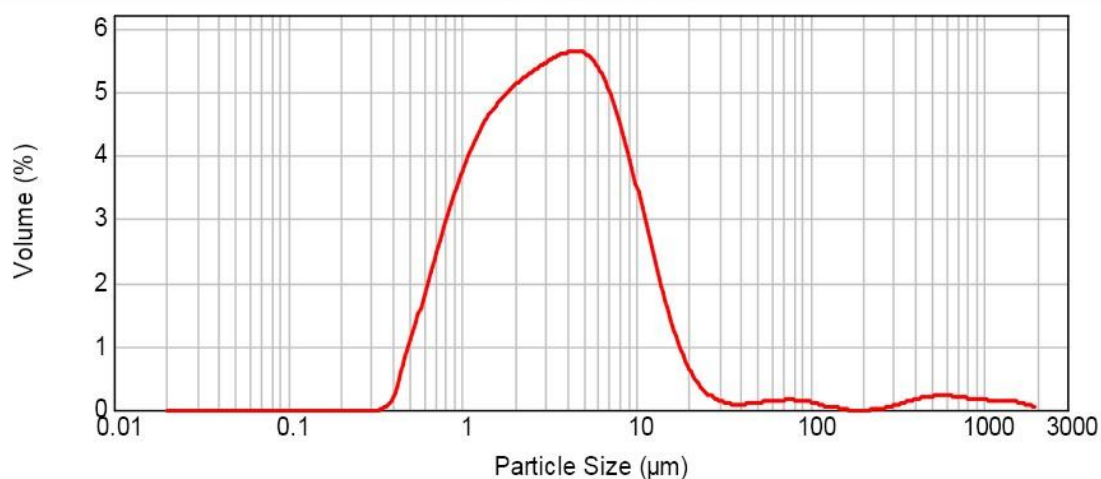


Figure 5.15. Particle size distribution of zinc borate produced at 90 °C (S-2) using 4.0 mol.dm<sup>-3</sup> boric acid with  $B_2O_3/ZnO$  molar ratio of 2.0 for 5.0 h, (Malvern Mastersizer 2000).

In most of the studies, higher boric acid concentration was emphasized for the synthesis of zinc borate of  $2ZnO \cdot 3B_2O_3 \cdot 3H_2O$  (Sawada et al., 2004, Eltepe et al. 2007, and Gürhan et al., 2009). In this part of study, 4.7 mol.dm<sup>-3</sup> boric acid concentration and

equivalent amount of zinc oxide according to the  $B_2O_3/ZnO$  molar ratio of 2.0 was examined for the zinc borate production for 5 h reaction time at 90 °C. FTIR spectrum and XRD pattern of zinc borate produced under those conditions are shown in Figure 5.16. and Figure 5.17., respectively. It can be inferred that zinc borate of  $2ZnO \cdot 3B_2O_3 \cdot 3H_2O$  does not contain water of crystallization in its structure since there is no peak at around  $1650\text{ cm}^{-1}$  wavenumber in its infrared spectrum (Figure 5.16). Also peaks between  $2500$  and  $3400\text{ cm}^{-1}$  are different than the other types of zinc borates,  $2ZnO \cdot 3B_2O_3 \cdot 7H_2O$  and  $ZnO \cdot B_2O_3 \cdot 2H_2O$ . The other major band values in that spectrum agree with the peaks given in Table 5.3. and explained for zinc borate of  $2ZnO \cdot 3B_2O_3 \cdot 3H_2O$ .

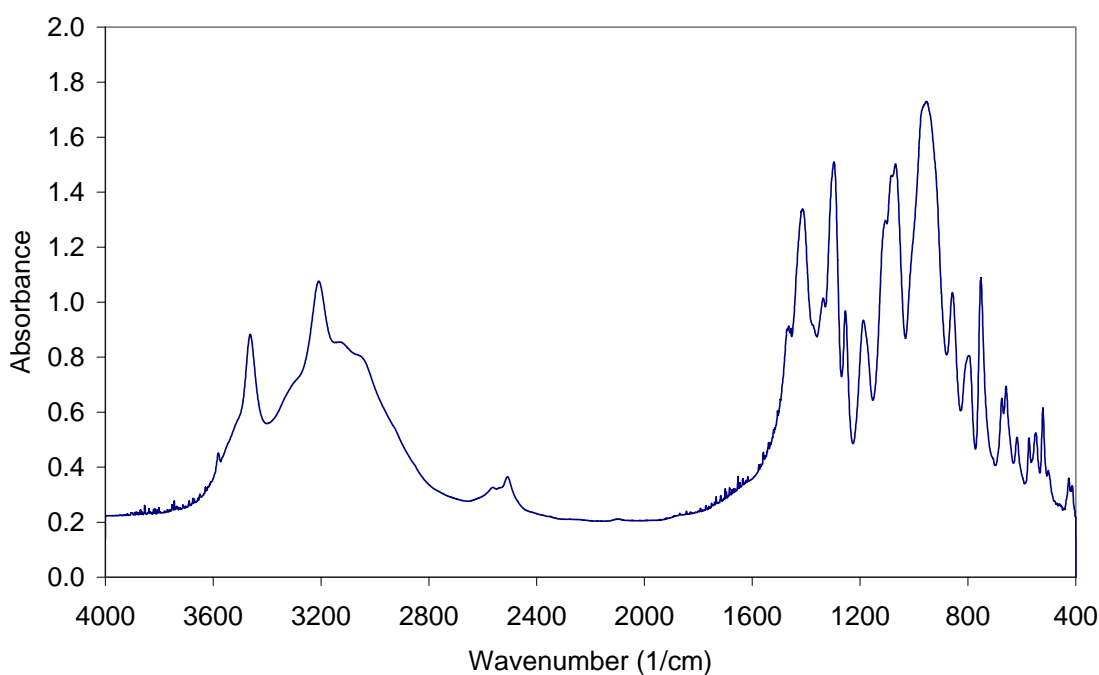


Figure 5.16. FTIR spectrum of zinc borate produced at 90 °C for 5 h, at  $B_2O_3/ZnO$  molar ratio of 2.0 and  $4.7\text{ mol}\cdot\text{dm}^{-3}$  boric acid (S-4).

The major peaks in Figure 5.17 start at  $2\theta$  value of  $18.0^\circ$  and end at  $36.6^\circ$ . The detailed characterization of those peaks was made in Table 2.7. According to the XRD pattern of zinc borate registered by Sawada and co-workers (2004) and JCPDS 32-1464 file product obtained at  $4.7\text{ mol}\cdot\text{dm}^{-3}$  boric acid concentration is zinc borate type of  $2ZnO \cdot 3B_2O_3 \cdot 3H_2O$ .

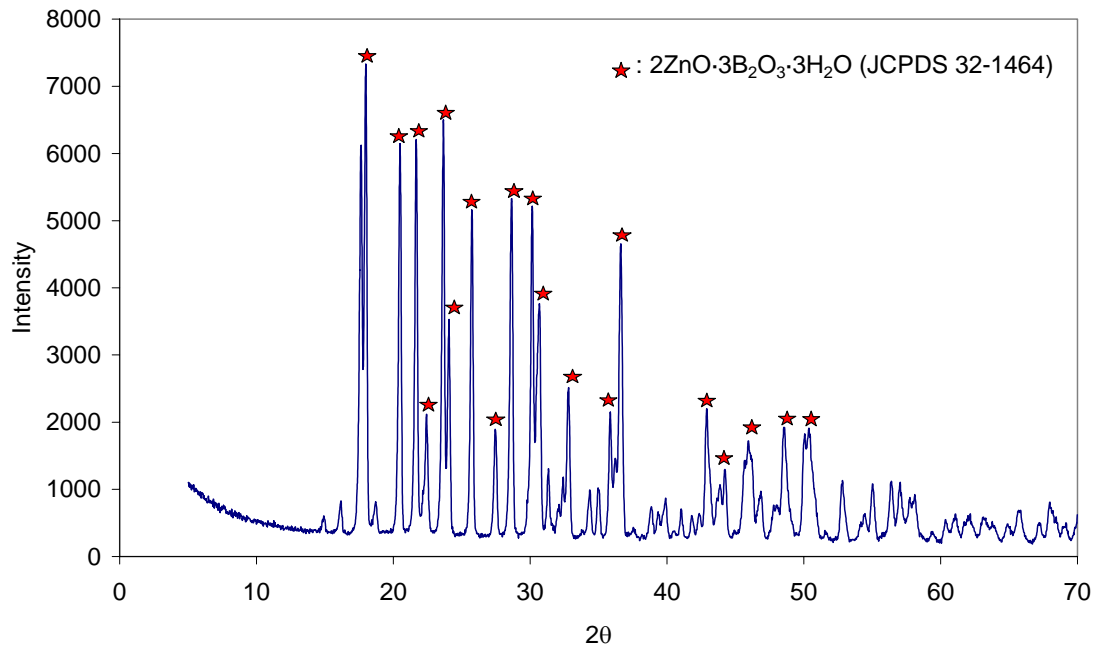


Figure 5.17. XRD pattern of zinc borate produced at 90 °C for 5 h, at B<sub>2</sub>O<sub>3</sub>/ZnO molar ratio of 2.0, 4.7 mol.dm<sup>-3</sup> boric acid (S-4).

Thermal behavior of zinc borate produced at 4.7 mol.dm<sup>-3</sup> boric acid concentration and equivalent amount of zinc oxide according to the B<sub>2</sub>O<sub>3</sub>/ZnO molar ratio of 2.0 is shown in Figure 5.18. Zinc borate sample began to lose mass at 290 °C and total mass loss occurred between 12.56-13.15 % which was comparable to the calculated value of 12.69 % for zinc borate of 2ZnO·3B<sub>2</sub>O<sub>3</sub>·3H<sub>2</sub>O. The observed mass loss is the result of condensation reaction of B-OH groups in zinc borate structure from which water is released. 2ZnO·3B<sub>2</sub>O<sub>3</sub>·3H<sub>2</sub>O degraded at temperatures between 290 and 450 °C to yield an amorphous product which corresponded to its dehydrated form (Equation 5.9). After the formation of amorphous structure, increasing temperature further induces the formation of anhydrous crystalline zinc borate having  $\alpha$  and  $\beta$  forms (Samyn et al., 2007).

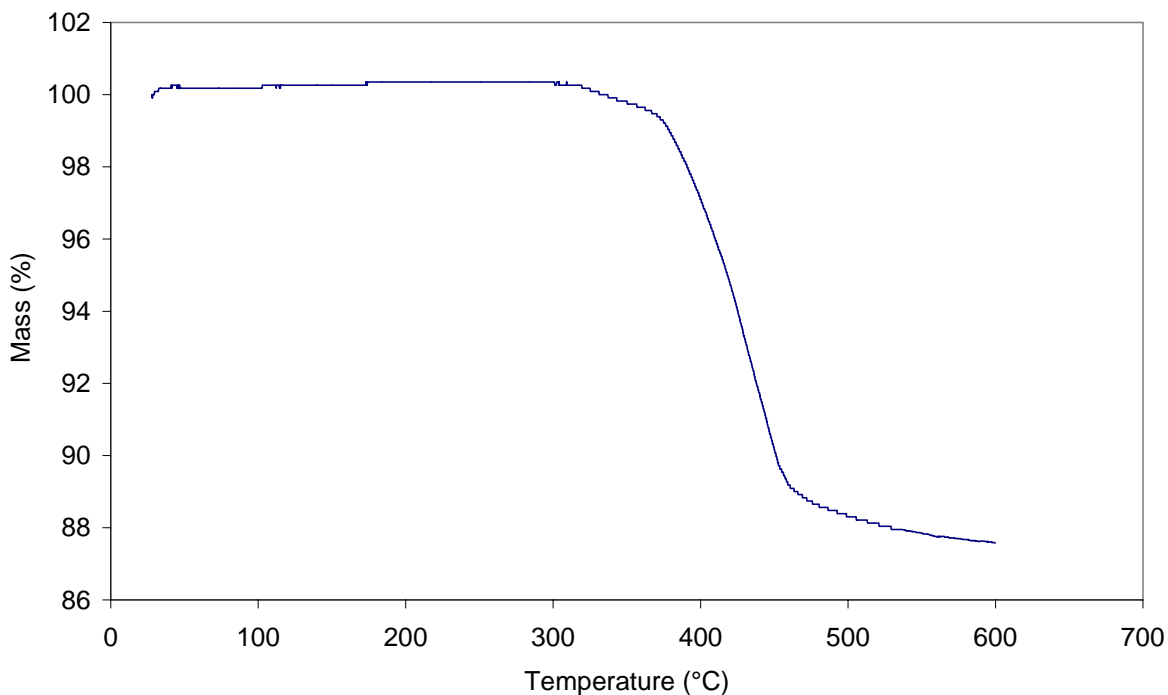


Figure 5.18. Thermogram of zinc borate produced at 90 °C for 5h, at B<sub>2</sub>O<sub>3</sub>/ZnO molar ratio of 2.0 and 4.7 mol.dm<sup>-3</sup> boric acid (S-4).

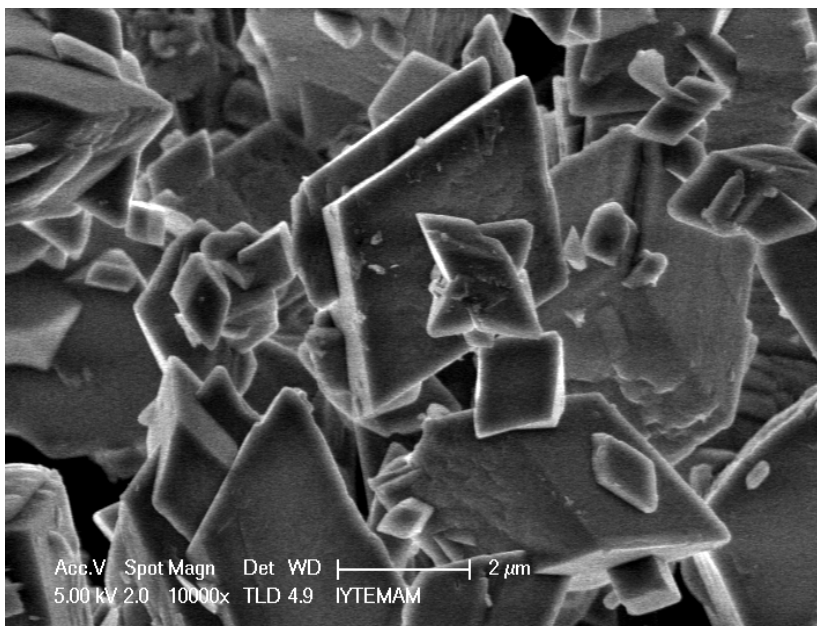


Figure 5.19. SEM microphotograph of zinc borate produced at 90 °C for 5 h, at B<sub>2</sub>O<sub>3</sub>/ZnO molar ratio of 2.0 and 4.7 mol.dm<sup>-3</sup> boric acid (S-4).

Figure 5.19 displays the SEM microphotograph of zinc borate particle morphology that was produced using 4.7 mol.dm<sup>-3</sup> boric acid concentration and equivalent amount of zinc oxide according to the B<sub>2</sub>O<sub>3</sub>/ZnO molar ratio of 2.0. Zinc borate particles are in the shape of prism and they can be classified into two groups

according to the particle size, larger particles with 2-4  $\mu\text{m}$  size and smaller particles lower than 1.0  $\mu\text{m}$ .

Particle size distribution of zinc borate produced at 90 °C using 4.7  $\text{mol}\cdot\text{dm}^{-3}$  boric acid concentration is shown in Figure 5.20. It has a bimodal distribution, smaller percent of particles had particle diameter lower than 1.0  $\mu\text{m}$  and greater percent had particle diameter greater than 6  $\mu\text{m}$  and volume-weighted mean diameter was found as 5.8  $\mu\text{m}$ .

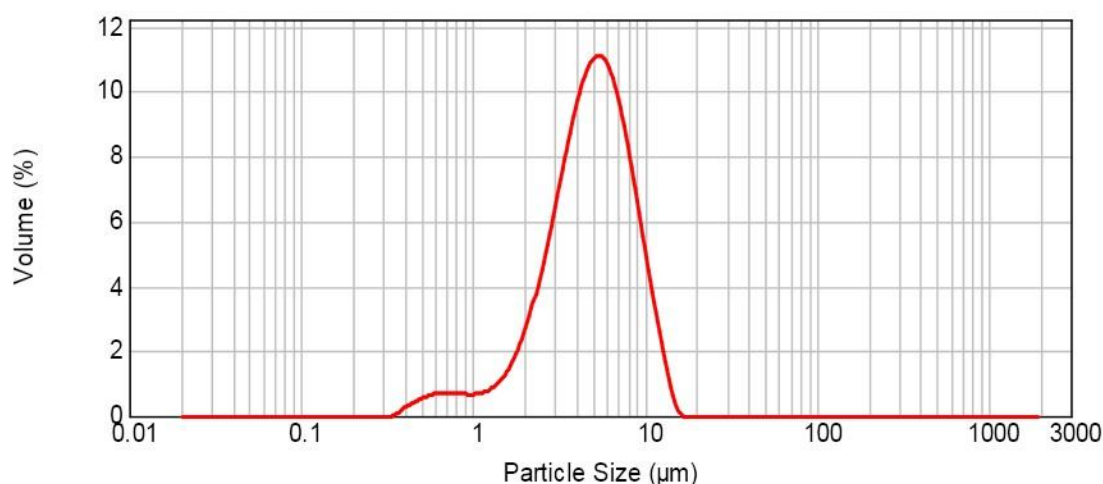


Figure 5.20. Particle size distribution of zinc borate produced at 90 °C for 5 h, at  $\text{B}_2\text{O}_3/\text{ZnO}$  molar ratio of 2.0 and 4.7  $\text{mol}\cdot\text{dm}^{-3}$  boric acid (S-4), (Malvern Mastersizer 2000).

### 5.3.3. Effect of Sonication

Sonication has been widely used in mixing, reactions and in various branches of science for many years. The chemical effects of ultrasound arise from acoustic cavitation, that is, the formation, growth, and implosive collapse of bubbles in a liquid. When solutions are exposed to strong ultrasound irradiation, bubbles in the solution are implosively collapsed by acoustic fields; as a result, the temperature can be as high as 5000 K, the pressure can reach over 1800 atm. and the cooling rate can be in excess of 106 K/s (Jiang et al., 2004). The influence of sonication in the reaction of zinc oxide and boric acid has not been examined yet according to the best of our knowledge. It is

expected that sonication might control particle size of final product in the reaction of boric acid and zinc oxide.

The use of sonication in the production of boric acid from colemanite was studied by Taylan and co-workers (2007). They found that ultrasound enhanced both dissolution rate of colemanite and precipitation rate of gypsum in the solution containing sulfuric acid after 1 h. They also reported that particle size of gypsum crystals was decreased by ultrasound.

The use of sonication in the reaction between zinc oxide and boric acid was studied using  $4.7 \text{ mol.dm}^{-3}$  boric acid concentration and adequate zinc oxide according to  $\text{B}_2\text{O}_3/\text{ZnO}$  molar ratio of 2.0 at  $90^\circ\text{C}$  for 5 h reaction time. The reaction was carried out in the 30 % of the maximum amplitude. It was expected that the use of sonication would decrease the particle size of formed product.

FTIR spectrum and XRD pattern of zinc borate produced in the presence of ultrasound are given in Figure 5.21 and Figure 5.22, respectively. From the comparison of both FTIR spectra and XRD patterns in the presence and absence of ultrasound, it can be deduced that ultrasound did not affect the formation of zinc borate type of  $2\text{ZnO}\cdot 3\text{B}_2\text{O}_3\cdot 3\text{H}_2\text{O}$  significantly. On the other hand, since ultrasound improves mass transfer rate between boric acid and zinc oxide, it consequently increases reaction rate. As the aim in the use of sonication was to examine its effects on particle size of final product, the improvement in the reaction rate was not investigated in details.

Zinc borate synthesized using sonication started to decompose at around  $300^\circ\text{C}$  and the total mass loss calculated as around 13.0 % corresponds to the theoretical water content of zinc borate having oxide formula of  $2\text{ZnO}\cdot 3\text{B}_2\text{O}_3\cdot 3\text{H}_2\text{O}$  as shown in Figure 5.23.

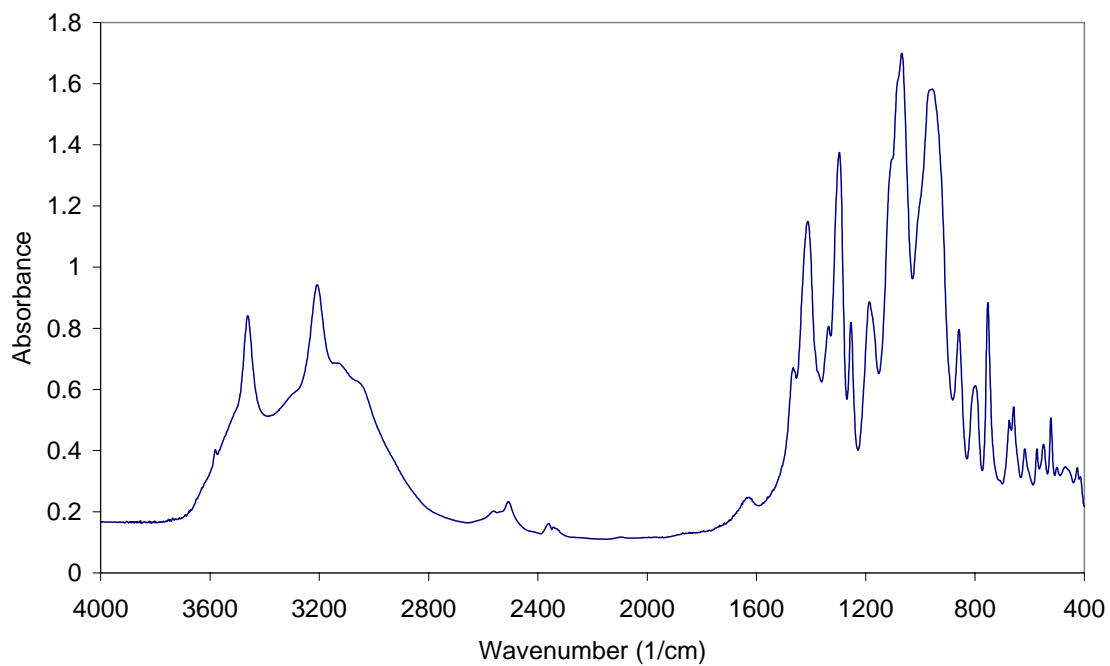


Figure 5.21. FTIR spectrum of zinc borate produced at 90 °C for 5 h, at  $B_2O_3/ZnO$  molar ratio of 2.0,  $4.7 \text{ mol}\cdot\text{dm}^{-3}$  boric acid and under sonication (S-5).

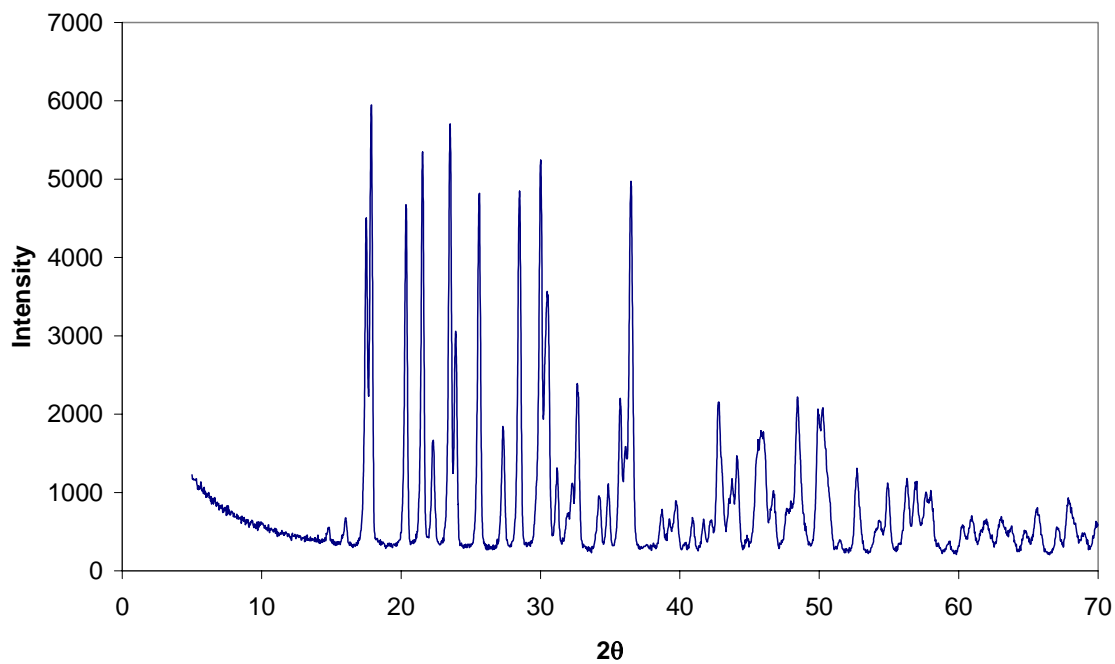


Figure 5.22. XRD pattern of zinc borate produced at 90 °C for 5h,  $B_2O_3/ZnO$  molar ratio of 2,  $4.7 \text{ mol}\cdot\text{dm}^{-3}$  boric acid and under sonication (S-5).



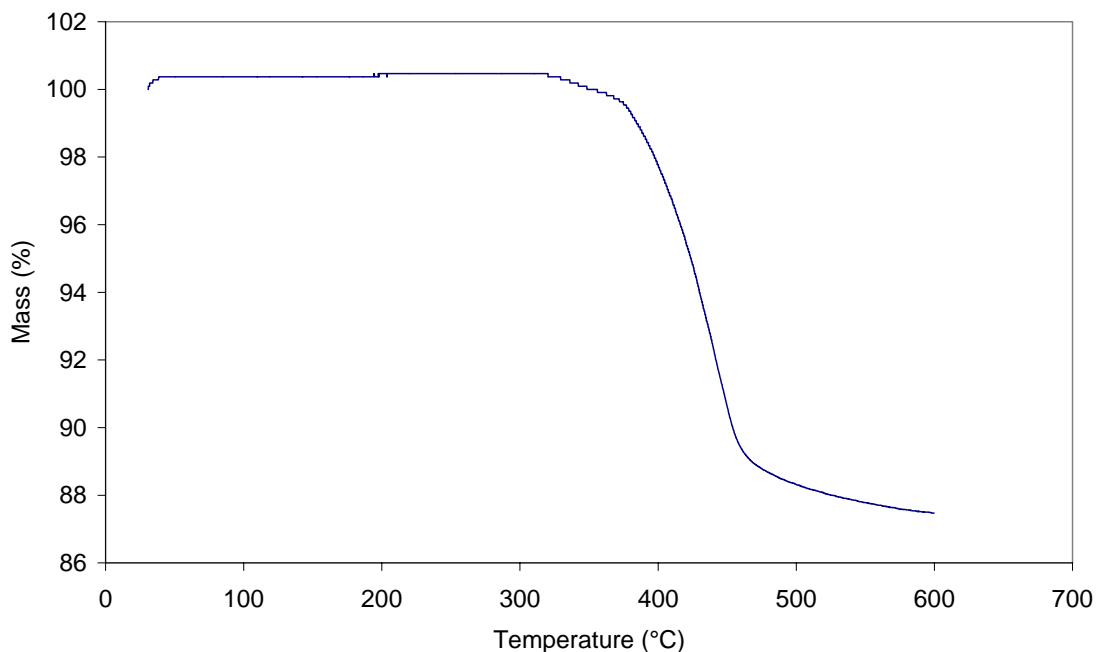


Figure 5.23. Thermogram of zinc borate produced at 90 °C for 5 h, at B<sub>2</sub>O<sub>3</sub>/ZnO molar ratio of 2.0, 4.7 mol.dm<sup>-3</sup> boric acid and under sonication (S-5).

SEM microphotograph of zinc borate produced in the presence of ultrasound is shown in Figure 5.24. Zinc borate particles are in the shape of prism and particle size is about 1-2 μm. When the particle morphology and size are compared with those of zinc borate produced under conventional mixing only, it can be seen implicitly that the use of sonication did not make a significant effect on the particle size and morphology of zinc borate.

Particle size distribution of zinc borate produced using sonication at 90 °C with 4.7 mol.dm<sup>-3</sup> boric acid concentration is shown in Figure 5.25. It has also a bimodal distribution; smaller percent of particles had volume-weighted mean diameter lower than 1.0 μm and greater percent had volume-weighted mean diameter of 5.1 μm. From the comparison of Figure 5.20 and Figure 5.25, it can be concluded that the use of sonication did not make any difference in particle size distribution.

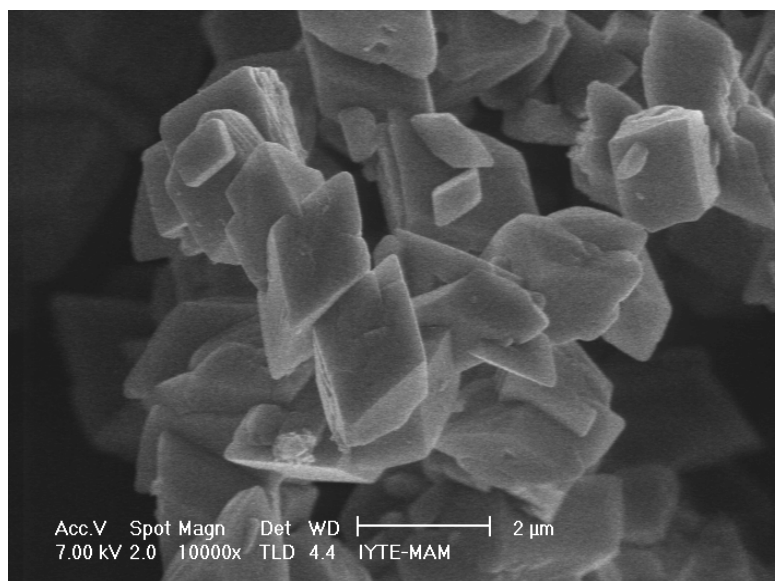


Figure 5.24. SEM microphotographs of zinc borate produced at 90 °C for 5 h, at  $B_2O_3/ZnO$  molar ratio of 2.0, 4.7 mol.dm<sup>-3</sup> boric acid and under sonication (S-5).

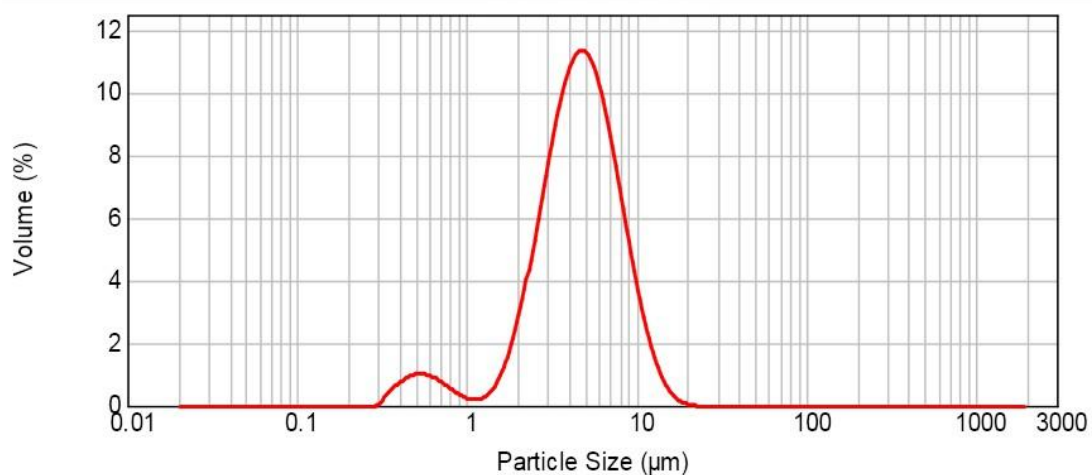


Figure 5.25. Particle size distribution of zinc borate produced at 90 °C for 5 h, at  $B_2O_3/ZnO$  molar ratio of 2.0, 4.7 mol.dm<sup>-3</sup> boric acid and under sonication (S-5), (Malvern Mastersizer 2000).

### 5.3.4. Effect of Zinc Oxide Particle Size

Particle size of reactant is one of the parameters that influence both the particle size of the product and the reaction rate. The reaction between zinc oxide and boric acid in aqueous media was assumed as a heterogeneous reaction and the influence of process variables on the particle size of formed zinc borate was investigated by Shete and co-

workers (2004). Unreacted core-model for the reaction between boric acid and zinc oxide should not be only mechanism as suggested by Shete et al., (2004). Nucleation and growth of zinc borate crystals by reaction of zinc cations and borate anions occur in the aqueous phase. It is known that boric acid dissolves in water accepting the hydroxyl group of the water and producing  $H^+$  proton in aqueous phase as mentioned in Equation 2.5. The pH of the  $0.75 \text{ mol.dm}^{-3}$  boric acid solution was given as 3.69 (Briggs, 2001). Thus, the reactant, zinc oxide, has to be dissolved under those conditions. Shete and co-workers reported that the particle size of zinc borate was close to the particle size of zinc oxide which means when particle size of zinc oxide is smaller, particle size of zinc borate becomes smaller. Thus, nanosized zinc oxide (particle size  $<100\text{nm}$ ) was used in the reaction to obtain nanosized zinc borate. From FTIR spectrum and XRD pattern it was obtained that zinc borate type of  $2\text{ZnO}\cdot 3\text{B}_2\text{O}_3\cdot 3\text{H}_2\text{O}$  was produced as shown in Figure 5.26. and Figure 5.27., respectively. But the particle size of zinc borate was not in nano level as it can be seen in Figure 5.29. The particle size of the zinc borate was as same as particle size of zinc borate produced with micron sized zinc oxide as shown in Figure 5.24. Zinc borate produced from nano zinc oxide starts to lose mass at about  $310^\circ\text{C}$  and ends at  $600^\circ\text{C}$  within one step as shown in Figure 5.28. The total mass loss was found as 12.7 %, which indicated the theoretical water content of zinc borate of  $2\text{ZnO}\cdot 3\text{B}_2\text{O}_3\cdot 3\text{H}_2\text{O}$  from Figure 5.28.

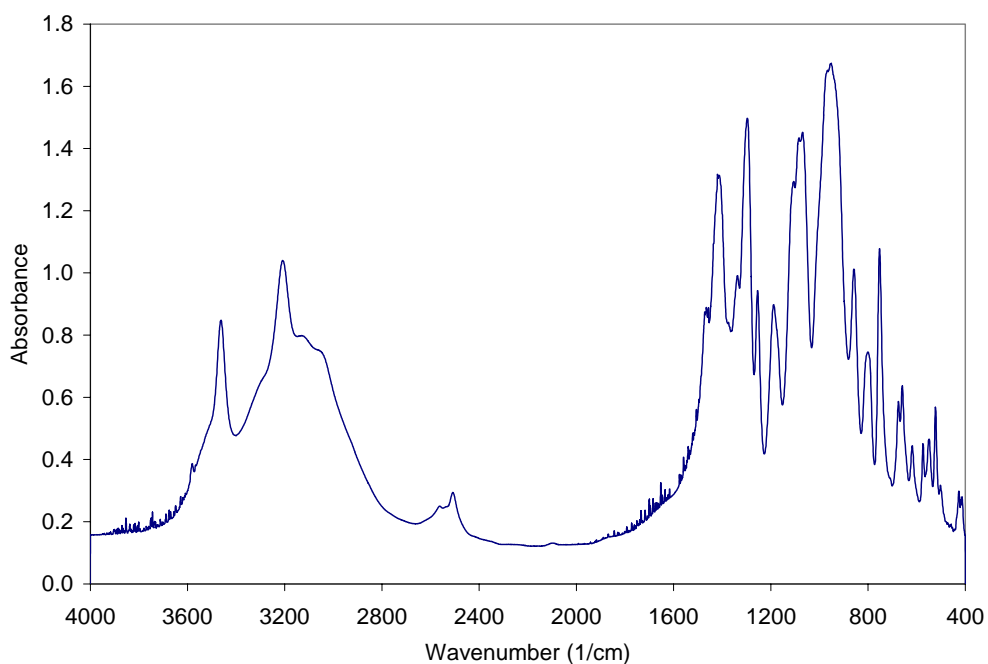


Figure 5.26. FTIR spectrum of zinc borate produced at  $90^\circ\text{C}$  for 5h, at  $\text{B}_2\text{O}_3/\text{ZnO}$  molar ratio of 2.0,  $4.7 \text{ mol.dm}^{-3}$  boric acid, and using nano zinc oxide (S-6).

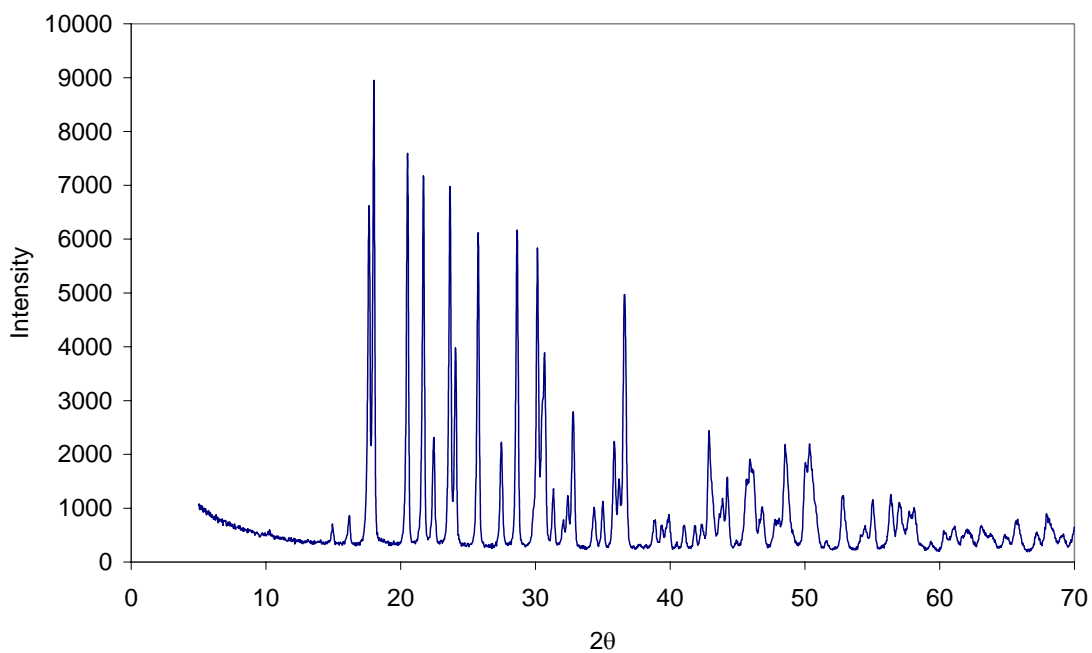


Figure 5.27. XRD pattern of zinc borate produced at 90 °C for 5 h, at  $B_2O_3/ZnO$  molar ratio of 2.0, 4.7 mol.dm<sup>-3</sup> boric acid and using nano zinc oxide (S-6).

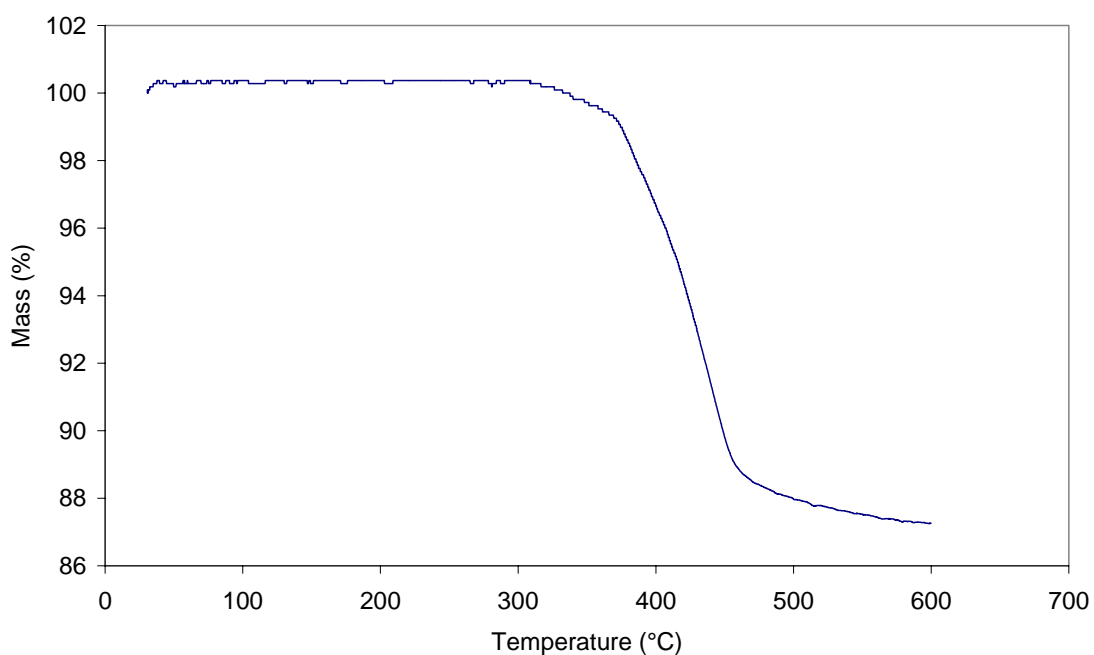


Figure 5.28. Thermogram of zinc borate produced at 90 °C for 5 h, at  $B_2O_3/ZnO$  molar ratio of 2.0, 4.7 mol.dm<sup>-3</sup> boric acid and using nano zinc oxide (S-6).

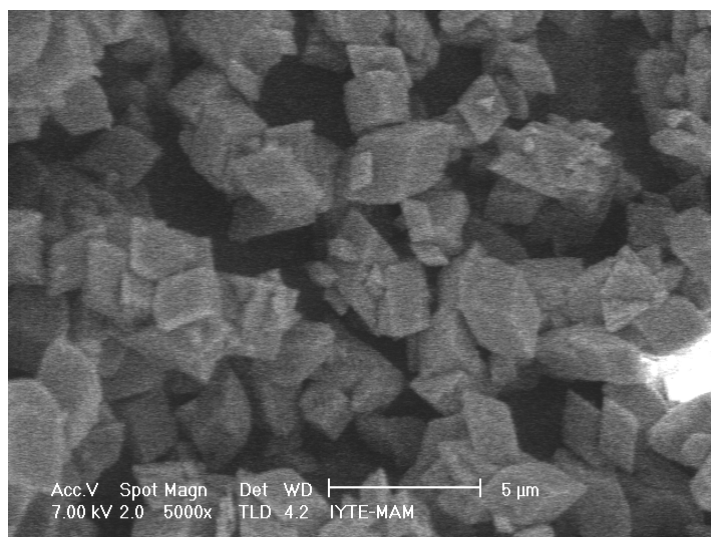


Figure 5.29. SEM microphotographs of zinc borate produced at 90 °C for 5 h, at  $B_2O_3/ZnO$  molar ratio of 2.0, 4.7 mol.dm<sup>-3</sup> boric acid and using nano zinc oxide (S-6).

Figure 5.30 displays particle size distribution of zinc borate produced using nano zinc oxide at 90 °C with 4.7 mol.dm<sup>-3</sup> boric acid concentration. A bimodal distribution; smaller percent of particles having particle size lower than 1.0 μm and volume-weighted mean diameter of 7.4 μm was observed. From the comparison of Figure 5.20 and Figure 5.30, that the use of nano zinc oxide was not effective also in controlling the particle size of the zinc borate. If unreacted core model was valid in the reaction of boric acid and zinc oxide as assumed by Shete and co-workers (2004), particle size of final product would be nanosized when nanosized zinc oxide was used.

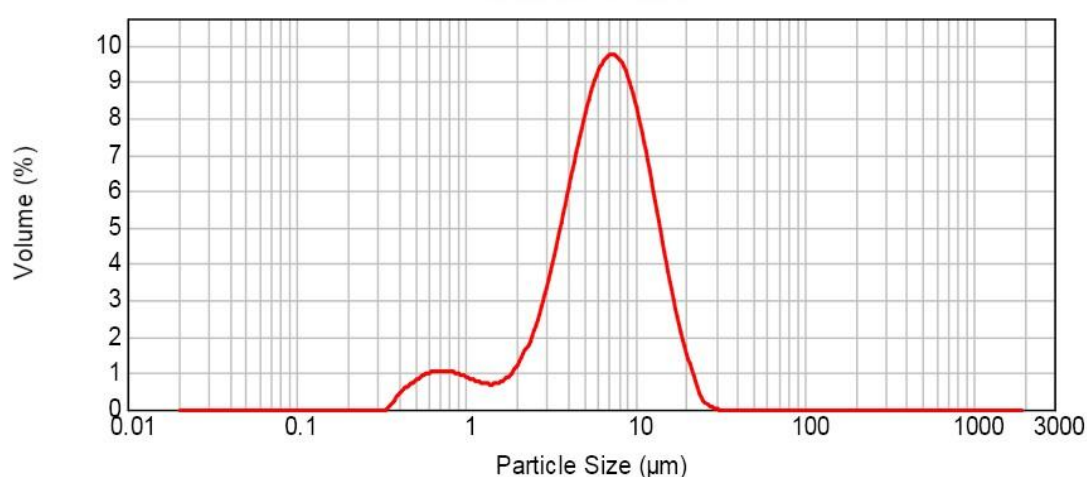


Figure 5.30. Particle size distribution of zinc borate produced at 90 °C for 5 h, at  $B_2O_3/ZnO$  molar ratio of 2.0, 4.7 mol.dm<sup>-3</sup> boric acid and using nano zinc oxide (S-6), (Malvern Mastersizer 2000).

### 5.3.5. Effect of Oleic Acid as a Modifying Agent

Modifying agents are used for controlling the particle size and morphology of the product during reaction. Tian and co-workers (2008) used oleic acid in the reaction of borax decahydrate and zinc sulfate hexahydrate at 70 °C for 6.5 h of reaction time. The optimum amount of oleic acid was pointed as 1.0 % of the final product mass. For controlling the particle size and morphology of the zinc borate, oleic acid 1.0 % of the reactants' mass was used in the reaction of boric acid and zinc oxide.

The FTIR spectrum and XRD pattern of zinc borate produced in the presence of oleic acid are shown in Figure 5.31. and Figure 5.32., respectively. From the examination of major peaks of IR spectrum and XRD pattern,  $\text{ZnO}\cdot\text{B}_2\text{O}_3\cdot 2\text{H}_2\text{O}$  was formed in the presence of oleic acid. Instead of the controlling particle size, oleic acid caused to formation of different zinc borate type. Thermal behavior of the zinc borate produced in the presence of oleic acid is given in Figure 5.33. The observed mass loss, 16.9 %, is very close to the theoretical water content of zinc borate ( $\text{ZnO}\cdot\text{B}_2\text{O}_3\cdot 2\text{H}_2\text{O}$ ).

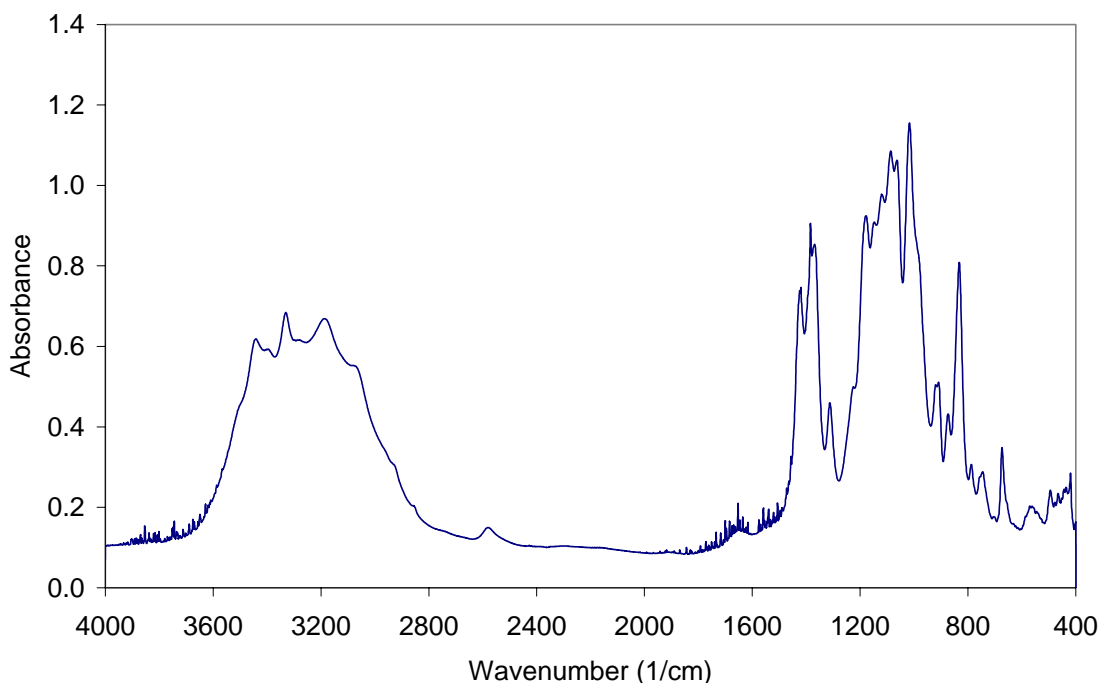


Figure 5.31. FTIR spectrum of zinc borate produced at 90 °C for 5 h, at  $\text{B}_2\text{O}_3/\text{ZnO}$  molar ratio of 2.0, 4.7 mol.dm<sup>-3</sup> boric acid and using oleic acid as modifying agent and ethanol (S-7).

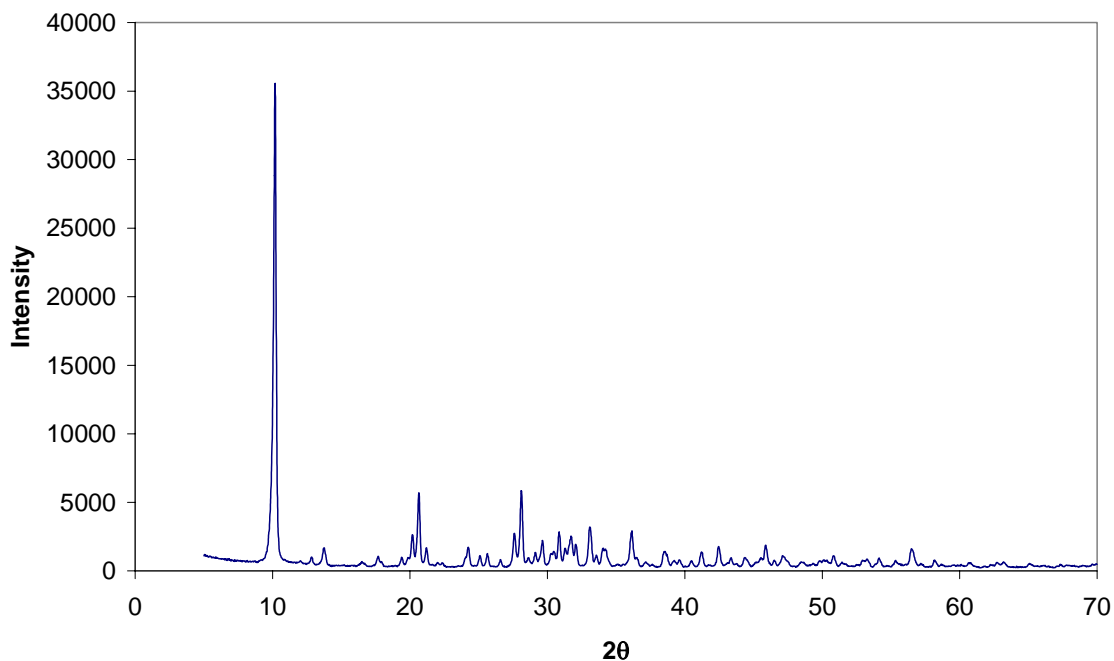


Figure 5.32. XRD pattern of zinc borate produced at 90 °C for 5 h, at  $B_2O_3/ZnO$  molar ratio of 2.0,  $4.7 \text{ mol.dm}^{-3}$  boric acid and using oleic acid as modifying agent and ethanol (S-7).

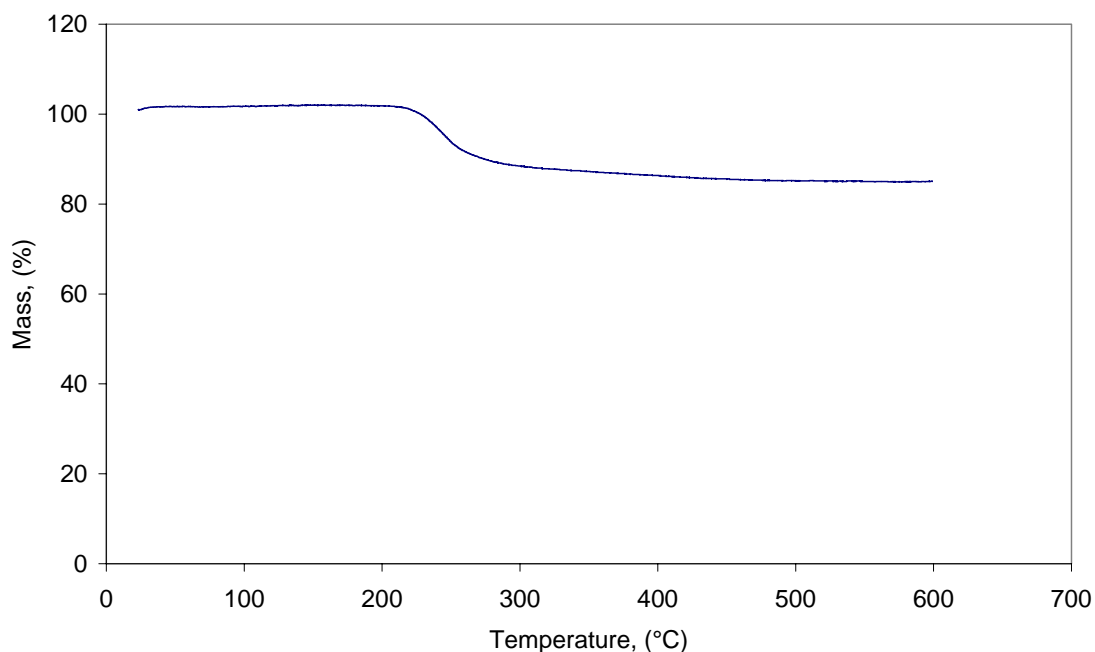


Figure 5.33. Thermogram of zinc borate produced at 90 °C for 5 h,  $B_2O_3/ZnO$  molar ratio of 2.0,  $4.7 \text{ mol.dm}^{-3}$  boric acid and using oleic acid as modifying agent and ethanol (S-7).

The particle size of the product was not in nano level as it can be seen in Figure 5.34. The type of zinc borate particles has the characteristics of  $ZnO \cdot B_2O_3 \cdot 2H_2O$ . Zinc

borate particles show a plate-like morphology rectangular shape and about 50 nm in thickness, 200-300 nm in width and 5-10  $\mu\text{m}$  in length.

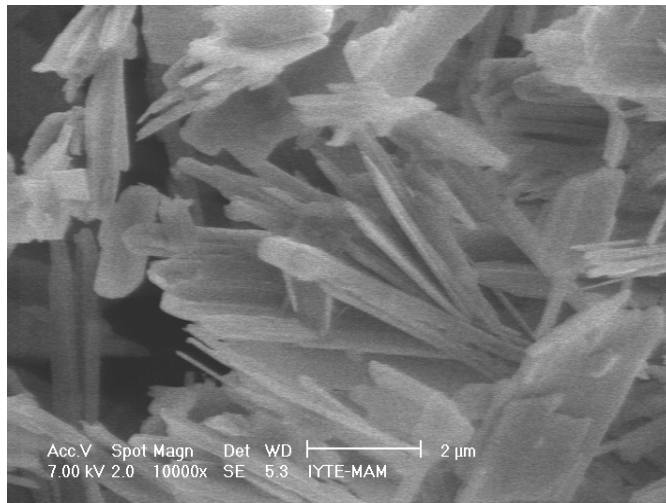


Figure 5.34. SEM microphotographs of zinc borate produced at 90 °C for 5 h, molar ratio of 2.0, 4.7  $\text{mol}\cdot\text{dm}^{-3}$  boric acid and using oleic acid as modifying agent and ethanol (S-7).

Figure 5.35 shows particle size distribution of zinc borate produced using 4.7  $\text{mol}\cdot\text{dm}^{-3}$  boric acid concentration and oleic acid as modifying agent at 90 °C. A bimodal distribution; smaller percent of particles had volume-weighted mean diameter lower than 3.0  $\mu\text{m}$  and greater percent with volume-weighted mean diameter of 13.6  $\mu\text{m}$  was observed. Actually, smaller particles (3  $\mu\text{m}$ ) include submicron particle as there is a shoulder peak in the first peak of size distribution. That the use of oleic acid as modifying agent was not a good choice in controlling the particle size for the determined zinc borate type as understood from the comparison of Figure 5.20 and Figure 5.35.



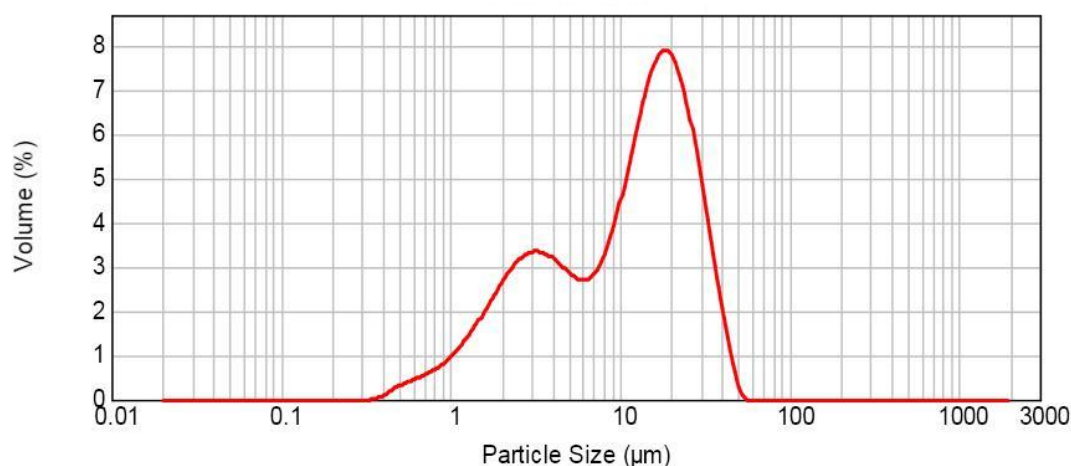


Figure 5.35. Particle size distribution of zinc borate produced at 90 °C for 5 h,  $B_2O_3/ZnO$  molar ratio of 2.0,  $4.7 \text{ mol.dm}^{-3}$  boric acid and using oleic acid as modifying agent and ethanol (S-7), (Malvern Mastersizer 2000).

### 5.3.6. Analytical Characterization

Zinc borate samples produced under different conditions were characterized by analytical titration. Results shown in Table 5.3., indicate that there are two different types of zinc borates based on the  $B_2O_3/ZnO$  molar ratio. The first one has the  $B_2O_3/ZnO$  molar ratio of around 1.2 and the latter one has the  $B_2O_3/ZnO$  molar ratio of about 1.5. At the same time, molar ratio usually indicates the alkalinity of the borate, low ratio not only corresponds to lower  $B_2O_3$  content but also to higher pH of the solution from which the borate is crystallized (Schubert, 2003).

Zinc borates produced using  $3.0 \text{ mol.dm}^{-3}$  boric acid concentration at 70 °C (S-1),  $4 \text{ mol.dm}^{-3}$  boric acid concentration at 90 °C (S-2),  $3.0 \text{ mol.dm}^{-3}$  boric acid concentration at 90 °C (S-3), and  $4.7 \text{ mol.dm}^{-3}$  boric acid concentration at 90 °C in the presence of oleic acid (S-7) have approximately same ZnO and  $B_2O_3$  contents. As indicated in Table 5.3,  $B_2O_3/ZnO$  molar ratio of zinc borate samples is around 1.1 which corresponds to the resolved oxide formula of  $ZnO \cdot B_2O_3 \cdot 2H_2O$  or  $Zn[BO(OH)_2]_2 \cdot H_2O$ . Based on those experimental data, the reaction depicted on Equation 5.8, took place when boric acid concentration was used as 3.0, 4.0  $\text{mol.dm}^{-3}$  and  $4.7 \text{ mol.dm}^{-3}$  with oleic acid as modifying agent at 90 °C.



On the other hand, zinc borates produced using  $4.7 \text{ mol.dm}^{-3}$  boric acid concentration (S-4) at  $90 \text{ }^\circ\text{C}$  and at different parameters; sonication (S-5), nano zinc oxide (S-6) have the  $\text{B}_2\text{O}_3/\text{ZnO}$  molar ratio of 1.5, which corresponds to the zinc borate formula of  $2\text{ZnO} \cdot 3\text{B}_2\text{O}_3 \cdot 3\text{H}_2\text{O}$  or  $\text{Zn}[\text{B}_3\text{O}_4(\text{OH})_3]$ .

Some borates contain isolated  $[\text{B}(\text{OH})_4]^-$  units, such as the mineral frovolute,  $\{\text{Ca}[\text{B}(\text{OH})_4]_2 = \text{CaO} \cdot \text{B}_2\text{O}_3 \cdot 4\text{H}_2\text{O}\}$  as shown in Figure 5.36.a. The condensation of two  $[\text{B}(\text{OH})_4]^-$  units produce the  $[\text{B}_2\text{O}(\text{OH})_6]^{2-}$  anion found in minerals, such as pinnoite,  $\{\text{Mg}[\text{B}_2\text{O}(\text{OH})_6] = \text{MgO} \cdot \text{B}_2\text{O}_3 \cdot 3\text{H}_2\text{O}\}$  as pointed in Figure 5.36.b. Further condensation leads to infinite chains of oxygen linked 4-coordinate boron that is found in the mineral vimsite,  $\{\text{Ca}[\text{BO}(\text{OH})_2]_2 = \text{CaO} \cdot \text{B}_2\text{O}_3 \cdot 2\text{H}_2\text{O}\}$ . The resolved oxide formula,  $\text{ZnO} \cdot \text{B}_2\text{O}_3 \cdot 2\text{H}_2\text{O}$ , of zinc borate having  $\text{B}_2\text{O}_3/\text{ZnO}$  molar ratio of 1.1 should have the same structure with vimsite except the metal cation. As it is clearly seen in those structures, water present in the structure is in the form of hydroxyl groups attached to the boron atom Figure 5.36.c.

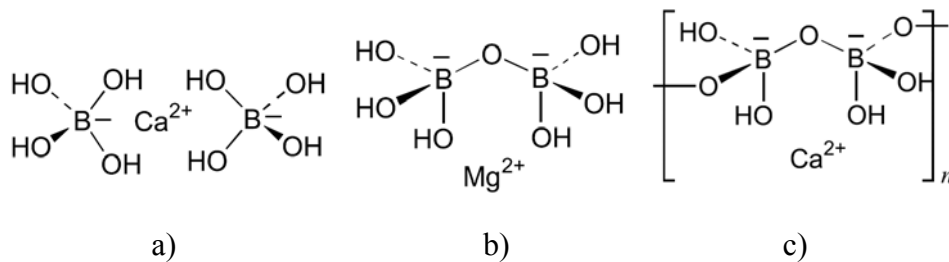


Figure 5.36. Schematic structures of some borate minerals, a) frovolute, b) pinnoite and c) vimsite (Source: Schubert, 2003).

When the FTIR spectra of those zinc borates (S-2, S-3, and S-7) were examined it was seen that these samples included interstitial water due to the presence of H-O-H bending peak at around  $1650 \text{ cm}^{-1}$ . Thus, the reaction given in Equation 5.8 produces  $\text{Zn}[\text{BO}(\text{OH})_2]_2 \cdot \text{H}_2\text{O}$  instead of  $\text{Zn}[\text{BO}(\text{OH})_2]_2$ .

Water content in resolved oxide formula of borate compound is usually related to the degree of condensation in borates. Water content of zinc borate samples (wt %), found by subtracting the sum of  $\text{B}_2\text{O}_3$  % and  $\text{ZnO}$  % from hundred confirmed the water content value obtained from TGA analysis for both zinc borate types ( $2\text{ZnO} \cdot 3\text{B}_2\text{O}_3 \cdot 3\text{H}_2\text{O}$  and  $\text{ZnO} \cdot \text{B}_2\text{O}_3 \cdot 2\text{H}_2\text{O}$ ). It is pointed that two forms of water can

easily be distinguished by TGA analysis as the dehydration reaction due to the condensation of hydroxyl groups occurs at significantly higher onset temperatures compared with the loss of interstitial (crystallization) water (Schubert, 2003). Based on this fact, zinc borate samples having a higher onset dehydration temperatures, such as (S-4, S-5, and S-6) have hydroxyl groups in their structures. The obtained onset temperatures (290-310 °C) for those samples are compatible with the given dehydration onset temperatures in the literature (Gürhan et al., 2009, Schubert et al., 2003). On the other hand, zinc borate samples with lower dehydration temperatures between 220-240 °C, for instance S-2, S-3, and S-7 have both water of crystallization and hydroxyl groups in their structures. Since zinc borate (S-1) has lower two different dehydration onset temperatures, 130 °C and 240 °C corresponding to two different types,  $2\text{ZnO}\cdot 3\text{B}_2\text{O}_3\cdot 7\text{H}_2\text{O}$  and  $\text{ZnO}\cdot \text{B}_2\text{O}_3\cdot 2\text{H}_2\text{O}$ , respectively it is a mixture of two types and has both water of crystallization and hydroxyl groups in its structure.

In Table 5.3, particle morphology of the zinc borate samples are also listed. While zinc borate of  $\text{ZnO}\cdot \text{B}_2\text{O}_3\cdot 2\text{H}_2\text{O}$  has long plate-like morphology, zinc borate of  $2\text{ZnO}\cdot 3\text{B}_2\text{O}_3\cdot 3\text{H}_2\text{O}$  has prismatic particles. Zinc borates having bimodal particle size distribution consist of both submicron and micron sized particles. Smaller peak in the size distributions shows submicron particles, and taller peak represents micron sized particles.

Table 5.3. ZnO, B<sub>2</sub>O<sub>3</sub>, H<sub>2</sub>O contents, dehydration onset temperature and particle morphology of zinc borate samples

Sample	Parameter	ZnO, (%)	B <sub>2</sub> O <sub>3</sub> , (%)	B <sub>2</sub> O <sub>3</sub> /ZnO Molar Ratio	H <sub>2</sub> O, (%)		Dehydration Onset Temperature (°C)	Particle Morphology	Mean Diameter (µm)
					From Chemical Analysis*	From TGA			
S-1	3.0 mol.dm <sup>-3</sup> boric acid concentration at 70 °C	38.95	40.41	1.21	19.64	22.14	130, 240	Long plate-like	7.6
S-2	4.0 mol.dm <sup>-3</sup> boric acid concentration at 90 °C	39.32	40.36	1.19	20.32	18.16	240	Long plate-like	4.5
S-3	3.0 mol.dm <sup>-3</sup> boric acid concentration at 90 °C	41.83	41.28	1.15	16.89	18.16	240	Long plate-like	5.9
S-4	4.7 mol.dm <sup>-3</sup> boric acid concentration at 90 °C	38.10	47.13	1.44	14.77	12.56	290	prismatic	5.8
S-5	4.7 mol.dm <sup>-3</sup> boric acid concentration at 90 °C under sonication	38.54	48.01	1.45	13.45	13.0	300	prismatic	5.1
S-6	4.7 mol.dm <sup>-3</sup> boric acid concentration at 90 °C using nano ZnO	38.44	50.26	1.52	11.30	12.7	310	prismatic	7.4
S-7	4.7 mol.dm <sup>-3</sup> boric acid concentration at 90 °C using oleic acid	42.60	41.40	1.13	16.00	16.9	220	Long plate-like	13.6

\*: Calculated by subtracting percent values of ZnO and B<sub>2</sub>O<sub>3</sub> from hundred.

## 5.4. Zinc Borate Production in a Mechanical-Stirred Stainless Steel Reactor

After determining the effects of reaction conditions and reactant amounts for zinc borate production from boric acid and zinc oxide in the glass reactor, zinc borate species were also produced in a stainless steel reactor with mechanical mixing apparatus. The effects of stirring using a four-bladed turbine type impeller and reaction time were investigated.

### 5.4.1. Effect of Reaction Time

In order to observe the progress of reaction between boric acid and zinc oxide, IR spectroscopy and X-ray diffraction were used. The experiments were carried out in a temperature and stirring-controlled stainless-steel reactor for different reaction times. Two steps at 60 °C and 90 °C were applied in the production: In the former one, the mixture of reactants was stirred at 60 °C for 90 min then it was further mixed at 90 °C for different reaction times e.g., 2 h, 3 h, and 4 h.

Before analyzing the effect of reaction time on the production of zinc borate, specific peaks of zinc borate species will be discussed. IR spectra of zinc borates that were obtained by KBr disc method (Colthup et al., 1990) are shown in Figure 5.37. All the observed vibration frequencies of FTIR spectra were assigned referring the literature on other metal borates (Jun et al., 1995 and Zhihong et al., 2003) and listed in Table 5.4. The IR spectra of hydrated zinc borates exhibited the following absorptions. The bands between  $2800\text{ cm}^{-1}$  and  $3600\text{ cm}^{-1}$  are due to O-H stretching. While  $2\text{ZnO}\cdot 3\text{B}_2\text{O}_3\cdot 7\text{H}_2\text{O}$  has only one broad strong peak,  $2\text{ZnO}\cdot 3\text{B}_2\text{O}_3\cdot 3\text{H}_2\text{O}$  has two sharp peaks at the same region. Configurational difference of hydroxyl groups or hydrogen bonding between them could be the reasons of why there is distinction between IR peaks of two zinc borate species. And that substantial distinction could be used to distinguish the zinc borate types (Eltepe et al., 2007). The band at  $2520\text{ cm}^{-1}$  and  $2682\text{ cm}^{-1}$  is the hydrogen bonded O-H stretching in the spectra of  $2\text{ZnO}\cdot 3\text{B}_2\text{O}_3\cdot 3\text{H}_2\text{O}$  and  $2\text{ZnO}\cdot 3\text{B}_2\text{O}_3\cdot 7\text{H}_2\text{O}$ ,

respectively. The band appearing at  $1652\text{ cm}^{-1}$  in the spectrum of  $2\text{ZnO}\cdot 3\text{B}_2\text{O}_3\cdot 7\text{H}_2\text{O}$  is assigned to the H-O-H bending mode, which correspond to the presence of crystal or interstitial water in the compound. Unlike  $2\text{ZnO}\cdot 3\text{B}_2\text{O}_3\cdot 3\text{H}_2\text{O}$ ,  $2\text{ZnO}\cdot 3\text{B}_2\text{O}_3\cdot 7\text{H}_2\text{O}$  contains the water of crystallization in its structure. The band at  $1652\text{ cm}^{-1}$  wavenumber can also be used to distinguish the zinc borate types as it is unique for  $2\text{ZnO}\cdot 3\text{B}_2\text{O}_3\cdot 7\text{H}_2\text{O}$ . The implicit chemical structure of  $2\text{ZnO}\cdot 3\text{B}_2\text{O}_3\cdot 7\text{H}_2\text{O}$  and  $2\text{ZnO}\cdot 3\text{B}_2\text{O}_3\cdot 3\text{H}_2\text{O}$  should be as following  $\text{Zn}[\text{B}_3\text{O}_3(\text{OH})_5]\cdot \text{H}_2\text{O}$  and  $\text{Zn}[\text{B}_3\text{O}_4(\text{OH})_3]$  based on results of IR and thermal analysis (Eltepe et al., 2007 and Schubert et al., 2003). The bands in  $1305\text{-}1425$  and  $864\text{-}960\text{ cm}^{-1}$  might be the asymmetric and symmetric stretching of  $\text{BO}_3$ , respectively. The bands at  $1228$  and  $1257\text{ cm}^{-1}$  are the in-plane bending of B-O-H. The bands in  $1000\text{-}1200$  and  $771\text{-}844\text{ cm}^{-1}$  are assigned as the asymmetric and symmetric stretching of  $\text{BO}_4$ , respectively. The band at a  $725\text{ cm}^{-1}$  is the out of plane bending mode of  $\text{BO}_3$ . The bands at  $624$  and  $650\text{ cm}^{-1}$  are assigned as the characteristic symmetric pulse vibration of  $\text{B}_3\text{O}_4(\text{OH})_3$ <sup>-2</sup> and  $\text{B}_3\text{O}_3(\text{OH})_5$ <sup>-2</sup>, respectively. The bands at  $526$  and  $586\text{ cm}^{-1}$  might be assigned to the bending mode of ( $\text{BO}_3$ ) and ( $\text{BO}_4$ ). The bands at  $430$  and  $468\text{ cm}^{-1}$  are assigned to the bending mode of ( $\text{BO}_4$ ).

In Figure 5.37., IR spectra of zinc borate samples that were produced at two heating steps, at  $60\text{ }^\circ\text{C}$  for 1.5 h and at  $90\text{ }^\circ\text{C}$  for different reaction times of 2, 3, and 4 h are shown. According to the characteristic IR peaks at  $3250$  and  $3500\text{ cm}^{-1}$  wavenumbers, zinc borate type of  $2\text{ZnO}\cdot 3\text{B}_2\text{O}_3\cdot 3\text{H}_2\text{O}$  was synthesized. It was concluded that 2 h reaction time at  $90\text{ }^\circ\text{C}$  was adequate for the synthesis of zinc borate type of  $2\text{ZnO}\cdot 3\text{B}_2\text{O}_3\cdot 3\text{H}_2\text{O}$  based on IR analysis. It was pointed out that zinc borate of  $2\text{ZnO}\cdot 3\text{B}_2\text{O}_3\cdot 7\text{H}_2\text{O}$  was synthesized in the first heating period at  $60\text{ }^\circ\text{C}$  according to the IR result (Eltepe et al., 2007). It is anticipated that same zinc borate ( $2\text{ZnO}\cdot 3\text{B}_2\text{O}_3\cdot 7\text{H}_2\text{O}$ ) was synthesized in the first heating period at  $60\text{ }^\circ\text{C}$  and it was converted into zinc borate of  $2\text{ZnO}\cdot 3\text{B}_2\text{O}_3\cdot 3\text{H}_2\text{O}$  either releasing water by condensation of OH groups or recrystallizing into a new structure.

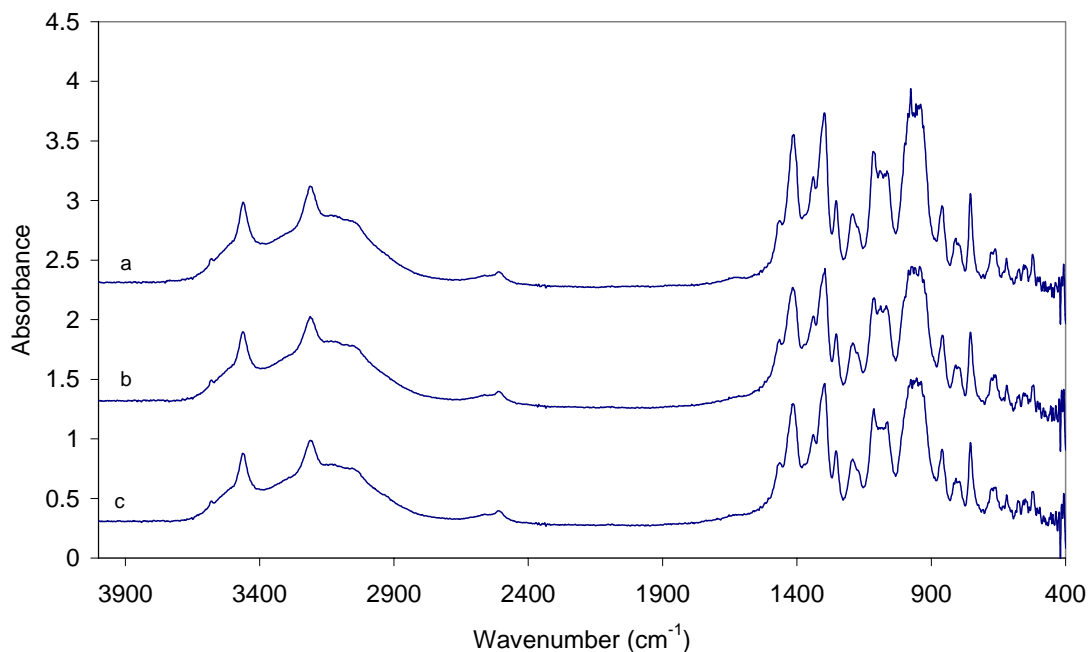


Figure 5.37. IR spectra of zinc borate samples produced at 90 °C for a) 2 h (S-8), b) 3 h (S-9), c) 4 h (S-10) (initially all samples were heated at 60 °C for 1.5 h).

Table 5.4. Observed frequencies of IR spectra of  $2\text{ZnO}\cdot 3\text{B}_2\text{O}_3\cdot 3\text{H}_2\text{O}$  and  $2\text{ZnO}\cdot 3\text{B}_2\text{O}_3\cdot 7\text{H}_2\text{O}$  (Source: Jun et al., 1995)

FT-IR ( $\text{cm}^{-1}$ )		
$2\text{ZnO}\cdot 3\text{B}_2\text{O}_3\cdot 3\text{H}_2\text{O}$	$2\text{ZnO}\cdot 3\text{B}_2\text{O}_3\cdot 7\text{H}_2\text{O}$	Assignment
3471	3606	$\nu(\text{O-H})$
3227	3373	
	3221	
2520	2682	
	1652	$\delta(\text{H-O-H})$
1425	1408	$\nu_{\text{as}}(\text{BO}_3)$
1346	1369	
1305		
1257	1228	$\delta(\text{B-O-H})$
1200	1130	$\nu_{\text{as}}(\text{BO}_4)$
1118	1070	
	1000	
960	941	$\nu_{\text{s}}(\text{BO}_3)$
864	891	$\nu_{\text{s}}(\text{BO}_4)$
816	844	
756	771	
	725	$\gamma(\text{BO}_3)$
624	650	$\nu_{\text{p}}(\text{B}_3\text{O}_4(\text{OH})_3)^{-2}$
553	586	$\delta(\text{BO}_3), \delta(\text{BO}_4)$
526	536	
432	468	$\delta(\text{BO}_4)$
	430	

IR spectra of zinc borate samples that were produced in different heating programs are given in Figure 5.38. When the IR spectra of zinc borates are compared, it is seen that the production of  $2\text{ZnO}\cdot 3\text{B}_2\text{O}_3\cdot 3\text{H}_2\text{O}$  at  $90\text{ }^\circ\text{C}$  is possible under appropriate mixing. As a result, the use of initial step carried out at  $60\text{ }^\circ\text{C}$  for 90 min in the production zinc borate ( $2\text{ZnO}\cdot 3\text{B}_2\text{O}_3\cdot 3\text{H}_2\text{O}$ ) is not needed.

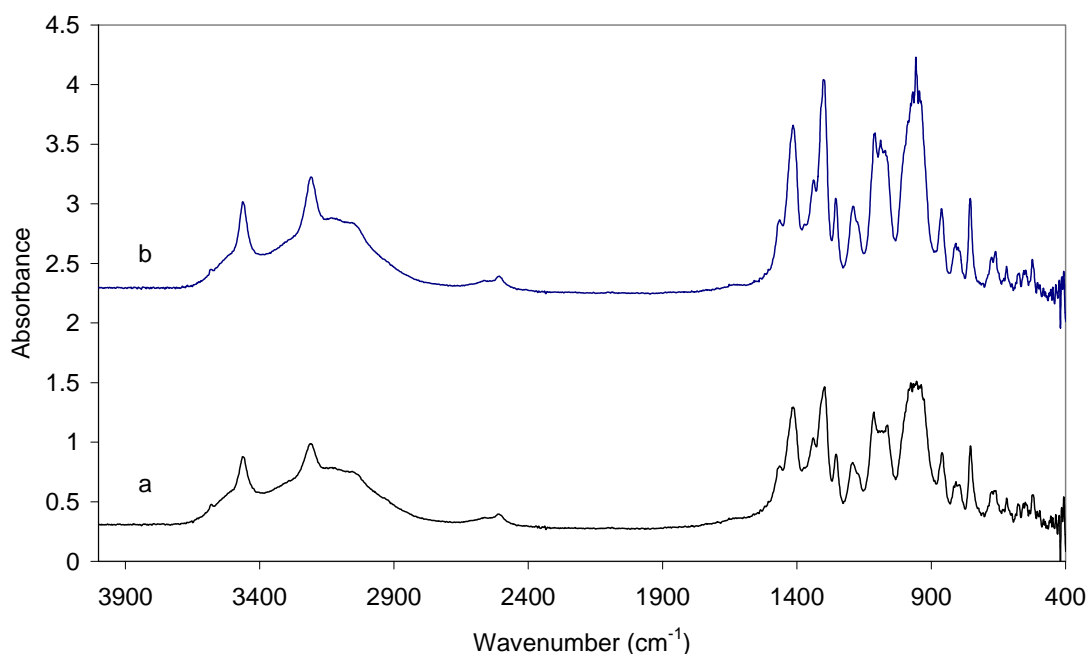


Figure 5.38. IR spectra of zinc borate samples produced a) at  $90\text{ }^\circ\text{C}$  for 4 h (S-10), (initially at  $60\text{ }^\circ\text{C}$  for 1.5 h), b) at  $90\text{ }^\circ\text{C}$  for 4 h (S-11).

X-ray diffraction diagrams of zinc borate samples produced in the reactor are given in Figure 5.39. Zinc borate of  $2\text{ZnO}\cdot 3\text{B}_2\text{O}_3\cdot 3\text{H}_2\text{O}$  was produced for all cases since the X-ray diffraction peaks observed were identical to that of  $2\text{ZnO}\cdot 3\text{B}_2\text{O}_3\cdot 3\text{H}_2\text{O}$  reported in the study of Sawada et al., (2004). It can be concluded that 2 h reaction time is enough for this reaction to form the desired material.

A comparison of two step process and one step process based on XRD patterns was given in Figure 5.40. It was seen that zinc borate obtained from two step process can also be produced by using a one step process at  $90\text{ }^\circ\text{C}$  in the presence of adequate mixing.



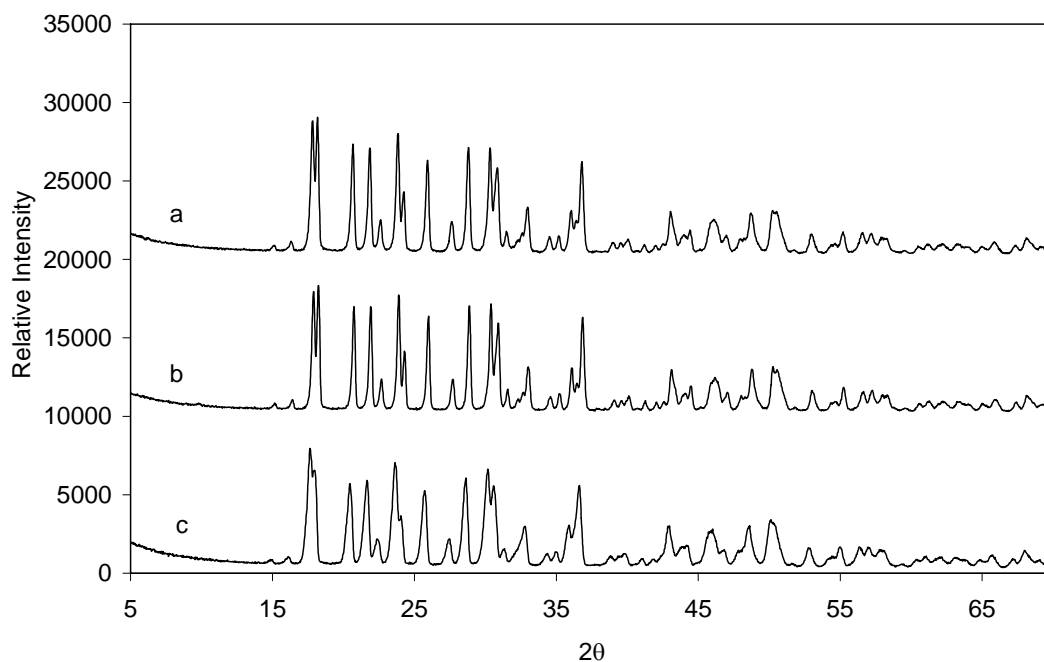


Figure 5.39. XRD patterns of zinc borate samples produced at 90 °C for a) 2 h (S-8), b) 3 h (S-9), c) 4 h (S-10) (initially all samples were heated at 60 °C for 1.5 h).

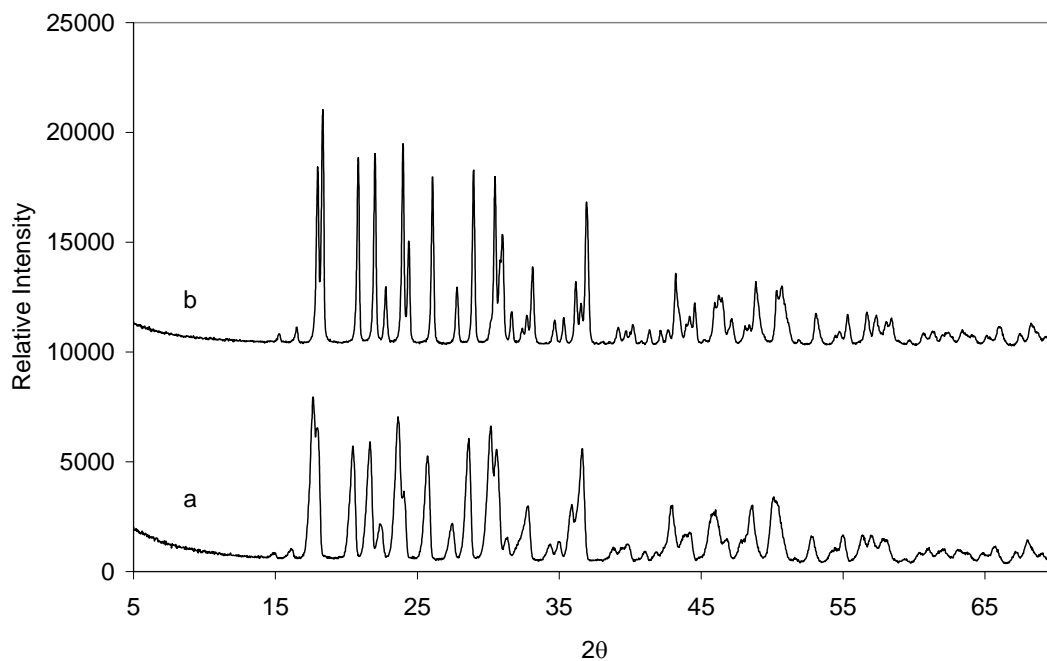
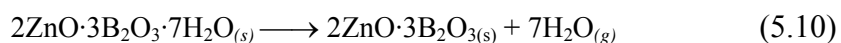


Figure 5.40. XRD patterns of zinc borate samples produced a) at 90 °C for 4 h (S-10), (initially at 60 °C for 1.5 h), b) at 90 °C for 4 h (S-11).

Thermogravimetric analysis shows the mass loss versus temperature data on programmed heating of a sample. It indicates mass loss due to the removal of volatile compounds from a sample. In the present study, the volatile compound is expected to be

water that formed from the condensation of OH groups. The upward slope of the TGA curves in Figure 5.41 during the initial periods of heating was due to a small drift in the baseline of the instrument.

Thermal behavior of zinc borate samples produced using two step processes in the reactor is shown in Figure 5.41. All zinc borate samples started to lose mass at 290 °C and mass losses occurred between 12.6-13.0 % which is comparable to the calculated value of 12.69 % for zinc borate of  $2\text{ZnO}\cdot 3\text{B}_2\text{O}_3\cdot 3\text{H}_2\text{O}$ . For all samples, the mass losses occurred mainly due to the removal of hydroxyl groups in the structure. Thermal degradation mechanisms of zinc borate samples may be proposed as given in Equation 5.9 and Equation 5.10.  $2\text{ZnO}\cdot 3\text{B}_2\text{O}_3\cdot 3\text{H}_2\text{O}$  decomposes at temperatures between 290 °C and 450 °C to yield an amorphous product which corresponds to its dehydrated form (Equation 5.9). After the formation of amorphous structure, with increasing temperature a crystalline zinc borate with  $\alpha$  and  $\beta$  phases occurred (Samyn et al., 2007). It is expected that zinc borate,  $2\text{ZnO}\cdot 3\text{B}_2\text{O}_3\cdot 7\text{H}_2\text{O}$ , should give same amorphous product according to Equation 5.10, when it is heated up to 140 °C.



DSC curves of zinc borate samples produced by two step process are shown in Figure 5.42. All samples gave one endotherm due to the condensation of B-OH groups in the structure. Dehydration reactions happen in two successive steps: Removal of water formed from weakly bonded O·H groups' condensation and removal of water by condensation which was formed from strongly bonded O-H groups. From DSC curves, one can conclude that zinc borate of  $2\text{ZnO}\cdot 3\text{B}_2\text{O}_3\cdot 3\text{H}_2\text{O}$  keeps its stability up to 300 °C, and then it starts to degrade to form water during heating finally degradation is completed at 450 °C. The area of endotherm gives the dehydration energy of the sample.

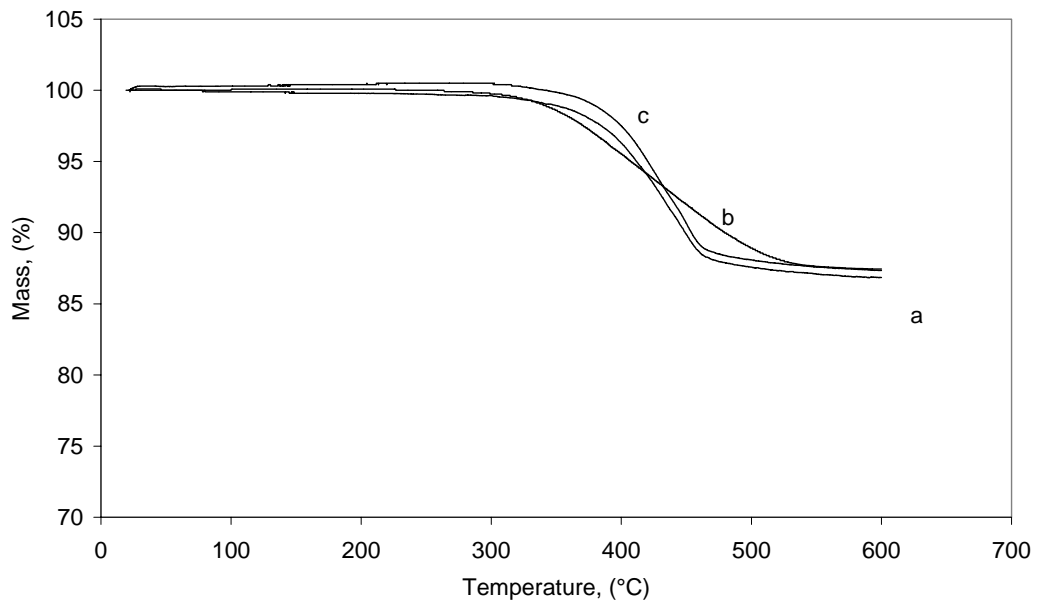


Figure 5.41. Thermograms of zinc borate samples produced at 90 °C for a) 2 h (S-8), b) 3 h (S-9), c) 4 h (S-10) (initially all samples were heated at 60 °C for 1.5 h).

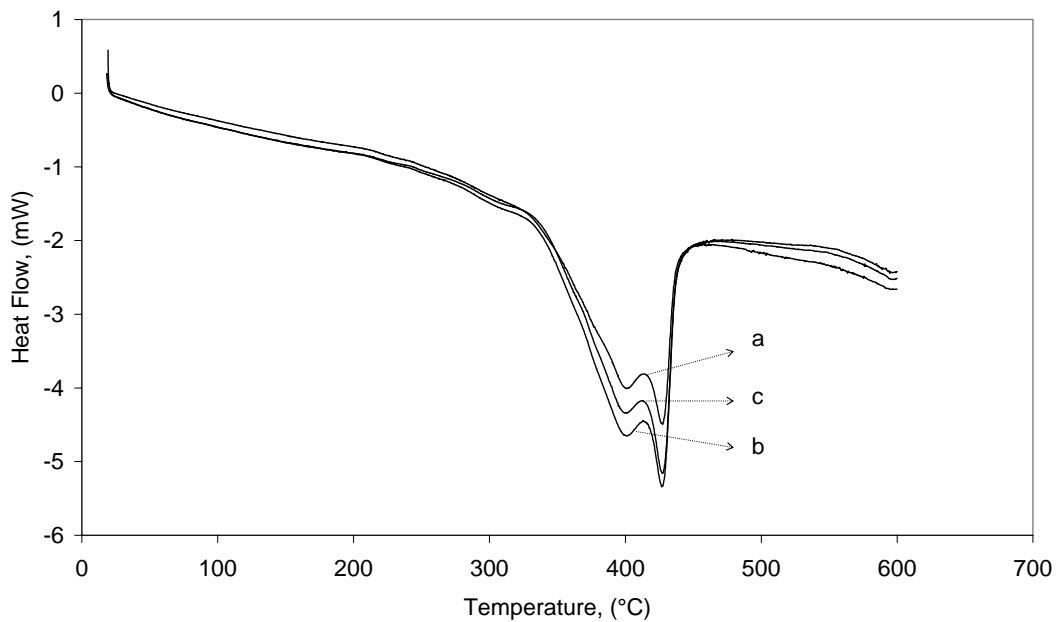


Figure 5.42. DSC curves of zinc borate samples produced at 90 °C for a) 2 h (S-8), b) 3 h (S-9), c) 4 h (S-10) (initially all samples were heated at 60 °C for 1.5 h).

The thermal behavior of zinc borate samples were compared using DSC and TGA in Figure 5.43 and Figure 5.44, respectively. Thermal properties of zinc borates obtained from two processes were same in the TGA and DSC analyses. Thus, two step process proposed by Sawada and co-workers (2004) is not needed for zinc borate synthesis. Zinc borate having same thermal properties with the one that was synthesized

from two step process can be produced using only one step of heating at 90 °C under sufficient mixing.

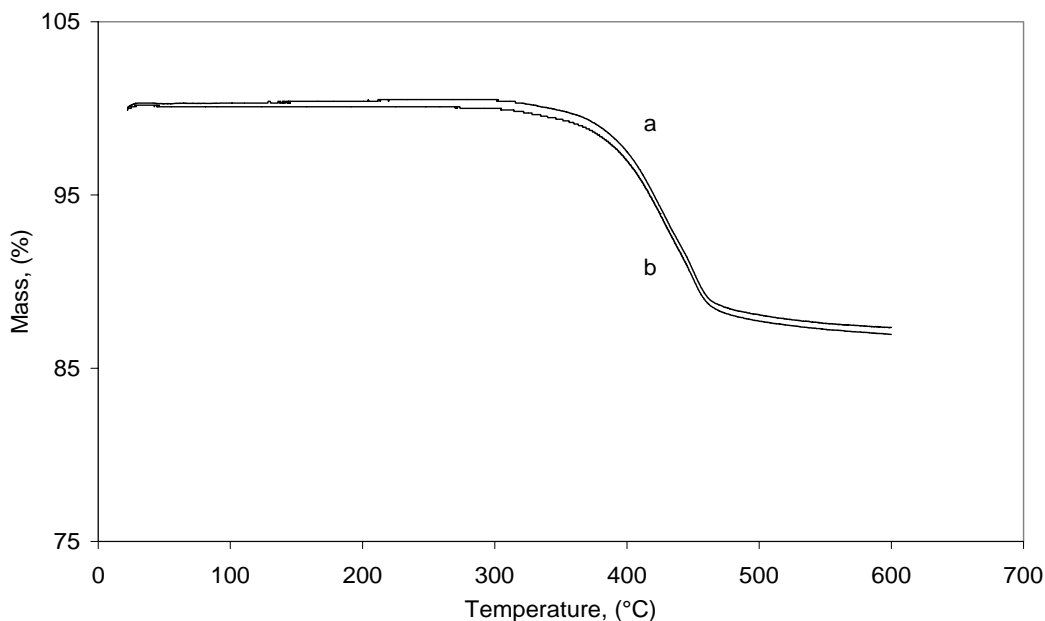


Figure 5.43. Thermograms of zinc borate samples produced a) at 90 °C for 4 h (S-10), (initially at 60 °C for 1.5 h), b) at 90 °C for 4 h (S-11).

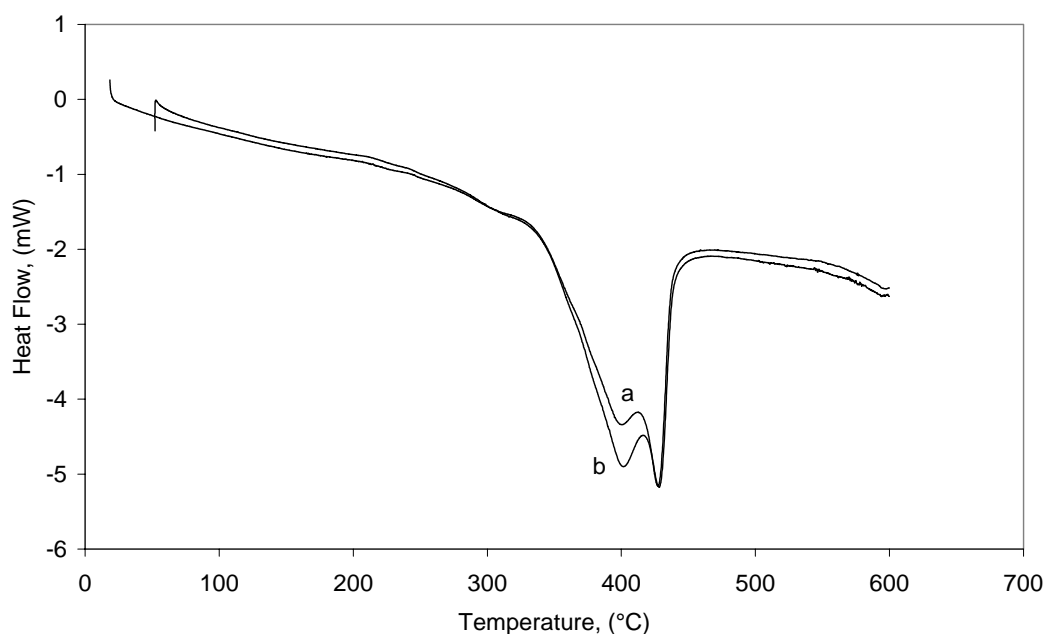


Figure 5.44. DSC curves of zinc borate samples produced a) at 90 °C for 4 h (S-10), (initially at 60 °C for 1.5 h), b) at 90 °C for 4 h (S-11).

Thermal properties of zinc borate samples produced using two step process and one step process are given in Table 5.5. The dehydration energy, which was calculated from peak areas in DSC curves, was between 385.7 and 457.3 J.g<sup>-1</sup>. These calculated energies were for the condensation of B-OH groups in zinc borate structure. It was

understood that much more energy ( $4275\text{-}5600 \text{ J}\cdot\text{g}^{-1}$ ) needed for removal of water from structure than required for only evaporation of water ( $2200 \text{ J/g H}_2\text{O}$ ).

Table 5.5. Dehydration behavior of zinc borates produced at  $90 \text{ }^\circ\text{C}$  for 2 h, 3 h, 4 h (initially samples were heated at  $60 \text{ }^\circ\text{C}$  for 1.5 h) and produced at only  $90 \text{ }^\circ\text{C}$  for 4 h.

Sample	Rxn time at $90 \text{ }^\circ\text{C}$ (h)	$\Delta\text{H}$ (J/g)	Peak ( $^\circ\text{C}$ )	On-set ( $^\circ\text{C}$ )	End-Set ( $^\circ\text{C}$ )	Mass Loss, (%)	$\Delta\text{H}$ (J/g $\text{H}_2\text{O}$ )
S-8*	2	385.7	427.7	395.3	442.3	9.0	4275.7
S-9*	3	414.5	426.7	388.6	441.0	7.4	5608.9
S-10*	4	392.7	427.4	388.4	440.9	7.9	4940.3
S-11	4	457.3	428.2	388.9	444.6	8.9	5092.7

\*: Reactants firstly mixed at  $60 \text{ }^\circ\text{C}$  for 1.5 h

Figure 5.45 shows the particle size distribution of zinc borate obtained in the stainless-steel reactor. The average particle size was determined as 2.91, 5.30, 3.15 and  $1.65 \text{ }\mu\text{m}$  for samples S-8, S-9, S-10, and S-11, respectively. The average crystal size of zinc borate samples were measured between  $1\text{-}3 \text{ }\mu\text{m}$  from SEM microphotographs as shown in Figure 5.46.

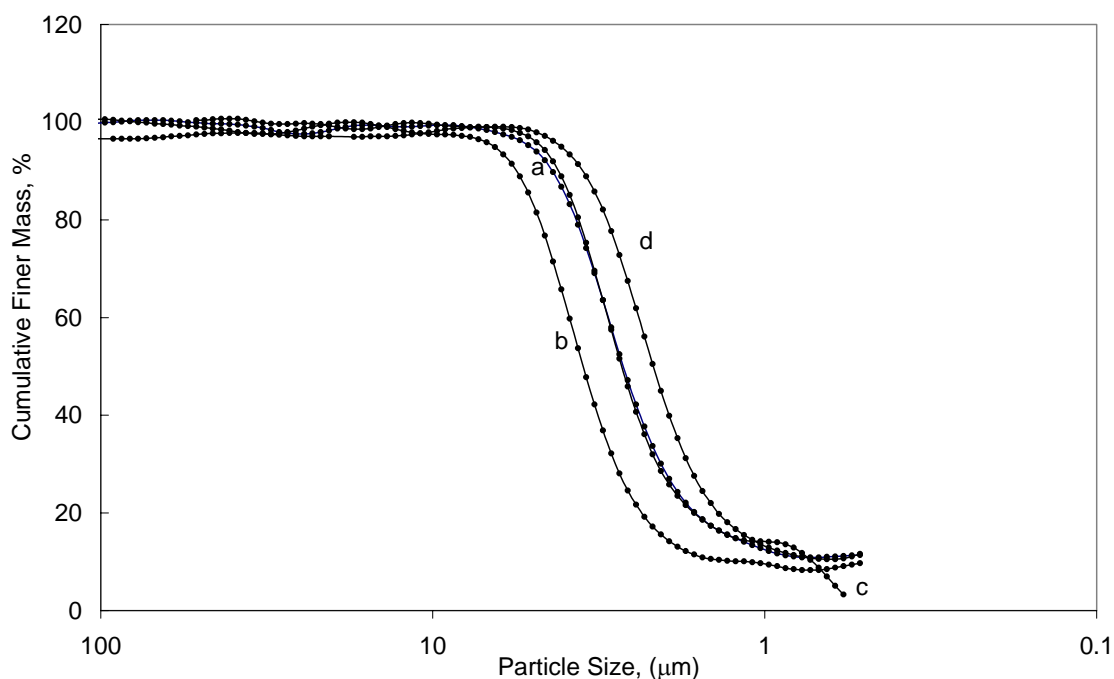


Figure 5.45. The particle size distributions of zinc borates produced at  $90 \text{ }^\circ\text{C}$  for a) 2 h (S-8), b) 3 h (S-9), c) 4 h (S-10) (initially all samples were heated at  $60 \text{ }^\circ\text{C}$  for 1.5 h) and produced at only  $90 \text{ }^\circ\text{C}$  for d) 4 h (S-11), (Sedigraph).

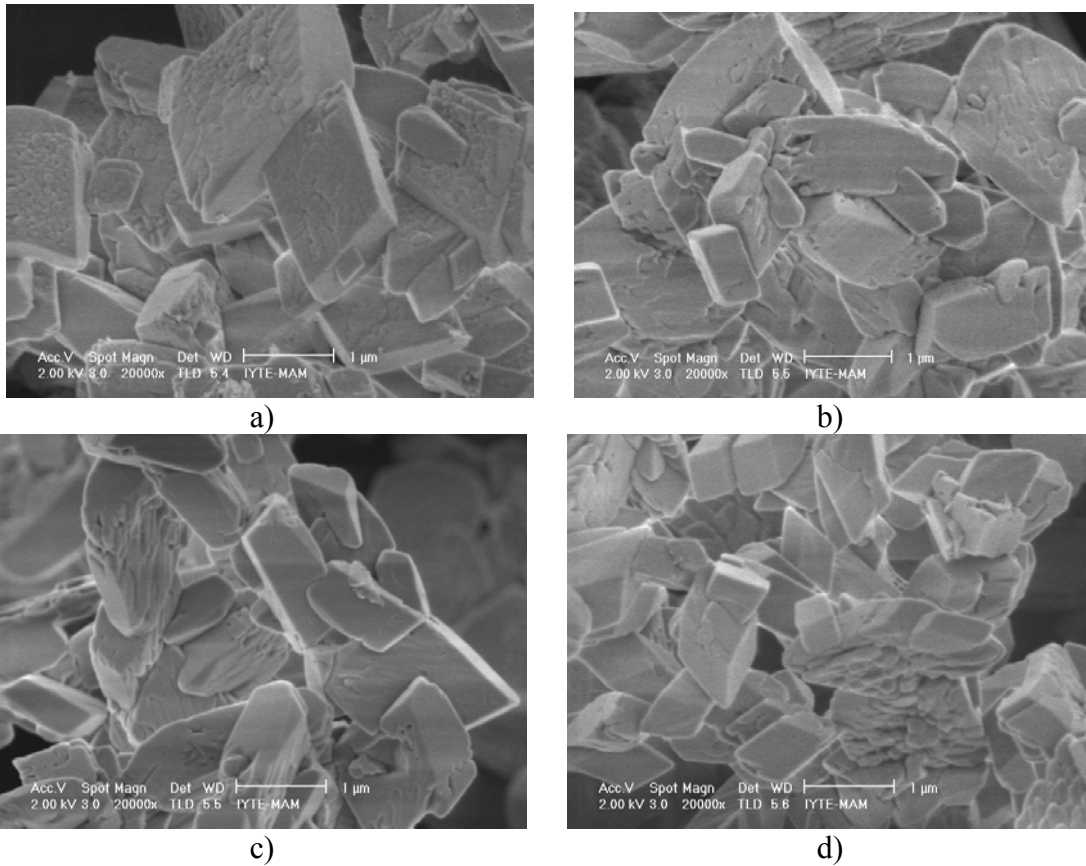


Figure 5.46. SEM microphotographs of zinc borates produced at 90 °C for a) 2 h (S-8), b) 3 h (S-9), c) 4 h (S-10) (initially all samples were heated at 60 °C for 1.5 h) and produced at only 90 °C for d) 4 h (S-11).

Figure 5.47 shows SEM image of zinc borate particles which was captured at 2500x magnification. Zinc borate crystals agglomerated in conventional drying due to the attractions between particles.

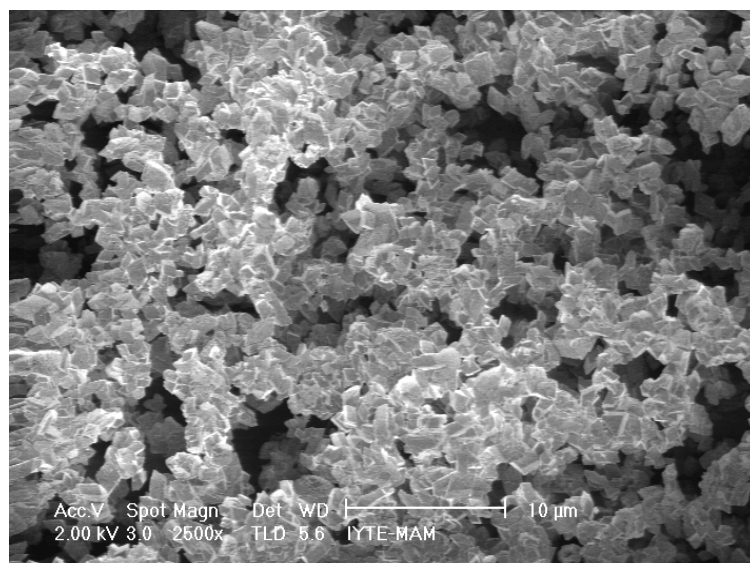


Figure 5.47. SEM microphotograph of zinc borate (S-11) produced at 90 °C for 4 h.

## 5.4.2. Analytical Characterization

The amount of unreacted boric acid in the aqueous phase of reaction mixture, and ZnO % and B<sub>2</sub>O<sub>3</sub> % contents of the zinc borate samples were determined by conventional titration technique. Results are given in Table 5.6. That zinc borates obtained in two step process (60 and 90 °C) could also be produced in a one step process at 90 °C as has been shown in XRD and FTIR results. B<sub>2</sub>O<sub>3</sub>/ZnO molar ratio of zinc borates produced in the two step process at different reaction times were different than each other. By elapsing reaction time at 90 °C, B<sub>2</sub>O<sub>3</sub>/ZnO molar ratio of samples decreased from 1.60 to 1.53 which is close to the theoretical value of 1.5. Theoretical values of ZnO %, B<sub>2</sub>O<sub>3</sub> %, and H<sub>2</sub>O % of zinc borate (2ZnO·3B<sub>2</sub>O<sub>3</sub>·3H<sub>2</sub>O) are 38.24 %, 49.06 %, and 12.69 % respectively. At this point, while the calculated value of ZnO % is close to the theoretical one, the value of B<sub>2</sub>O<sub>3</sub> % is about 2 % higher than the theoretical one for zinc borate samples. However, H<sub>2</sub>O % values of zinc borate samples are lower than the theoretical value. Since H<sub>2</sub>O % value is obtained by subtracting the summation of the other two values, all the experimental errors propagate in the result of H<sub>2</sub>O %. Actual values of H<sub>2</sub>O % was obtained from TG analysis. Density of zinc borate samples are also given in Table 5.6, increasing reaction time increased the density of the zinc borate formed from 2.38 to 2.52 kg.dm<sup>-3</sup>. The density of zinc borate produced for 4 h reaction time is very close to a value (2.86 kg.dm<sup>-3</sup>) given by Schubert et al. (2003).

Table 5.6. B(OH)<sub>3</sub> content, and B<sub>2</sub>O<sub>3</sub>/ZnO molar ratio and density of solid phase of zinc borates produced at 90 °C for 2 h, 3 h, 4 h (initially samples were heated at 60 °C for 1.5 h) and produced at only 90 °C for 4 h.

Sample	Rxn time at 90 °C (h)	B <sub>2</sub> O <sub>3</sub> , (%)	ZnO, (%)	B <sub>2</sub> O <sub>3</sub> /ZnO Molar Ratio	H <sub>2</sub> O, (%)	Density (kg.dm <sup>-3</sup> )
S-8*	2	50.50	37.93	1.60	10.60	2.38
S-9*	3	52.28	38.50	1.56	10.55	2.25
S-10*	4	50.50	38.80	1.53	10.60	2.52
S-11	4	50.80	37.81	1.57	11.05	2.47

\*: Reactants firstly mixed at 60 °C for 1.5 h

In the examination of wet zinc borates produced from boric acid and zinc oxide in moisture analyzer, it was found that wet samples, after filtration, contain about 45-50

% (wt) free water that should be removed during drying operation. Actually, the amount of free water is directly proportional to the filtration efficiency of the samples.

## **5.5. Zinc Borate Production from Borax Decahydrate and Zinc Nitrate Hexahydrate**

Alternatively, zinc borates can be produced from borax decahydrate and zinc nitrate hexahydrate. Hereafter, borax decahydrate and zinc nitrate hexahydrate will be named shortly as borax and zinc nitrate, respectively. The use of borax as a boron source for the nanosized metal borate synthesis has increased recently (Tian et al., 2008 and Zheng et al., 2009). The reaction between borax and zinc nitrate was initially carried out in a 0.25 dm<sup>3</sup> volume glass reactor to elucidate the reaction mechanism and products formed at the end of certain reaction times. Secondly, the production of zinc borate was studied using the same reactants in 0.30 dm<sup>3</sup> volume stainless steel reactor based on the outputs of previous experiments and literature data.

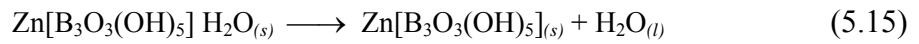
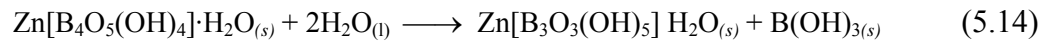
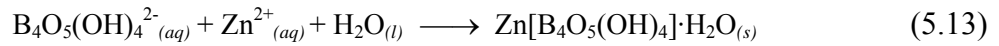
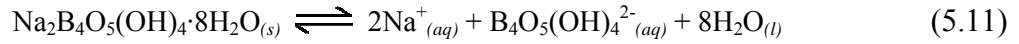
### **5.5.1. Reaction Mechanism**

While borax and zinc nitrate are soluble in water, zinc borate formed is sparingly soluble in water. The reaction is called as heterogeneous because of solid zinc borate in aqueous phase. The reaction was carried out in equivalent amounts of zinc nitrate and borax at 70 °C for different reaction periods.

Borax dissolves in aqueous phase according to Equation 5.11 to form tetra borate anion  $[B_4O_5(OH)_4]^{2-}$  and sodium cation, since it is soluble at 70 °C as shown in Figure 2.3. In Equation 5.12, zinc nitrate dissolves to produce zinc cations and nitrate anions. These reactions are anticipated ones based on literature data of borate and polyborate anions (Briggs, 2001 and Schubert, 2003). The formed polyborate anions and zinc cations precipitate when mixed together as shown in Equation 5.13. There are various types of zinc borate species which can be produced by changing reaction



parameters or reactants' molar ratio. After the precipitation, formed building blocks, (Zn[B<sub>4</sub>O<sub>5</sub>(OH)<sub>4</sub>]), rearrange and produce the Zn[B<sub>3</sub>O<sub>3</sub>(OH)<sub>5</sub>]·H<sub>2</sub>O or Zn[B<sub>3</sub>O<sub>3</sub>(OH)<sub>5</sub>] as depicted in Equation 5.14 and Equation 5.15, respectively. Further polymerization of these units result in sheets and networks of three dimensional structures. In those reactions, by product, sodium nitrate, formation was not taken into consideration since it was soluble and removed from the product by washing.



As soon as borax and zinc nitrate solutions were mixed, a white precipitate was formed from borate anion and zinc cation in the mixture. Since zinc borate species is sparingly soluble in aqueous phase, supersaturation is exceeded immediately after mixing. In this reactive crystallization, nucleation, crystal growth on formed nuclei, and interaction of those formed crystals take place. The progress of crystallization with respect to reaction time was examined from characterization results.

## 5.6. Zinc Borate Production in a Magnetically-Stirred Glass Reactor

### 5.6.1. Effect of Reaction Time

The progress of reaction between borax and zinc nitrate was observed by FTIR spectroscopy and X-ray diffraction. In these experiments that were carried out in a temperature and stirring-controlled glass reactor, samples taken at different reaction

times were analyzed by FTIR and XRD, TGA, and SEM. Reaction was carried out at 70 °C using equivalent amounts of zinc nitrate and borax under 1100 rpm mixing rate with a magnetic stirrer.

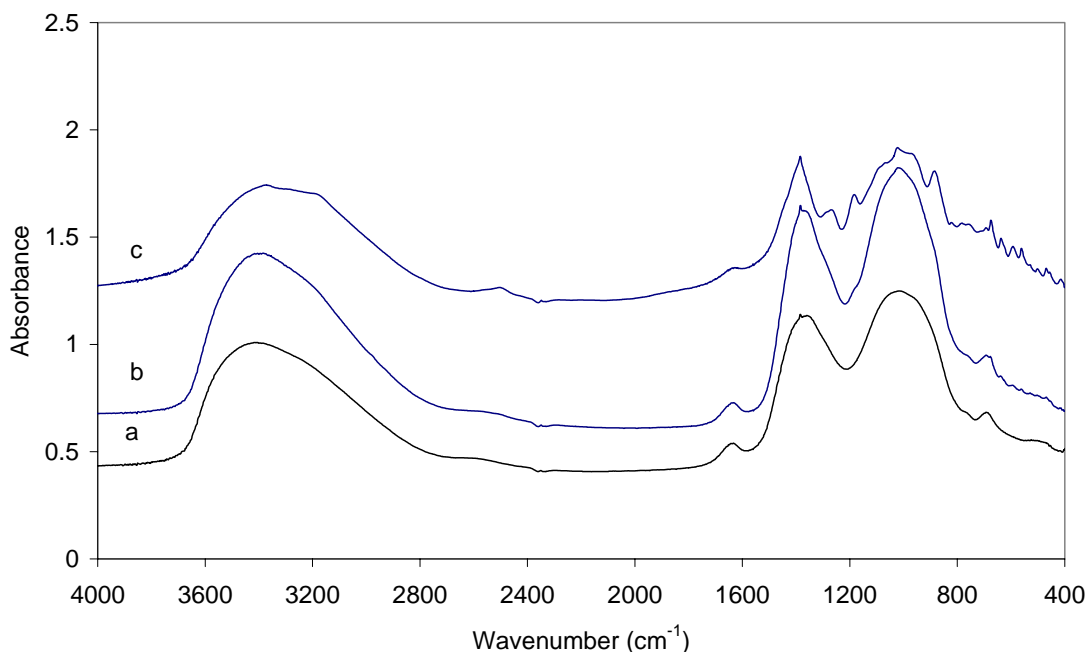


Figure 5.48. FTIR spectra of zinc borates produced from 1 mol.dm<sup>-3</sup> zinc nitrate and 1 mol.dm<sup>-3</sup> borax at 70 °C, mole ratio of borax/zinc nitrate =1.0 for reaction times a) 1h (S-12), b) 2h (S-13), c) 3h (S-14).

FTIR spectra of formed zinc borate samples are given in Figure 5.48. There are two different infrared spectra corresponding to two different zinc borate species. At the end of 1 h reaction time, isolated borate ions reacted with zinc cations to form fundamental building blocks of zinc borate. As it is seen from Figure 5.48.b there is further change in the structure of formed building blocks at the end of 2 h of reaction time. When the mixture was further stirred at 70 °C for 3 h, there was significant change in its coordination as inferred from its spectrum (Figure 5.48.c). The bands at 1386 cm<sup>-1</sup> due to the asymmetric stretching of BO<sub>3</sub> coordination, at 1030 cm<sup>-1</sup> caused by asymmetric stretching of BO<sub>4</sub> coordination and at 700 cm<sup>-1</sup> because of the out of plane bending of BO<sub>3</sub> indicate trihedral and tetrahedral boron-oxygen coordination in polyborate ion as shown in Figure 5.48.a and Figure 5.48.b. All types of zinc borates produced from borax contain water of crystallization in their structures as there is a peak at 1650 cm<sup>-1</sup> corresponding to the H-O-H bending mode. The broad peak between 2800 cm<sup>-1</sup> and 3600 cm<sup>-1</sup> indicates that there are hydroxyl groups attached to the main

structure. Another result from those spectra (Figure 5.48.a and Figure 5.48.b) that there is no hydrogen bonding between OH groups since there is no peak at  $2510\text{ cm}^{-1}$  wavenumber. The structure of zinc borate changed significantly and hydrogen bonding formed at the end of 3 h of reaction time (Figure 5.48.c). Zinc borate clusters transformed into a new structural configuration. There is a dynamic equilibrium between formed zinc borate clusters other ions, e.g.,  $\text{Zn}^{2+}$ ,  $\text{Na}^+$ ,  $\text{NO}_3^-$ , and borate ions. This part of reaction, up to 3 h reaction time, was called as nucleation of zinc borate clusters that would be utilized in the formation of zinc borate crystals.

When the mixture was further stirred at  $70\text{ }^\circ\text{C}$  for 4 h, 5 h, and 6 h there is no change in the structure of formed product at all except water of crystallization as understood from Figures 5.49.a-c. The peak at  $2510\text{ cm}^{-1}$  wavenumber in Figure 5.49.a and Figure 5.49.b, and Figure 5.49.c. shows the interaction of OH groups due to the hydrogen bonding. That peak shifted to the wavenumber of  $2590\text{ cm}^{-1}$  for zinc borate (Figure 5.49.d). Initially formed zinc borate structure lost its crystal water for the longer reaction times, such as 4, 5, and 6 hours. However, when the mixture was stirred for longer reaction times, such as 16 h, structure of zinc borate underwent a change as shown in Figure 5.49.d. This product includes also interstitial water in its structure since there is H-O-H bending vibration at  $1650\text{ cm}^{-1}$  wavenumber. Another considerable result is that zinc borate obtained from borax at the end of 16 h reaction time and zinc borate that was synthesized using  $3.0\text{ mol.dm}^{-3}$  and  $4.0\text{ mol.dm}^{-3}$  boric acid for 5 h reaction time are same type according to the infrared spectra (Figure 5.11.).

In this period of reaction (3-6 h), zinc borate crystals have grown on the clusters formed initially. When the reaction time increased to 16 h, a phase transformation took place and structural configuration of zinc borate changed completely. Dissolution and re-crystallization steps might be responsible for the phase transformation in zinc borate structure.

XRD patterns of zinc borates that were produced at different reaction times are shown through Figures 5.50-52. The existence of broad peak and absence of sharp peaks in XRD pattern as shown in Figure 5.50.a indicated that product formed at the end of 1 h reaction time had an amorphous structure. in XRD pattern of product prepared At the end of 2 h reaction time, a crystalline structure was determined from sharp peaks in the XRD pattern as illustrated in Figure 5.50.b. The existence of those sharp peaks pointed out that crystal growth began on the nuclei formed by consuming precursors from the aqueous solution.

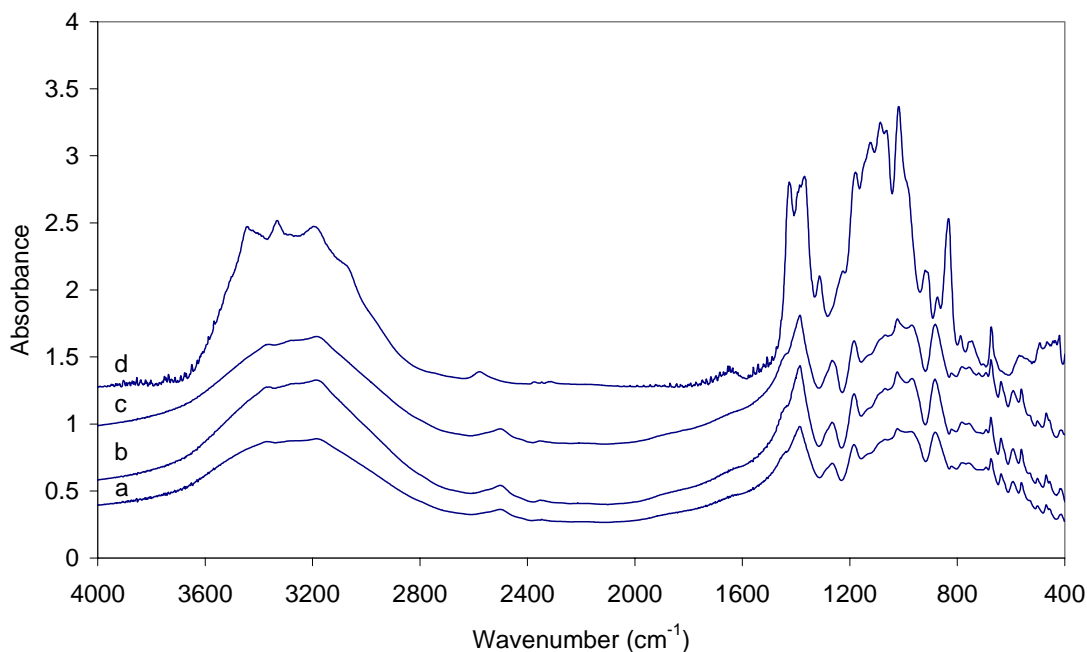


Figure 5.49. FTIR spectra of zinc borates produced from 1 mol.dm<sup>-3</sup> zinc nitrate and 1 mol.dm<sup>-3</sup> borax at 70 °C, mole ratio of borax/zinc nitrate =1.0 for reaction times a)- 4 h (S-15), b)- 5 h (S-16), c)- 6 h (S-17), d)- 16 h (S-18).

That new crystalline structure of zinc borate completely formed at the end of 3 h of reaction time as shown in Figure 5.51.a. It can be summarized that both nucleation and crystal formation had been occurred for 3 h of reaction time. Increasing the reaction time further did not make any change in the crystal structure of zinc borate as understood from Figure 5.51.b and Figure 5.51.c. However, another growth mechanism, Ostwald ripening, was responsible for the reaction period between 3 and 6 hours. During this period, smaller zinc borate crystals dissolved in favor of larger crystals. It was clearly inferred that with elapsing reaction time different zinc borate species were formed based on the XRD and FTIR results. After 3 h and 6 h of reaction time, zinc borate of  $2\text{ZnO}\cdot 3\text{B}_2\text{O}_3\cdot 7\text{H}_2\text{O}$  (JCPDS 75-0766 and Sawada et al., 2004) was formed and then at the end of 16 h it was converted into zinc borate type of  $\text{ZnO}\cdot \text{B}_2\text{O}_3\cdot 2\text{H}_2\text{O}$ . The major peaks in XRD pattern of zinc borate produced for 16 h of reaction time occurred at 10.2°, 20.6°, 28.2°, and 33.2° 2θ values as shown in Figure 5.52.a. The results obtained from XRD patterns confirmed the IR analysis results that three different zinc borate types were prepared in the reaction.

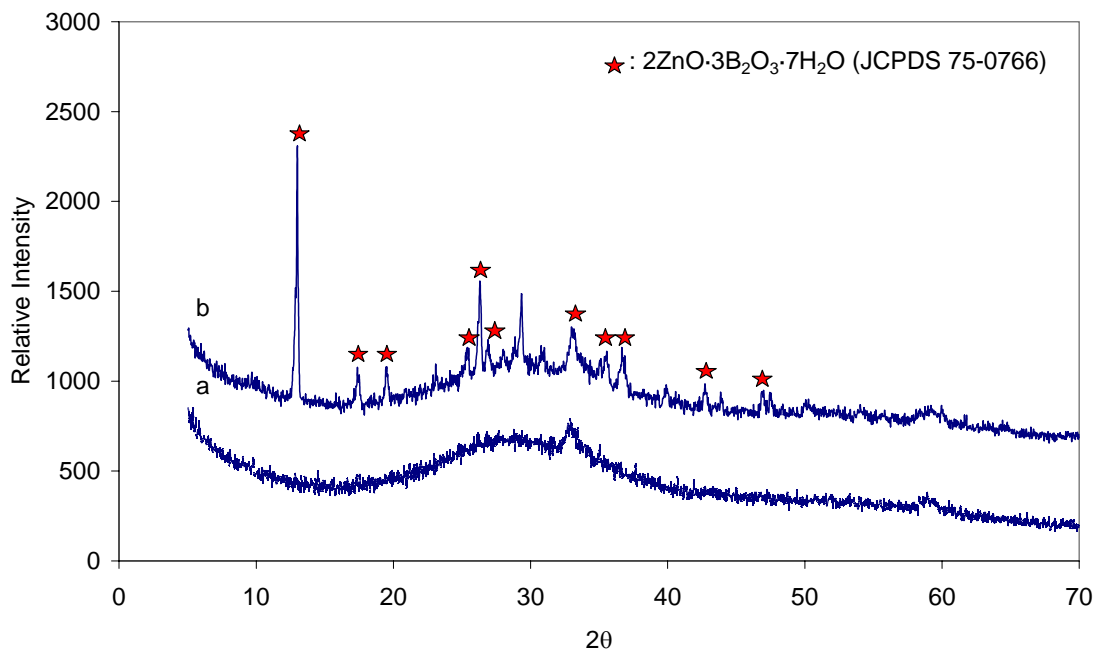


Figure 5.50. XRD patterns of zinc borates produced from  $1 \text{ mol.dm}^{-3}$  zinc nitrate and  $1 \text{ mol.dm}^{-3}$  borax at  $70^\circ \text{C}$ , mole ratio of borax/zinc nitrate = 1.0, for reaction times a) 1 h (S-12), b) 2 h (S-13).

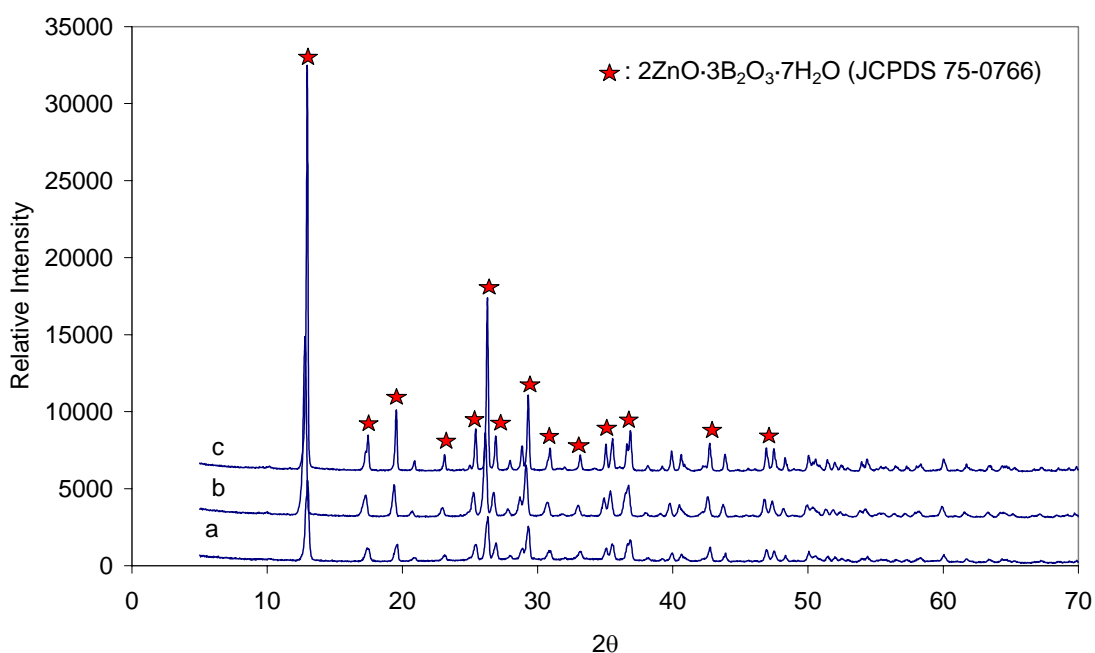


Figure 5.51. XRD patterns of Zinc Borates produced from  $1 \text{ mol.dm}^{-3}$  zinc nitrate and  $1 \text{ mol.dm}^{-3}$  borax at  $70^\circ \text{C}$ , mole ratio of borax/zinc nitrate = 1.0, for reaction times a) 3 h (S-14), b) 4 h (S-15), c) 5 h (S-16).

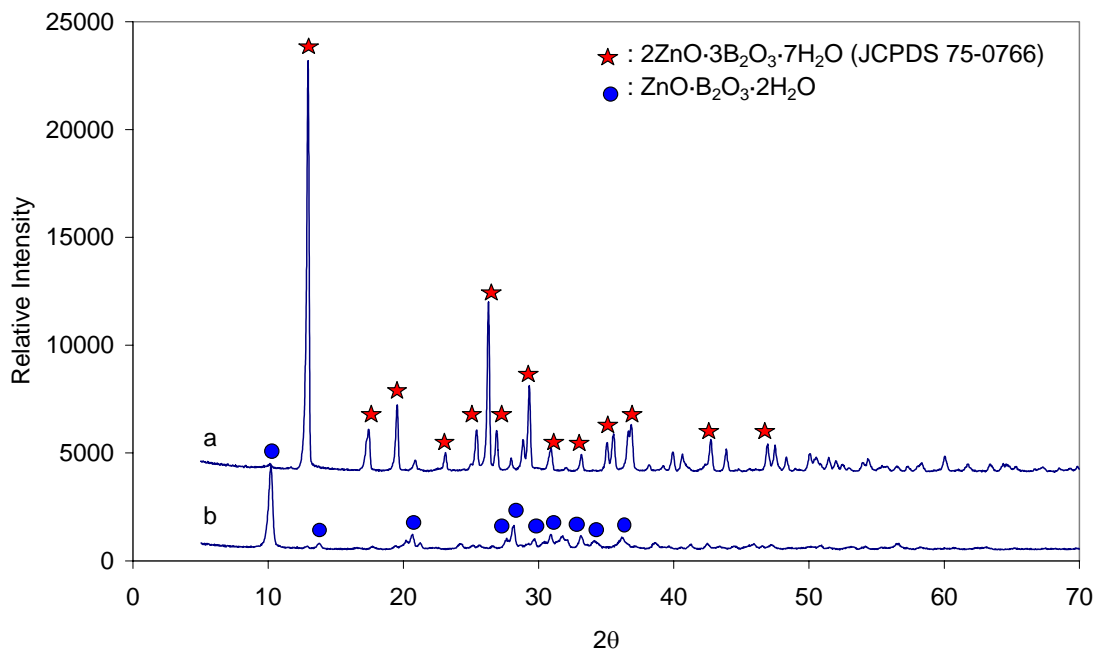


Figure 5.52. XRD patterns of zinc borates produced from 1 mol.dm<sup>-3</sup> zinc nitrate and 1 mol.dm<sup>-3</sup> borax at 70 °C, mole ratio of borax/zinc nitrate = 1.0, for reaction times a) 6 h (S-17), b) 16 h (S-18),

Thermal behaviors of zinc borates obtained at different reaction times (1-16 h) are shown in Figure 5.53. and Figure 5.54. While zinc borate obtained at the end of 1 h of reaction time began to lose mass upon heating, zinc borate obtained at the end of 3 h of reaction time showed only one dehydration step which started at around 190 °C as shown in Figure 5.53.a and Figure 5.53.b. Since the zinc borate clusters produced for 1 h of reaction time has an amorphous structure, coordination of hydroxyl groups is not so strong or they are not as stable as others. Thus, they are easily removed when they are exposed to heating even at lower than 100 °C. On the other hand, zinc borate produced at the end of 3 h reaction time has a mass loss of about 23.0 % due to the removal of water of crystallization or water formed from the polymerization of hydroxyl groups (B-OH). Based on the mass losses, chemical structure of zinc borate synthesized for 3 h of reaction time was determined as 2ZnO·3B<sub>2</sub>O<sub>3</sub>·7H<sub>2</sub>O and no chemical formula was estimated for the zinc borate obtained at the end of 1 h of reaction time based on the TGA analysis.

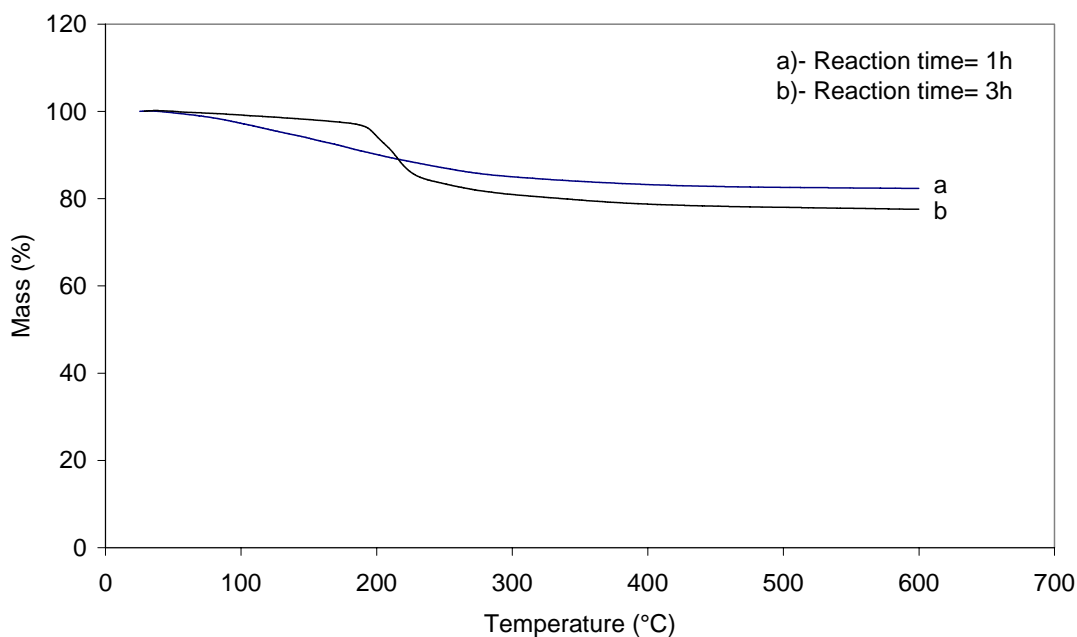


Figure 5.53. Thermograms of zinc borates produced from  $1 \text{ mol}\cdot\text{dm}^{-3}$  zinc nitrate and  $1 \text{ mol}\cdot\text{dm}^{-3}$  borax at  $70 \text{ }^\circ\text{C}$ , mole ratio of borax/zinc nitrate = 1.0, for reaction times a) 1 h (S-12), b) 3 h (S-14).

Thermograms of zinc borates produced at the end of 6 h and 16 h of reaction time are shown in Figure 5.54. Since FTIR spectra of those zinc borates produced between 3-6 h reaction periods are same, only zinc borate produced at the end of 6 h reaction time was examined in TGA analysis. Both thermograms decomposed in one step between  $200 \text{ }^\circ\text{C}$  and  $400 \text{ }^\circ\text{C}$  temperature range. The total mass loss occurred as 25.0 % when the zinc borate produced for 6 h of reaction time was heated from ambient temperature to  $600 \text{ }^\circ\text{C}$  as shown in Figure 5.54.a. The observed mass loss of 25.0 % corresponds to the water content value of  $2\text{ZnO}\cdot 3\text{B}_2\text{O}_3\cdot 7\text{H}_2\text{O}$ . Zinc borate produced at the end of 16 h reaction time started to lose mass at around  $240 \text{ }^\circ\text{C}$  and beyond  $400 \text{ }^\circ\text{C}$  no mass loss was observed till  $600 \text{ }^\circ\text{C}$  as shown in Figure 5.54.b. The mass loss of 20.0 % occurred due to the condensation of hydroxyl groups (B-OH) in that temperature range corresponds to the water content value, 19.25 %, in zinc borate ( $\text{ZnO}\cdot\text{B}_2\text{O}_3\cdot 2\text{H}_2\text{O}$ ) structure. It can be inferred that increasing reaction time caused zinc borate of  $2\text{ZnO}\cdot 3\text{B}_2\text{O}_3\cdot 7\text{H}_2\text{O}$  to lose water and it was converted into zinc borate of  $\text{ZnO}\cdot\text{B}_2\text{O}_3\cdot 2\text{H}_2\text{O}$ . In this phase transformation, zinc borate of  $2\text{ZnO}\cdot 3\text{B}_2\text{O}_3\cdot 7\text{H}_2\text{O}$  dissolved and recrystallized to form zinc borate of  $\text{ZnO}\cdot\text{B}_2\text{O}_3\cdot 2\text{H}_2\text{O}$ .

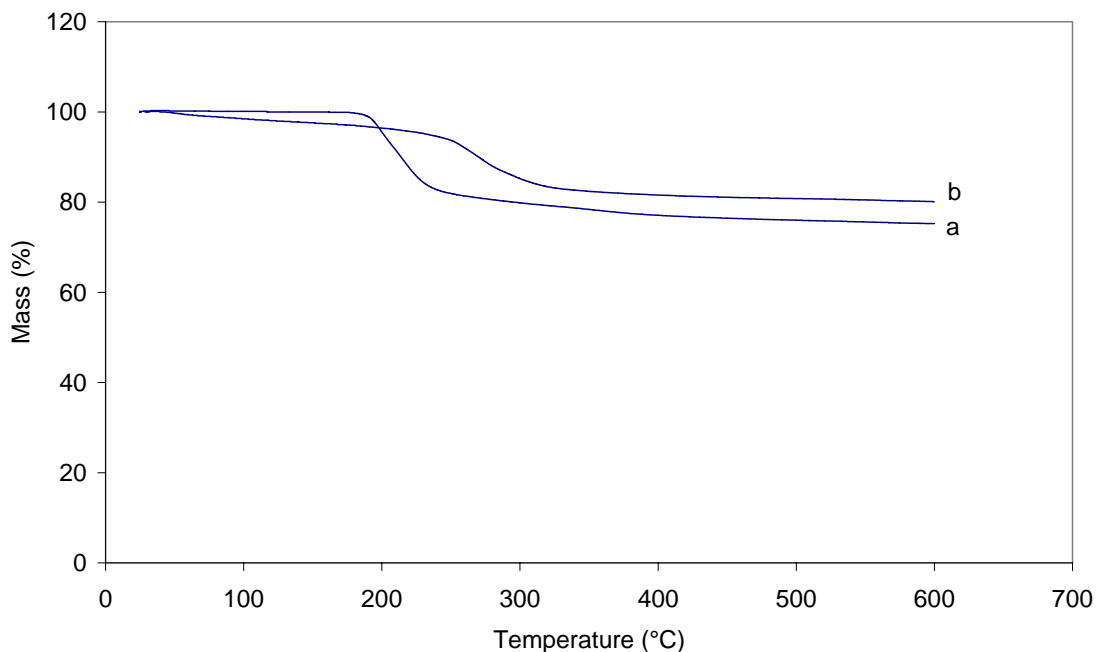


Figure 5.54. Thermograms of zinc borates produced from 1 mol.dm<sup>-3</sup> zinc nitrate and 1 mol.dm<sup>-3</sup> borax at 70 °C, mole ratio of borax/zinc nitrate =1.0, for reaction times a) 5 h (S-16), b) 16 h (S-18).

SEM microphotographs of zinc borates produced for different reaction periods (1-16 h) are shown in Figure 5.55 and Figure 5.56. Agglomerated nanoparticles that were formed for 1 h reaction time are shown in Figure 5.55.a. It was anticipated that zinc borate clusters were initially prepared from the reaction of precursors in aqueous phase. Those nanosized particles formed agglomerates due to attraction forces (Van der Waals) between them. Additionally, these clusters might have bonded to each other by hydrogen bonding, which was formed between OH groups. Because, this intermediate product began to lose mass even below 100 °C in TGA analysis. In Figure 5.55.b, agglomerated clusters and particles with plate-like structure are observed. The presence of plate-like structures supported the XRD data in which crystalline phase was determined in XRD pattern of the zinc borate. Figure 5.55.c displays the zinc borate particles produced at the end of 3 h reaction time. It is clearly seen that all the particle have plate-like morphology in submicron size and no evidence for nanoparticles was observed.



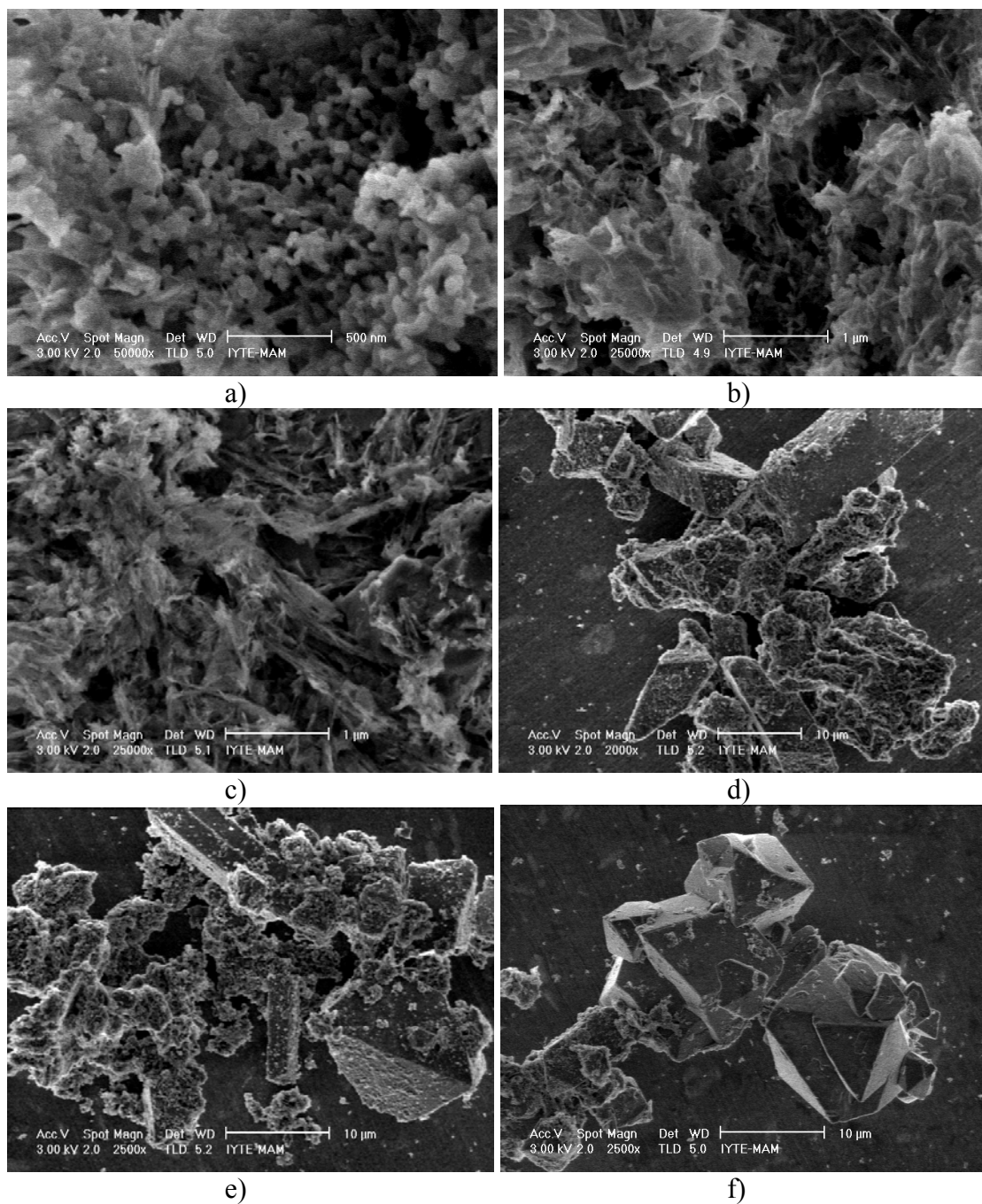


Figure 5.55. SEM microphotographs of zinc borates produced from  $1 \text{ mol.dm}^{-3}$  zinc nitrate and  $1 \text{ mol.dm}^{-3}$  borax at  $70 \text{ }^\circ\text{C}$ , mole ratio of borax/zinc nitrate =1.0, for reaction times a) 1 h (S-12), b) 2 h (S-13), c) 3 h (S-14), d) 4 h (S-15), e) 5 h (S-16), f) 6 h (S-17).

Both nucleation and crystal formation occurred simultaneously in the reaction period of 3 h. As soon as critical supersaturation was exceeded nucleation started and then crystal formation took place on nuclei formed. After 3 h of reaction time, crystal growth took place for reaction time of 4 h, 5 h, and 6 h. SEM microphotographs of zinc borates produced at the end of 4, 5, and 6 h are shown in Figure 5.55.d, Figure 5.55.e,

and Figure 5.55.f, respectively. Micron-sized prismatic zinc borate crystals were formed for these reaction times.

Figure 5.56 shows the zinc borate particles produced at the end of 16 h of reaction time. Increasing the reaction time induced a change in the morphology and crystal structure of particles, crystalline zinc borate of  $2\text{ZnO}\cdot 3\text{B}_2\text{O}_3\cdot 7\text{H}_2\text{O}$  dissolved and recrystallized to form zinc borate of  $\text{ZnO}\cdot \text{B}_2\text{O}_3\cdot 2\text{H}_2\text{O}$  with a flake-like morphology.

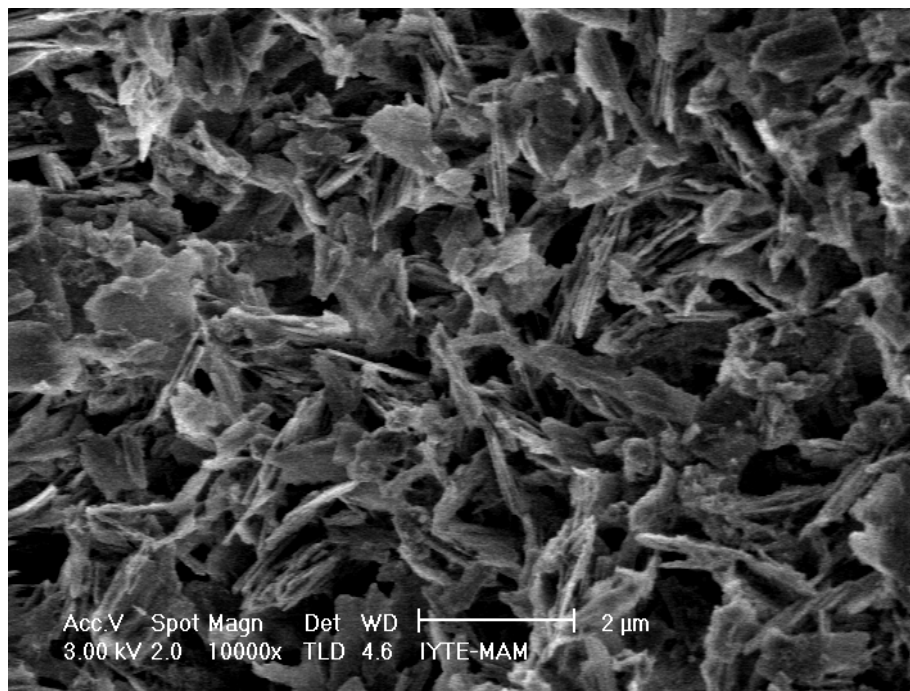


Figure 5.56. SEM microphotograph of zinc borate produced from  $1 \text{ mol}\cdot\text{dm}^{-3}$  zinc nitrate and  $1 \text{ mol}\cdot\text{dm}^{-3}$  borax at  $70 \text{ }^\circ\text{C}$ , mole ratio of borax/zinc nitrate =1.0, for reaction time of 16 h (S-18).

The volume-weighted particle size distribution of zinc borate samples produced from borax and zinc nitrate at different reaction times are shown through Figure 5.57 and Figure 5.59. From the comparison of Figure 5.55.a and Figure 5.57, it could be inferred easily that nanoparticles agglomerated and formed larger particles, thus particle size distribution had three different size groups: 400-500 nm nanosized particles, and particles lower than  $10 \text{ }\mu\text{m}$  and particles larger than  $10 \text{ }\mu\text{m}$ .

Particle size distribution of zinc borate produced from borax and zinc nitrate under 3 h of reaction time has a bimodal distribution (Figure 5.58). The first group, which is lower than  $1 \text{ }\mu\text{m}$ , indicates the individual particles and the second group represents the agglomeration of those nanoparticles. Figure 5.59 shows the particle size distribution of zinc borate that was produced at 5 h of reaction time using borax and

zinc nitrate. In this distribution, there were also two groups of particles: smaller particles having 400-500 nm of particle size and larger crystals having about 10  $\mu\text{m}$  particle size. As it was supported by SEM images, zinc borate clusters were initially formed at the end of 1 h reaction time and then crystals were grown on nuclei formed. Zinc borate crystals were formed at the end of 3 h reaction time and crystal growth took place at the end of 6 h reaction time.

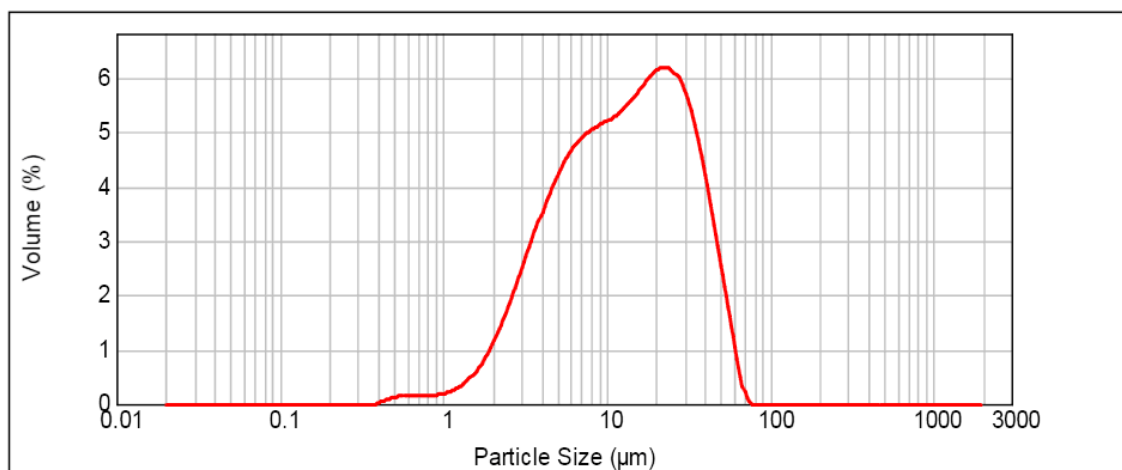


Figure 5.57. Particle size distribution of zinc borate produced from 1 mol.dm<sup>-3</sup> zinc nitrate and 1 mol.dm<sup>-3</sup> borax at 70 °C, mole ratio of borax/zinc nitrate =1.0, for reaction time of 1 h (S-12), (Malvern Mastersizer 2000).

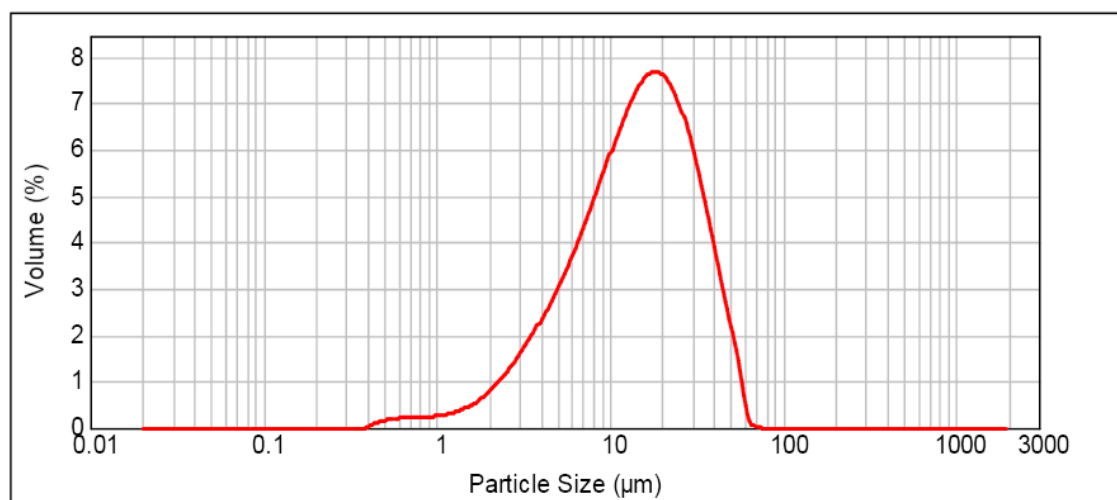


Figure 5.58. Particle size distribution of zinc borate produced from 1 mol.dm<sup>-3</sup> zinc nitrate and 1 mol.dm<sup>-3</sup> borax at 70 °C, mole ratio of borax/zinc nitrate =1.0, for reaction time of 3 h (S-14), (Malvern Mastersizer 2000).

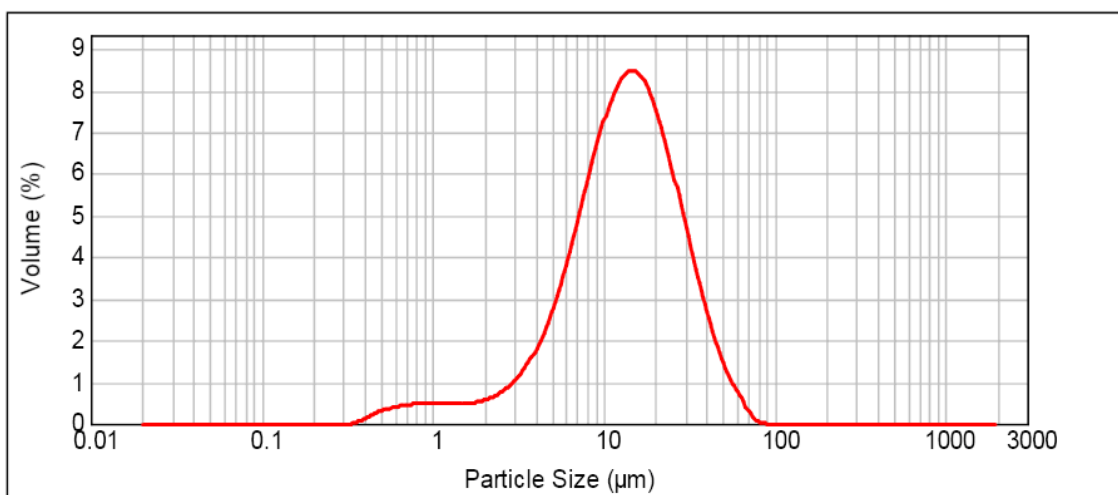


Figure 5.59. Particle size distribution of zinc borate produced from  $1 \text{ mol.dm}^{-3}$  zinc nitrate and  $1 \text{ mol.dm}^{-3}$  borax at  $70 \text{ }^\circ\text{C}$ , mole ratio of borax/zinc nitrate =1.0, for reaction time of 5 h (S-16), (Malvern Mastersizer 2000).

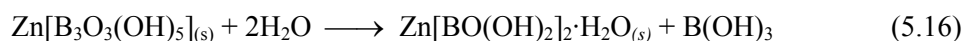
Based on these results obtained from XRD, FTIR, SEM and TGA, the production of zinc borate from borax decahydrate and zinc nitrate hexahydrate must be carried out for the reaction time of between 3 h and 6 h to obtain the crystalline zinc borate of  $2\text{ZnO}\cdot 3\text{B}_2\text{O}_3\cdot 7\text{H}_2\text{O}$ . At the beginning of the reaction (1-2 h) isolated borate units, such as  $[\text{B}(\text{OH})_4]^-$  precipitates with metal cation ( $\text{Zn}^{2+}$ ) to form amorphous zinc borate clusters as understood from XRD patterns (Figure 5.50). In the reaction time of 3 h and 6 h, initially formed amorphous product recrystallized and turned into crystalline zinc borate of  $2\text{ZnO}\cdot 3\text{B}_2\text{O}_3\cdot 7\text{H}_2\text{O}$ . Increasing the reaction time further (16 h) caused zinc borate of  $2\text{ZnO}\cdot 3\text{B}_2\text{O}_3\cdot 7\text{H}_2\text{O}$  to lose water and to transform into new structure. Since the reactions were carried out in magnetically stirred glass reactor, it was anticipated that mixing of reactants, impeller type could influence the reaction rate, consequently zinc borate type. Mechanical stirred reactor was used to clarify above issues in the production study of zinc borate from borax and zinc nitrate.

## 5.6.2. Analytical Characterization

Zinc borate samples produced under different reaction times were characterized by analytical titration. As shown in Table 5.7, there are two different crystalline zinc borates based on the  $\text{B}_2\text{O}_3/\text{ZnO}$  molar ratio except amorphous products formed initially.

The first one has the B<sub>2</sub>O<sub>3</sub>/ZnO molar ratio of around 1.5 and the latter one has the B<sub>2</sub>O<sub>3</sub>/ZnO molar ratio of about 1.0. As this molar ratio indicates the alkalinity of the borate, initially produced amorphous zinc borates had lower B<sub>2</sub>O<sub>3</sub> content and pH of the solution from which they were crystallized was high.

Zinc borates produced using 1 mol.dm<sup>-3</sup> borax and 1 mol.dm<sup>-3</sup> zinc nitrate at 70 °C for reaction time of 1 h (S-12), for reaction time of 2h (S-13) have approximately same ZnO contents (49.0%) and B<sub>2</sub>O<sub>3</sub>/ZnO molar ratio of 0.80 and 1.19, respectively. As it is seen from XRD patterns, initially formed product has amorphous structure and at the end of 3h reaction time (S-14), it is converted into crystalline product. As indicated in Table 5.7, it has B<sub>2</sub>O<sub>3</sub>/ZnO molar ratio of 1.15. Increasing reaction time from 3 to 6 hour, B<sub>2</sub>O<sub>3</sub>/ZnO molar ratio has increased from 1.15 to 1.49. The value of B<sub>2</sub>O<sub>3</sub>/ZnO molar ratio, which is around 1.50, corresponds to the resolved oxide formula of 2ZnO·3B<sub>2</sub>O<sub>3</sub>·7H<sub>2</sub>O. Based on those experimental data, when the reaction time of 16h is applied zinc borate of 2ZnO·3B<sub>2</sub>O<sub>3</sub>·7H<sub>2</sub>O has undergone a chemical change as given in Equation 5.16. In this reaction, formed product had water of crystallization in its structure as understood from its FTIR spectrum (Figure 5.48.d) which has H-O-H bending peak at around 1650 cm<sup>-1</sup>.



In Table 5.7, particle morphology of the zinc borate samples are also listed. While zinc borate of 2ZnO·3B<sub>2</sub>O<sub>3</sub>·7H<sub>2</sub>O has prismatic morphology, zinc borate of ZnO·B<sub>2</sub>O<sub>3</sub>·2H<sub>2</sub>O has flake-like morphology.

Water contents of zinc borate samples, obtained by subtracting the summation of B<sub>2</sub>O<sub>3</sub> % and ZnO % from hundred, support the water content value found from TGA results for both zinc borate types (2ZnO·3B<sub>2</sub>O<sub>3</sub>·7H<sub>2</sub>O and ZnO·B<sub>2</sub>O<sub>3</sub>·2H<sub>2</sub>O). Two types of water can easily be distinguished by TGA analysis as the dehydration of water due to the condensation of hydroxyl groups occurs at significantly higher onset temperatures compared with the loss of interstitial water (Schubert, 2003). Based on this fact, zinc borate produced at the end of 1 h reaction time (S-12) consists of mostly interstitial water. Zinc borate obtained at the end of 3 h reaction time (S-14) has both hydroxyl groups and interstitial water in its structure since there is mass loss at around 100 °C and 190 °C. On the other hand, zinc borate obtained at the end of 5 h reaction time (S-16) has only hydroxyl groups in its structure since there is mass loss at around 190 °C.

Zinc borate produced at the end of 16 h reaction time (S-18) has both hydroxyl groups and interstitial water in its structure since there are mass losses at around 100 °C and mostly at 240 °C.

## 5.7. Zinc Borate Production in a Mechanical-Stirred Stainless Steel Reactor

In order to see the effects of stirring, reaction between borax and zinc nitrate was also carried out in the stainless steel reactor using an impeller instead of magnetic bar. The progress of reaction was observed by FTIR spectroscopy and X-ray diffraction. The samples taken at the end of 4 and 5 h reaction times were analyzed by FTIR and XRD, TGA, and SEM. The reaction was carried out at 70 °C using equivalent amounts of zinc nitrate and borax under 900 rpm mixing rate.

The functional groups of the samples obtained for different reaction periods were analyzed by FTIR spectroscopy and obtained FTIR spectra are shown in Figure 5.60. FTIR spectrum of zinc borate obtained at the end of 4 h reaction time resembles FTIR spectrum of product produced at the end of 5 h reaction period.

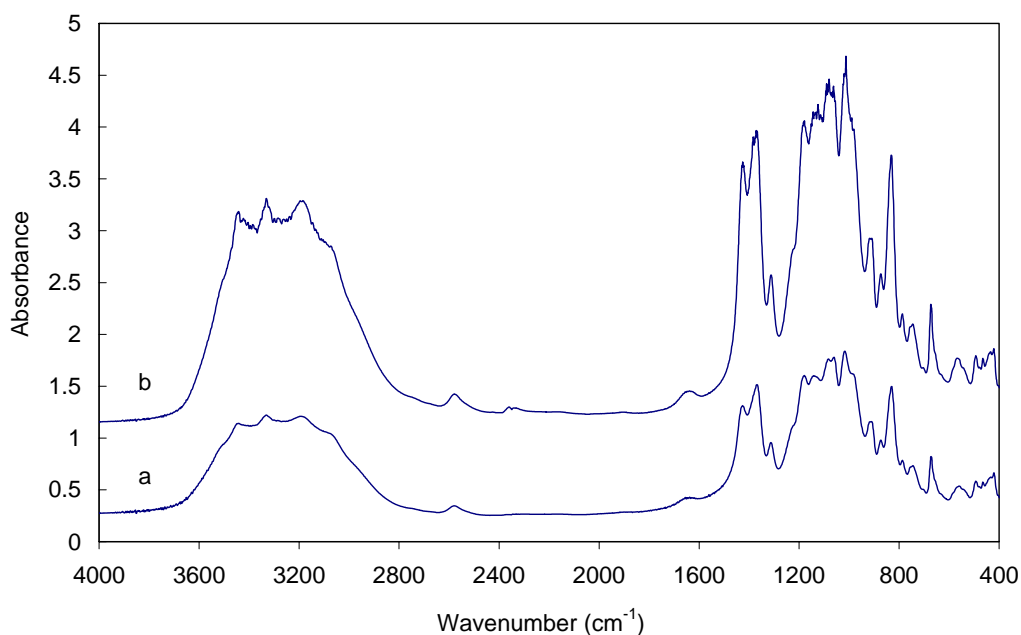


Figure 5.60. FTIR spectra of zinc borates produced in a reactor for a) 4 h (S-19), b) 5 h (S-20), reaction time at 70 °C.

Table 5.7. ZnO, B<sub>2</sub>O<sub>3</sub>, H<sub>2</sub>O contents, dehydration onset temperature and particle morphology of samples

Sample	Reaction time, h	ZnO, (%)	B <sub>2</sub> O <sub>3</sub> , (%)	B <sub>2</sub> O <sub>3</sub> /ZnO Molar Ratio	H <sub>2</sub> O, (%)		Dehydration Onset Temperature (°C)	Particle Morphology	Mean Diameter (µm)
					From Chemical Analysis*	From TGA			
S-12	1	49.12	33.38	0.80	17.50	17.66	50	Nanosized spheres	18.9
S-13	2	48.31	27.55	1.19	24.14	-	-	Nanosized flakes	-
S-14	3	40.39	39.56	1.15	20.05	22.43	190	Nanosized flakes	17.5
S-15	4	34.51	41.58	1.42	23.91	-	-	Prismatic crystals	-
S-16	5	34.76	40.91	1.39	24.32	24.78	190	Prismatic crystals	16.3
S-17	6	34.85	44.16	1.49	20.99	-	-	Prismatic crystals	-
S-18	16	44.94	33.42	0.88	21.65	20.0	230	Micronized flakes	-
S-19*	4	40.14	42.93	1.20	18.08	18.0	240	Micronized flakes	0.5 and 1.9
S-20*	5	40.94	41.19	1.18	17.86	19.0	240	Micronized flakes	0.3 and 0.9

\*: Calculated by subtracting percent values of ZnO and B<sub>2</sub>O<sub>3</sub> from hundred.

The peaks observed between  $1450\text{-}1300\text{ cm}^{-1}$  and  $1200\text{-}1000\text{ cm}^{-1}$  are related to asymmetric stretching vibrations of trihedral borate ( $\text{BO}_3$ ), and tetrahedral borate ( $\text{BO}_4$ ) groups, respectively. The other peaks between  $960\text{-}740\text{ cm}^{-1}$  belong to symmetric stretching vibrations of ( $\text{BO}_3$ ) and ( $\text{BO}_4$ ) groups (Jun et al., 1995). Moreover, the peaks between  $3200\text{-}3600\text{ cm}^{-1}$  and the at  $2590\text{ cm}^{-1}$  belong to stretching vibrations of OH groups and stretching vibrations due to hydrogen bonding in the structure of zinc borate. This product includes interstitial water in its structure since there is H-O-H bending vibration at  $1650\text{ cm}^{-1}$  wavenumber.

Figure 5.61 shows the XRD patterns of the zinc borates produced at the end of 4 and 5 h reaction periods. The presence of peaks with high intensity shows that the product has a crystalline structure. The major peaks in XRD patterns of zinc borate at  $10.22^\circ$ ,  $20.75^\circ$ ,  $28.20^\circ$ , and  $33.18^\circ$   $2\theta$  values are different than the other well known zinc borates, such as  $2\text{ZnO}\cdot 3\text{B}_2\text{O}_3\cdot 7\text{H}_2\text{O}$ ,  $2\text{ZnO}\cdot 3\text{B}_2\text{O}_3\cdot 3\text{H}_2\text{O}$  (Sawada et al., 2004) and  $4\text{ZnO}\cdot \text{B}_2\text{O}_3\cdot \text{H}_2\text{O}$  (Schubert, 1995). These XRD results confirmed the IR results that zinc borate had different structure.

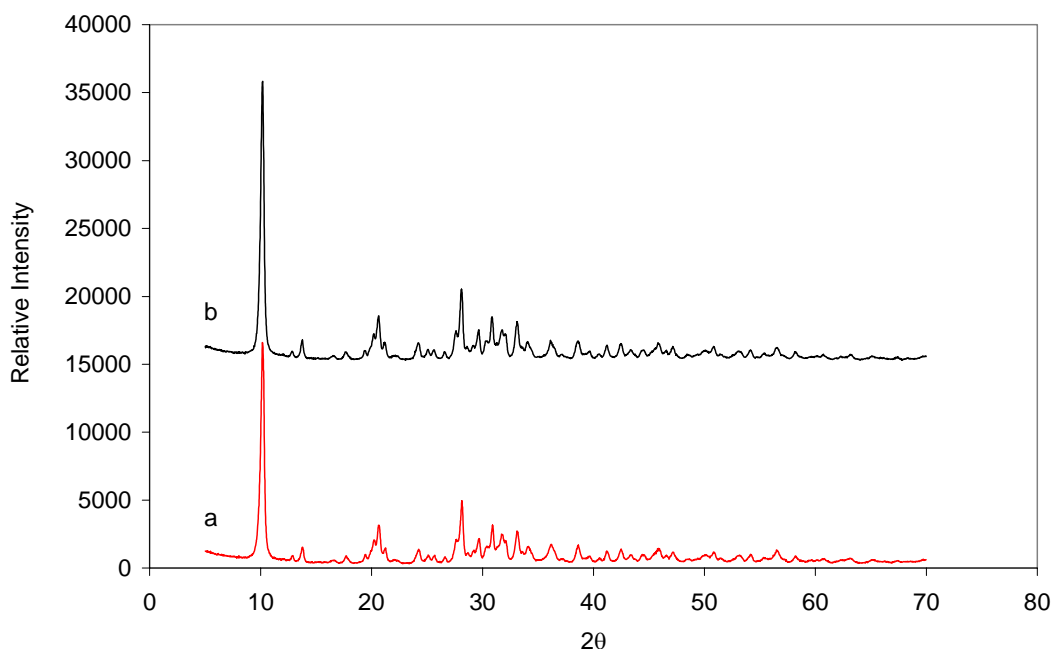


Figure 5.61. XRD patterns of zinc borates produced in a reactor at  $70^\circ\text{C}$  for a) 4 h (S-19), and b) 5 h (S-20) reaction time.

TGA curves of zinc borates produced for 4 h and 5 h of reaction with a mixing rate of 900 rpm are shown in Figure 5.62. Both products decomposed in one step



between 160 °C and 400 °C temperature range. The total mass losses occurred as 18.0 % and 19.0 % for zinc borates produced for 4 h and 5 h reaction times, respectively. The mass loss of 19.0 % occurred due to the removal of water corresponds to the H<sub>2</sub>O content of ZnO·B<sub>2</sub>O<sub>3</sub>·2H<sub>2</sub>O and could be compared to the calculated water content value of 19.25 %. It can be inferred that both zinc borate samples have the structure of ZnO·B<sub>2</sub>O<sub>3</sub>·2H<sub>2</sub>O based on H<sub>2</sub>O content.

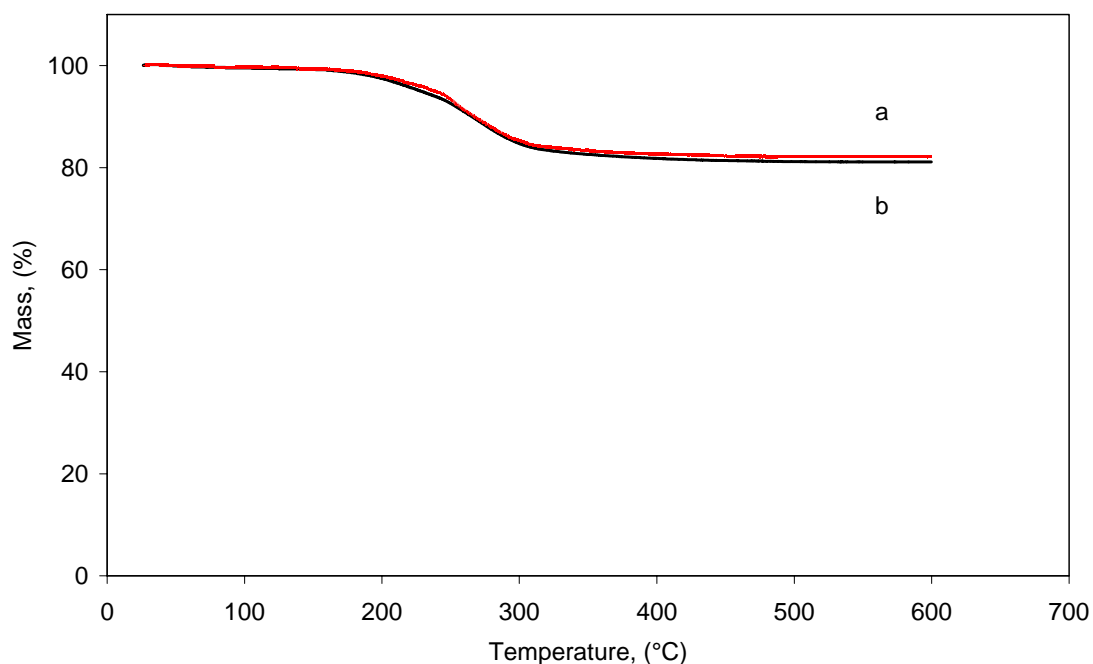


Figure 5.62. TGA thermograms of zinc borate products obtained at the end of a) 4 h (S-19) and b) 5 h (S-20) reaction time at 70 °C.

DSC curves of zinc borate samples produced at the end of 4 and 5 h reaction time are shown in Figure 5.63. Dehydration energy of zinc borate samples produced for 4 and 5 hours were calculated using peak areas in DSC curves as 5575 and 3835 J.g<sup>-1</sup> H<sub>2</sub>O, respectively. Those energies are much more than the one required for only evaporation of water (2200 J/g H<sub>2</sub>O). Since there is water of crystallization in the structure of zinc borate samples, broad endotherm occurred. Initial part of endotherm is due to the removal of interstitial water and the rest represents the water formed from the condensation of OH groups.

SEM microphotographs of zinc borates produced for 4 h and 5 h reaction time in reactor are shown in Figure 5.64. Zinc borate particles are in the form flakes and the sizes are smaller than 2 μm.

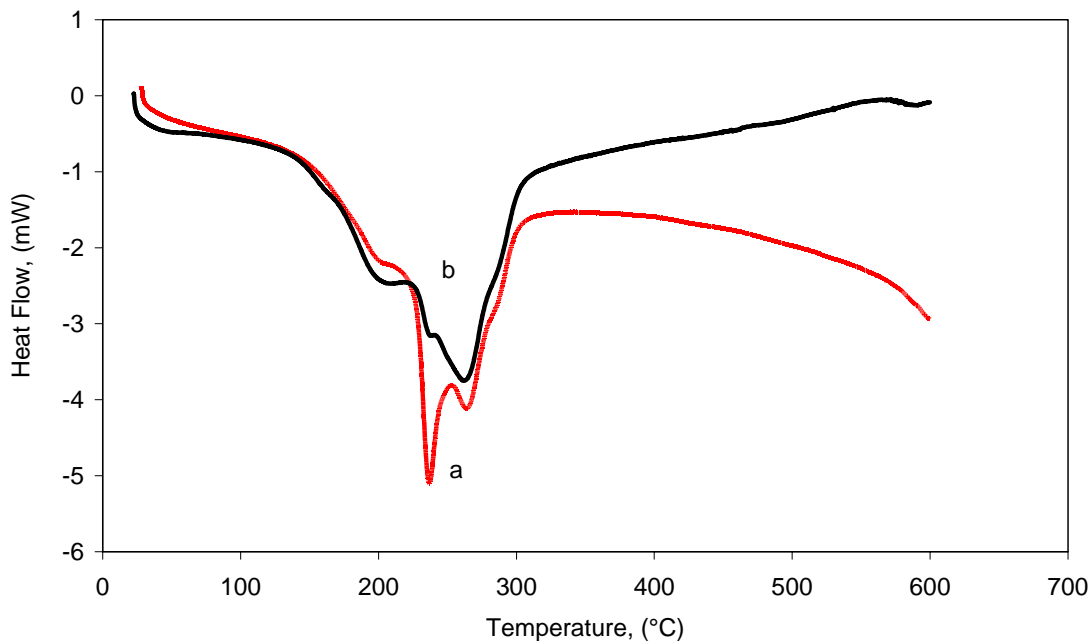


Figure 5.63. DSC curves of zinc borate products obtained at the end of a) 4 h (S-19) and b) 5 h (S-20) reaction time at 70 °C.

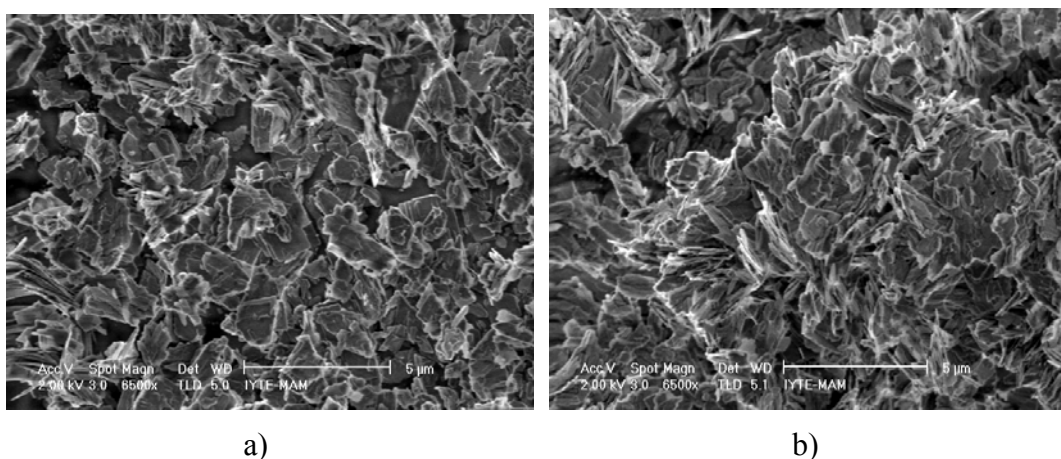


Figure 5.64. SEM microphotographs of zinc borate particles produced in a reactor for reaction time of a) 4 h (S-19), b) 5 h (S-20) at 70 °C.

To determine the particle size distribution of zinc borates, Sedigraph was firstly utilized. Figure 5.65 shows the particle size distribution of zinc borate obtained for 4 h and 5 h reaction time in the reactor. It can be proposed that half of the particles are smaller than 1 µm according to the Figure 5.65. Since dispersion of zinc borate particles in water is difficult even in the presence of surfactant, particle size analysis using Zetasizer sounds more reasonable. Before analyzing the zinc borate in Zetasizer, they were initially washed by ethanol. Particle size distributions of zinc borate samples show a bimodal distribution as shown in Figure 5.66. Zinc borate produced at the end of 4 h

reaction time has particles in two ranges; the first group has an average particle size of 460 nm and second group has mean particle size of 1.9  $\mu\text{m}$ . On the other hand, zinc borate synthesized at the end of 5 h of reaction period has an average particle size of 277 nm and 858 nm for two groups as shown in Figure 5.66.b.

In Table 5.7, particle morphology,  $\text{B}_2\text{O}_3/\text{ZnO}$  molar ratio, and  $\text{H}_2\text{O}$  content of the zinc borate samples produced for 4 h and 5 h reaction time (S-19 and S-20) are given. Both of zinc borate samples have particles with flake-like morphology. Water content of samples obtained from analytical titration (by subtracting the summation of  $\text{B}_2\text{O}_3$  % and  $\text{ZnO}$  % from hundred) and from TGA analysis supports the theoretical water content value of  $\text{ZnO}\cdot\text{B}_2\text{O}_3\cdot 2\text{H}_2\text{O}$ .

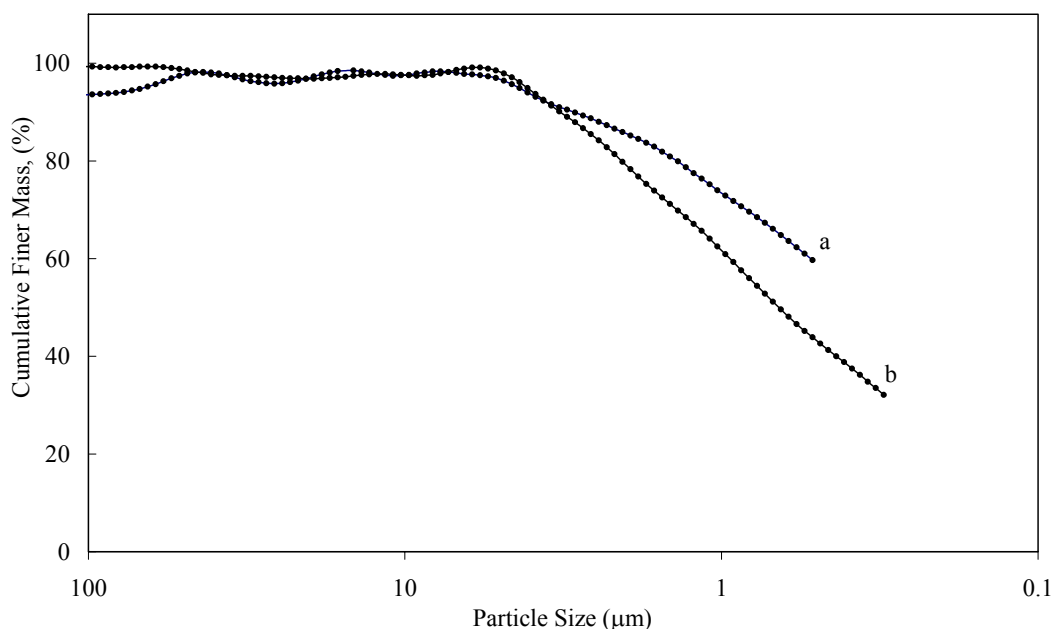


Figure 5.65. Particle size distribution of zinc borate particles produced in a reactor for reaction time of a) 4 h (S-19), b) 5 h (S-20) at 70  $^{\circ}\text{C}$ , (Sedigraph).

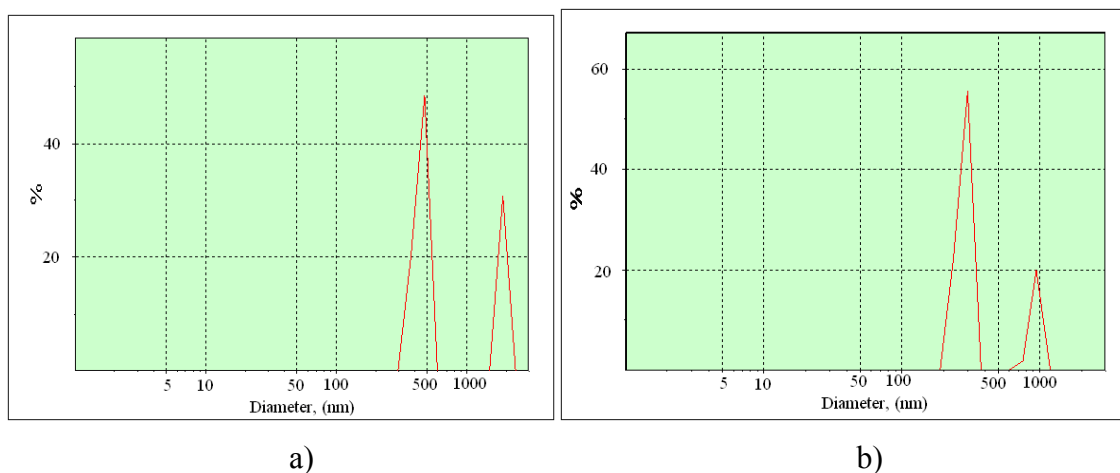


Figure 5.66. Particle size distribution of zinc borates produced in a reactor for reaction time of a) 4 h (S-19), b) 5 h (S-20) at 70 °C, (Malvern Zetasizer 3000 HSA).

That the zinc borate of  $2\text{ZnO}\cdot 2\text{B}_2\text{O}_3\cdot 7\text{H}_2\text{O}$  was initially synthesized product in the reaction of borax and zinc nitrate was determined from the effect of reaction time study. The use of stainless steel reactor with four-bladed impeller increased the reaction rate, and zinc borate of  $2\text{ZnO}\cdot 2\text{B}_2\text{O}_3\cdot 7\text{H}_2\text{O}$  converted into  $\text{ZnO}\cdot \text{B}_2\text{O}_3\cdot 2\text{H}_2\text{O}$  even for 4 h reaction time. It is obvious that zinc borates synthesized for same reaction periods using different stirrers are completely different from each other. It was concluded that the use of four-bladed turbine type impeller instead of magnetic bar not only increased the reaction rate but also changed morphology of the synthesized products.

## 5.8. Supercritical Carbon Dioxide ( $\text{CO}_2$ ) Drying of Zinc Borate Species

Nanoparticles agglomerate due to the influence of interfacial tension during conventional drying (Brinker, 1990). Supercritical fluid drying where the solvent is removed above its critical temperature ( $T_c$ ) and critical pressure ( $P_c$ ) is suggested to overcome the agglomeration and sticking of nanoparticles. In other words, since the liquid-vapor interface and capillary pressure are eliminated in supercritical fluid drying, particles do not tend to agglomerate. Supercritical fluids have been used in areas ranging from natural products extraction, materials cleaning, chemical reactions,

nanoparticle preparation and drying (Perrut, 2000; O'Neil and Watkins, 2005) The production of nanosized metal borates was studied using supercritical ethanol drying and supercritical CO<sub>2</sub> drying (Dong and Hu 1998, Hu et al., 2002). Supercritical CO<sub>2</sub> drying has been utilized in many applications owing to the fact that carbon dioxide is inexpensive, environmentally benign, not flammable, non toxic and can be regenerated easily by a cycle system. The preparation of nanometer copper borate with supercritical carbon dioxide drying was studied by Hu and co-workers (1999).

In those studies, there are some drawbacks, such as types of metal borates not determined and given, interaction of borate with solvent under supercritical conditions not taken into account. In this section, supercritical carbon dioxide drying of zinc borates produced from both borax and boric acid was investigated to elucidate above debatable points.

### **5.8.1 Characterization of Supercritical CO<sub>2</sub> Dried Zinc Borate Produced from Boric Acid and Zinc Oxide**

The zinc borate (S-4) prepared from boric acid and zinc oxide at 90 °C for 5 h reaction time is a zinc borate species with the oxide formula of 2ZnO·3B<sub>2</sub>O<sub>3</sub>·3H<sub>2</sub>O. The mole ratio of B<sub>2</sub>O<sub>3</sub>/ZnO was determined as 1.50 from analytical titration and water content was determined by thermal gravimetric analysis as 13.3 % (Table 5.8) that corresponds to its theoretical value of 12.7 %. FTIR spectrum of conventionally dried compound (Figure 5.67.b) shows some important properties of 2ZnO·3B<sub>2</sub>O<sub>3</sub>·3H<sub>2</sub>O. All hydrated borate salts have a broad peak at 2200-3600 cm<sup>-1</sup> resulting from stretching vibrations of OH groups (Jun et al., 1995) in their structure, 2ZnO·3B<sub>2</sub>O<sub>3</sub>·3H<sub>2</sub>O has two major sharp peaks at 3210 and 3470 cm<sup>-1</sup> in this region which is accepted as characteristics of this type (Eltepe et al., 2007). Another important feature of this product is that it does not have crystallization water in its structure since it does not have a peak at 1635 cm<sup>-1</sup> belonging to bending vibrations of H<sub>2</sub>O molecules in its IR spectrum.

Table 5.8. Composition of the samples

Sample	N%	C%	CO <sub>2</sub> %		H%	H <sub>2</sub> O%		B <sub>2</sub> O <sub>3</sub> / ZnO	ZnCO <sub>3</sub> %
			From C%	From TGA		From H%	From TGA		
S-4	-	-	-	-	-	-	13.31	1.5	-
S-4-SC	-	0.26	0.95	-	1.43	12.87	13.16	1.5	-
S-16	0.23	0.15	0.56	-	2.52	22.68	23.01	1.35	-
S-16-SC1	-	1.26	4.62	4.78	2.26	20.3	16.88	-	13.87
S-16-SC2	-	1.43	5.24	5.50	2.22	19.98	15.35	-	15.67
S-16-SC3	-	1.47	5.39	5.76	2.24	20.10	15.27	-	16.41

The chemical structure of zinc borate of this type has been recently updated by Schubert and co-workers (2003) as  $(\text{Zn}[\text{B}_3\text{O}_4(\text{OH})_3])$  which has a polymeric network structure. Figure 5.67.a shows the FTIR spectrum of zinc borate that was dried by supercritical CO<sub>2</sub> for 2 h. It can be inferred that there is no change in the chemical structure of zinc borate during supercritical drying. Conventionally dried and supercritical CO<sub>2</sub> dried zinc borate ( $2\text{ZnO}\cdot 3\text{B}_2\text{O}_3\cdot 3\text{H}_2\text{O}$ ) samples had identical spectra in which major peaks were summarized in Table 5.4.

X-ray diffraction patterns of zinc borate samples dried by supercritical CO<sub>2</sub> and conventionally at 110 °C are given in Figure 5.68.a and Figure 5.68.b, respectively. This zinc borate species has a crystal structure that is identical to that of  $2\text{ZnO}\cdot 3\text{B}_2\text{O}_3\cdot 3\text{H}_2\text{O}$  (Sawada et al., 2004). The most important characteristic of this zinc borate species is that the major peaks begin to occur at  $2\theta$  18.0° value, and other important peaks in the XRD pattern observed at about 20.0°, 22.0°, 24°, 26°, 29°, 30° and 36°  $2\theta$  values. And it can be concluded from the comparison of Figure 5.68.a and Figure 5.68.b that there is no change in the crystal structure of zinc borate after supercritical CO<sub>2</sub> drying.

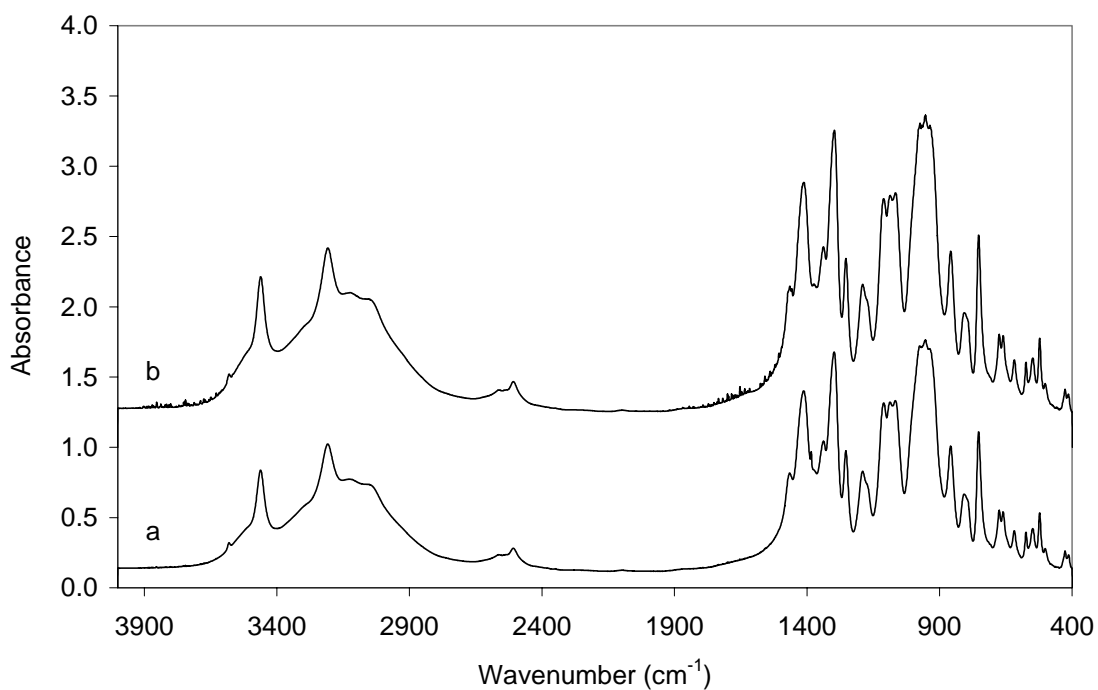


Figure 5.67. FTIR spectra of zinc borate (S-4) dried a) by SC CO<sub>2</sub> for 2h and b) by conventionally at 110 °C.

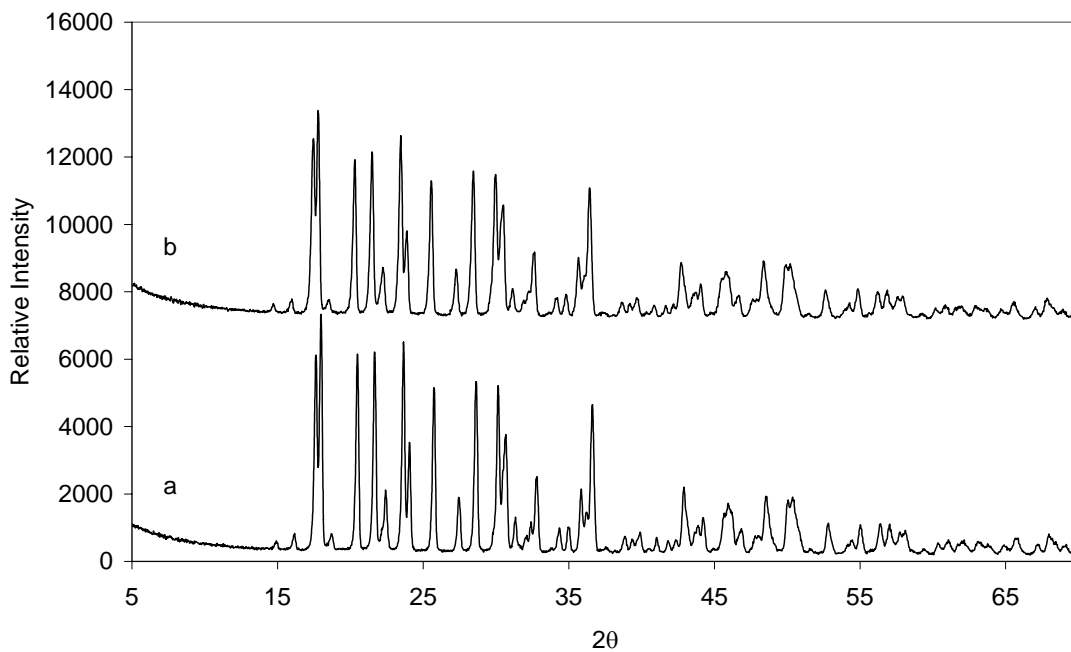


Figure 5.68. XRD patterns of zinc borate (S-4) dried a) by SC CO<sub>2</sub> for 2 h and b) by conventionally at 110 °C.

From SEM microphotographs of conventionally dried particles (Figure 5.69.a) particle size was determined about 2  $\mu\text{m}$  size. Particles stick to each other and supercritical  $\text{CO}_2$  has no influence on separation of these particles (Figure 5.69.b). Particles in both Figure 5.69.a and Figure 5.69.b have smooth surface and random shapes.

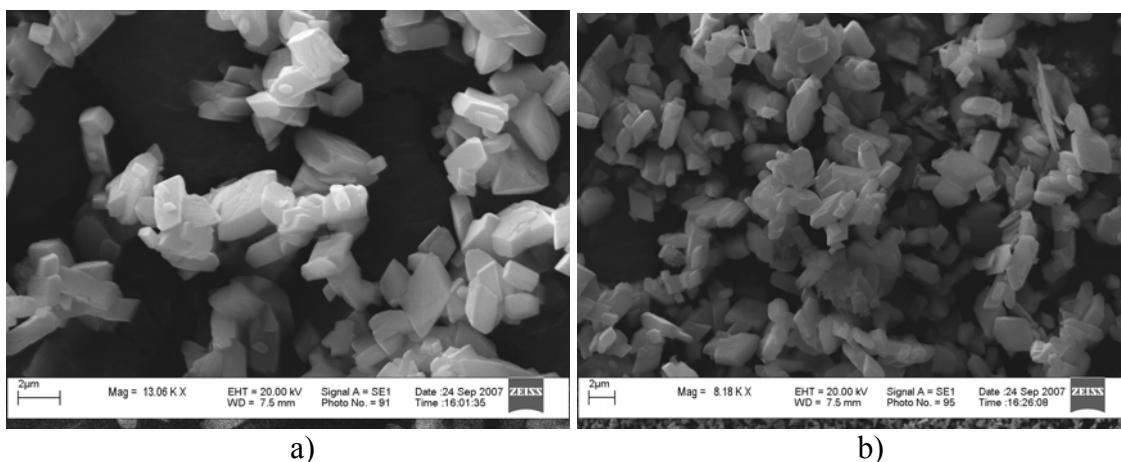


Figure 5.69. SEM microphotographs of zinc borate (S-4) dried a) by conventionally at 110 °C, b) by SC  $\text{CO}_2$ .

In order to determine the water content of zinc borate and supercritical  $\text{CO}_2$  drying effect, samples were analyzed by TGA. Figure 5.70 shows the TGA plots of zinc borates dried conventionally at 110 °C and by supercritical  $\text{CO}_2$ . Conventional dried zinc borate (S-4) started to lose mass at 290 °C; supercritical  $\text{CO}_2$  dried zinc borate began to lose mass at 303 °C as shown in Table 5.9. The total mass loss of both samples was about 13.0 % which was very close to theoretical value of 12.69 % for  $2\text{ZnO}\cdot 3\text{B}_2\text{O}_3\cdot 3\text{H}_2\text{O}$  until 600 °C. The water content was also determined as 12.81 % from elemental H content of supercritically dried sample (Table 5.8).



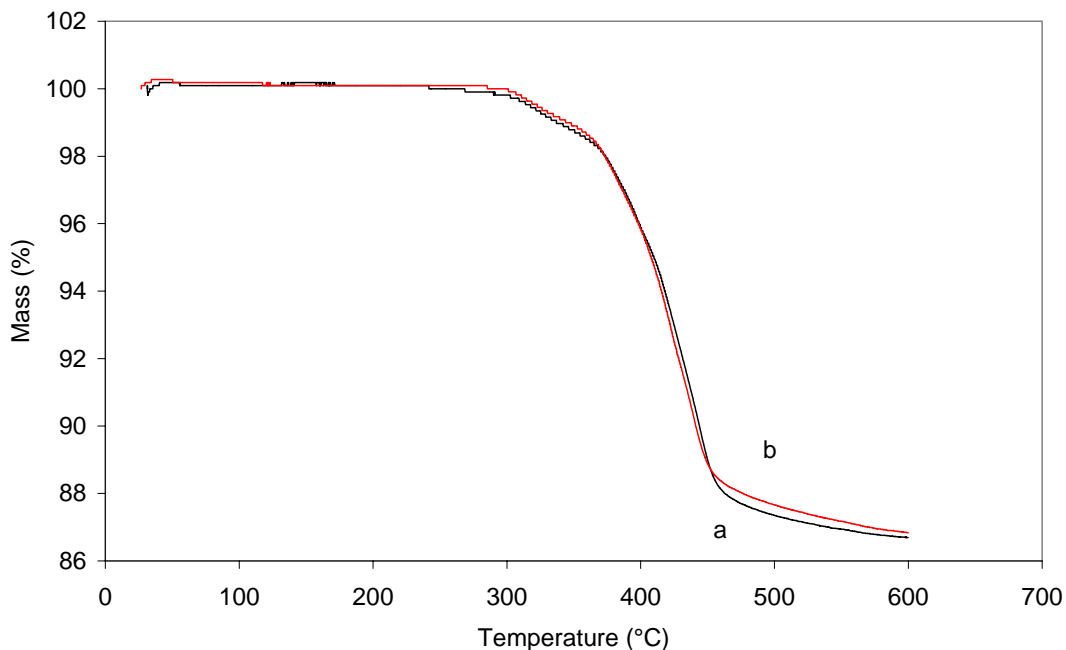


Figure 5.70. TGA curves of zinc borate (S-4) dried a) by conventionally at 110 °C, b) dried by SC CO<sub>2</sub> for 2 h.

It can be concluded that zinc borate produced from boric acid (S-8) was not affected chemically by supercritical carbon dioxide drying.

### 5.8.2. Supercritical CO<sub>2</sub> Drying of Zinc Borate Produced from Borax Decahydrate and Zinc Nitrate Hexahydrate

From analytical titration method, the mole ratio of B<sub>2</sub>O<sub>3</sub>/ZnO was calculated as 1.35 (Table 5.8) which was very close to the theoretical formula of 2ZnO·3B<sub>2</sub>O<sub>3</sub>·7H<sub>2</sub>O. FTIR spectra of zinc borates produced from borax decahydrate and zinc nitrate hexahydrate conventionally and supercritical CO<sub>2</sub> dried for 2, 3 and 4 h are shown in Figure 5.71. The spectrum in Figure 5.71.a indicates that zinc borate species has identical spectrum with 2ZnO·3B<sub>2</sub>O<sub>3</sub>·7H<sub>2</sub>O (Eltepe et al., 2007). A small peak at 1635 cm<sup>-1</sup> shows that there was crystal water in the structure of zinc borate of this type (Fig. 5.71.a) and bound water was not removed during the supercritical CO<sub>2</sub> drying. The other major peaks in the spectrum of zinc borate were given in Table 5.4.

The peaks at about  $1450\text{ cm}^{-1}$  (shoulder peak) and  $870\text{ cm}^{-1}$  in FTIR spectra of supercritically dried zinc borate samples in Fig.5.71.b, c and d. belong to carbonate ions (Kanari et al., 2004). It is inferred from the comparison of Figure 5.71.a and Figure 5.71.b, c and d that zinc borate species interacts chemically with carbon dioxide under supercritical conditions. No methanol was present in the samples since peaks related to C-H vibrations of methanol at  $2900\text{ cm}^{-1}$  was not observed in the FTIR spectra.

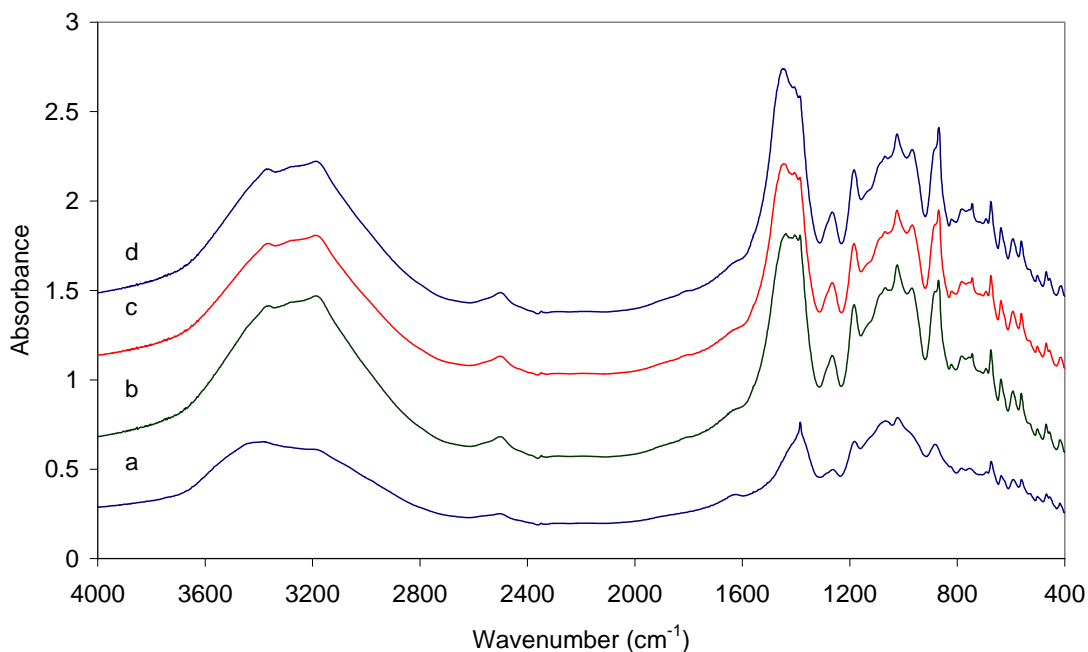


Figure 5.71. FTIR spectra of zinc borate (S-16) dried a: by conventionally at  $110\text{ }^{\circ}\text{C}$ , by SC  $\text{CO}_2$  at different drying time b) 2 h, c) 3 h, d) 4 h.

Figure 5.72.a shows the XRD pattern of zinc borate produced from borax decahydrate and zinc nitrate hexahydrate and dried at  $110\text{ }^{\circ}\text{C}$ . As the major peaks at  $2\theta$  values of  $13.0^{\circ}$ ,  $18.0^{\circ}$ ,  $20.0^{\circ}$ ,  $27.0^{\circ}$  and  $30.0^{\circ}$  are identical to the peaks of  $2\text{ZnO}\cdot 3\text{B}_2\text{O}_3\cdot 7\text{H}_2\text{O}$  given in the JCPDS 75-0766 data file, it was concluded that the product was  $2\text{ZnO}\cdot 3\text{B}_2\text{O}_3\cdot 7\text{H}_2\text{O}$ . Figure 5.72.b represents the XRD pattern of zinc borate that dried by supercritical  $\text{CO}_2$ . This pattern was redrawn while the intensity value was constrained to 8000 so that the small peaks can be seen easily. From the comparison of Figure 5.72.a and Figure 5.72.b. it can be inferred that there are extra peaks in the XRD pattern of supercritical  $\text{CO}_2$  dried zinc borate.

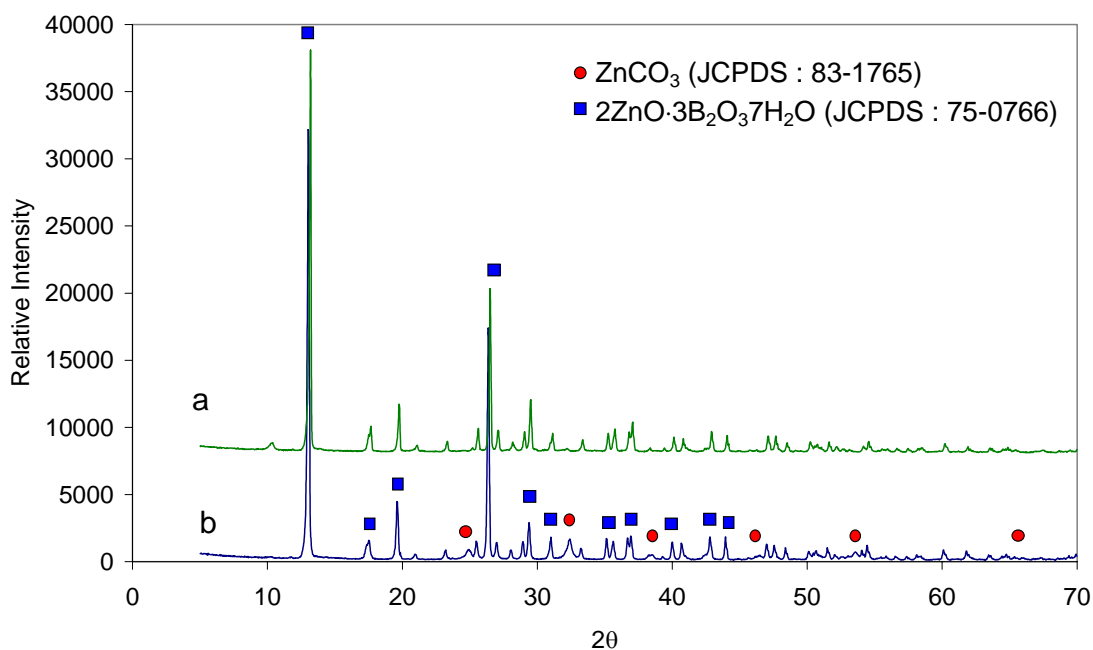


Figure 5.72. XRD patterns of zinc borate (S-16) dried a: by conventionally at 110 °C, b: by supercritical CO<sub>2</sub> for 4h.

The peaks at  $2\theta$  values of  $24.96^\circ$ ,  $32.45^\circ$ , and  $53.67^\circ$  indicated by arrows belong to zinc carbonate (Wu and Jiang, 2006). During the supercritical CO<sub>2</sub> drying under 10 MPa and 40 °C, zinc borate gave reaction with CO<sub>2</sub> to produce zinc carbonate. The formation of zinc carbonate during drying was also supported by FTIR analysis.

SEM microphotographs of zinc borate and supercritical CO<sub>2</sub> dried zinc borate samples are shown in Figure 5.73.a to Figure 5.73.d. Figure 5.73.a clearly shows that there are two types of particles; one is prismatic rods with micron size and the second one is nanosized flakes. By comparison of the SEM image of Figure 5.73.a with that of Figure 5.73.d, it can be seen that reaction started on the surface of the micron sized particles and the amount of zinc borate reacted with CO<sub>2</sub> on the surface has increased with increasing drying time. The particle size of spherical particles on the surface of zinc borate varies between 200 nm to 500 nm.

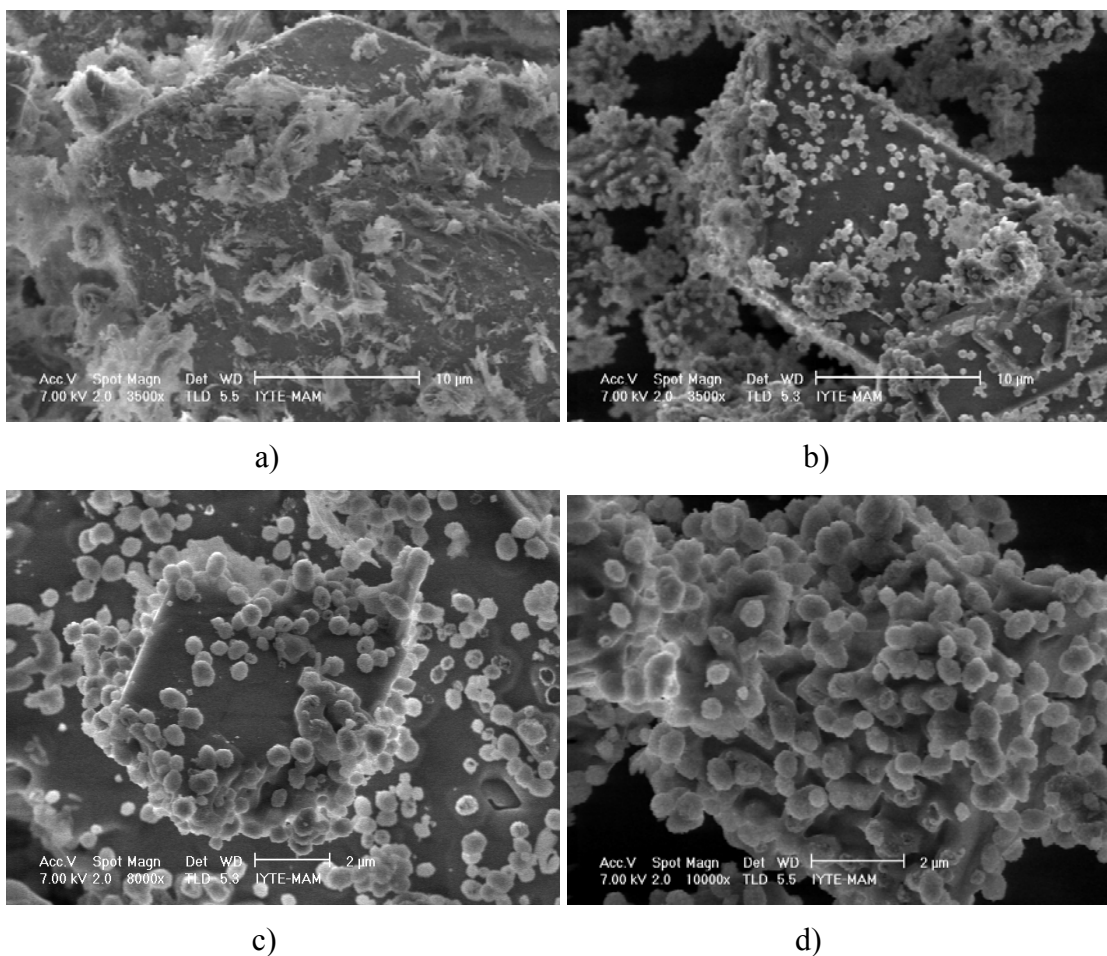


Figure 5.73. SEM microphotographs of zinc borate (S-16) dried a) by conventionally at 110 °C, by SC CO<sub>2</sub> at different drying time b) 2 h, c) 3 h, d) 4 h.

TGA curves of zinc borate samples produced from borax decahydrate and zinc nitrate hexahydrate and supercritical CO<sub>2</sub> dried samples are given in Figure 5.74 and Figure 5.75. In these thermograms, the first step starts at around 180 °C, (T1), and it represents the removal of water from structure by evaporation of crystallization water and water formed by condensation of B-OH groups. The second step which occurs at around 370 °C, (T2), is due to the removal of CO<sub>2</sub> from zinc carbonate structure. Conventionally dried zinc borate at 110 °C begins to lose its hydration water at 180 °C with a mass loss of 23.0 % (Figure 5.74.a) which is close to the theoretical value 25.32 % calculated from the formula of 2ZnO·3B<sub>2</sub>O<sub>3</sub>·7H<sub>2</sub>O. On the other hand, zinc borates dried by supercritical CO<sub>2</sub> under 10 MPa and 40 °C for drying time of 2 h, 3 h, and 4 h show two steps in TGA curves as shown by Figure 5.75.a, Figure 5.75.b and Figure 5.74.b, respectively. The first step started at 180 °C with a mass loss of 16.88 % belongs to water loss of zinc borate and the second step occurred at 370 °C with a mass loss of 4.78 % (S-16SC-1), pertaining to the decomposition of zinc carbonate (Wu and Jiang,

2006). After supercritical CO<sub>2</sub> drying, the approximate composition of ultimate product is zinc borate (85 %) and zinc carbonate (15 %) as calculated from the CO<sub>2</sub> mass loss. CO<sub>2</sub> % found from C content and TGA and H<sub>2</sub>O % from H content and TGA were very close to each other as reported in Table 5.8. The thermal stability properties of zinc borates and samples that were dried by supercritical CO<sub>2</sub> are summarized in Table 5.9. The CO<sub>2</sub> content of S-16-SC1, S-16-SC2 and S-16-SC-3 samples were determined by TGA as 4.78 %, 5.50 % and 5.76 %, respectively (Table 5.8). They contained 13.87-16.41 % (wt) ZnCO<sub>3</sub> as listed in Table 5.8.

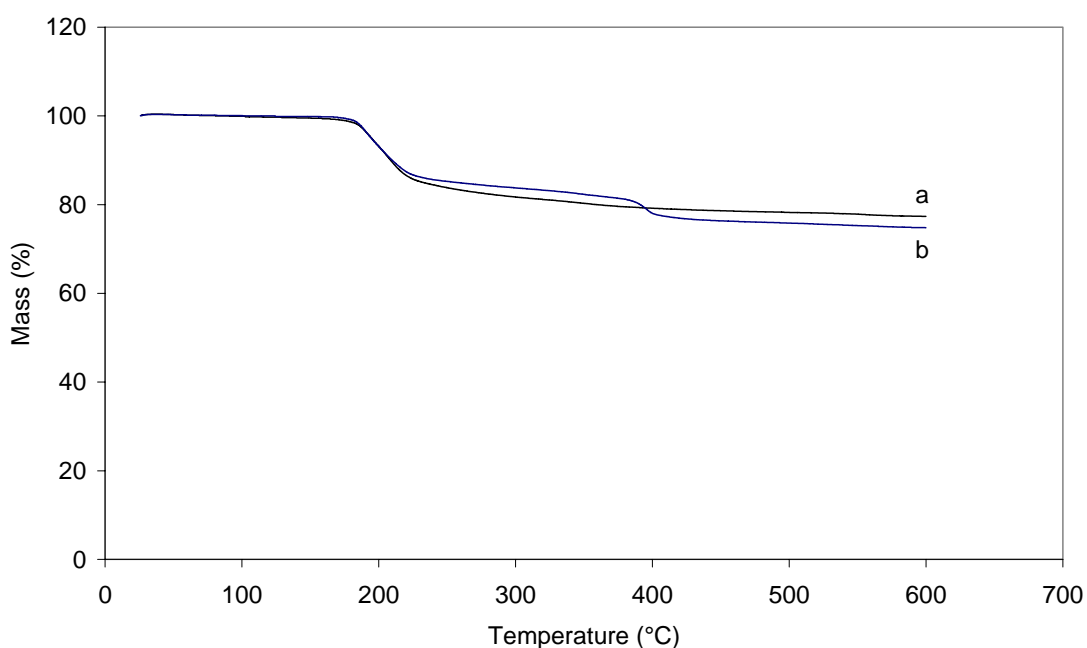


Figure 5.74. TGA thermograms of zinc borate (S-16) dried a) by conventionally at 110 °C, b) dried by SC CO<sub>2</sub> for 4 h.

DSC curves of zinc borates dried by conventionally at 110 °C and by supercritical CO<sub>2</sub> supporting the TG data are shown in Figure 5.76. Zinc borate dried conventionally has only one endotherm between (165-240 °C) which indicates the removal water from the product (Figure 5.76.a). On the other hand, zinc borate dried by supercritical CO<sub>2</sub> has two endotherms between (165-240 °C) and (365-400 °C) which represent removal of water and carbon dioxide, respectively (Figure 5.76.b).

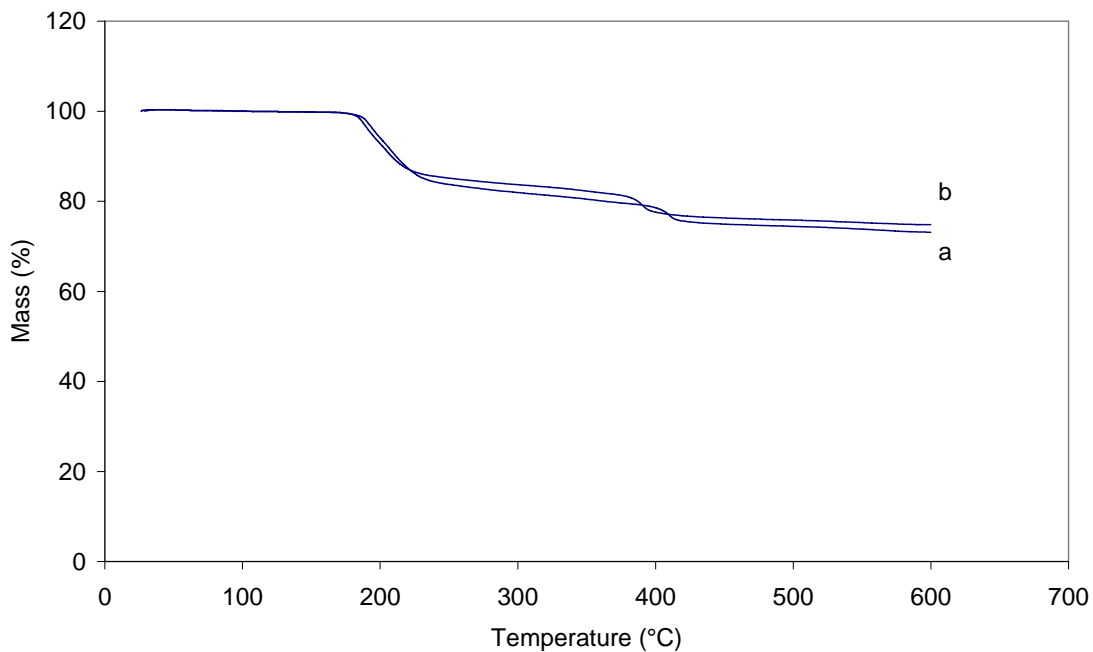


Figure 5.75. TGA thermograms of zinc borate (S-16) dried by Supercritical CO<sub>2</sub> for a) 2 h, and b) 3 h.

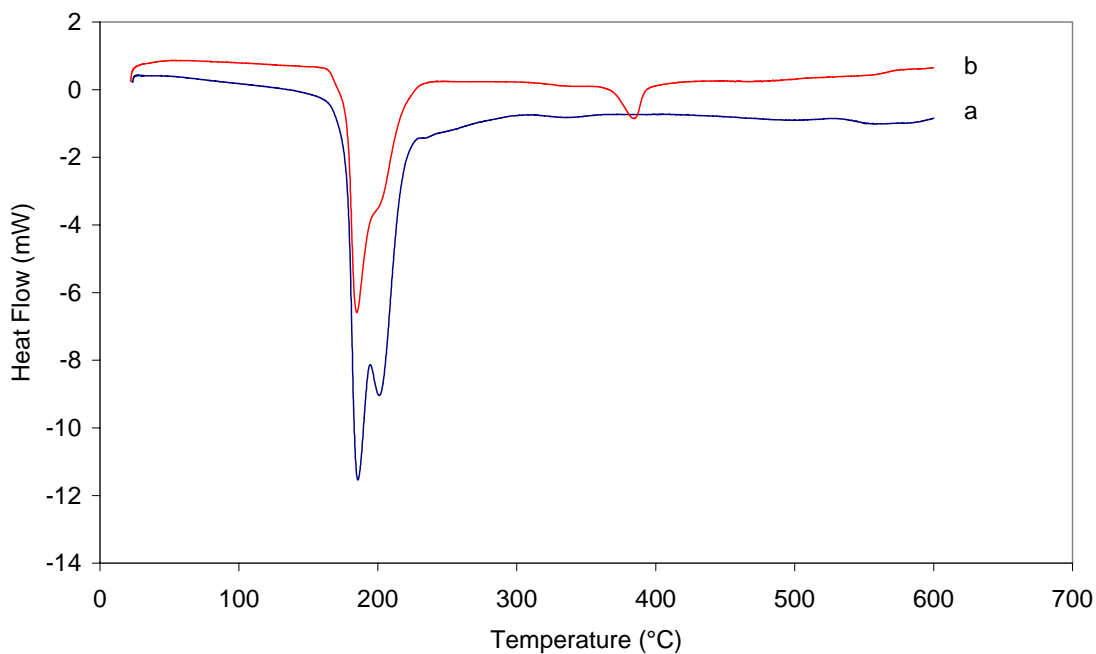


Figure 5.76. DSC curves of zinc borate (S-16) dried a) by conventionally at 110 °C, b) dried by SC CO<sub>2</sub> for 4 h.

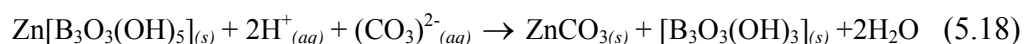
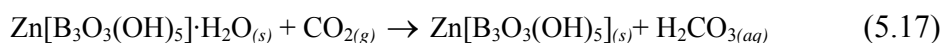
In order to determine the elemental composition of zinc borate samples and the effect of supercritical CO<sub>2</sub> drying, C, H, N contents of samples that were produced from “borax decahydrate and zinc nitrate hexahydrate”, (S-4) and “boric acid and zinc oxide”, (S-16) and supercritical CO<sub>2</sub> dried samples were determined as shown in Table 5.8. Hydrogen content of zinc borate produced from borax and zinc nitrate hexahydrate (S-16) was found as 2.52 % which is very close to the theoretical value of 2.84 %. Carbon and nitrogen contents of zinc borate (S-16) were negligible and indicating that it was washed efficiently formed nitrate ions present in the reaction mixture. Presence of carbon in (S-16) was not expected any way. However, it can be seen that during supercritical carbon dioxide drying due to reaction of carbon dioxide with sample, the carbon content of sample increased to 1.26 % for 2 h dried sample. With the increase of drying time to 3 and 4 h, the carbon content increased from 1.26 % to values of 1.43 % and 1.47 %, respectively. Another considerable change occurred in the H content of zinc borate during supercritical drying, it decreased from 2.52 % to 2.22 % as carbon dioxide flow caused the removal of some OH groups, as well. On the other hand, hydrogen content of supercritical dried zinc borate (S-4-SC) obtained from boric acid and zinc oxide was found as 1.43 % which corresponded to the theoretical value 1.42 %. Nitrogen was not present and carbon content was not significant as expected for this sample. Conventional dried zinc borate produced from boric acid and zinc oxide was not examined in the elemental analysis.

Table 5.9. Thermal behavior of zinc borate samples

Sample	T1 (°C)	H <sub>2</sub> O Loss %	T2 (°C)	CO <sub>2</sub> Loss %
S-4	290	13.31	-	-
S-4-SC	303	13.16	-	-
S-16	180	23.01	-	-
S-16-SC1	180	16.88	386	4.78
S-16-SC2	180	15.35	370	5.50
S-16-SC3	180	15.27	370	5.76

### 5.8.3. Interaction Between Carbon Dioxide and Zinc Borates

Since carbon dioxide is widely used in supercritical fluid processes, it is also considered as a solvent in the drying of zinc borate species. Since methanol has a good solubility in supercritical CO<sub>2</sub>, water in zinc borate samples was replaced by methanol. Although the supercritical CO<sub>2</sub> extracted all of the methanol from samples, zinc borate (2ZnO·3B<sub>2</sub>O<sub>3</sub>·7H<sub>2</sub>O) having the structure of Zn[B<sub>3</sub>O<sub>3</sub>(OH)<sub>5</sub>]·H<sub>2</sub>O reacted with CO<sub>2</sub> under supercritical conditions. It was anticipated that carbonic acid was formed from the dissolution of carbon dioxide in water that was released from zinc borate structure under supercritical conditions as shown in Equation 5.17. Then, zinc borate-methanol mixture reacted with carbonic acid as shown in Equation 5.18.



Since the structure of Zn[B<sub>3</sub>O<sub>4</sub>(OH)<sub>3</sub>] is quite stable and has no water of crystallization, no carbonate formation was observed in the drying of that zinc borate (2ZnO·3B<sub>2</sub>O<sub>3</sub>·3H<sub>2</sub>O). The larger particle size of that product might be another reason for not observing any reaction, since the reaction between zinc borate and carbon dioxide takes places on the surface of the solid particles.

## 5.9. Subcritical and Supercritical Ethanol Drying of Zinc Borate Species

As the zinc borate produced from borax and zinc nitrate reacted with CO<sub>2</sub> and formed zinc carbonate during supercritical CO<sub>2</sub> drying, it was decided to use supercritical ethanol drying technique in the project. Supercritical ethanol drying has been used in the production of inorganic oxide aerogels, such as Al, Si. Those aerogels are used as a catalyst support and isolation material since they have low thermal



conductivity and high surface area (Sunol et al. 1995). The fundamental idea of supercritical ethanol drying is to prevent the particle agglomeration which occurs inevitably in thermal drying. As the liquid-gas interface is removed in supercritical drying, particles can not agglomerate and can not form bigger particles. In the supercritical region where both liquid and gas densities become equal, there is no liquid-vapor interface and capillary pressure.

In supercritical ethanol drying after placing the zinc borate sample and adequate ethanol into high pressure reactor, critical pressure was provided by heating the closed vessel. Both of the experimental and theoretical pressure of ethanol with increasing temperature in the closed reactor is shown in Figure 5.77. The experimental pressure was read from pressure gauge in the system. Theoretical pressure was calculated using the ancillary equation (Dillon and Penoncello, 2004). In this ancillary equation, ethanol critical temperature (513.9 K) and pressure (6.148 MPa) were used as given below.

$$\ln \frac{P}{P_c} = \frac{T_c}{T} (-0.0514771\theta^{1/2} - 8.27075\theta - 5.49245\theta^3 + 5.64829\theta^{11/2}) \quad (5.19)$$

where  $\theta = 1 - (T/T_c)$ . It was pointed that Equation 5.19 could be used to predict the vapor pressure of ethanol within  $\pm 0.4\%$ .

Process safety is one of the main concepts while studying with flammable liquids. In order to prevent any risky situation, oxygen must be removed from the reactor before starting to heating. This step is one of the crucial points in the supercritical ethanol drying where flammable materials (ethanol) and much energy for burning are present. The presence of very little amount of oxygen in such a process may trigger oxidation and/or other reactions and cause pressure built up and energy release in the system. The change of pressure and temperature with respect to time in the closed reactor is given in Figure 5.78.

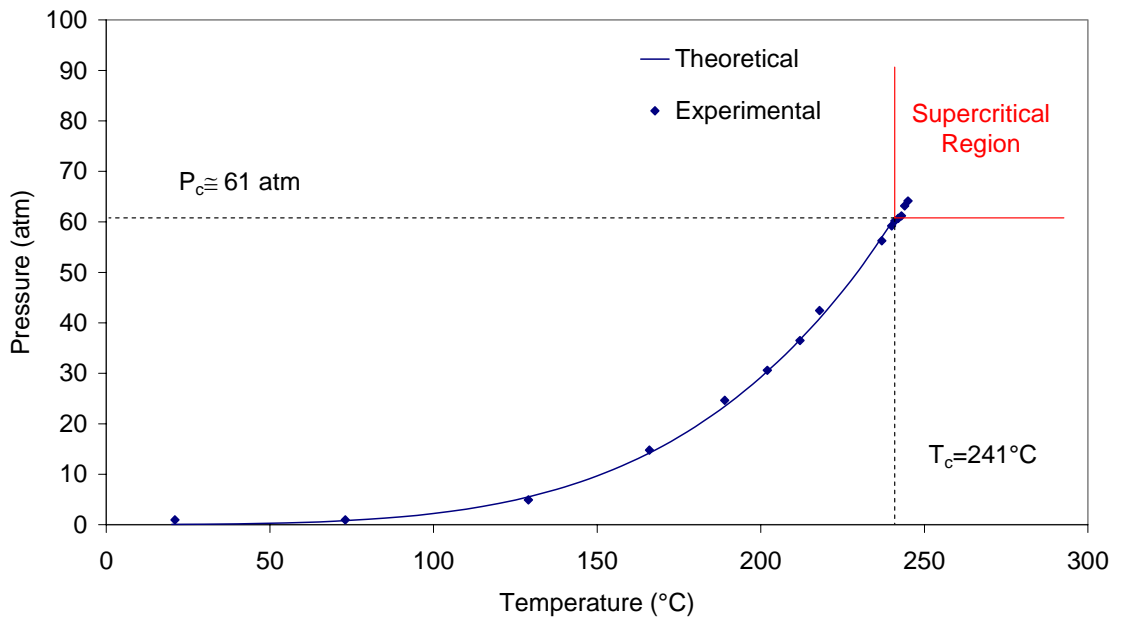


Figure 5.77. Pressure-Temperature relation of ethanol in closed reactor.

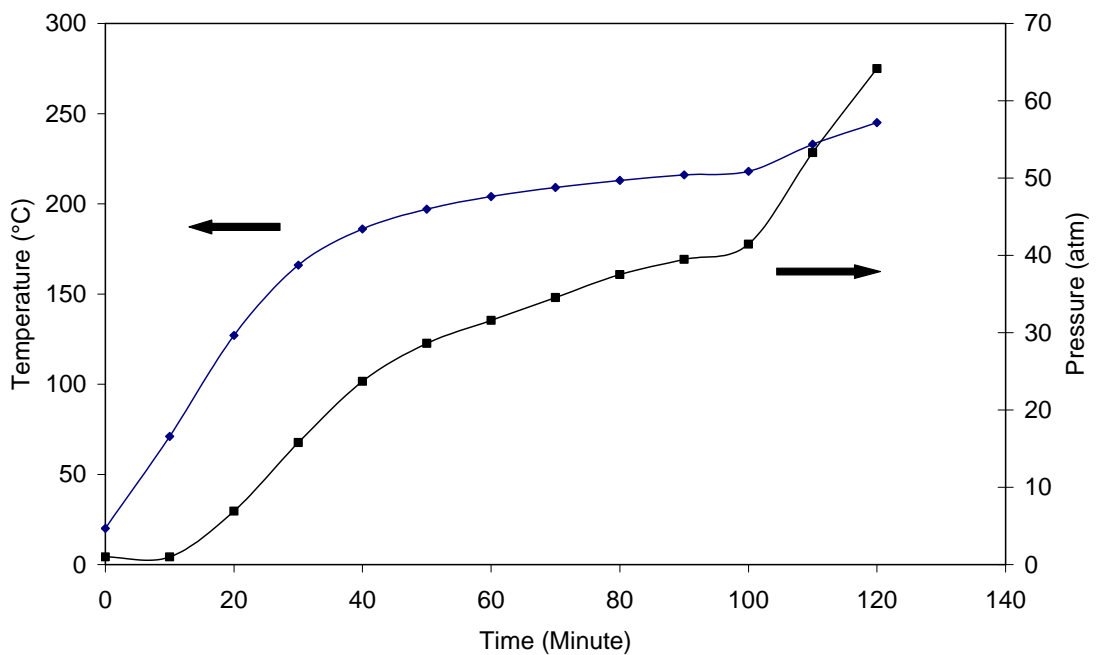


Figure 5.78. The change of temperature and pressure with time in closed reactor.

It was seen that supercritical pressure was obtained after 2 h of heating in the system. As the heating of reactor was carried out in room temperature, the heating period might show variations from time to time. After reaching to critical temperature and pressure of ethanol, system pressure was released so slowly into expansion vessel

under constant temperature. Two different procedures were used in this step. In the former one, system was maintained under supercritical conditions for 30 minutes and then ethanol was released and in latter one, as soon as reaching supercritical conditions ethanol started to release from system.

In that part of study, two different types of zinc borates  $2\text{ZnO}\cdot 3\text{B}_2\text{O}_3\cdot 3\text{H}_2\text{O}$  and  $\text{ZnO}\cdot \text{B}_2\text{O}_3\cdot 2\text{H}_2\text{O}$  that were produced in our laboratory and a commercial product with a given formula of  $2\text{ZnO}\cdot 3\text{B}_2\text{O}_3\cdot 3.5\text{H}_2\text{O}$  were dried by supercritical ethanol drying and by removal of ethanol at different temperatures, such as 200 °C and 150 °C. Actually, the commercial product has the oxide formula of  $2\text{ZnO}\cdot 3\text{B}_2\text{O}_3\cdot 3\text{H}_2\text{O}$  but it is known with the formula of  $2\text{ZnO}\cdot 3\text{B}_2\text{O}_3\cdot 3.5\text{H}_2\text{O}$  in trade literature. The detailed characterization of only zinc borates (ZnB1-SCE and ZnB7-SCE) produced and commercial zinc borate dried by supercritical ethanol drying were given in this part. In order to reveal the effect of drying temperature, zinc borates dried by ethanol removal at 200 °C and 150 °C were characterized and the results were discussed.

### **5.9.1. Supercritical Ethanol Drying of Zinc Borate Produced from Boric Acid and Zinc Oxide**

**Morphology of Particles:** In the determination of particle morphology both SEM and TEM analyses were utilized. The chemical characterization of zinc borate (S-4) that was produced from boric acid and zinc oxide at 90 °C,  $\text{B}_2\text{O}_3/\text{ZnO}$  molar ratio of 2.0 and dried conventionally at 110 °C was made previously. Zinc borate having the structure of  $2\text{ZnO}\cdot 3\text{B}_2\text{O}_3\cdot 3\text{H}_2\text{O}$  has particle size between 2-4  $\mu\text{m}$  as shown in Figure 5.79.a and Figure 5.79.b. In supercritical ethanol drying, transformation of micron sized particles into nanosized particles was expected. Particles with smaller size agglomerate during conventional drying due to the attraction of particles. In the supercritical ethanol drying of zinc borate particles, removal of water from the zinc borate structure and recrystallization of remained constituents forming a smaller nanosized anhydrous zinc borate species were expected.

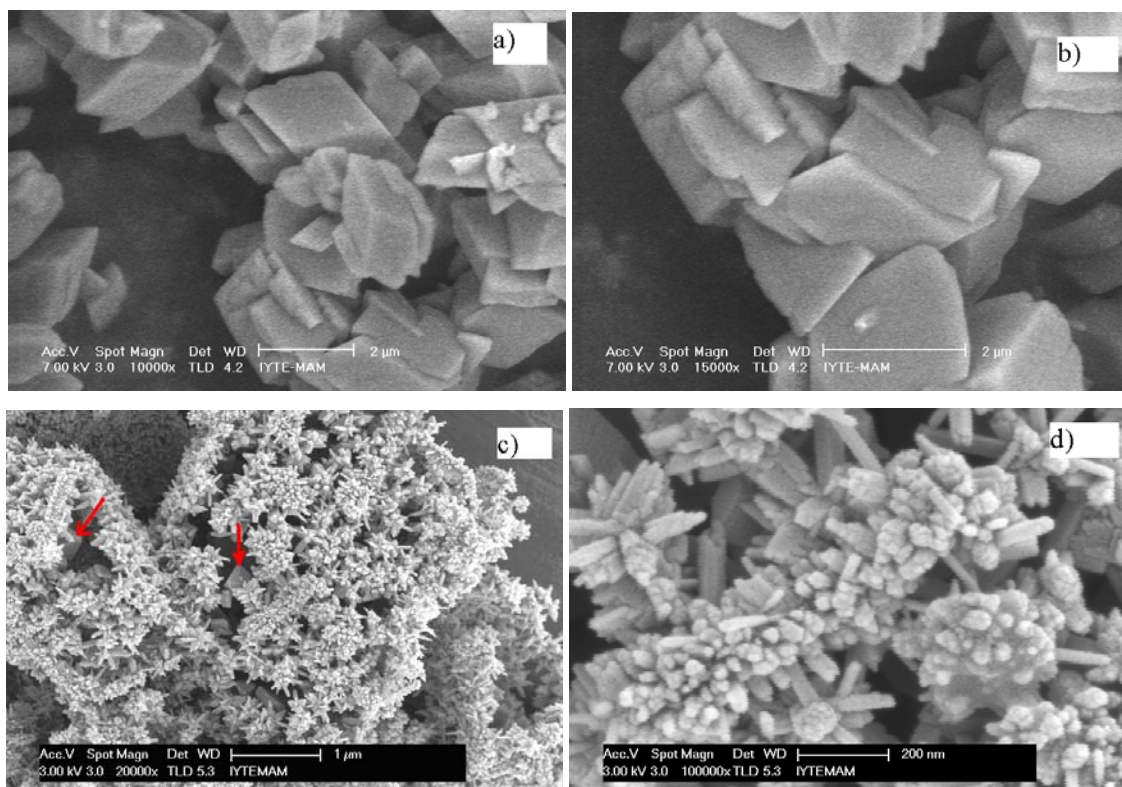


Figure 5.79. SEM microphotographs of zinc borate sample (S-4) that were produced from boric acid and zinc oxide at 90 °C and with B<sub>2</sub>O<sub>3</sub>/ZnO molar ratio of 2.0 a) and b) before supercritical drying c) and d) after supercritical drying (ZnB1-SCE).

Although zinc borate of 2ZnO·3B<sub>2</sub>O<sub>3</sub>·3H<sub>2</sub>O was known as stable while heating up to 290 °C under atmospheric pressure, a significant change in morphology of that product was observed during supercritical ethanol drying. Figure 5.79.c and Figure 5.79.d show the SEM microphotographs of zinc borate after supercritical ethanol drying at different magnifications. It was anticipated that zinc borate (2ZnO·3B<sub>2</sub>O<sub>3</sub>·3H<sub>2</sub>O) has undergone a chemical change and turned into a new chemical configuration due to the high pressure (6.5 MPa) and temperature (250 °C) during supercritical ethanol drying. When SEM microphotograph of zinc borate shown in Figure 5.79.c is examined it is observed that there are three different types of particle morphology: Larger particles at background, rod like particles and broccoli type particles. The larger particles shown by arrows at background might belong to anhydrous zinc borate. Rod-like particles are anticipated to be zinc oxide that formed from the decomposition of initial material. These rod-like particles are in length of 200 nm and in diameter of 30 nm. Broccoli-like particles might be also anhydrous zinc borate that loses its water during supercritical ethanol drying and their particle size changes between 20-40 nm. These small particles have tendency of agglomeration due to attractive forces (Van der Waals) between them.

From the SEM microphotographs taken before and after supercritical ethanol drying, it might be concluded that zinc borate of  $(2\text{ZnO}\cdot 3\text{B}_2\text{O}_3\cdot 3\text{H}_2\text{O})$  either dissolved in supercritical ethanol and formed a new phase after removal of ethanol or decomposed into its initial constituents' boron oxide, zinc oxide and water.

TEM microphotographs of zinc borate samples after supercritical ethanol drying at different magnification are shown in Figure 5.80. Three different morphologies determined in SEM images were also observed in TEM microphotographs. It was clearly distinguished from those microphotographs that nanoparticles agglomerated due to attractive forces.

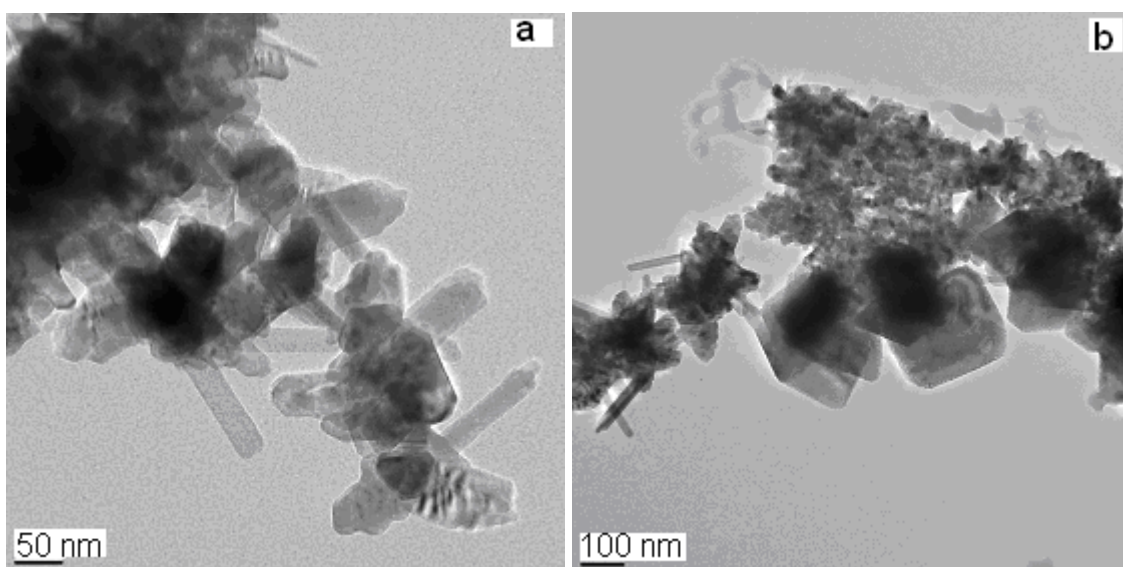


Figure 5.80. TEM microphotographs of zinc borate sample (ZnB1-SCE) that were produced from boric acid and zinc oxide at 90 °C and with  $\text{B}_2\text{O}_3/\text{ZnO}$  molar ratio of 2.0, and dried by supercritical ethanol drying a) 50 nm b)100 nm.

**Functional Groups of the Product:** FTIR spectrum of zinc borate after supercritical ethanol drying is shown in Figure 5.81. The peak at  $400\text{ cm}^{-1}$  wavenumber shows the presence of zinc oxide in the powder product. It can be concluded that chemical structure of zinc borate was changed completely during supercritical ethanol drying. After drying, the powder obtained contains zinc oxide as inferred from FTIR analysis. The peaks at  $1290$  ve  $720\text{ cm}^{-1}$  wavenumbers in that spectrum belong to boron-oxygen coordination in  $\text{BO}_3$  units but exact structure of that compound could not be determined. The formed product at the end of supercritical ethanol drying might have affinity to water because some peaks related to water molecule were observed at  $3470$  ve  $1650\text{ cm}^{-1}$  wavenumbers.

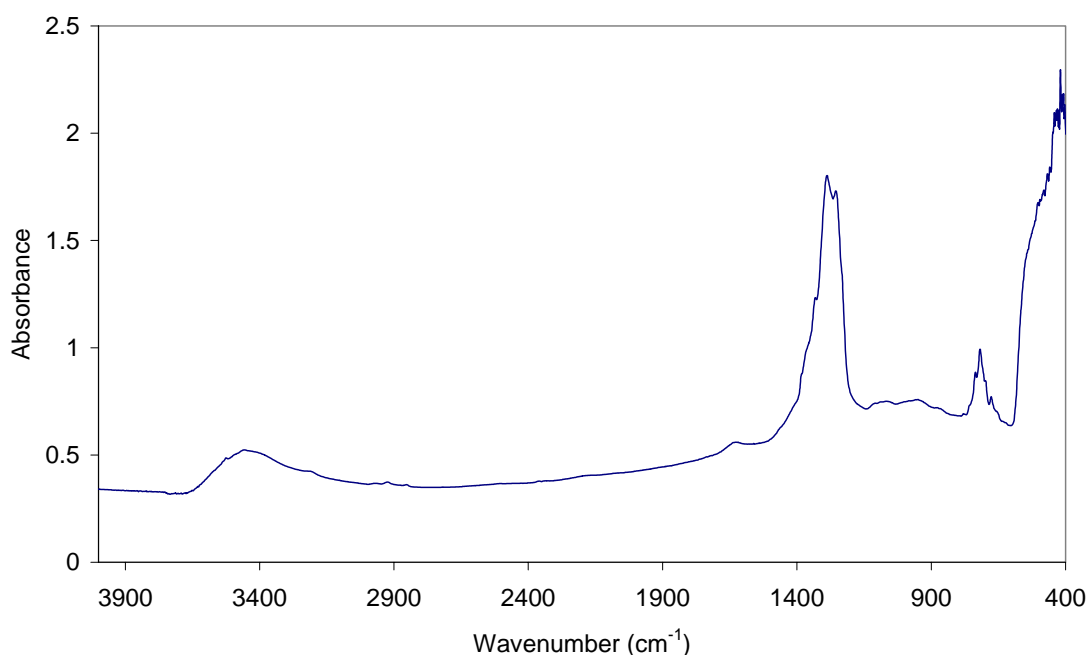


Figure 5.81. FTIR spectrum of zinc borate after supercritical drying (ZnB1-SCE).

Zinc borate produced from zinc oxide and boric acid decomposed into zinc oxide and boron-oxygen compound in supercritical ethanol drying process. In the decomposition of zinc borate and new boron-oxygen compound formation, it was anticipated that critical temperature and pressure of ethanol played a significant role. That zinc borate decomposed into its initial components was determined by characterizing zinc oxide peak from infrared analysis. If so, the other decomposition product had to be boric acid and it might be in the powder product or in the ethanol phase. In order to determine the boric acid, liquid ethanol used in supercritical drying was characterized in infrared analysis. A portion of that ethanol was vaporized and remaining white powder was examined using infrared spectroscopy. FTIR spectrum of white powder obtained from ethanol phase is shown in Figure 5.82. The peak at 3230  $\text{cm}^{-1}$  wavenumber indicates that there is O-H groups in the powder. O-H groups in zinc borate structure were utilized in the formation of boric acid in ethanol solution. The peaks observed at different wavelengths was summarized in Table 5.10. From those peaks it can be understood that white powder obtained from ethanol was boric acid (Medvedev and Komarevskaya, 2007).

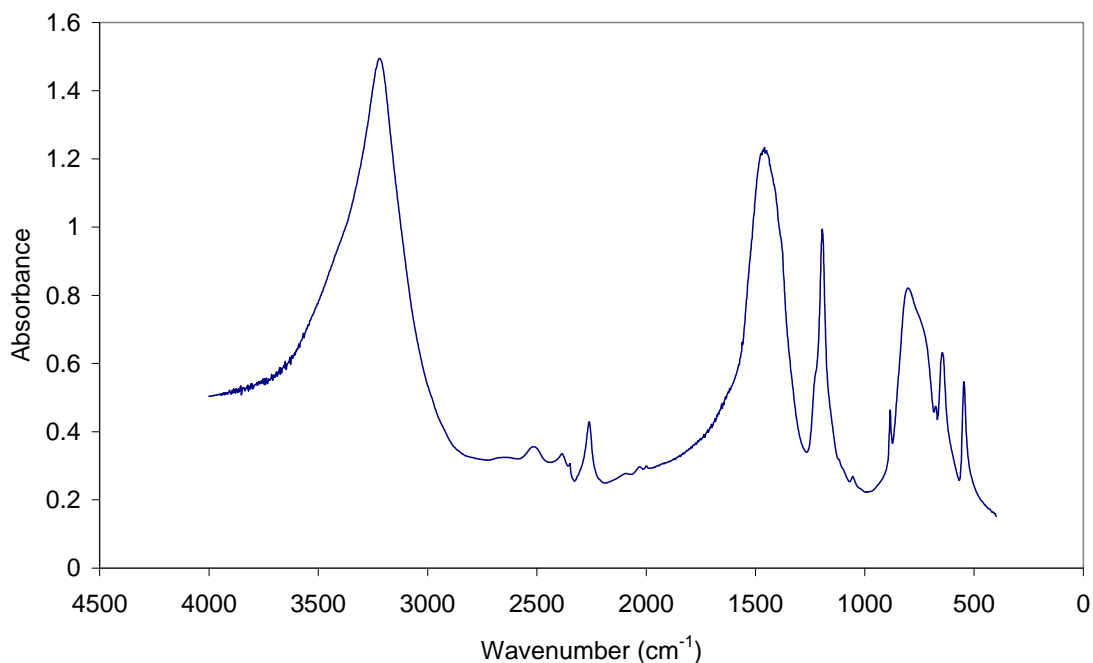
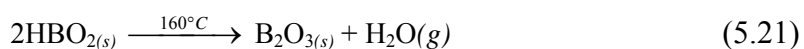
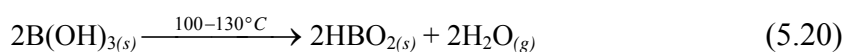


Figure 5.82. FTIR spectrum of white powder obtained from ethanol phase.

Table 5.10. Observed peaks in IR spectrum of white powder obtained from ethanol

Position in spectrum (cm <sup>-1</sup> )	Structure
547	B-O-B bond
650	B-O bond deformation
817	Out of plane bending of B-O-H
885	Symmetric (BO <sub>3</sub> )
1195	In plane bending of B-O-H
1473	Asymmetric stretching of (BO <sub>3</sub> )

The thermal phase change of boric acid was given by Pankajavalli and co-workers (2007) in Equations 5.20 and 5.21. According to this reaction mechanism, orthoboric acid was firstly transformed into metaboric acid in the temperature range of 100-130 °C and then that product was converted into anhydrous boron oxide (B<sub>2</sub>O<sub>3</sub>) compound by releasing a mole of H<sub>2</sub>O at 160 °C. Zinc borate (2ZnO·3B<sub>2</sub>O<sub>3</sub>·3H<sub>2</sub>O) decomposed partially forming the anhydrous zinc borate and other constituents, e.g. zinc oxide, boron oxide and water during the supercritical ethanol drying. As diboron trioxide (B<sub>2</sub>O<sub>3</sub>) has great affinity to water, it may form metaboric acid or orthoboric acid with water according the reverse reactions given in the Equations 5.20 and 5.21.



It was anticipated that diboron trioxide ( $\text{B}_2\text{O}_3$ ) and water were extracted from mixture of decomposition products of zinc borate. When ethanol was released to expansion vessel where it was cooled to room temperature, diboron trioxide ( $\text{B}_2\text{O}_3$ ) and ( $\text{H}_2\text{O}$ ) reacted to form the boric acid in ethanol phase.

**Crystal Structure of the Product:** After supercritical ethanol drying of zinc borate, obtained product consists of nanoparticles. As shown in Figure 5.83., the peaks in the XRD pattern were classified into two groups; peaks shown by circle and star. The peaks having higher intensity were compared with literature and it was concluded that they belong to zinc oxide (Wahab et al., 2007) and (JCPDS 80-0075). Additionally, the peaks having low intensity and shown by star belong to zinc oxide borate according to the data file of (JCPDS 85-1778).

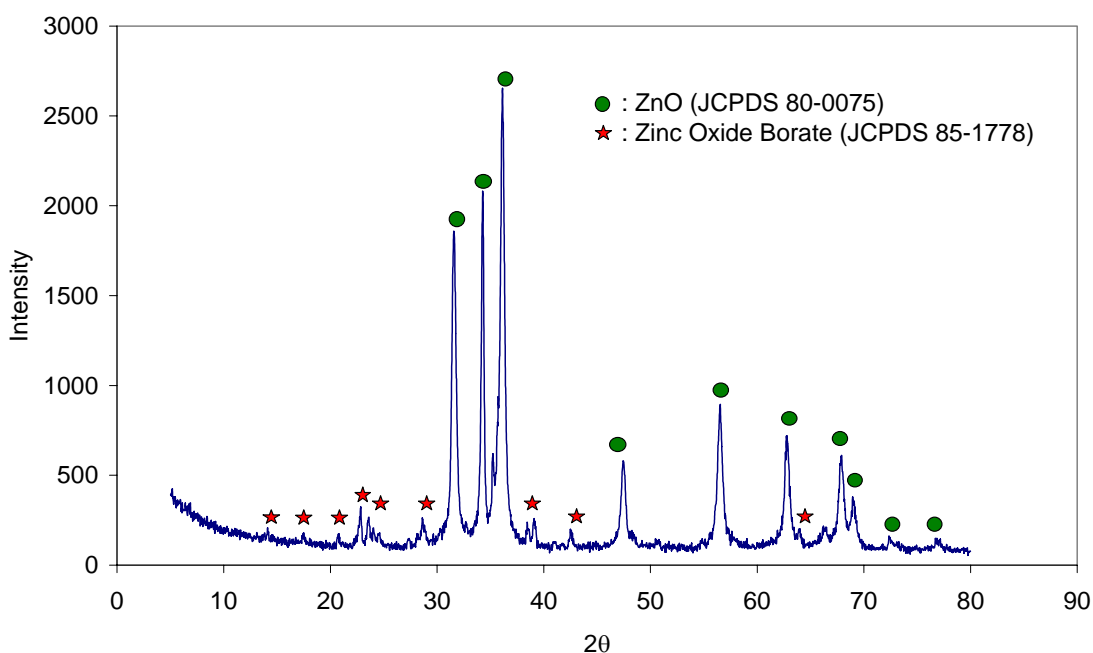


Figure 5.83. XRD pattern of supercritical ethanol dried zinc borate (ZnB1-SCE).



**Thermal Behaviour of the Product:** TGA thermogram of zinc borate obtained after supercritical ethanol drying is shown in Figure 5.84. It was comprehended that product was stable up to 600 °C and it did not contain any volatile compound. The water which was determined from peaks at 3400  $\text{cm}^{-1}$  and 1650  $\text{cm}^{-1}$  in FTIR spectrum could not be removed from structure up to 600 °C.

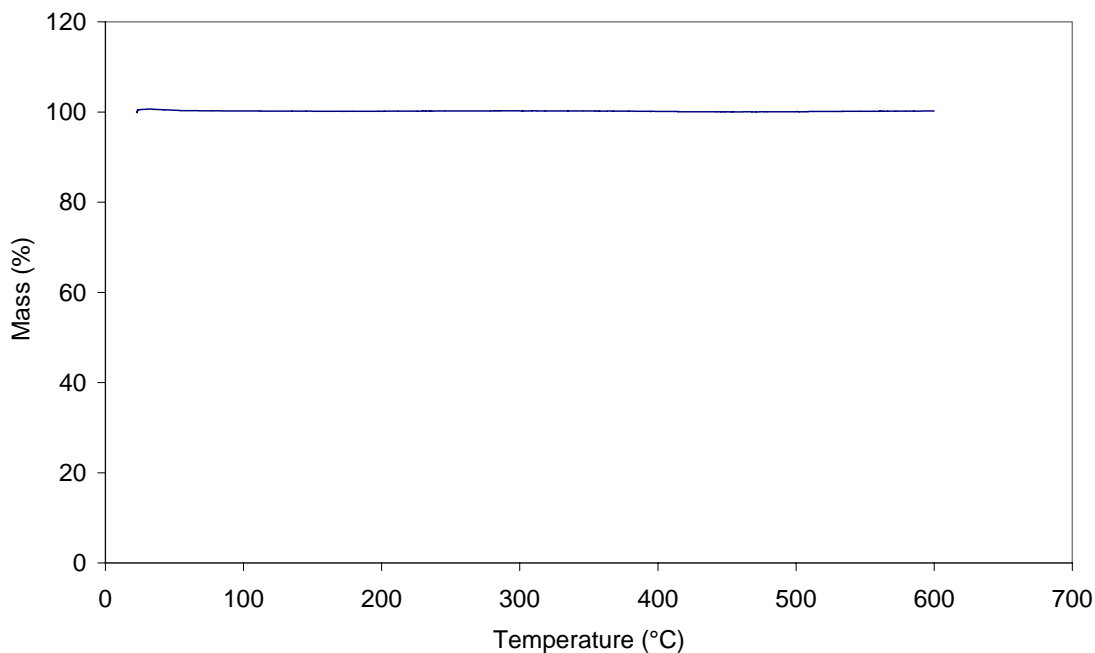
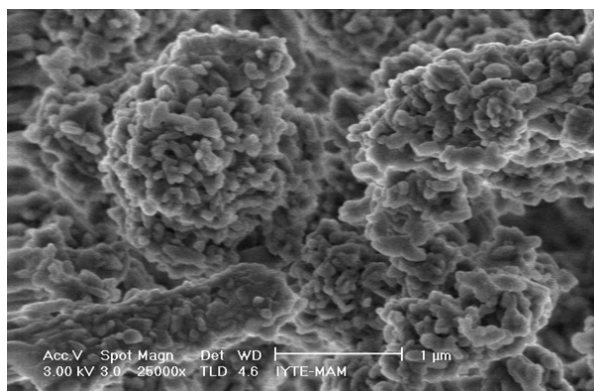


Figure 5.84. TGA thermogram of supercritical ethanol dried zinc borate (ZnB1-SCE).

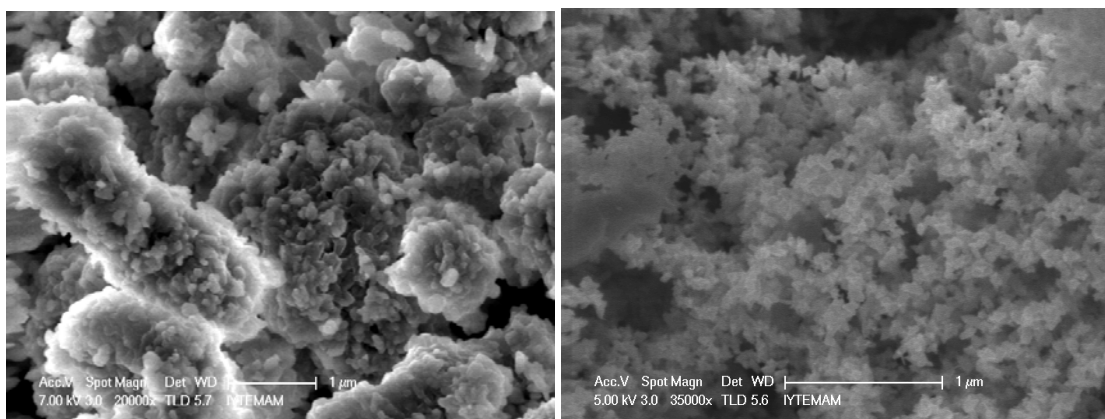
### 5.9.2. Effect of Temperature in Ethanol Drying

Zinc borate,  $2\text{ZnO}\cdot 3\text{B}_2\text{O}_3\cdot 3\text{H}_2\text{O}$ , has decomposed partially into its constituents, zinc oxide, boron oxide and water during supercritical ethanol drying which was carried out at 250 °C and 6.5 MPa. The effect of ethanol drying at lower temperatures, such as 150 °C and 200 °C were also examined.

The particle morphology of the zinc borate samples before and after drying at 150 °C and 200 °C was observed by SEM. As shown in Figure 5.85.a and Figure 5.85.b, there is no significant change in the morphology of the particles. The removal of ethanol at 200 °C, caused a change in the particle morphology of the zinc borate (Figure 5.85.c). Zinc borate decomposed into zinc oxide and smaller particles on the surface of large particles represent zinc oxide.



a)



b)

c)

Figure 5.85. SEM microphotographs of a) commercial product, zinc borates dried by removing ethanol at b) 150 °C (ZnB4-SCE), c) 200 °C (ZnB5-SCE).

Figure 5.86 shows the volume-weighted particle size distribution of zinc borate that was dried by removing ethanol at 200 °C. There are two groups of particles; smaller particles having 64 nm average particle size and the larger particles having average particle size of 540 nm. It was concluded that larger particles were formed from agglomeration of those nanosized particles.

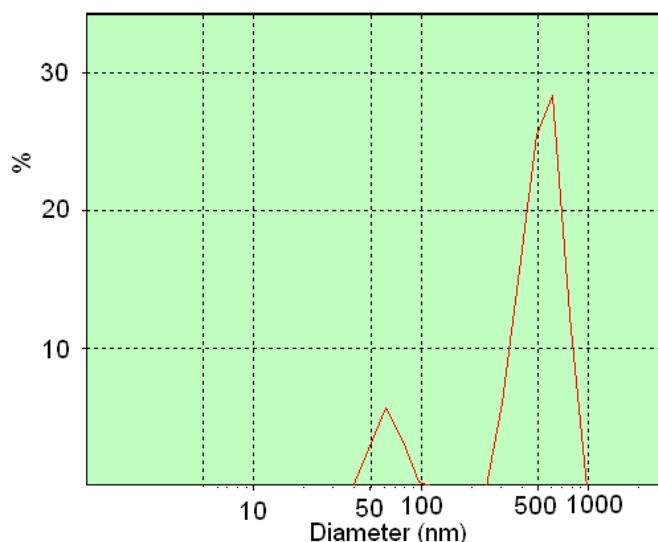


Figure 5.86. Particle size distribution of zinc borate dried by removing ethanol at 200 °C (ZnB5-SCE), (Malvern Zetasizer 3000 HSA).

FTIR spectra of zinc borate samples dried at 200 °C and 150 °C are shown in Figure 5.87. The peak at 400  $\text{cm}^{-1}$  wavenumber in Figure 5.87.a indicates that there is free zinc oxide in the product. The presence of ZnO in the final product means that zinc borate decomposed during the drying even at 200 °C. On the other hand, drying of zinc borate at 150 °C did not make a significant alteration neither on the particle morphology nor the structure of product as inferred from Figure 5.87.b.

Changes in crystallinity and chemical structure of zinc borates during ethanol drying at different temperatures were examined also by XRD analysis. XRD patterns of zinc borates dried at 200 °C and 150 °C are shown in Figure 5.88.a and 5.88.b, respectively. Zinc borate that was dried by ethanol drying at 150 °C was not affected under those condition as the X-ray diffraction peaks observed in Figure 5.88.a were identical to that of  $2\text{ZnO}\cdot 3\text{B}_2\text{O}_3\cdot 3\text{H}_2\text{O}$  reported in the study of Sawada et al., (2004). On the other hand, XRD pattern of zinc borate dried at 200 °C was different than the XRD pattern of zinc borate dried at 150 °C as shown in Figure 5.88.a. In other words, there are extra peaks, 31.7°, 34.1°, 36.2°, 56.6°, 62.9°, and 68.0° at  $2\theta$  values rather than the peaks of zinc borate of  $2\text{ZnO}\cdot 3\text{B}_2\text{O}_3\cdot 3\text{H}_2\text{O}$ . The extra peaks in Figure 5.88.b represents the presence of zinc oxide (Wahab et al., 2007) and (JCPDS 80-0075) that resulted from the decomposition of zinc borate during drying at 200 °C.

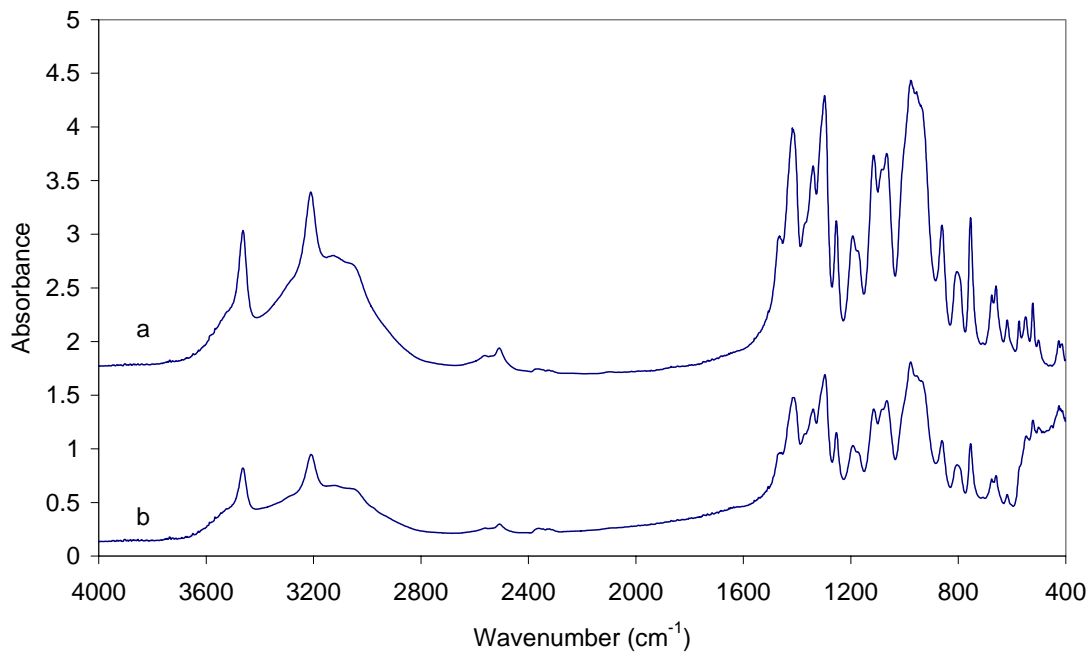


Figure 5.87. FTIR spectra of zinc borates dried by removing ethanol at a) 150 °C (ZnB4-SCE), b) 200 °C (ZnB5-SCE).

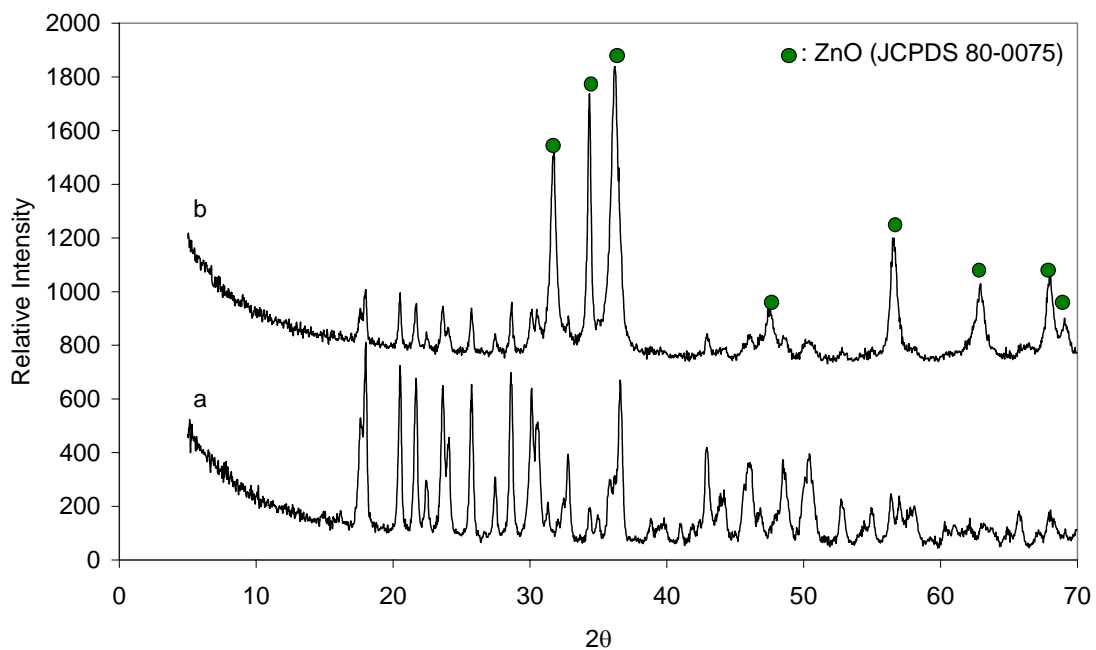


Figure 5.88. XRD patterns of zinc borates dried by removing ethanol at a) 150 °C (ZnB4-SCE) b) 200 °C (ZnB5-SCE).

### 5.9.3 Supercritical Ethanol Drying of Zinc Borate Produced from Borax Decahydrate and Zinc Nitrate Hexahydrate

Zinc borate produced from  $1 \text{ mol.dm}^{-3}$  borax decahydrate and  $1 \text{ mol.dm}^{-3}$  zinc nitrate hexahydrate at  $70 \text{ }^\circ\text{C}$  for 5 h reaction time was dried by supercritical ethanol drying. Results obtained from the characterization of final product are given as follows.

**Morphology of Particles:** SEM microphotographs of material obtained from supercritical ethanol drying of zinc borate are given in Figure 5.89. From the examination of these microphotographs, there are two types of morphology; rod-like particles and spherical particles. It is believed that both types of spherical and rod-like particles formed from the decomposition of zinc borate belonged to zinc oxide. The length of those rods was about 200 nm and their diameter was between 20-30 nm. It was determined that spherical particles were between 40-60 nm.

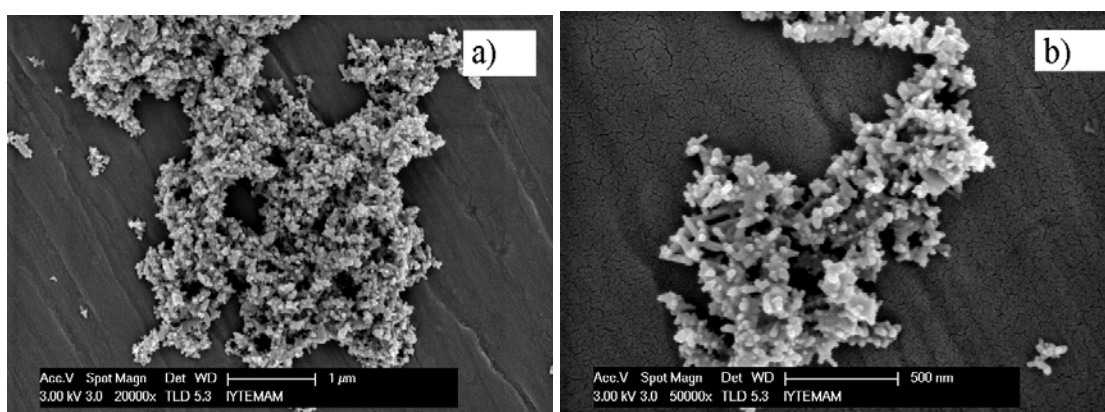


Figure 5.89. SEM microphotographs of supercritical ethanol dried zinc borate (ZnB6-SCE) that were produced from  $1.0 \text{ mol.dm}^{-3}$  borax decahydrate and  $1 \text{ mol.dm}^{-3}$  zinc nitrate hexahydrate at  $70 \text{ }^\circ\text{C}$  for 5 h a) 20.000x, b) 50.000x.

TEM microphotographs of samples obtained from supercritical ethanol drying of zinc borate were shown in Figure 5.90. In those photographs, particles are in the shape of rod which is 20-30 nm in diameter and 100-200 nm in length. It was observed that these nanosized particles formed bigger particles due to attractive forces between them.

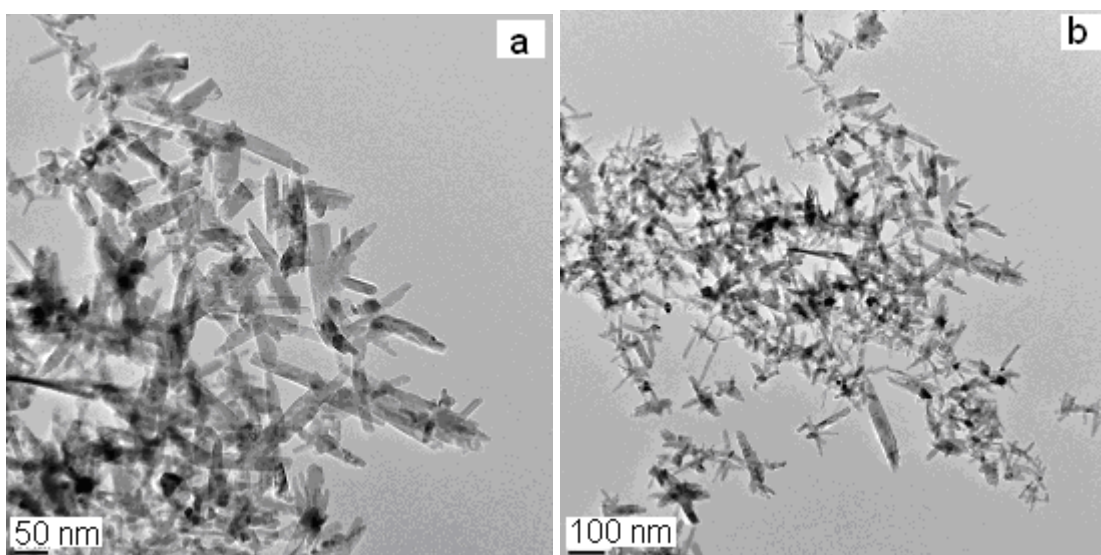


Figure 5.90. TEM microphotographs of supercritical ethanol dried zinc borate (ZnB6-SCE) that were produced from  $1.0 \text{ mol.dm}^{-3}$  Borax decahydrate and  $1 \text{ mol.dm}^{-3}$  zinc nitrate hexahydrate at  $70 \text{ }^\circ\text{C}$  for 5 h a) 50 nm, b)100 nm.

Figure 5.91 displays the particle size distribution of zinc borate before supercritical ethanol drying. As we know from the characterization of zinc borate produced from borax and zinc nitrate, it has two groups of particles. The first group consists of micron sized and nanosized particles, the second group generally includes micron sized larger particles and mean value of particle size considering two groups is  $5.8 \text{ }\mu\text{m}$ .

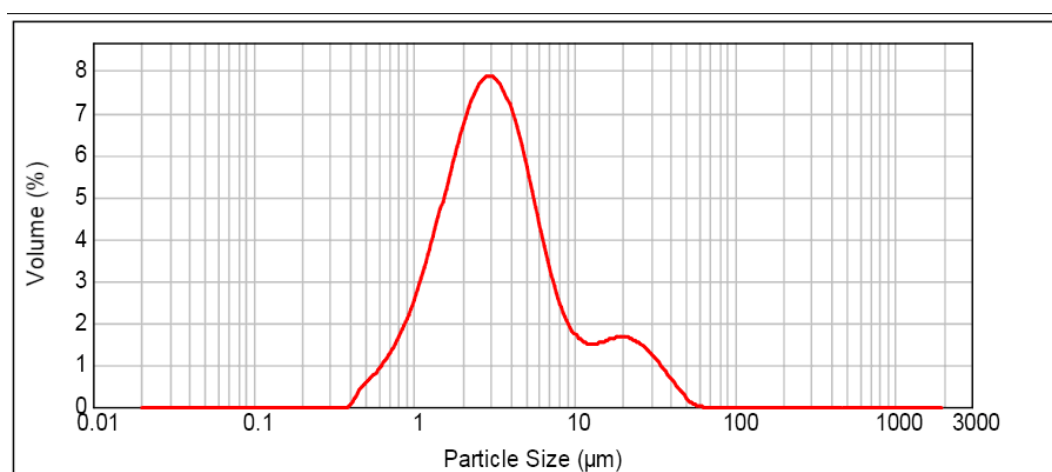


Figure 5.91. Particle size distribution of zinc borate (ZnB6-SCE) that was produced from  $1.0 \text{ mol.dm}^{-3}$  borax decahydrate and  $1.0 \text{ mol.dm}^{-3}$  zinc nitrate hexahydrate at  $70 \text{ }^\circ\text{C}$  for 5 h and conventional dried, (Malvern Mastersizer 2000).

Figure 5.92 shows the particle size distribution of zinc borate that was treated by supercritical ethanol drying. After supercritical ethanol drying of zinc borate, nanosized smaller particles have emerged in the distribution. It is highly believed that nanosized particles form larger particles due to attraction between them. The volume weighted mean value of particle size was found as 3.8  $\mu\text{m}$ .

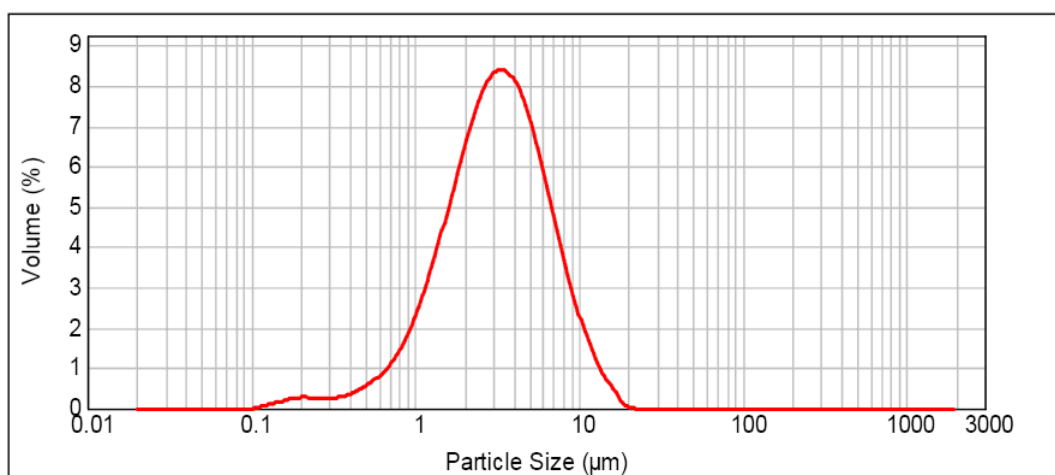


Figure 5.92. Particle size distribution of zinc borate (ZnB6-SCE) that was produced from  $1.0 \text{ mol.dm}^{-3}$  borax decahydrate and  $1.0 \text{ mol.dm}^{-3}$  zinc nitrate hexahydrate at  $70 \text{ }^\circ\text{C}$  for 5 h, and supercritical ethanol dried, (Malvern Mastersizer 2000).

**Functional Groups of the Product:** Zinc borate produced from boric acid and zinc oxide decomposed during supercritical ethanol drying was determined previously. In the decomposition of zinc borate, the temperature and pressure of the supercritical drying process had a significant role. In the drying of zinc borate produced from borax decahydrate and zinc nitrate hexahydrate, same sort of decomposition took place as it was understood from FTIR spectrum in Figure 5.93. The peak at  $400 \text{ cm}^{-1}$  wavenumber shows the presence of zinc oxide in the powder product. It can be deduced that chemical structure of zinc borate has been changed completely during supercritical ethanol drying. After drying, the obtained powder contains zinc oxide. The peaks at  $1290$  and  $720 \text{ cm}^{-1}$  wavenumbers in that spectrum belong to boron-oxygen coordination but exact structure of that compound could not be proposed. The presence of peaks at  $3470$  and  $1650 \text{ cm}^{-1}$  which shows the water molecule or OH groups in the product can be explained by the affinity of formed product to water molecule.

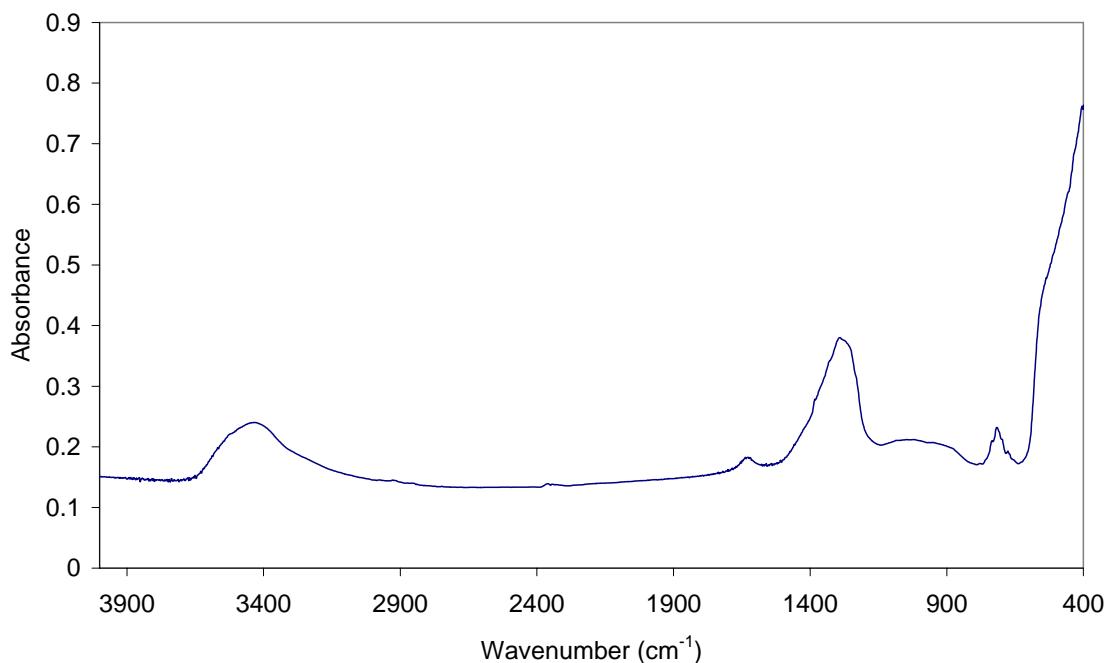


Figure 5.93. FTIR spectrum of supercritical ethanol dried zinc borate (ZnB6-SCE).

FTIR spectrum of powder obtained from ethanol which was used as a solvent in supercritical drying is given in Figure 5.94. After the decomposition of zinc borate produced from borax decahydrate and zinc nitrate hexahydrate during supercritical ethanol drying,  $B_2O_3$  and OH groups in the zinc borate structure are expected to form the boric acid. Since the solubility of boric acid in ethanol is extremely high (94.4 g/L) (Briggs, 2001), it can be easily extracted from the mixture of zinc borate and decomposition products. Solid boric acid was obtained by evaporating ethanol boric acid mixture. The peaks observed at different wavelengths in Figure 5.94 were identified in Table 5.10. From those identified peaks, white powder obtained from ethanol was boric acid (Medvedev and Komarevskaya, 2007).

Another important phenomenon in the transportation of boric acid from high pressure vessel to the expansion vessel is the state of boric acid. As it is given in literature, boric acid has a great solubility in liquid ethanol and it has a vapor pressure (Attina et al. 1992). The vapor pressure of boric acid was measured in the temperature range 326–363 K. The standard enthalpy of sublimation,  $\Delta H_{sub}^{\circ}$ , of  $H_3BO_3$  was estimated to be  $174.1 \pm 4.7 \text{ kJ.mol}^{-1}$  (Pankajavalli et al. 2007). There is no information regarding to vapor pressure or sublimation of boric acid in ethanol above critical temperature and pressure of ethanol. From this experiment, one may draw either of the



following conclusions; boric acid could have also dissolved in supercritical ethanol or it may have easily sublimated into vapor form under supercritical ethanol drying conditions.

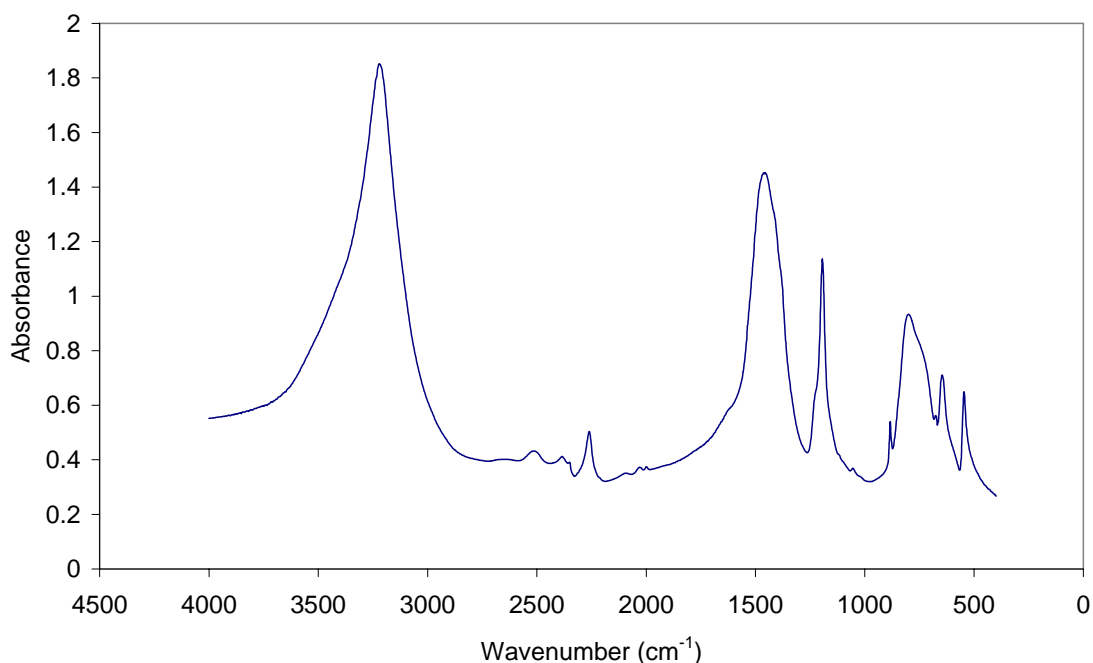


Figure 5.94. FTIR spectrum of white powder obtained from ethanol phase.

**Crystal Structure of the Product:** After supercritical ethanol drying of zinc borate produced from borax decahydrate and zinc nitrate hexahydrate nanosized white powder was obtained. In order to determine its crystal structure and its constituents X-ray diffraction analysis was utilized for those samples. Sharp peaks in XRD pattern as shown in Figure 5.95. indicate that powder obtained after supercritical ethanol drying has crystalline structure. By comparing that pattern with literature it was concluded that powder at the end of supercritical ethanol drying was zinc oxide (Wahab et al., 2007). Another important emerging result in this pattern is that it belonged to only one component, zinc oxide. There is no evidence for other compounds, such as anhydrous zinc borate or other boron-oxygen compounds.

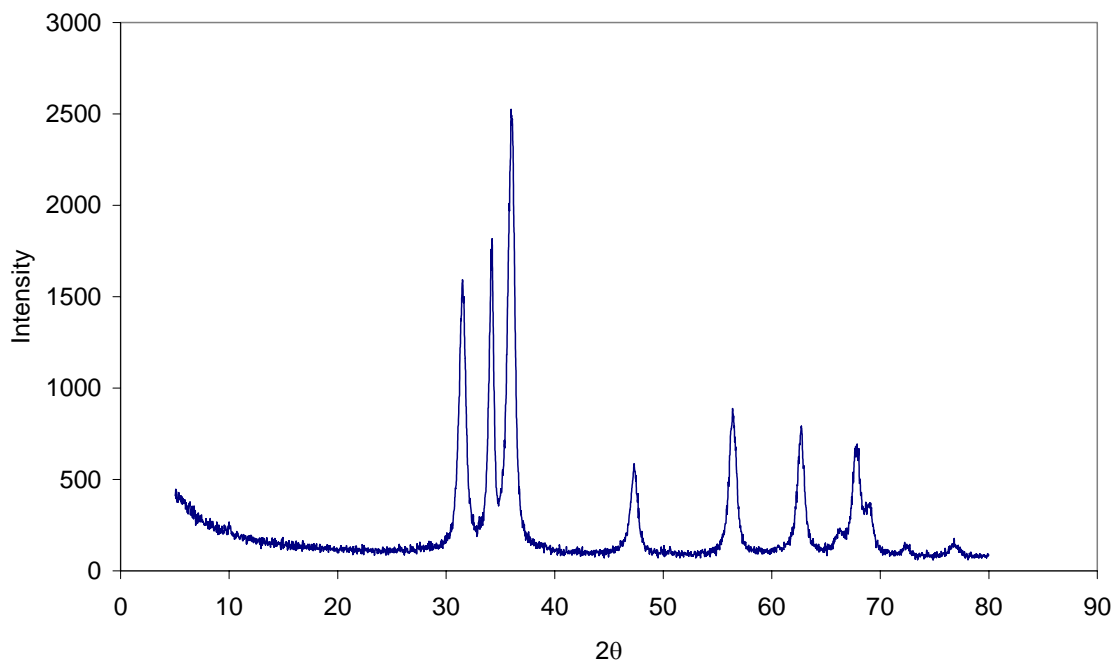


Figure 5.95. XRD pattern of supercritical ethanol dried zinc borate (ZnB6-SCE).

**Thermal Behaviour of the Product:** TGA thermogram of supercritical ethanol dried zinc borate produced from borax decahydrate and zinc nitrate hexahydrate is shown in Figure 5.96. It was comprehended that product was stable up to 600 °C and it did not contain any volatile and organic compounds. The water as shown by peaks at 3400  $\text{cm}^{-1}$  and 1650  $\text{cm}^{-1}$  in FTIR spectrum could not be removed from structure up to 600 °C.

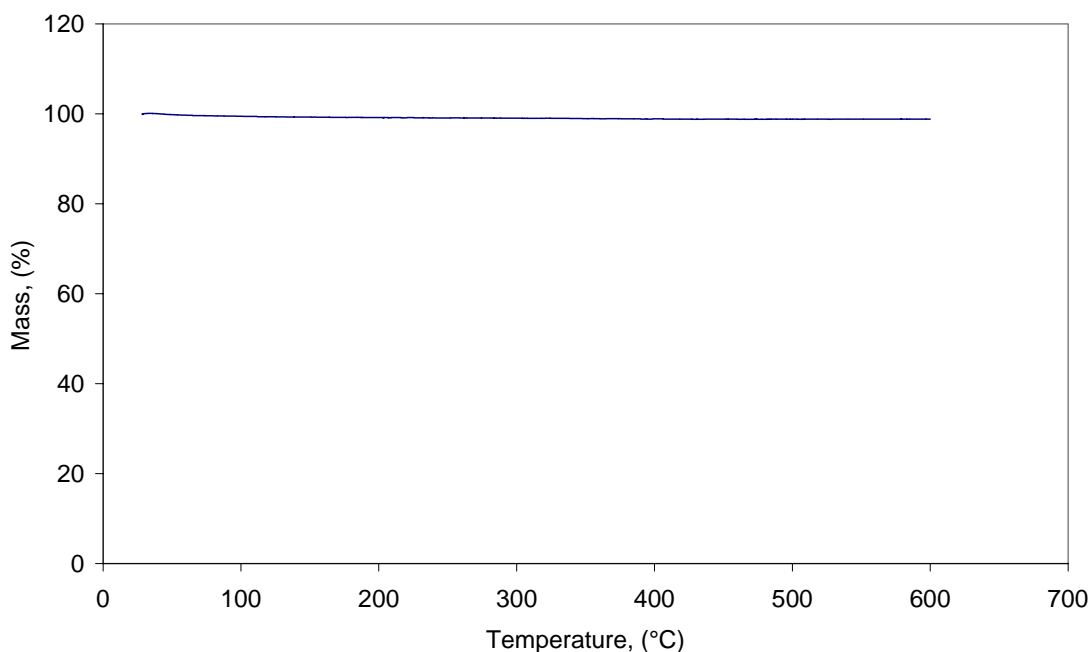
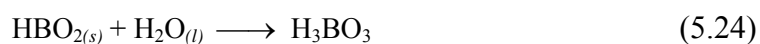
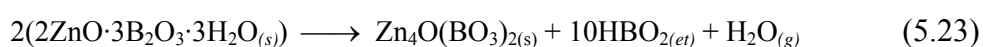
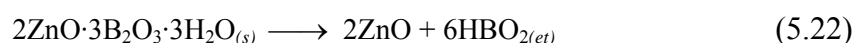


Figure 5.96. TGA thermogram of supercritical ethanol dried zinc borate (ZnB6-SCE).

#### 5.9.4. Material Balance Around Supercritical Ethanol Drying Process

Zinc borate having formula of  $2\text{ZnO}\cdot 3\text{B}_2\text{O}_3\cdot 3\text{H}_2\text{O}$  decomposes partially into its component according to Equation 5.22 and loses hydroxyl groups (B-OH) and forms anhydrous zinc borate according to Equation 5.23 in supercritical ethanol drying process. The presence of anhydrous zinc borate,  $\text{Zn}_4\text{O}(\text{BO}_3)_2$ , was determined from XRD analysis. The other decomposition product metaboric acid,  $\text{HBO}_2$ , dehydrates further to form anhydrous boron oxide,  $\text{B}_2\text{O}_3$  as given in Equation 5.21. In the presence of water dehydrated from zinc borate structure, both metaboric acid and boron oxide react with water to synthesize boric acid,  $\text{B}(\text{OH})_3$ , as given in Equation 5.24.



On the other hand, zinc borate having 2 moles of water in its structure decomposes completely according to Equation 5.25. The formed HBO<sub>2</sub> in ethanol gives reaction with water and produces boric acid according to Equation 5.24.



Both orthoboric acid (H<sub>3</sub>BO<sub>3</sub>) and metaboric acid (HBO<sub>2</sub>) dissolve spontaneously in ethanol and they are anticipated to vaporize from liquid state with ethanol under supercritical conditions of ethanol. During the removal of ethanol from high pressure vessel to expansion vessel, not only ethanol was separated but also boric acid in gaseous state was removed. When adiabatic expansion of ethanol from 6.5 MPa to atmospheric pressure is considered, the temperature decreases from 250 °C to 161 °C. As there is no isolation material around the pipeline between two vessels, the ethanol expanded is also cooled by the surrounding air. Thus, it liquefies until reaching to the expansion vessel. The remarkable conclusion of that separation process is that supercritical ethanol is a good solvent for the extraction of boric acid from inorganic hydrated metal borate structure. Boric acid is usually manufactured from minerals colemanite, kernite and tincal using sulphuric acid and crystallization techniques (Roskill, 2006). The use of supercritical ethanol extraction of boric acid from those minerals can be an alternative production method. After separating and crystallizing the boric acid, ethanol can be used in the process without producing any aqueous waste streams. That phenomenon can be utilized to extract boric acid from natural boron minerals, such as colemanite, ulexite, and borax.

The streams defined in the supercritical ethanol drying system are shown in Figure 5.97. In that system, **A** is zinc borate sample; **B** is ethanol; **C** is powder product formed at the end of supercritical ethanol drying; **D** is ethanol and by-product (boric acid) mixture; **E** is solid boric acid and **F** is the ethanol that regained.

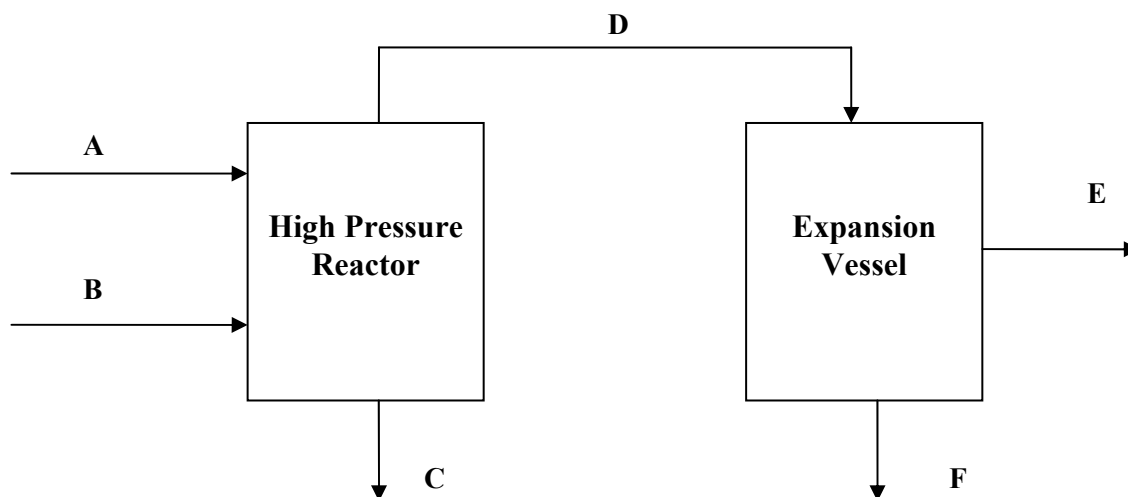


Figure 5.97. Streams in supercritical ethanol drying system.

Amounts of materials obtained in both liquid and solid phases at the end of supercritical ethanol drying of zinc borates that were obtained from both borax decahydrate and boric acid, and subcritical ethanol drying of commercial zinc borates are given in Table 5.11. That the product separated from zinc borate by supercritical ethanol drying was boric acid was determined from both FTIR and XRD analyses. As zinc borate ( $2\text{ZnO}\cdot 3\text{B}_2\text{O}_3\cdot 3\text{H}_2\text{O}$ ) has a dehydration onset temperature at  $290\text{ }^\circ\text{C}$  under atmospheric pressure, it was not expected that aforementioned zinc borate would not decompose during supercritical ethanol drying conditions of  $250\text{ }^\circ\text{C}$  and  $6.5\text{ MPa}$ . However, that high pressure  $6.5\text{ MPa}$  should be responsible in the decomposition of zinc borate during supercritical drying. On the other hand, when that decomposition was examined, it was clearly seen that not only diboron trioxide ( $\text{B}_2\text{O}_3$ ) but also ( $\text{H}_2\text{O}$ ) in the structure of zinc borate ( $2\text{ZnO}\cdot 3\text{B}_2\text{O}_3\cdot 3\text{H}_2\text{O}$ ) released from structure due to high temperature and pressure. In that decomposition during supercritical ethanol drying, temperature is greater than the temperature of water removal from metaboric and orthoboric acid structures according to Equation 5.19. Thus, both of the  $\text{B}_2\text{O}_3$  and  $\text{H}_2\text{O}$  react to form boric acid in liquid ethanol or at temperatures lower than  $100\text{ }^\circ\text{C}$ . Boric acid that dissolved in ethanol was separated by evaporating of ethanol.

Zinc borate (S-4) that was produced in our laboratory at  $90\text{ }^\circ\text{C}$  with  $\text{B}_2\text{O}_3/\text{ZnO}$  molar ratio of 2.0 and commercial zinc borates were dried by supercritical ethanol for 30 minute and commercial zinc borates were dried by supercritical ethanol by releasing ethanol as soon as reaching critical temperature and pressure. Amounts of zinc borate samples before the operation and amounts of solid samples remained in the reactor and

dissolved in ethanol are given in Table 5.11. As it is seen, mass balance around the supercritical drying is consistent and excess amount of powder product can be attributed to moisture uptake from air. The density of the solid product obtained at the end of supercritical ethanol drying is also given in Table 5.11. The densities are average values of ten different measurements at 25 °C. All of these densities are lower than the density ( $5.7 \text{ g.cm}^{-3}$ ) of zinc oxide pointing that final product is a mixture of zinc oxide and other zinc boron oxygen compound having density lower than that of zinc oxide. Another approach for the difference in the densities of ZnO formed at the end of supercritical ethanol drying of zinc borates might be amorphous structure of some part of zinc oxide. After the supercritical drying of zinc borate (ZnB1-SCE) for 30 minute, 3.25 g powder product left in the high pressure reactor and 4.87 g product was removed in ethanol. Same procedure was applied to commercial product (ZnB2-SCE), 3.64 g powder product obtained in the reactor and 5.35 g product carried by ethanol to expansion chamber. For both experiments, initial and final masses after the drying are close to each other and small variations can be attributed to error propagation in the experiments and titration analysis. In the drying of zinc borate, (ZnB3-SCE), ethanol was released as soon as reaching the supercritical conditions. For that product, 3.34 g powder product and 5.15 g product that dissolved in ethanol were obtained. When the mass balance around the drying process was examined it could be said that inlet material was almost equal to outlet products in which it was assumed that all of water in zinc borate was consumed in the boric acid formation.

Table 5.11. Mass and density of samples obtained from supercritical and subcritical ethanol drying of zinc borates

Sample	Drying time (min.)	A (g)	C (g)	E (g)	Final mass (C+E), (g)	Density of C ( $\text{g.cm}^{-3}$ )
ZnB1-SCE	30	8.25	3.25	4.87	8.12	5.1
ZnB2-SCE	30	8.25	3.64	5.35	8.99	4.5
ZnB3-SCE	0	8.25	3.34	5.15	8.49	4.5
ZnB4-SCE	0	10.00	9.50	0.15	9.65	2.8
ZnB5-SCE	0	10.00	5.04	6.71	11.75	3.8
ZnB6-SCE	0	5.26	2.20	2.77	4.97	4.8
ZnB7-SCE	0	4.03	2.39	2.10	4.49	4.5

Samples obtained at the end of drying of commercial zinc borates at 150 °C (ZnB4-SCE) and 200 °C (ZnB5-SCE) were also analysed. That zinc borate was not affected from drying at 150 °C could be inferred as there was no difference between initial and final masses. On the other hand, zinc borate dried at 200 °C decomposed partially since half of the initial mass was lost at the end of drying. The densities of those (ZnB4-SCE) and (ZnB5-SCE) samples are 2.8, which is very close to density of the zinc borate (2.86 g.cm<sup>-3</sup>), and 3.8 g.cm<sup>-3</sup>, that is mixture of zinc oxide and zinc borate, respectively.

Zinc borate (S-20) produced by using 50 mL 1 mol.dm<sup>-3</sup> borax decahydrate and 50 mL 1 mol.dm<sup>-3</sup> zinc nitrate at 70 °C for 5 h reaction time in our laboratory was dried by supercritical ethanol. That zinc borate had 2 moles of water in its structure was determined previously. Zinc borate sample (ZnB6-SCE) was dried by supercritical ethanol drying and that run was repeated (ZnB7-SCE). The initial mass of zinc borate samples, final mass remained in the reactor and by-product removed by ethanol are given Table 5.11. For the drying of zinc borate having 2 moles of water, initial masses are close to final masses that are summation of powder product and by-product in the ethanol considering residues left in the pipelines and reactors.

Compositions of powder remained in the reactor and the solid obtained from ethanol phase at the end of supercritical ethanol drying of zinc borates determined by analytical titration are given in Table 5.12.

Table 5.12. Composition of products: powder remained in reactor and product dissolved ethanol

Sample	Powder remained in reactor c)		Product Dissolved in Ethanol (E)	
	%ZnO	% B <sub>2</sub> O <sub>3</sub>	%ZnO	% B <sub>2</sub> O <sub>3</sub>
ZnB1-SCE	90.8	16.8	0.7	54.3
ZnB2-SCE	82.8	10.3	0.9	54.8
ZnB3-SCE	89.8	10.2	1.6	55.4
ZnB4-SCE	34.3	49.8	-	-
ZnB5-SCE	71.6	27.6	-	56.9
ZnB6-SCE	92.5	1.4	3.4	54.5
ZnB7-SCE	92.0	2.7	1.3	56.3

(-): could not be measured.

From those results, it can be proposed that remained product in the reactor has high zinc oxide content and product dissolved in ethanol is rich in boric acid. In the

supercritical ethanol drying of zinc borate (ZnB1-SCE) for 30 minute, powder remained in the reactor consisted of zinc oxide in 90.8 % by weight and  $B_2O_3$  in 16.8 % by weight and the product dissolved in ethanol consisted of  $B_2O_3$  in 54.3 % by weight and zinc oxide 0.7 % by (wt). The equivalent amount of  $B_2O_3$  percent in boric acid content is 56.25 % by (wt). Thus, it can be concluded that product dissolved in ethanol was mainly boric acid. In the supercritical ethanol drying of commercial zinc borate (ZnB2-SCE) for 30 min., obtained product in the reactor composed of 82.8 % zinc oxide and 10.3 %  $B_2O_3$  by weight as shown in Table 5.12. The product dissolved in ethanol consisted of 54.8 %  $B_2O_3$  and only 0.9 % zinc oxide. The commercial product dried by supercritical ethanol without waiting after reaching the supercritical conditions (ZnB3-SCE) had same composition with the run which had dried for 30 minute. Since no difference was observed between the compositions of products dried by supercritical ethanol drying for 30 min. and without waiting under supercritical conditions, no waiting period was applied for the supercritical ethanol drying of other zinc borate samples. Chemical composition of zinc borate (ZnB4-SCE) dried at 150 °C is very similar to the composition of zinc borate ( $2ZnO \cdot 3B_2O_3 \cdot 3H_2O$ ), that means that no interaction took place. Since the percent value of ZnO is greater and percent value of  $B_2O_3$  is lower than the theoretical values, zinc borate, (ZnB5-SCE), decomposed partially during drying at 200 °C.

The chemical compositions of powder remained in the reactor after the supercritical ethanol drying of zinc borate samples (ZnB6-SCE and ZnB7-SCE) are also given in Table 5.12. From these results, that powder product was mainly consisted of zinc oxide 92 % and  $B_2O_3$  in ratios between 1-3 % by weights. On the other hand, the product dissolved in ethanol was mainly boric acid with 98-99 % by weight. From those results, it was determined that zinc borate of ( $ZnO \cdot B_2O_3 \cdot 2H_2O$ ) was less stable than zinc borate of ( $2ZnO \cdot 3B_2O_3 \cdot 3H_2O$ ) during supercritical ethanol drying.

To determine the surface area of the products obtained at the end of supercritical ethanol drying, nitrogen adsorption isotherms were obtained for those samples, ZnB3-SCE and ZnB7-SCE, as shown in Figure 5.98 and Figure 5.99, respectively.



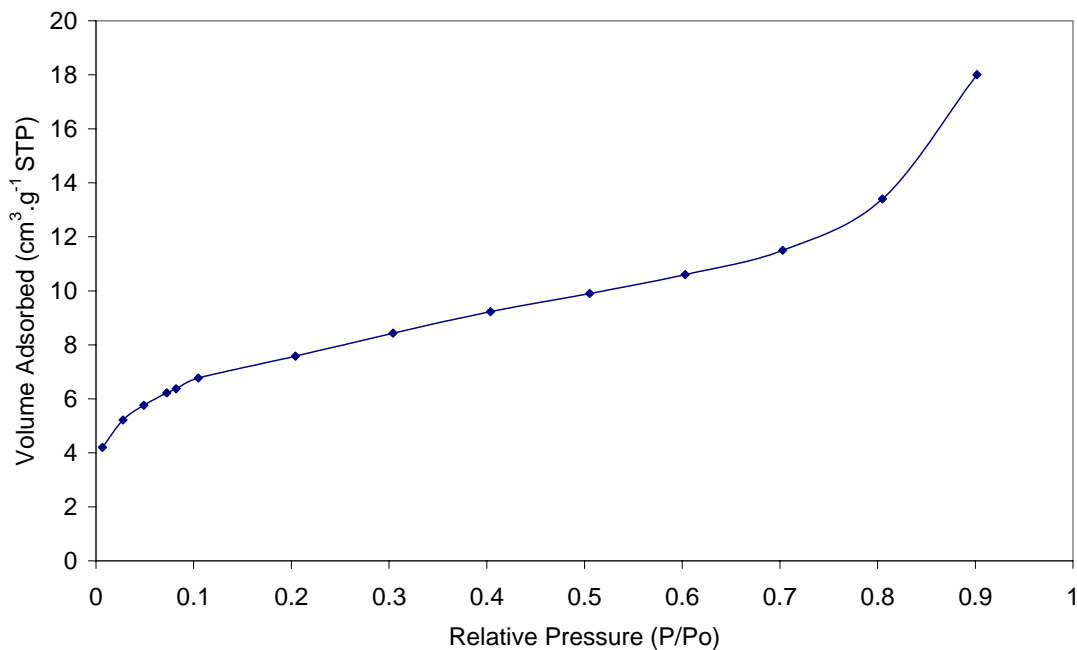


Figure 5.98. Nitrogen adsorption isotherms of zinc borate after supercritical ethanol drying (ZnB3-SCE).

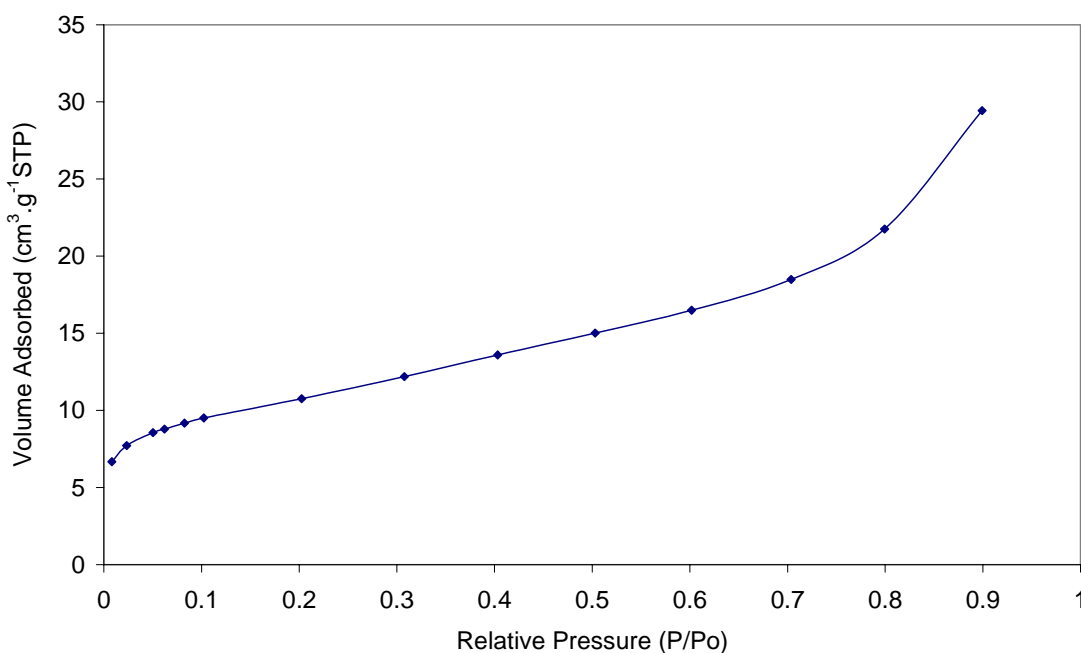


Figure 5.99. Nitrogen adsorption isotherms of zinc borate after supercritical ethanol drying (ZnB7-SCE).

The BET analysis results showed that the specific surface areas of ZnB3-SCE and ZnB7-SCE were  $25.9 \text{ m}^2.\text{g}^{-1}$  and  $37.0 \text{ m}^2.\text{g}^{-1}$ , respectively. Conventionally dried zinc borates surface areas were so low that it could not be measured using nitrogen adsorption in Micromeritics ASAP 2010.

Assuming that all particles are spherical and size distribution is monodisperse, average particle diameter,  $D$  ( $\mu\text{m}$ ), can be estimated using following equation:

$$D = \frac{6}{(S_{sp}\rho_a)} \quad (5.26)$$

where  $S_{sp}$  is the specific surface area per unit mass of the sample ( $\text{m}^2\cdot\text{g}^{-1}$ ) and  $\rho_a$  is the density ( $\text{g}\cdot\text{cm}^{-3}$ ). Average particle size of ZnB3-SCE and ZnB7-SCE were calculated as 51 and 36 nm using BET surface area, and measured densities.

## 5.10. Freeze Drying of Zinc Borate Species

Freeze drying was studied as an alternative technique to the supercritical fluid drying in the drying of zinc borates, which were produced in magnetically stirred glass reactor and mechanical stirred stainless steel reactor. Zinc borate (S-21) was produced using  $1 \text{ mol}\cdot\text{dm}^{-3}$  borax and  $1 \text{ mol}\cdot\text{dm}^{-3}$  zinc nitrate at  $70 \text{ }^\circ\text{C}$  and at 550 rpm stirring rate for 4 h of reaction time in glass reactor. Zinc borate (S-22) was produced using  $1 \text{ mol}\cdot\text{dm}^{-3}$  borax and  $1 \text{ mol}\cdot\text{dm}^{-3}$  zinc nitrate at  $70 \text{ }^\circ\text{C}$  and at 900 rpm stirring rate for 4 h of reaction time in stainless steel reactor. In the freeze drying, frozen water is sublimated from the zinc borate samples at a low temperature,  $-51 \text{ }^\circ\text{C}$ , and under vacuum of 0.020 mbar.

### 5.10.1. Freeze Drying of Zinc Borate Produced in Glass Reactor

FTIR spectrum of freeze dried zinc borate is shown in Figure 5.100. A broad band between  $2800$  and  $3600 \text{ cm}^{-1}$  indicates the presence of hydroxyl groups attached to the main structure. The presence of bands at  $1386 \text{ cm}^{-1}$ , which is due to asymmetric stretching of  $\text{BO}_3$  coordination,  $1030 \text{ cm}^{-1}$  that is caused by asymmetric stretching of  $\text{BO}_4$  coordination and  $700 \text{ cm}^{-1}$  that is because of out of plane bending of  $\text{BO}_3$  on Figure

5.100 show that formed product includes both  $\text{BO}_3$  and  $\text{BO}_4$  units. Besides them, the band at  $1650\text{ cm}^{-1}$  corresponding to the H-O-H bending mode indicates there is water of crystallization in the structure. FTIR spectrum of zinc borate (S-21) obtained by freeze drying is different than the one (S-15) obtained by conventional drying at  $110\text{ }^\circ\text{C}$  at the same reaction time. The only difference, mixing rate, can be the factor that affected the particle morphology of the product. Actually, zinc borate produced at 550 rpm stirring rate for 4 h of reaction time did not begin to crystallize, so particle size and morphology is lower than that of zinc borate produced at 900 rpm stirring rate with a four-bladed impeller for 4 h of reaction time. Another approach for clarifying the phenomenon was considered as the difference in drying techniques. Zinc borate produced using conventional drying at  $110\text{ }^\circ\text{C}$  might have continued a solid state reaction to form new crystal structure while free water was being removed from the product.



Figure 5.100. FTIR spectrum of freeze dried zinc borate produced from borax and zinc nitrate (S-21).

Figure 5.101 displays the XRD pattern of the zinc borate that was dried by freeze drying. A broad peak at  $2\theta$  value of  $20^\circ$  and  $40^\circ$  indicates that zinc borate has mainly an amorphous structure.

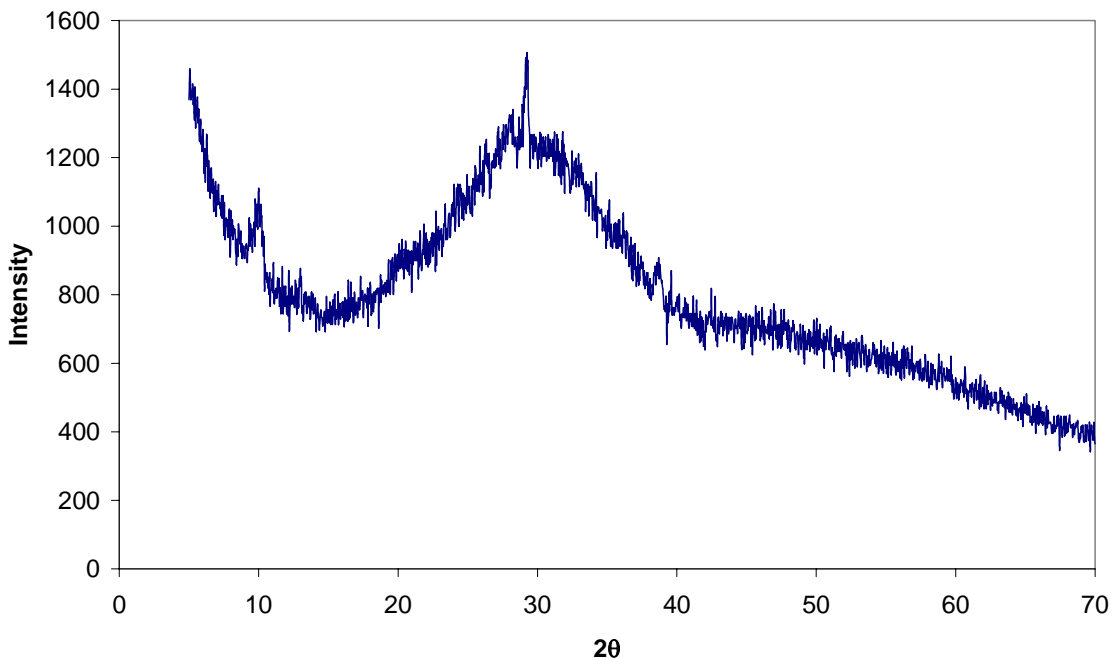


Figure 5.101. XRD pattern of freeze dried zinc borate produced from borax and zinc nitrate (S-21).

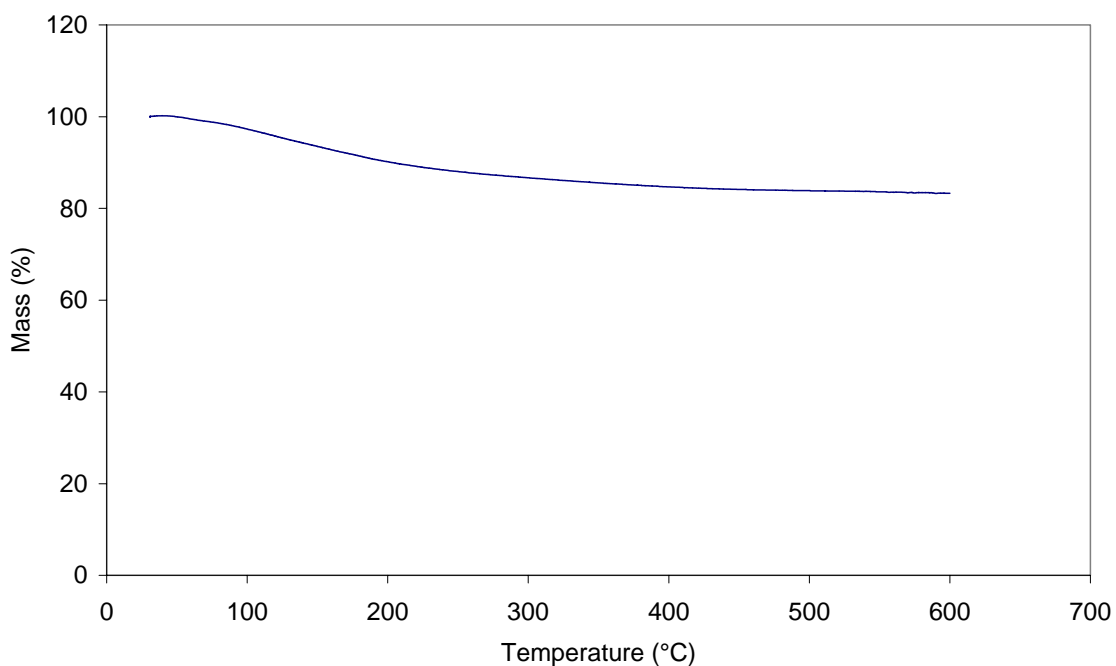


Figure 5.102. TG thermogram of freeze dried zinc borate produced from borax and zinc nitrate (S-21).

Thermal behavior of freeze dried zinc borate is given in Figure 5.102. From that TG curve, it was easily seen that sample started to lose mass before 100 °C which indicated that sample had initially interstitial water inside the structure. The total mass

loss was determined as about 17 % during heating up to 600 °C which was close to the H<sub>2</sub>O content (19.2 %) obtained from analytical titration as shown in Table 5.13.

Table 5.13. ZnO, B<sub>2</sub>O<sub>3</sub>, and H<sub>2</sub>O contents, dehydration onset temperature and particle morphology of freeze dried zinc borates

Sample	ZnO, (%)	B <sub>2</sub> O <sub>3</sub> , (%)	B <sub>2</sub> O <sub>3</sub> /ZnO Molar Ratio	H <sub>2</sub> O, (%)		Dehydration Onset Temperature (°C)	Particle Morphology
				From Chemical Analysis*	From TGA		
S-21	43.5	37.3	1.0	19.2	17.0	50	Nanosized discs
S-22	38.8	41.5	1.2	19.7	18.0	190	Nanosized plates

Figure 5.103. shows the SEM microphotographs of freeze dried zinc borate samples at different magnification. In both photographs particles are around 100 nm in size and there is a few agglomerate of them. The number-weighted nicomp distribution of freeze dried zinc borate is given in Figure 5.104. There is bimodal distribution showing both size around 100 nm individual particles and agglomeration of them at around 500 nm. Nanoparticles attract each other owing to the attractive forces between them, such as Van der Waals.

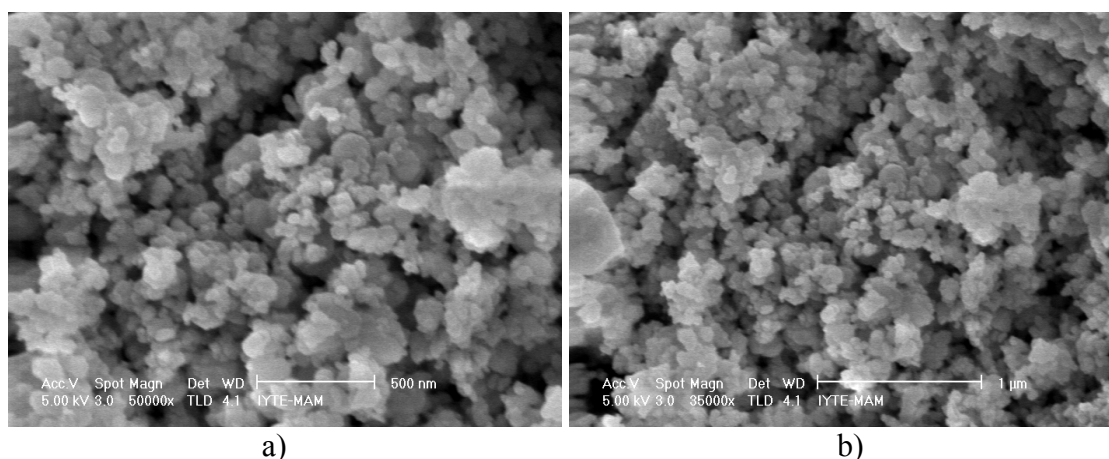


Figure 5.103. SEM microphotographs of freeze dried zinc borate produced from borax and zinc nitrate (S-21) a) 50000x, and b) 35000x.

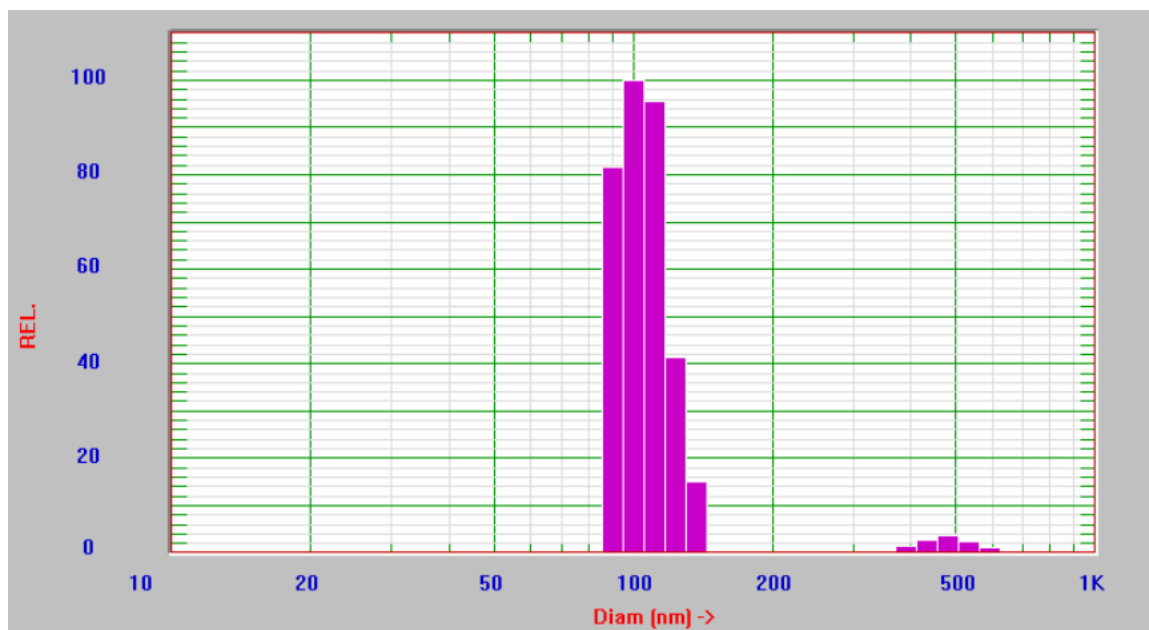


Figure 5.104. Number-weighted nicomp distribution of freeze dried zinc borate particles (S-21), (PSS Nicomp 380).

### 5.10.2. Freeze Drying of Zinc Borate Produced in Stainless Steel Reactor

Zinc borate, which was produced from borax and zinc nitrate in stainless steel reactor using 900 rpm stirring rate, was dried by freeze drying to observe the drying effects. Figure 5.105 shows the FTIR spectrum of freeze dried zinc borate produced from borax and zinc nitrate. The characteristic peaks defined previously in Figure 5.5.b. were observed in the FTIR spectrum of freeze dried sample. That zinc borate type of  $\text{ZnO} \cdot \text{B}_2\text{O}_3 \cdot 2\text{H}_2\text{O}$  synthesized was determined from those characteristic peaks.

Figure 5.106. represents TGA plots of the zinc borate produced by freeze drying. The total mass loss occurred as 18.0 % when the sample was heated from ambient temperature to 600 °C. Zinc borate sample started to lose mass at around 190 °C and no further mass loss was observed between 400 °C and 600 °C. The mass loss of 18.0 % occurred due to the condensation of hydroxyl groups in that temperature range corresponds to water content of  $\text{ZnO} \cdot \text{B}_2\text{O}_3 \cdot 2\text{H}_2\text{O}$  and can be compared to the calculated water content value of 19.25 %.  $\text{B}_2\text{O}_3/\text{ZnO}$  molar ratio for zinc borate (S-22) was calculated as 1.2 from analytical titration results as given in Table 5.13. This result supported the zinc borate structure of  $\text{ZnO} \cdot \text{B}_2\text{O}_3 \cdot 2\text{H}_2\text{O}$ .

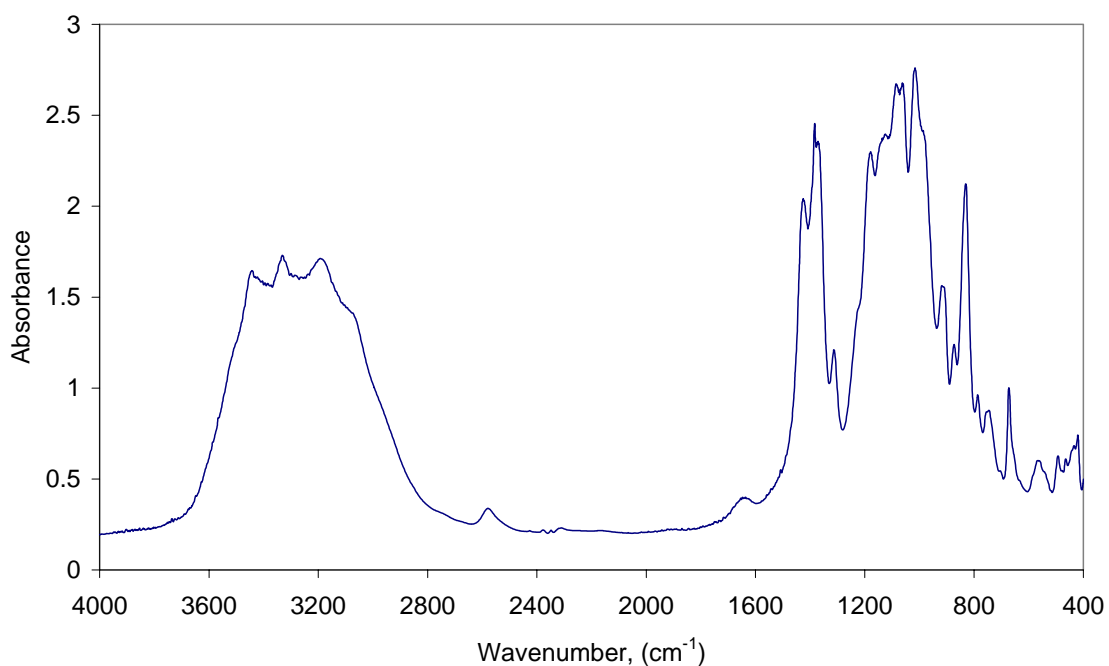


Figure 5.105. FTIR spectrum of freeze dried zinc borate produced from borax and zinc nitrate (S-22).

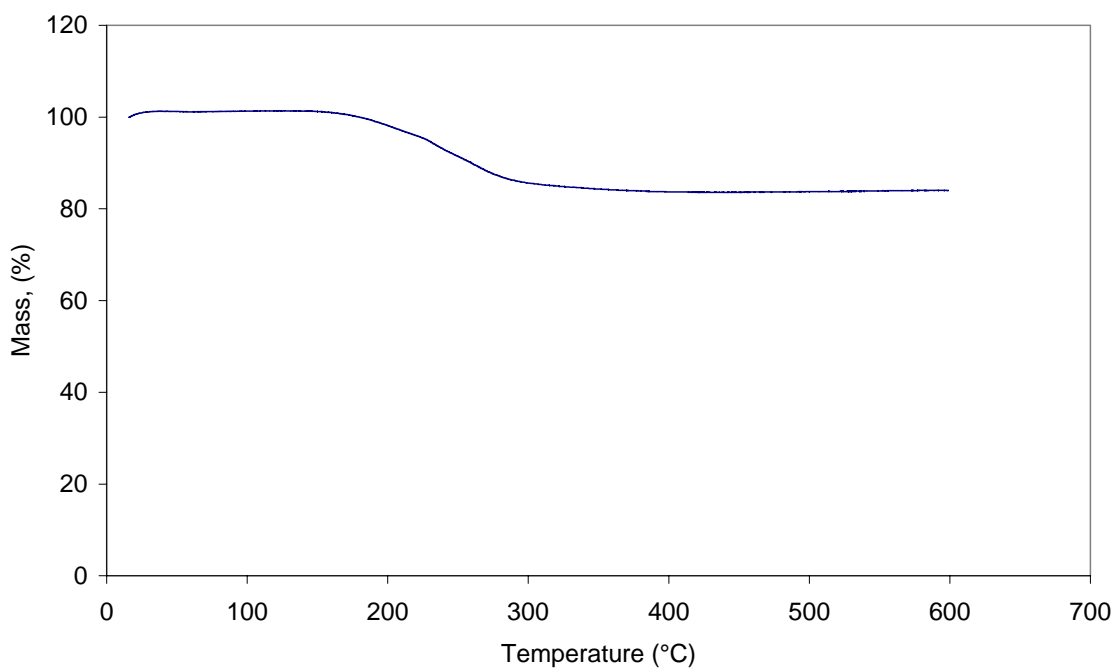


Figure 5.106. TGA thermogram of freeze dried zinc borate produced from borax and zinc nitrate (S-22).

SEM images of freeze dried zinc borate at different magnifications are shown in Figure 5.107. Particles have a plate-like morphology and they are agglomerated due to attractive forces between them. Since the water is frozen in the bulk of product, particles

are enforced to orient in certain place (layer by layer). After the removal of water from solid to gas phase by sublimation, particles are obtained in an agglomerated form.

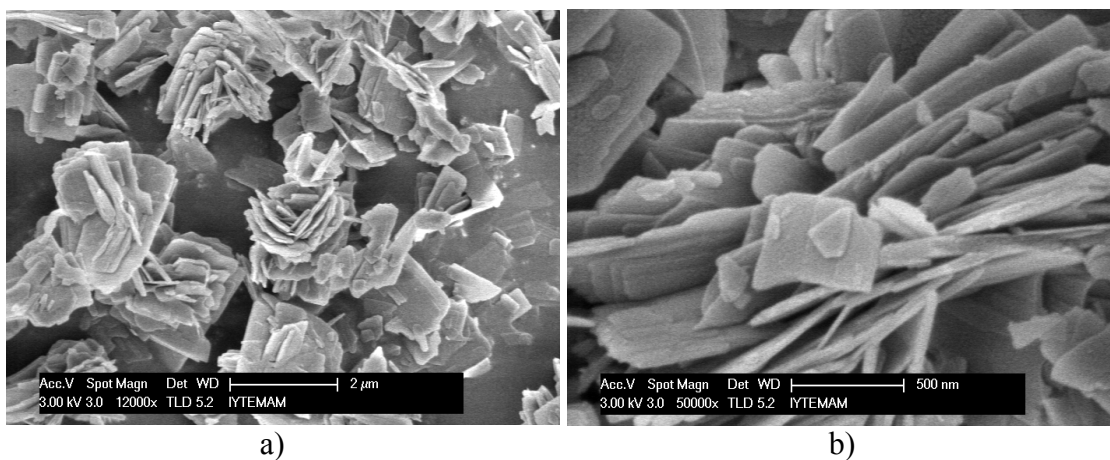


Figure 5.107. SEM microphotograph of freeze dried zinc borate produced from borax and zinc nitrate (S-22) a) 12000x, and b) 50000x.

Finally, it can be concluded that freeze drying makes a significant effect if the particle size of zinc borate sample is smaller enough. Nanosized products can be obtained as long as particles agglomeration is inhibited.

### 5.11. Nucleation, Growth and Phase Transformation in Zinc Borate Crystallization

Zinc borate production either using borax decahydrate-zinc nitrate hexahydrate or using boric acid-zinc oxide was carried out in aqueous phase. Boron content of mother liquids was determined based on boric acid equivalents. Boron and zinc contents in mother liquid indicate the progress of reaction with time. At the beginning of reaction, small zinc borate clusters are formed and their concentration increases until a critical supersaturation is reached. As soon as reaching critical supersaturation concentration ( $C_{min}^*$ ), rapid nucleation of those clusters takes place. Below this value, no further nucleation occurs. It was pointed that nuclei were unstable in the reaction mixture and had the highest chemical potential of the species present (Ahrenstorf et al., 2008). Then, growth on the nuclei formed occurs via consuming the molecular precursors produced by chemical reaction. The growth proceeds until reaction stops due



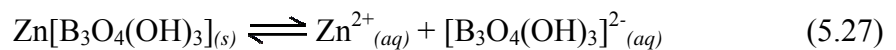
to equilibrium concentration ( $C_s$ ). Desired particle size of zinc borate can be obtained by controlling both of the aforementioned steps; nucleation and growth.

In order to evaluate the crystallization of zinc borates from the reactions, where borax and boric acid were used as boron sources, pH, boric acid concentration, and zinc content in mother liquids were measured. Results are given in Table 5.14.

In the zinc borate production from boric acid and zinc oxide, boric acid dissolved in aqueous phase to which, zinc oxide in solid form was added. Because the initial pH of the solution before adding ZnO was measured as 3.5 and the final pH was measured as 5.0 at the end of reaction, reaction was carried out in acidic medium and in the excess of boric acid to consume all zinc oxide. Based on zinc borate solubility data, 0.1 g/100 ml H<sub>2</sub>O, given by Gürhan et al. (2009), the solubility product was calculated as  $7.8 \times 10^{-6}$  using the dissociation of zinc borate in water as given in Equation 5.27.

Table 5.14. Analyses of mother liquids in zinc borate production from borax-zinc nitrate and boric acid-zinc oxide pairs

Parameter		Boric acid-zinc oxide	Borax-zinc nitrate
pH	initial	3.5	9.5
	final	5.0	5.1
B(OH) <sub>3</sub> (mol.dm <sup>-3</sup> )		0.5	0.28
Zn <sup>2+</sup> (mol.dm <sup>-3</sup> )		$1.4 \times 10^{-3}$	$1.5 \times 10^{-2}$
Na <sup>+</sup> (mol.dm <sup>-3</sup> )		-	1.0
(NO <sub>3</sub> ) <sup>-</sup> (mol.dm <sup>-3</sup> )		-	1.0



Zn<sup>2+</sup> concentration of mother liquid was determined using as  $1.4 \times 10^{-3}$  mol.dm<sup>-3</sup>, which was below the concentration of zinc cations,  $2.8 \times 10^{-3}$  mol.dm<sup>-3</sup>, in solutions in equilibrium with zinc borate. Solubility product of zinc borate is given as follow:

$$K_{sp} = [\text{Zn}^{2+}][(\text{B}_3\text{O}_4(\text{OH})_3)^{2-}] \quad (5.28)$$

The reaction between borax decahydrate and zinc nitrate hexahydrate was carried out by adding 1 mol.dm<sup>-3</sup> aqueous solution of zinc nitrate into 1 mol.dm<sup>-3</sup> borax solution at 70 °C. Borax solution had pH of 9.5 at the beginning of reaction and pH of mother liquid was measured as 5.1 at the end of reaction. Since concentrated reactants

were used in zinc borate synthesis, nucleation and crystal growth of zinc borate occurred simultaneously and rapidly. As soon as zinc nitrate solution was added drop wise into borax solution, precipitate was formed under these conditions. Measured  $Zn^{2+}$  concentration in mother liquid was found to be  $1.5 \times 10^{-2} \text{ mol.dm}^{-3}$  which was above the concentration of zinc cations,  $2.8 \times 10^{-3} \text{ mol.dm}^{-3}$ , in solutions in equilibrium with zinc borate. This could be explained by the presence of nano zinc borate particles passed through membrane filter during filtration.

The growth medium in both systems contains a high concentration of boric acid ( $0.5 \text{ mol.dm}^{-3}$  and  $0.28 \text{ mol.dm}^{-3}$ ). Borax-zinc nitrate system includes also other dissolved ions, such as  $Na^+$  and  $NO_3^-$  ions. The presence of those ions in equilibrium with crystals formed in the medium affects crystallization process. The crystals dissolve, reform, and transform to the different zinc borate species during long reaction periods. Crystal composition changes as shown by FTIR spectra in Figures 5.48 and 5.49. Particle size distribution of zinc borate crystals also changes during this period as representatively shown in Figures 5.57 and 5.59. Larger crystals were formed at the expense of smaller ones. On the other hand, the number of crystals in nanosize increases with reaction time indicating new nuclei formation in the medium.

## CHAPTER 6

### CONCLUSIONS

Zinc borates have gained a remarkable interest not only in scientific area but also in various branches of industry. Especially the developments in nanoparticle synthesis techniques enabled production of novel borate compounds and extended the application areas of zinc borates. The following conclusions are made based on this research which was conducted in two main subjects: Zinc borate production and supercritical fluid drying of those zinc borate species. The production of zinc borate from “boric acid-zinc oxide” and “borax decahydrate-zinc nitrate hexahydrate” pairs was studied altering various variables, such as raw materials concentration, temperature, reaction time, sonication, raw material particle size, and modifying agent in the reaction. Then, those zinc borate species were dried using supercritical carbon dioxide and ethanol drying techniques and freeze drying method to see the effects of those drying methods on particle morphology and size of product.

In the production of zinc borate using zinc oxide and boric acid, three different zinc borate species ( $2\text{ZnO}\cdot 3\text{B}_2\text{O}_3\cdot 3\text{H}_2\text{O}$ ,  $2\text{ZnO}\cdot 3\text{B}_2\text{O}_3\cdot 7\text{H}_2\text{O}$ , and  $\text{ZnO}\cdot \text{B}_2\text{O}_3\cdot 2\text{H}_2\text{O}$ ) were synthesized under different reaction conditions. Dissolution of zinc oxide in acidic reaction medium was proposed and formed zinc cations reacted with borate anions to produce zinc borate. Zinc borate type of  $2\text{ZnO}\cdot 3\text{B}_2\text{O}_3\cdot 3\text{H}_2\text{O}$  can be produced using one step process carried out at 90 °C instead of using conventional two step process performed at 60 °C and 90 °C when boric acid concentration is  $4.7 \text{ mol}\cdot\text{dm}^{-3}$  and the  $\text{B}_2\text{O}_3/\text{ZnO}$  molar ratio is 2.0. A mixture of zinc borates,  $2\text{ZnO}\cdot 3\text{B}_2\text{O}_3\cdot 7\text{H}_2\text{O}$ , and  $\text{ZnO}\cdot \text{B}_2\text{O}_3\cdot 2\text{H}_2\text{O}$ , was produced at reaction temperature of 70 °C using  $3.0 \text{ mol}\cdot\text{dm}^{-3}$  boric acid with  $\text{B}_2\text{O}_3/\text{ZnO}$  molar ratio of 2.0 for 5.0 h. At lower boric acid concentrations, such as 3.0 and 4.0  $\text{mol}\cdot\text{dm}^{-3}$  keeping the  $\text{B}_2\text{O}_3/\text{ZnO}$  molar ratio as 2.0 at 90 °C for 5 h of reaction time, zinc borate type of  $\text{ZnO}\cdot \text{B}_2\text{O}_3\cdot 2\text{H}_2\text{O}$  was formed. Generally, it was concluded that zinc borate,  $2\text{ZnO}\cdot 3\text{B}_2\text{O}_3\cdot 7\text{H}_2\text{O}$ , could be synthesized at lower boric acid concentration and at low temperatures, such as 60, 70 °C. Increasing

the reaction temperature caused zinc borate of  $2\text{ZnO}\cdot 3\text{B}_2\text{O}_3\cdot 7\text{H}_2\text{O}$  to lose water and turn into new structure,  $\text{ZnO}\cdot \text{B}_2\text{O}_3\cdot 2\text{H}_2\text{O}$ . XRD pattern of zinc borate,  $\text{ZnO}\cdot \text{B}_2\text{O}_3\cdot 2\text{H}_2\text{O}$ , was introduced by defining major peaks and d-spacing for the first time in literature according to the best of our knowledge. Water content determined from TGA analysis confirmed the theoretical water content value for the zinc borate of  $\text{ZnO}\cdot \text{B}_2\text{O}_3\cdot 2\text{H}_2\text{O}$ . The average particle size of zinc borate ( $2\text{ZnO}\cdot 3\text{B}_2\text{O}_3\cdot 3\text{H}_2\text{O}$ ) was between 2-4  $\mu\text{m}$ . Additionally, it was found that the use of oleic acid as a modifying agent, ultrasonic treatment and nanosized zinc oxide in the reaction did not make any difference in controlling the particle size of the product. The effect of reaction time was studied in the reaction of borax decahydrate and zinc nitrate hexahydrate to examine the formation of zinc borate species, their morphology and size. Nanosized zinc borate clusters were obtained for 1-3 h reaction period. Particle size of zinc borate produced from borax and zinc nitrate increased with increasing reaction time. Three hours of reaction time was a critical value after which crystal growth began and larger crystals were formed. Zinc borate of  $2\text{ZnO}\cdot 3\text{B}_2\text{O}_3\cdot 7\text{H}_2\text{O}$  was synthesized first in the reaction at the end 3 h of reaction time. With elapsing reaction time up to 6 h,  $2\text{ZnO}\cdot 3\text{B}_2\text{O}_3\cdot 7\text{H}_2\text{O}$  was crystallized and formed larger crystals. It was observed that a new type of zinc borate ( $\text{ZnO}\cdot \text{B}_2\text{O}_3\cdot 2\text{H}_2\text{O}$ ) was formed at the end of 16 h of reaction time.

Four-bladed turbine type impeller utilized in the reactor increased reaction rate, even for 4 and 5 h of reaction time produced zinc borate of  $\text{ZnO}\cdot \text{B}_2\text{O}_3\cdot 2\text{H}_2\text{O}$  which could not be obtained at the end of 6 h of reaction time in the magnetically stirred reactor. Zinc borate obtained from borax and zinc nitrate at the end of 16 h reaction time and zinc borate that was synthesized using  $3.0 \text{ mol}\cdot \text{dm}^{-3}$  and  $4.0 \text{ mol}\cdot \text{dm}^{-3}$  boric acid for 5 h reaction time were same type according to the IR and XRD analyses.

The supercritical  $\text{CO}_2$  drying of zinc borate species,  $2\text{ZnO}\cdot 3\text{B}_2\text{O}_3\cdot 3\text{H}_2\text{O}$  and  $2\text{ZnO}\cdot 3\text{B}_2\text{O}_3\cdot 7\text{H}_2\text{O}$ , was studied under 10 MPa and 40  $^\circ\text{C}$ . It was expected that supercritical  $\text{CO}_2$  would extract methanol without inducing agglomeration, but on the contrary  $\text{CO}_2$  reacted with zinc borate of  $2\text{ZnO}\cdot 3\text{B}_2\text{O}_3\cdot 7\text{H}_2\text{O}$  and formed zinc carbonate. However, it did not interact with zinc borate of  $2\text{ZnO}\cdot 3\text{B}_2\text{O}_3\cdot 3\text{H}_2\text{O}$ . Furthermore, formation of carbonic acid because of dissolution of  $\text{CO}_2$  in water that was released from zinc borate structure induced the chemical reaction. Interaction with  $\text{CO}_2$  at high supercritical pressures is a possible side effect of supercritical  $\text{CO}_2$  drying. The size of spherical particles on zinc borate surface varies between 200 nm and 500 nm.

The supercritical ethanol drying of zinc borate species was studied to obtain nanosized product at 6.5 MPa and 250 °C. While zinc borate of  $2\text{ZnO}\cdot 3\text{B}_2\text{O}_3\cdot 3\text{H}_2\text{O}$  decomposed partially, zinc borate of  $\text{ZnO}\cdot \text{B}_2\text{O}_3\cdot 2\text{H}_2\text{O}$  decomposed completely during the supercritical ethanol drying. Instability of zinc borates in supercritical ethanol drying conditions was also an undesired side effect. Zinc borate,  $2\text{ZnO}\cdot 3\text{B}_2\text{O}_3\cdot 3\text{H}_2\text{O}$ , started to decompose during the drying with ethanol even at 200 °C as determined from chemical analysis and XRD results. As inferred from characterization of powder product and product dissolved in ethanol phase, zinc borate of  $2\text{ZnO}\cdot 3\text{B}_2\text{O}_3\cdot 3\text{H}_2\text{O}$  decomposed to produce zinc oxide and anhydrous zinc borate in nanosized powder form and boric acid that dissolved in ethanol and transferred by it. The powder obtained in supercritical ethanol drying of  $2\text{ZnO}\cdot 3\text{B}_2\text{O}_3\cdot 3\text{H}_2\text{O}$  was composed of about 90 % zinc oxide and 10 %  $\text{B}_2\text{O}_3$ . However, the powder obtained in supercritical ethanol drying of  $\text{ZnO}\cdot \text{B}_2\text{O}_3\cdot 2\text{H}_2\text{O}$  was composed of about 92 % zinc oxide and only 1-3 %  $\text{B}_2\text{O}_3$ . Extraction of boron oxide by supercritical ethanol can be used in the production of boric acid from boron minerals.

It was concluded that both zinc borates,  $2\text{ZnO}\cdot 3\text{B}_2\text{O}_3\cdot 7\text{H}_2\text{O}$  and  $\text{ZnO}\cdot \text{B}_2\text{O}_3\cdot 2\text{H}_2\text{O}$ , are less stable than the other type of zinc borate,  $2\text{ZnO}\cdot 3\text{B}_2\text{O}_3\cdot 3\text{H}_2\text{O}$  in both supercritical  $\text{CO}_2$  and supercritical ethanol drying.

It would be possible to obtain nano particles of zinc borates in freeze drying if initial particle size of wet zinc borates was nanosized.

Further studies should be made to explain the mechanism of interaction between carbon dioxide and zinc borate ( $2\text{ZnO}\cdot 3\text{B}_2\text{O}_3\cdot 7\text{H}_2\text{O}$ ) and to clarify the decomposition of zinc borate ( $2\text{ZnO}\cdot 3\text{B}_2\text{O}_3\cdot 3\text{H}_2\text{O}$ ), which is known as thermally stable at 290 °C, in supercritical ethanol drying. In particular, extraction of boric acid from boron minerals can be studied using supercritical and/or subcritical ethanol.

## REFERENCES

- Adams R. M. *Boron, Metallo Boron Compounds and Boranes*. Wiley: New York, **1964**.
- Ahrenstorf, K.; Heller, H.; Kornowski, A.; Broekaert, J. A. C.; Weller H. Nucleation and Growth Mechanism of Ni<sub>x</sub>Pt<sub>1-x</sub> Nanoparticles. *Adv. Funct. Mater.* **2008**, 18, 3850-3856.
- Akgerman, A.; Erkey, C.; Orejuela, M. Limiting Diffusion Coefficients of Heavy Molecular Weight Organic Contaminants in Supercritical Carbon Dioxide. *Ind. Eng. Chem. Res.* **1996**, 35, 911-917.
- Arai, Y.; Sako, T.; Takebayashi, Y. *Supercritical Fluids Molecular Interactions, Physical Properties, and New Applications*. Springer Series in Material Processing, Berlin, **2002**.
- Attina, M.; Cacace, F.; Occhiucci, G.; Riccit, A. Gaseous Borate and Polyborate Anions. *Inorg. Chem.* **1992**, 31, 3114-3117.
- Biswick. T.; Jones. W.; Pacula. A.; Serwicka. E.; Podobinski. J. The role of anhydrous zinc nitrate in the thermal decomposition of the zinc hydroxy nitrates Zn<sub>5</sub>(OH)<sub>8</sub>(NO<sub>3</sub>)<sub>2</sub>·2H<sub>2</sub>O and ZnOHNO<sub>3</sub>·H<sub>2</sub>O *J. Solid State Chem.* **2007**, 180, 1171-1179.
- Bouchard A., Jovanovic N., Jiskoot W., Mendes E., Witkamp G.J., Crommelin D.J.A., Hofland G.W., Lysozyme particle formation during supercritical fluid drying: Particle morphology and molecular integrity, *J. Supercrit. Fluids.* **2007**, 40, 293-307.
- Brinker C. J.; Scherer G. W. *Sol-Gel Science: The Physics and Chemistry of Sol-Gel Processing*. Academic Press: San Diego, 1990.
- Briggs, M. Boron Oxides, Boric Acid, and Borates. *Kirk-Othmer Encyclopedia of Chemical Technology* [Online]; Wiley & Sons, Posted July 13, 2001. <http://mrw.interscience.wiley.com/emrw/9780471238966/kirk/article/borosmit.a01/current/pdf> (accessed April 1, 2009).
- Cansell, F.; Aymonier, C.; Loppinet-Serani, A. Review on Materials Science and Supercritical Fluids. *Curr. Opin. Solid State Mater. Sci.* **2003**, 7, 331-340.

- Cao, Y.; Hu, J.; Hong, Z.; Deng, J.; Fan, K. Characterization of high surface area zirconia aerogel synthesized from combined alcohothermal and supercritical fluid drying techniques. *Catal. Lett.* **2002**, 81, 107-112.
- Chang, R. *Chemistry*. McGraw-Hill: New York, **1994**; p 323.
- Chattopadhyay, P.; Gupta, R. B. Production of Antibiotic Nanoparticles Using Supercritical CO<sub>2</sub> as Antisolvent with Enhanced Mass Transfer. *Ind. Eng. Chem. Res.* **2001**, 40, 3530-3539.
- Colthup, N. B.; Daly, L. H.; Wiberley, S. E. Introduction to Infrared and Raman Spectroscopy; Academic Press:San Diego, CA, **1990**; p 88.
- Dillon, H. E. and Penoncello, S. G., A Fundamental Equation for Calculation of the Thermodynamic Properties of Ethanol, *Int. J. Thermophys.* **2004**, 25(2), 321-335.
- Dong, J. X.; Hu, Z. S. A study of the anti-wear and friction-reducing properties of the lubricant additive, nanometer zinc borate. *Tribol. Int.* **1998**, 31, 219-223.
- Eltepe, H. E.; Balköse, D.; Ülkü, S. Effect of Temperature and Time on Zinc Borate Species Formed from Zinc Oxide and Boric Acid in Aqueous Medium. *Ind. Eng. Chem. Res.* **2007**, 46(8), 2367-2371.
- Erdemir, A.; Halter, M.; and Fenske, G. R. Preparation of ultralow-friction surface films on vanadium diboride. *Wear.* **1997**, 205, 236-239.
- Erdemir, A. Lubrication with Boric Acid Additives. U.S. Patent 6025306, February 15, 2000.
- Eti Maden, URL: <http://www.etimaden.gov.tr/>, (accessed on March 23, **2009**).
- Gallagher, P. M.; Coffey, M. P.; Krukonis, V. J.; Klasutis, N. Gas Antisolvent Recrystallization: New Process To Recrystallize Compounds Insoluble in Supercritical Fluids. In *Supercritical Fluid Science and Technology*; Johnston, K. P., Penninger, J. M. L. Eds., ACS Symposium Series, 406, ACS Publishing:Washington, DC, **1989**.
- Geffen, N.; Semiat, R.; Eisen, M. S.; Balazs, Y.; Katz, I.; Dosoretz, C. G. Boron removal from water by complexation to polyol compounds. *J. Membr. Sci.* **2006**, 286, 45-51.
- Genovese, A.; Shanks, R. A. Structural and thermal interpretation of the synergy and interactions between the fire retardants magnesium hydroxide and zinc borate. *Polym. Degrad. Stab.* **2007**, 92, 2-13

- Giudice, C. A.; Benitez, J.C. Zinc borates as flame-retardant pigments in chlorine-containing coatings. *Prog. Org. Coat.* **2001**, 42, 82–88.
- Gürhan, D.; Çakal, G. Ö.; Eroğlu, I.; Özkar, S. Improved synthesis of fine zinc borate particles using seed crystals. *J. Cryst. Growth.* **2009**, 311, 1545–1552.
- Hu, Z. S.; Dong, J. X.; Chen, G. X. Replacing Solvent Drying Technique for Nanometer Particle Preparation. *J. Colloid Interface Sci.* **1998**, 208, 367-372.
- Hu, Z. S.; Dong, J. X.; Chen, G. X.; Lou, F. Preparation of nanometer copper borate with supercritical carbon dioxide drying. *Powder Technol.* **1999**, 102, 171-176.
- Hu, Z. S.; Lai, R.; Lou, F.; Wang, L.; G., Chen.; Z. L.; Chen, G. X.; Dong, J. X. Preparation and tribological properties of nanometer magnesium borate as lubricating oil additive. *Wear*, **2002**, 252, 370–374.
- Jiang, L.; Xu, S.; Zhu, J.; Zhang, J.; Zhu, J.; Chen, H., Ultrasonic-Assisted Synthesis of Monodisperse Single-Crystalline Silver Nanoplates and Gold Nanorings. *Inorg. Chem.* **2004**, 43, 5877-5883.
- Jovanovic, N.; Bouchard, A.; Hofland, G. W.; Witkamp, G.; Crommelin, D. J. A.; Jiskoot, W. Distinct effects of Sucrose and trehalose on protein stability during supercritical fluid drying and freeze-drying. *Eur. J. Pharm. Sci.* **2006**, 27, 336-345.
- Jun L., Shuping X., Shiyang G. FT-IR and Raman Spectroscopic Study of Hydrated Borates. *Spectrochimica Acta.* **1995**, 51A (4), 519-532.
- Kanari, N.; Mishra, D.; Gaballah, I.; Dupré, B. Thermal decomposition of zinc carbonate hydroxide. *Thermochim. Acta.* **2004**, 410, 93–100.
- Karpinski, P. H.; Wey J. S. Precipitation Processes. In *Handbook of Industrial Crystallization*; Myerson A. S., Ed.; BH: Boston, 2002; pp 141-160.
- Kar, Y.; Şen, N.; Demirbaş, A. Boron Minerals in Turkey, Their Application Areas and Importance for the Country's Economy. *Minerals And Energy-Raw Materials Report.* **2006**, 20(3-4), 2-10.
- Kistler, S. S. Method of Making Aerogels, U.S. Patent 2,249,767, July 22, 1941.
- Knez, Z.; Weidner, E. Particles formation and particle design using supercritical. *Curr. Opin. Solid State Mater. Sci.* **2003**, 7, 353–361.
- Kocon, L.; Despetis, F.; Phalippou, J. Ultralow density silica aerogels by alcohol supercritical drying, *J. Non-Cryst. Solids.* **1998**, 225, 96–100.



- Levenspiel, O. *Chemical Reactor Engineering*; Wiley: New York, 1972, pp 357-400.
- Lide, D. R. Ed. *CRC Handbook of Chemistry and Physics*; CRC Press. Boca Raton FL, **2004**, pp 8–141.
- Liu Q.; Xiao, Y.; Rong, W.; Yuan, L. Large-Scale Synthesis of Monodisperse  $2\text{ZnO}\cdot 3\text{B}_2\text{O}_3\cdot 3\text{H}_2\text{O}$  Micro/Nano Single Crystals and Their Effect in Polypropylene. *Soft Materials*. **2009**, 7(2), 67-78.
- Luzenac, **2009**, Zinc Borate Applications, [http://www.luzenac.com/plastics\\_zinc\\_borate.htm](http://www.luzenac.com/plastics_zinc_borate.htm) (accessed March 25, 2009).
- Matson, D. W.; Fulton, J. L.; Petersen, R. C.; Smith, R. D. Rapid Expansion of Supercritical Fluid Solutions: Solute Formation of Powders, Thin Films, and Fibers. *Ind. Eng. Chem. Res.* **1987**, 26, 2298-2306.
- Medvedev, E. F.; Komarevskaya, A. S. IR Spectroscopic Study Of The Phase Composition Of Boric Acid As A Component Of Glass Batch. *Glass Ceram.* **2007**, 64(1–2), 42-46.
- Mizushima, Y.; Hori, M. Alumina aerogel catalysts prepared by two supercritical drying methods used in methane combustion. *J. Mater. Res.* **1995**, Vol. 10-6, 1424-1428.
- Mukhopadhyay, M. *Natural Extracts Using Supercritical Carbon Dioxide*. CRC Press: Boca Raton, FL, 2000, pp 84-95.
- Myhren, A. J.; Nelson, E. W. Manufacture of Zinc Borate. U.S. Patent 2,405,366, August 6, 1946.
- Nies, N. P.; Hulbert, R. W. Zinc Borate of Low Hydration and Method for Preparing the Same. U.S. Patent 3,549,316, December 22, 1970.
- O’Neil, A.; Watkins, J. J. Fabrication of Device Nanostructures Using Supercritical Fluids, *MRS Bull.* **2005**, 30, 967-975.
- Pankajavalli, R.; Anthonysamy, S.; Ananthasivan, K.; Vasudeva, Rao P. R. Vapour pressure and standard enthalpy of sublimation of  $\text{H}_3\text{BO}_3$ . *J. of Nucl. Mater.* **2007**, 362, 128–131.
- Perrut, M. Supercritical Fluid Applications: Industrial Developments and Economic Issues, *Ind. Eng. Chem. Res.*, **2000**, 39, 4531-4535.
- Roskill Reports on Metals and Minerals. The Economics of Boron. 11<sup>th</sup> Edition. Roskill Information Service: London, 2006.

- Samyn, F.; Bourbigot, S.; Duquesne, S.; Delobel, R. Effect of zinc borate on the thermal degradation of ammonium polyphosphate. *Thermochim. Acta.* **2007**, 456, 134–144.
- Sawada, H.; Igarashi, H.; Sakao, K. Zinc Borate and Production Method and Use Thereof. U. S. Patent No: 6780913 B2, 2004.
- Schubert, D. M. Zinc Borate. U.S. Patent 5,472,644, December 5, 1995.
- Schubert, D. M.; Alam, F.; Visi, M. Z.; Knobler, C. B. Structural Characterization and Chemistry of Industrially Important Zinc Borate  $Zn[B_3O_4(OH)_3]$ . *Chem. Mater.* **2003**, 15, 866-871.
- Schubert, D. M. Borates in Industrial Use. *Group 13 Chemistry III Industrial Applications* [Online] Roesky, H.W., Atwood, D.A. Eds. Structure & Bonding. Springer: Berlin, 2003, 105, pp 1-40. <http://www.springerlink.com/content/mj26plqvva2b/?p=fc56c8e2f98a4ae4b47b8f1fd0d47c18&pi=0> (accessed July 10, 2007).
- Schubert, D. M. Zinc Borate. U.S. Patent 6,919,036 B2, July 19, 2005.
- Sengers, J. M. H. L. Supercritical Fluids: Their Properties and Applications. In *Supercritical Fluids Fundamentals and Applications*; Kiran, E., Debenedetti, P. G., Peters, C. J., Eds.; Nato Science Series E: Applied Science 366; Kluwer Academic: Dordrecht, 2000, 1-29.
- Shen, K. K.; Kochesfahani, S.; and Jouffret, F. Zinc borates as multifunctional polymer additives, *Polym. Adv. Technol.*, **2008**, 19, 469–474.
- Shete, A. V.; Sawant, S. B.; Pangarkar, V. G. Kinetics of fluid-solid reaction with an insoluble product: zinc borate by the reaction of boric acid and zinc oxide. *J. Chem. Technol. Biotechnol.* **2004**, 79, 526-532.
- Shi, X.; Li, M.; Yang, H.; Chen, S.; Yuan L.; Zhang, K.; Sun J. PEG-300 assisted hydrothermal synthesis of  $4ZnO \cdot B_2O_3 \cdot H_2O$  nanorods. *Mater. Res. Bull.* **2007**, 42, 1649–1656.
- Shi, X.; Yuan, L.; Sun, X.; Chang, C.; Sun, J. Controllable Synthesis of  $4ZnO \cdot B_2O_3 \cdot H_2O$  Nano-/Microstructures with Different Morphologies: Influence of Hydrothermal Reaction Parameters and Formation Mechanism. *J. Phys. Chem. C.* **2008a**, 112, 3558-3567.
- Shi, X.; Xiao, Y.; Li, M.; Yuan, L.; Sun, J. Synthesis of an industrially important zinc borate,  $2ZnO \cdot 3B_2O_3 \cdot 3H_2O$ , by a rheological phase reaction method. *Powder Technol.* **2008b**, 186, 263-266.

- Shi, X.; Xiao, Y.; Yuan, L.; Sun, J. Hydrothermal synthesis and characterizations of 2D and 3D  $4\text{ZnO}\cdot\text{B}_2\text{O}_3\cdot\text{H}_2\text{O}$  Nano-/Microstructures with Different Morphologies *Powder Technol.* **2009**, 189, 462-465.
- Smith, J. M.; Ness, H. C. V.; Abbott, M. M. *Introduction to Chemical Engineering Thermodynamics*, McGraw-Hill: New York, **1996**.
- Subra, P.; Jestin; P. Powders elaboration in supercritical media: comparison with conventional routes. *Powder Technol.* **1999**, 103, 2-9.
- Sunol, S. G.; Sunol, A. K.; Keskin, O.; Guney, O. Supercritical Fluid Aided Preparation of Aerogels and their Characterization. ACS Symposium Series 608: Innovations in Supercritical Fluids Science and Technology, Ch. 17, K. W. Hutchenson and N. R. Foster eds., Washington, DC, 1995. pp. 258-268.
- Tang, Q.; Wang, T. Preparation of silica aerogel from rice hull ash by supercritical carbon dioxide drying. *J. Supercrit. Fluids.* **2005**, 35, 91-94.
- Taylan, N.; Gürbüz, H.; Bulutcu, A. N. Effects of ultrasound on the reaction step of boric acid production process from colemanite. *Ultrason. Sonochem.* **2007**, 14, 633-638.
- Tihminlioğlu, F.; Ülkü S. Use of Clinoptilolite in Ethanol Dehydration. *Sep. Sci. Technol.* **1996**, Vol. 31, 20, 2855-2865.
- Tian, Y.; Guo, Y.; Jiang, M.; Sheng, Y.; Hari, B.; Zhang, G.; Jiang, Y.; Zhou, B.; Zhu, Y.; Wang, Z. Synthesis of hydrophobic zinc borate nanodiscs for lubrication. *Mater. Lett.* **2006**, 60, 2511-2515.
- Tian, Y.; He, Y.; Yu, L.; Deng, Y.; Zheng, Y.; Sun, F.; Liu, Z.; Wang, Z. In situ and one-step synthesis of hydrophobic zinc borate nanoplatelets. *Colloids and Surfaces A: Physicochem. Eng. Aspects.* **2008**, 312, 99-103
- Ting, C.; Jian-Cheng, D.; Long-Shuo, W.; Gang, F. Preparation and characterization of nano-zinc borate by a new method. *J. Mater. Process. Technol.* **2009**, 312, 4076-4079.
- Tsuyumoto, I.; Oshio, T.; Katayama, K. Preparation of highly concentrated aqueous solution of sodium borate. *Inorg. Chem. Commun.* **2007**, 10, 20-22
- Vemavarapu, C.; Mollan, M. J.; Lodaya, M.; Needham, T. E. Design and Process aspects of laboratory scale SCF particle formation systems. *Int. J. Pharm.* **2005**, 292, 1-16.
- Wahab, R.; Ansari, S. G.; Kim, Y. S.; Seo, H. K.; Kim, G. S.; Khang, G.; Shin, H. S. Low temperature solution synthesis and characterization of ZnO nano-flowers. *Mater. Res. Bull.* **2007**, 42, 1640-1648.

- Waclawska, I. Controlled Rate Thermal Decomposition of Borax. *J. Therm. Anal.* **1995**, 43, 261-269.
- Waclawska, I. Controlled Rate Thermal Analysis of Hydrated Borates. *J. Therm. Anal.* **1998**, 53, 519-532.
- Ward, D.; Ko, E. I. Preparing Catalytic Materials by the Sol-Gel Method. *Ind. Eng. Chem. Res.* **1995**, 34, 421-433
- Wahlbrink, T., Küpper, D., Bolten, J., Möller, M., Lemme, M.C., Kurz, H., Supercritical drying for high aspect-ratio HSQ nano-structures, *Microelectron. Eng.* **2007**, 84, 1045–1048.
- Weibel, G. L.; Ober, C. K An overview of supercritical CO<sub>2</sub> applications in microelectronics processing. *Microelectron. Eng.* **2003**, 65, 145–152.
- Wu, W.; Jiang, Q. Preparation of nanocrystalline zinc carbonate and zinc oxide via solid-state reaction at room temperature, *Mater. Lett.* **2006**, 60, 2791-2794.
- Zabaloy, M. S.; Vasquez, V. R.; Macedo, E. A. Viscosity of pure supercritical fluids. *J. of Supercrit. Fluids.* **2005**, 36, 106–117.
- Zheng, Y.; Tian, Y.; Ma H.; Qu, Y.; Wang, Z.; An, D.; Guan, S.; Gao, X. Synthesis and performance study of zinc borate nanowhiskers. *Colloids Surf., A: Physicochem. Eng. Aspects*, **2009**, 339, 178-184.
- Zhihong, L.; Bo, G.; Mancheng, H.; Shuni, L.; Shuping, X. FT-IR and Raman spectroscopic analysis of hydrated cesium borates and their saturated aqueous solutions. *Spectrochim. Acta, Part A.* **2003**, 59, 2741-2745.

## **APPENDICES**

The features of equipments used in the experiments (temperature controller, thermocouple, and pressure gauges) are given in Appendix A. The detailed drawing of reactor system including pipelining and valves, is given in Appendix B.

## APPENDIX A

### TEMPERATURE CONTROLLER AND PRESSURE GAUGE PROPERTIES

#### Temperature Controller Properties:

Model	: Parr 4836
Input Thermocouple Type	: J
Operating Range	: 0-800 °C
Readout Resolution	: 1 °C
Setpoint Resolution	: 1 °C
System Accuracy	: +/- 2 °C
Control Type	: PID controller

#### Pressure Gauge Properties:

Pressure range	: 1-3000 psi
Type	: T316 stainless steel Bourdon tube
System Accuracy	: +/- 1%

# APPENDIX B

## VESSEL AND PIPING LAYOUT

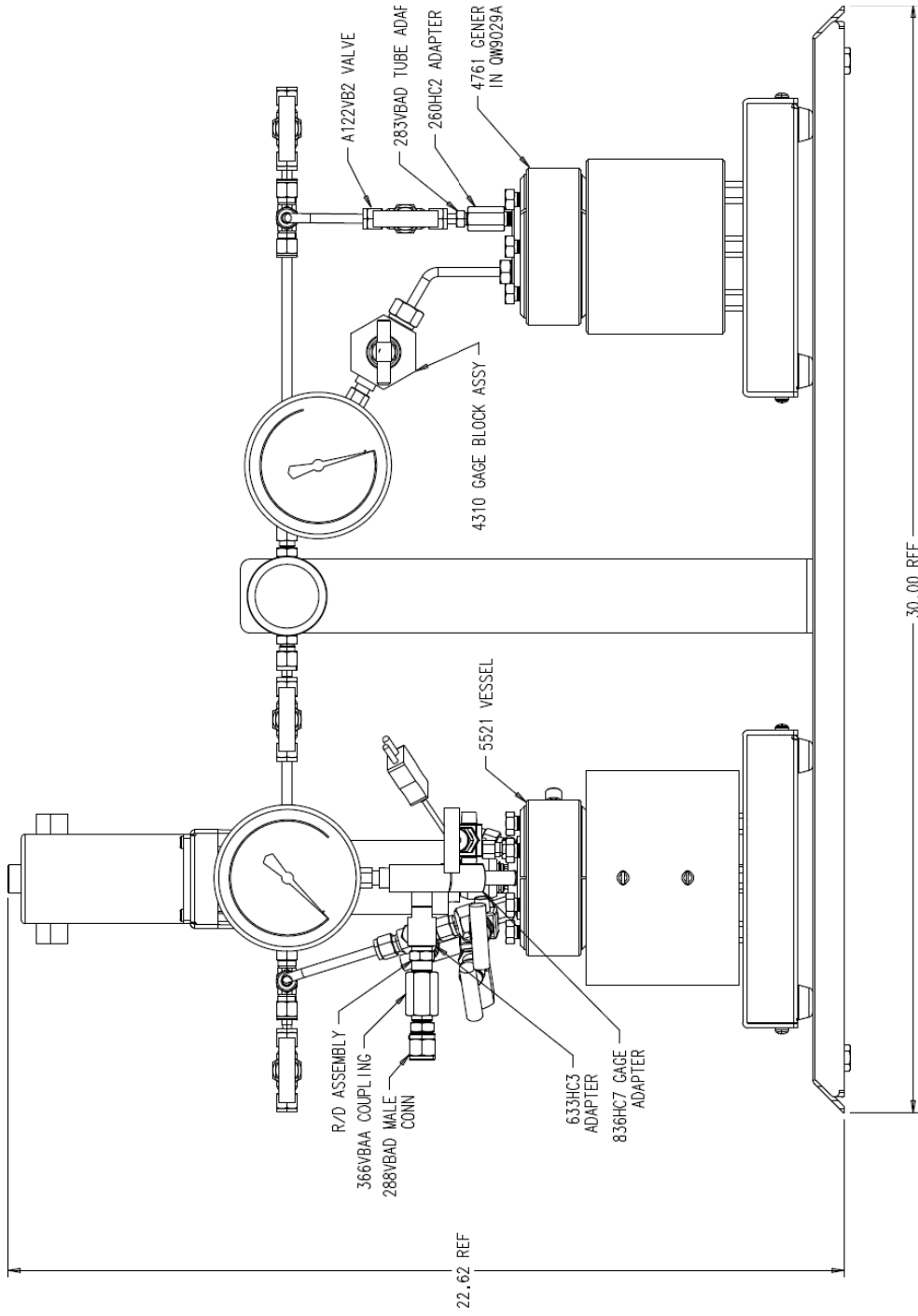


Figure B.1. Front view of reactor drawing (All dimensions are in inches)

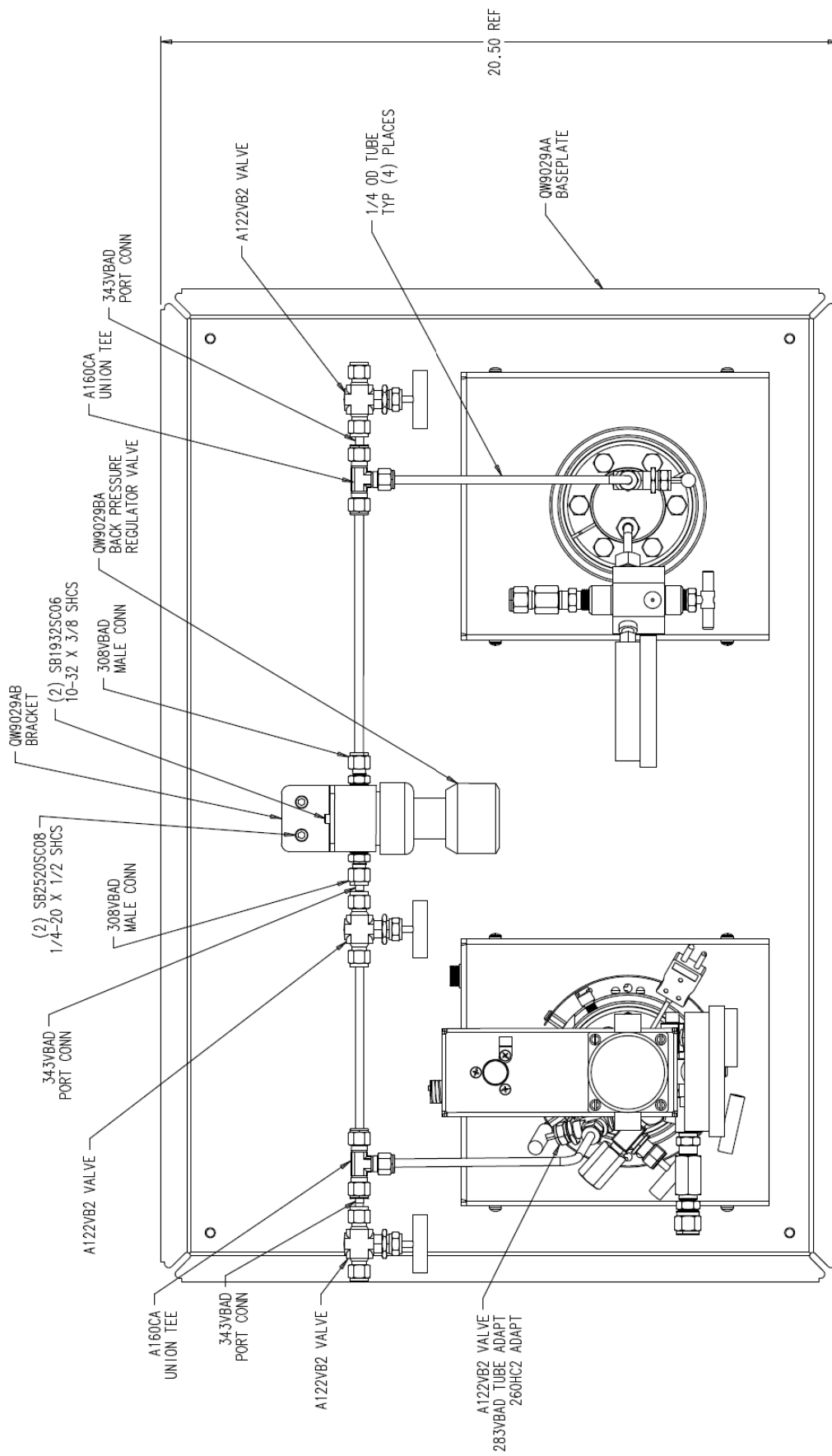


Figure B.2. Top view of reactor drawing (All dimensions are in inches)



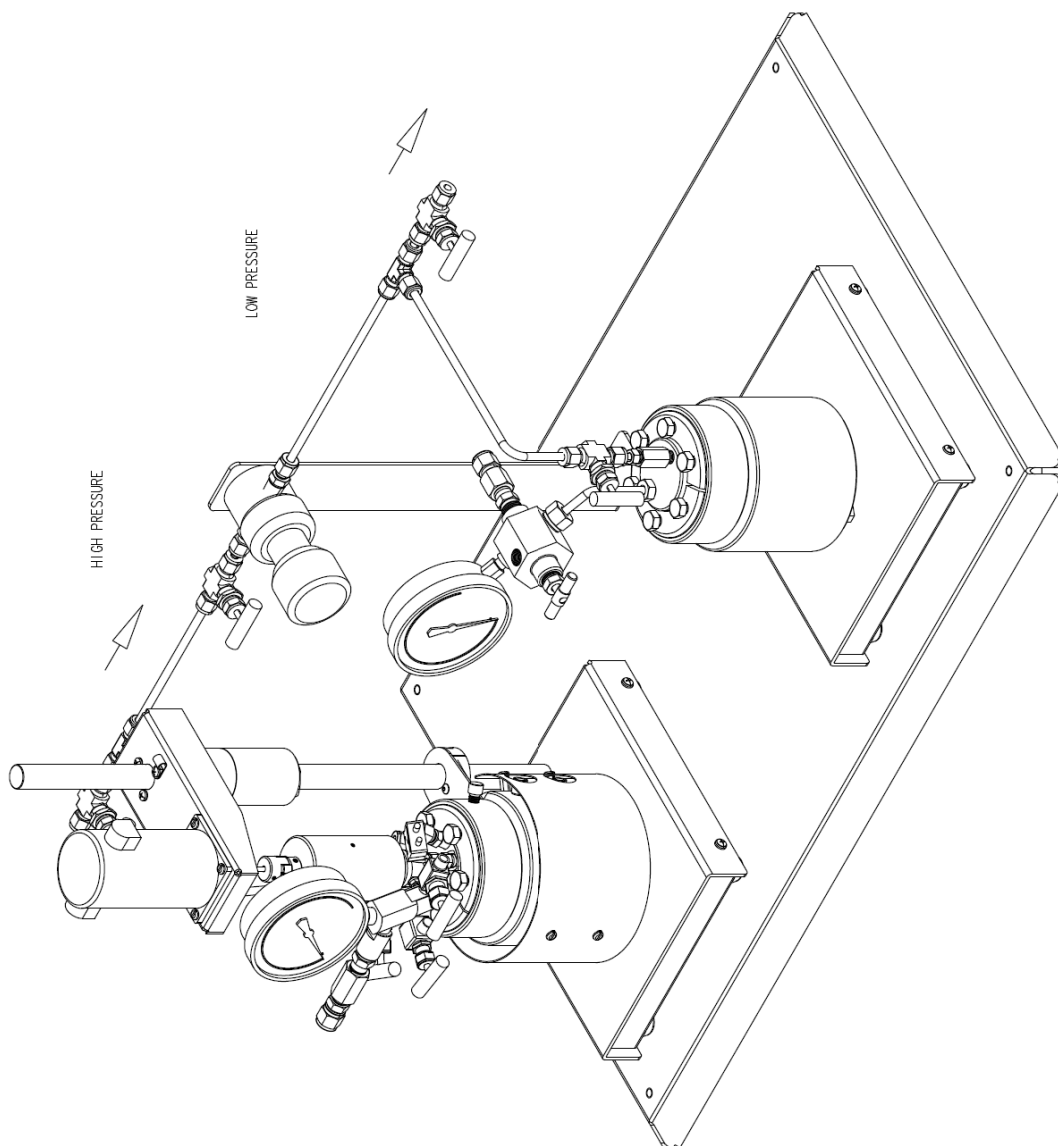


Figure B.3. Perspective of reactor drawing

# VITA

## PERSONALITY

**Date of Birth:** March 24, 1976

**Place of Birth:** SÖKE

## EDUCATION

**2009 Philosophy of Doctorate (Ph.D.)** İzmir Institute of Technology, Department of Chemical Engineering

**2003 Master of Science (M.S.)** İzmir Institute of Technology, Department of Chemical Engineering

**1999 Bachelor of Science (B.S.)** Ege University, Department of Chemical Engineering, with 74.94 GPA and as a second graduate of class.

## PUBLICATIONS

M. Gönen, D. Balköse, R. B. Gupta, S. Ülkü, “Supercritical Carbon Dioxide Drying of Methanol–Zinc Borate Mixtures”, *Ind. Eng. Chem. Res.*, 2009, 48, 6869-6876.

## PRESENTATIONS

M. Gönen, D. Balköse, F.B. Alp, S.A. Savrık, S. Ülkü, “Supercritical Ethanol Drying of Zinc Borates”, *Fourth International Boron Symposium*, Eskişehir, Turkey, 15-17 October, 2009 (accepted as an oral presentation).

M. Gönen, D. Balköse, B. Alp, S. Ülkü, “Thermal Decomposition of Hydrated Zinc Borates of  $2\text{ZnO}\cdot 3\text{B}_2\text{O}_3\cdot 3\text{H}_2\text{O}$  and  $4\text{ZnO}\cdot \text{B}_2\text{O}_3\cdot \text{H}_2\text{O}$ ”, *32<sup>nd</sup> International Vacuum Microbalance and Thermoanalytical Techniques Conference*, Kazimierz-Dolny Poland, June 21-25, 2009.

M. Gönen, S. Atakul, B. Alp, R. B. Gupta, D. Balköse, S. Ülkü, “Drying of Zinc Borate Particles by Supercritical Carbon Dioxide”, *II. National Boron Symposium*, Ankara, 17-18 Nisan, 2008.

## MEMBERSHIP

- Chamber of Chemical Engineers, (Member of Administrative Board of Chamber of Chemical Engineers Ege Branch, between January 2006 and June 2007).